Zeolite synthesis from coal fly ash and its application to heavy metals remediation from wastewater

Sofi Buzukashvili

Department of Mining and Materials Engineering

McGill University

Montreal, Quebec, Canada

January 2025

A thesis submitted to McGill University in partial fulfilment of the requirements of the degree of Doctor of Philosophy

Abstract

Industrial growth over the last few decades has resulted in the generation of a significant volume of contaminated wastewater. The unique properties of zeolites, such as their microporous structure and ion exchange capacity, make them a promising material for water treatment applications. This work explores the synthesis of zeolites from coal fly ash (CFA) using the microwave fusion and hydrothermal synthesis method and investigates their effectiveness in removing heavy metal ions, specifically Cu^{2+}, Zn^{2+}, Ni^{2+}, and Pb^{2+}, from an aqueous solution.

The environmental and economic implications of using CFA-derived zeolites (CFAZ) are profound. By repurposing CFA, a dangerous industrial waste product, this thesis aims to not only reduce environmental pollution but also provide an effective alternative to conventional adsorbent materials.

Moreover, to overcome the challenge of extracting fine zeolite particles from treated water, a novel method using colloidal PVA solutions to bind magnetite nanoparticles to zeolite was used. The obtained magnetic CFA zeolite (M-CFAZ) was investigated for its adsorption performance and ability to be recovered from water in both batch and continuous flow systems. The successful integration of magnetic separation technology facilitates the easy recovery and reuse of the zeolites, enhancing the overall sustainability of the process. In this work, magnetic separation technology, in particular, lab scale Wet High Intensity Magnetic Separator (WHIMS) was used to extract metal-laden zeolites from treated solutions. The results obtained in this thesis demonstrated that fine particles of synthesized magnetic zeolite can be efficiently extracted from treated solutions using a single cycle of wet high-intensity magnetic separation.

Furthermore, investigations into the adsorption kinetics revealed a competitive nature between the investigated metal ions for the free sites available on CFAZ. These results suggest that in an industrial scale application, it may be beneficial to employ a sequential adsorption process, whereby heavy metal ions are removed in multiple cycles. This approach could involve the removal of Pb in an initial cycle, followed by the removal of other metal ions in subsequent cycles, to avoid competition for available sites on the zeolite surface. This strategy could potentially

enhance the efficiency and speed of the adsorption process, providing an effective means of heavy metal removal from water contaminated with a mixture of ions. Further investigation is needed to determine the optimal parameters for such a sequential adsorption process and to assess its feasibility for practical application.

The implications for industrial applications are also significant. Industries such as mining, which often face challenges with heavy metal contamination, could greatly benefit from this technology. The ability to integrate magnetic CFA zeolites into existing water treatment systems, especially those employing magnetic separation, could streamline operations and reduce costs. Additionally, this technology can be tailored to treat various water compositions, making it versatile and adaptable to different industrial needs.

To investigate the relevance of the synthesized magnetic CFA zeolite into real-world systems, a continuous flow system was designed and tested. The results demonstrated effective heavy metal removal and efficient magnetic particles' recovery from the treated water. The adsorption performance was investigated under various operational conditions, maintaining a consistent selectivity order of Pb > Cu > Zn > Ni, matching the selectivity order found in the batch extraction studies the magnetic CFA zeolite. Furthermore, regeneration of metal-laden magnetic zeolites through desorption experiments was investigated by enhancing the ion-exchange process using a saturated NaCl solution.

This study highlights the potential of CFA-synthesized zeolites for the effective removal of heavy metal pollutants from wastewater. It provides valuable insights into the mechanisms underlying their adsorption behavior, elucidating how these materials interact with various metal ions. Furthermore, the research demonstrated that the synthesized magnetic CFA zeolite holds substantial promise for practical water treatment applications. As an effective and sustainable material, it offers a viable solution for the removal of heavy metal pollutants from wastewater.

Résumé

La croissance industrielle au cours des dernières décennies a entraîné la production d'un volume substantiel d'eaux usées contaminées. Les propriétés uniques des zéolites, telles que leur structure microporeuse et leur capacité d'échange ionique, en font un matériau prometteur pour les applications de traitement de l'eau. Cette thèse explore la synthèse de zéolites à partir de cendres volantes de charbon (CFA) en utilisant la méthode de fusion par micro-ondes et la synthèse hydrothermale, et étudie leur efficacité dans l'élimination des ions métalliques lourds, spécifiquement Cu^{2+}, Zn^{2+}, Ni^{2+} et Pb^{2+}, d'une solution aqueuse.

Les implications environnementales et économiques de l'utilisation des zéolites dérivées de CFA (CFAZ) sont profondes. En réutilisant les CFA, un déchet industriel dangereux, cette thèse vise non seulement à réduire la pollution environnementale, mais aussi à fournir une alternative efficace aux matériaux adsorbants conventionnels.

De plus, pour surmonter le défi de l'extraction des fines particules de zéolites de l'eau traitée, une nouvelle méthode utilisant des solutions colloïdales de PVA pour lier des nanoparticules de magnétite aux zéolites a été employée. La zéolite magnétique obtenue à partir de CFA (M-CFAZ) a été étudiée pour ses performances d'adsorption et sa capacité d'être récupérée de l'eau dans des systèmes en batch et en écoulement continu. L'intégration réussie de la technologie de séparation magnétique facilite la récupération et la réutilisation aisée des zéolites, améliorant ainsi la durabilité globale du procédé. La technologie de séparation magnétique, en particulier la séparatrice magnétique à haute intensité en milieu humide (WHIMS) à l'échelle du laboratoire, a été utilisée pour extraire les zéolites chargées de métaux des solutions traitées. Les résultats obtenus dans cette thèse ont démontré que les fines particules de zéolite magnétique synthétisée peuvent être extraites des solutions traitées à l'aide d'un seul cycle de WHIMS.

De plus, les études sur la cinétique d'adsorption ont révélé une concurrence entre les ions métalliques étudiés pour les sites libres sur les CFAZ. Ces résultats suggèrent que, dans une application à l'échelle industrielle, il pourrait être avantageux d'employer un procédé d'adsorption séquentielle où les ions métalliques lourds sont éliminés en plusieurs cycles. Cette approche

pourrait impliquer l'élimination du Pb lors d'un premier cycle, suivie de l'élimination des autres ions métalliques lors des cycles suivants, afin d'éviter la concurrence pour les sites disponibles à la surface de la zéolite. Cette stratégie pourrait potentiellement améliorer l'efficacité et la rapidité du procédé d'adsorption, offrant un moyen efficace d'éliminer les métaux lourds des eaux contaminées par un mélange d'ions. Des recherches supplémentaires sont nécessaires pour déterminer les paramètres optimaux de ce procédé d'adsorption séquentielle et pour évaluer sa faisabilité pour une application pratique.

Les implications pour les applications industrielles sont également significatives. Des industries telles que l'exploitation minière, qui sont souvent confrontées à des problèmes de contamination par les métaux lourds, pourraient grandement bénéficier de cette technologie. La possibilité d'intégrer les zéolites magnétiques dérivées de CFA dans les systèmes de traitement de l'eau existants, en particulier ceux qui utilisent la séparation magnétique, pourrait rationaliser les opérations et réduire les coûts. De plus, cette technologie peut être adaptée pour traiter diverses compositions d'eau, la rendant polyvalente et adaptable à différents besoins industriels.

Pour étudier la pertinence des zéolites magnétiques synthétisées à partir de CFA dans des systèmes réels, un système à écoulement continu a été conçu et testé. Les résultats ont démontré une élimination efficace des métaux lourds et une récupération efficace des particules magnétiques de l'eau traitée. Les performances d'adsorption ont été étudiées dans diverses conditions opérationnelles, en maintenant un ordre de sélectivité constant de Pb > Cu > Zn > Ni, correspondant à l'ordre de sélectivité trouvé dans les études d'extraction en batch avec les zéolites magnétiques de CFA. En outre, la régénération des zéolites magnétiques chargées de métaux a été étudiée à travers des expériences de désorption en améliorant le procédé d'échange ionique à l'aide d'une solution saturée de NaCl.

Cette étude met en évidence le potentiel des zéolites synthétisées à partir de CFA pour l'élimination efficace des polluants métalliques lourds des eaux usées. Elle fournit des informations précieuses sur les mécanismes sous-jacents à leur comportement d'adsorption, expliquant comment ces matériaux interagissent avec divers ions métalliques. De plus, la recherche a démontré que la zéolite magnétique synthétisée à partir de CFA présente un potentiel considérable pour des

applications pratiques dans le traitement de l'eau. En tant que matériau efficace et durable, elle offre une solution viable pour l'élimination des polluants métalliques lourds des eaux usées.

Acknowledgements

First and foremost, I would first like to express my sincere gratitude to my supervisor Professor Kristian E. Waters, for his support and guidance throughout the time of my PhD program at the Mineral Processing group at McGill University. I am incredibly thankful for the opportunities you have given me, both at McGill and through traveling, to conduct and present my research. I sincerely appreciate your insightful comments and helpful suggestions on numerous occasions of this thesis preparation and for the papers we have written. I am also very thankful for your support, patience and guidance.

I am thankful for the McGill Engineering Doctoral Award (MEDA) from the Faculty of Engineering at McGill University. Also, I would like to express my gratitude for the financial support provided by the Natural Sciences and Engineering Research Council of Canada (NSERC), Teck Resources Limited, COREM, SGS Canada Inc. and Flottec.

I am grateful to the McGill staff for their help and support, especially Barbara Hanley, Raymond Langlois, Ranjan Roy, Andrew Golsztajn and Aleksandra Djuric.

I would like to thank Dr. Ozan Kökkılıç, Dr. Shiva Mohammadi-Jam, Dr. Yue Hua Tan, Ray Langlois, Dzmitry Pashkevich, Ronghao Li, Justin Paris, Jeff Opoku, Chukwuma O. Collins, Weiqing Hu and Tian Zhao for their invaluable input and help on the different stages of this thesis. I would also like to thank all the current and alumni members of the mineral processing group who I am proud to know and who made my time at McGill fun and memorable.

I would like to thank Dr. Sidney Omelon and Dr. Philippe Ouzilleau for many interesting discussions about this project, collaborations and support over the years. Special thanks to Dr. Roberto Sommerville for his invaluable assistance in deepening my understanding of zeolites and for collaboration in published papers.

I would also like to thank all my friends, who became online friends when I moved to Montreal. Thank you for staying with me through the years, without your friendship it would have been too difficult to survive through pandemic times and completing the PhD would be much harder. I am

grateful to all the amazing people who I was lucky to meet in Montreal and who became my friends - thank you for making me feel in Montreal like at home.

I would like to thank my late parents, Maria and Iosif Buzukashvili for everything you taught me and all the love you gave me. My father was a brilliant engineer and without his example, I would not be able to be where I am today. I know you would be proud seeing me now. I would also want to thank my extended family, my uncle, my stepmom and my mother-in-law for their unconventional support. Also, I would like to acknowledge Jordy, for being the best fluffy friend in the world and for emotional support over these years.

Finally, I want to thank Lior Goldstien, for being the best partner, who always supports and encourages me, for moving through half of the world for me to be able to fulfill my dream and for being there through the worst times. Thank you for everything you are doing for us and for being the best partner ever. Without you all that would not be possible.

Table of Contents

List of Figures

List of Tables

Nomenclature

Abbreviations

Initials	Description
ACs	Activated Carbons
ATSDR	Agency for Toxic Substances and Disease Registry
BET	The Brunauer-Emmett-Teller method
CB	Conduction Band
CE	Circular Economy
CEC	Cation Exchange Capacity
CFA	Coal Fly Ash
CFAZ	CFA-derived Zeolite
CNS	Cashew Nutshell
CNT	Classical Nucleation Theory
CNTs	Carbon Nanotubes
DMS	Dense Medium Separation
EDS	Energy Dispersive X-ray Spectroscopy
EPA	U.S. Environmental Protection Agency
GDP	Gross Domestic Product
ICP-OES	Inductively Coupled Plasma - Optical Emission Spectrometry
IZA	International Zeolite Association
LE	Linear Economy
LOI	Loss on Ignition
LTA	Linde Type A Zeolite
LTAZ	LTA Synthesized Zeolite
M-CFAZ	Magnetic CFA-derived Zeolite
MF	Microfiltration
M-LTAZ	Magnetic LTA-synthesized Zeolite
MZ0.1	Magnetic LTA zeolite synthesized with addition of 0.1 g iron oxide nanoparticles

Initials	**Description**
MZ0.5	Magnetic LTA zeolite synthesized with addition of 0.5 g iron oxide nanoparticles
MZ1	Magnetic LTA zeolite synthesized with addition of 1 g iron oxide nanoparticles
MZ2	Magnetic LTA zeolite synthesized with addition of 2 g iron oxide nanoparticles
NF	Nanofiltration
PSA	Particle Size Analysis
PVA	Polyvinyl alcohol
PVC	Polyvinyl Chloride
RHA	Rice Husk Ash
RO	Reverse Osmosis
SDG	Sustainable Development Goals
SEM	Scanning Electron Microscopy
TFC	Thin Film Composite
UF	Ultrafiltration
VB	Valence Band
VSM	Vibrating Sample Magnetometer
WHIMS	Wet High Intensity Magnetic Separator
WHO	World Health Organization
XPS	X-ray Photoelectron Spectroscopy
XRD	X-Ray Diffraction Analysis

List of Symbols

Symbol	Description	Units
B	Magnetic induction	T
C_0	Initial concentrations of metal ions in solution	mg/L
C_e	Concentrations of metal ions in solution and after the adsorption process	mg/L
d	Lattice spacing	Å
dB/dx	Magnetic field gradient	T/m
F_x	Magnetic force on the particle	N
H	Applied magnetic field strength	A/m
K_f	Freundlich constant related to the adsorption capacity	L/g
K_L	Langmuir constant	L/mg
m	Adsorbent dosage	g
M	Intensity of magnetization	A/m
n	Adsorption intensity	
q_d	Amount of metal desorbed per unit mass of desorbing	mg/g
q_e	Adsorbed fraction	mg/g
q_m	Maximum adsorption capacity	mg/g
Q_{sat}	Monolayer adsorption capacity	mg/g
q_t	Amount of metal adsorbed onto the mineral per unit mass of adsorbent at equilibrium	mg/g
R^2	Correlation coefficient	
t_g	Time taken for said nucleus to grow to a detectable size	min
t_n	Time taken for a stable nucleus to form	min
t_r	Equilibration time for reagents to reach temperature and silicate and aluminate ion distribution	min
V	Solution volume	L
θ	Angle of incidence	°
λ	Wavelength	nm

Symbol	Description	Units
μ_0	Permeability of free space	kg·m/s·A²
τ	Nucleation induction period	min
χ	Magnetic susceptibility	
χ_f	Magnetic susceptibility of the fluid	emu/cm^3
V	Particle volume	m^3

Chapter 1
Introduction

1.1 Background

Human activities and industrial developments generate large volumes of polluted wastewater, which is a severe environmental problem [1,2]. Water pollution is one of the leading reasons for water shortages [3] and can also affect other significant aspects of our life, such as public health, industrial and agricultural production, and the economy [4].

There are a wide range of factors generating water pollution [5]. Industrial wastewater may consist of different pollutant types depending on the generating process [6]. The most common pollutants in wastewaters are specific organic constituents, high salinity, and heavy metals [6]. The term heavy metals is often used as a group name for metals and metalloids that have been associated with contamination and potential toxicity in the environment [7,8]. Heavy metals are generally described as metals with a density greater than 5 g/cm^3 [9,10], the most common being lead (Pb), zinc (Zn), mercury (Hg), nickel (Ni), cadmium (Cd), copper (Cu), chromium (Cr), and arsenic (As) [11]. One common source of heavy metals environmental contaminations is wastewater originating through, mining operations, chemical production, metal plating facilities, agriculture, batteries and other industries [12,13]. The concentration of heavy metals in wastewater has been rising due to the expansion of industrial activities and other human endeavors, which is a threat for both the ecosystem and human health [11].

In recent years, significant efforts have been dedicated to developing efficient techniques for heavy metal removal, including ion exchange, chemical precipitation, electrochemistry, membrane filtration, and adsorption [11,14]. Adsorption is recognized as an efficient and cost-effective technology for heavy metals removal from water, offering the benefits of adsorbent recovery and reuse [15]. This study investigates the adsorption of heavy metal ions from aqueous solutions using synthetic adsorbents, namely zeolites.

Zeolites are crystalline aluminosilicates with well-defined micropores and distinctive physicochemical properties, including cation exchange capacity, large surface area, molecular sieving, catalytic activity, and sorption capabilities[16]. Typically, zeolites are constructed from TO_4 tetrahedra (T = tetrahedral atom, e.g. Si, Al) and oxygen atoms bridging the tetrahedral atoms [17-19]. Zeolites are widely used in diverse applications, including the removal of heavy metals from wastewater [20-22].

Natural zeolites are primarily hydrothermal and of volcanic origin, with examples being faujasite, mordenite, offretite, ferrierite, erionite and chabazite [23]. They can be found in crystallized forms within igneous, metamorphic rocks and sedimentary rocks [24,25], and are widely used in the field of heterogeneous catalysis and have many other industrial applications. However, due to the limited variety of natural zeolite microstructures and surface chemistry, synthetic zeolites often outperform natural zeolites [24,26]. The sorption capacity of synthetic zeolites developed through various synthesis methods with designed chemical properties and pore size has been the subject of many studies. Synthetic zeolites are highly pure, with uniform crystal sizes, making them particularly useful for industrial applications [27,28]. Moreover, synthetic zeolites can be made for specific application needs [29]. As such, synthetic zeolites have garnered significant interest among researchers and scientists due to their high flexibility and excellent adaptability. The advancements in the field of zeolite synthesis over the recent years can be attributed to innovations in synthetic strategies and a deeper understanding of the zeolite crystallization process [30].

In laboratory settings, hydrothermal processes can be simulated using elevated temperature or pressure along with natural raw materials and/or synthetic silicates [24]. Synthesis reactions necessitate specialized equipment, pure substrates, and energy, making the product potentially much more expensive than natural zeolites [27]. Current research trends in zeolite synthesis are influenced by environmental considerations, promoting the use of natural or waste raw materials [24,27]. As such, the raw material for zeolite synthesis investigated in this study is coal fly ash.

Coal fly ash (CFA) is a by-product of the combustion of coal that is mainly composed of spherical aluminosilicate glass particles [31]. Coal is originated millions of years ago from deposited plant material, which was transformed into carbon-rich coal through geological processes [31,32]. CFA

is produced at 1200–1700°C from the various inorganic and organic constituents of the feed coal and is currently generated in large quantities [33,34]. CFA is considered to be a human carcinogen with a small particle size (average size smaller than 75 μm [34,35]). The continued reliance on coal by some of the world's largest coal-dependent countries is expected to increase CFA generation in the coming years [36,37]. However, a significant portion of CFA is stored in landfills, ash ponds, surface impoundments, or stacked [38]. Given the potential hazards of CFA, utilizing it for the synthesis of zeolites presents a promising field of research [39,40].

Before treated water can be discharged, zeolite particles should be removed. The separation of fine zeolite particles after the adsorption process poses a significant challenge, as conventional methods have limitations for removal of such fine particles [41,42]. One promising method to address the challenge of separating fine zeolite particles from water is the synthesis of magnetic zeolite composites, which can be sequentially removed after adsorption of heavy metals by the application of external magnetic field [43,44]. For that, the zeolite can be embedded with magnetic particles, such as magnetite (Fe_3O_4) or maghemite (Fe_2O_3), among others [45,46]. When binding iron oxide nanoparticles with zeolite, the zeolite is likely to acquire the iron oxide's properties such as superparamagnetism, while maintaining or even enhancing its adsorption capacity.

After metal ions removal, magnetic zeolite can be extracted using magnetic separation technologies. While other research had successfully synthesized magnetic zeolites that can be attracted to magnets and tested it in heavy metal ions removal that is covered in more details in Section 4.2 of this thesis, no work has previously been published on the extraction of magnetic zeolite particles from treated water in a way that could be industrially applicable.

1.2 Thesis Objectives and Motivation

Industrial wastewater often contains high concentrations of heavy metals, which are known to be among the most dangerous environmental contaminants due to their toxicity and carcinogenicity. Among various methods to reduce heavy metal concentrations in wastewater, adsorption is often considered one of the most effective. Zeolites, known for their unique properties such as high porosity and large surface area, are highly suitable for water treatment applications.

This study investigates novel synthetic magnetic zeolites from coal fly ash (CFA) and laboratory-grade Linde Type A (LTA) zeolite enhanced with nano magnetite particles for the remediation of heavy metal ions (Pb^{2+}, Cu^{2+}, Zn^{2+}, Ni^{2+}) from wastewater. To address the challenge of extracting fine zeolite particles from treated water, a novel method using colloidal polyvinyl alcohol (PVA) solutions to bind iron oxide nanoparticles to zeolite was developed. This research not only investigates the adsorption performance of synthesized magnetic zeolite in both batch and continuous flow systems but also explores the ease of extracting the zeolite from water post-adsorption and its regeneration through desorption experiments.

The main objectives of this thesis can be split into two categories - synthesis of magnetic CFA-derived zeolite and its application in industrially relevant water remediation process.

1. To synthesise magnetic CFA zeolite:
   a. Zeolite synthesis from CFA (CFAZ).
   b. CFAZ application for heavy metals remediation from water: CFAZ maximum adsorption capacity for selected metal ions in single and mixed ions systems; insights into adsorption mechanisms.
   c. Develop a method for magnetic CFAZ (M-CFAZ) synthesis.
2. To investigate adsorption performance of magnetic M-CFAZ:
   a. Compare adsorption performance to non-magnetic CFAZ in the same experimental conditions to investigate if M-CFAZ is still efficient for the removal of selected metal ions.
   b. Develop a method for full extraction of M-CFAZ from treated solution.
   c. Design and build continuous flow system for water treatment using M-CFAZ.
   d. Examine regeneration of extracted metal-laden M-CFAZ and possibility of its reuse.

Overall, this research aims to utilize one waste stream (CFA) to synthesize an adsorbent material (zeolite) for the remediation of another waste stream (contaminated wastewater). By modifying the CFA-derived zeolite to become magnetic, this study enhances the process's sustainability, allowing for the extraction, regeneration, and reuse of the zeolite. This contributes to both the environmental and economic viability of water treatment processes.

1.3 Thesis Structure

This thesis is presented as a traditional monograph thesis comprised of 8 chapters and 3 appendices. The chapters summarize information from relevant literature on zeolites, their synthesis and application in water treatment from heavy metal ions (Chapter 1-4). The experimental methods employed throughout the thesis are described in the Experimental Methods chapter (Chapter 5). Synthesized non-magnetic zeolites (LTAZ and CFAZ) and their magnetic modifications (M-LTAZ and M-CFAZ) are described in Chapter 6. The results of heavy metals removal from aqueous solutions using non-magnetic and magnetic zeolites in both batch and continuous flow systems are summarized in Chapter 7. Additionally, Chapter 7 covers removal of magnetic zeolite from treated solutions and its regeneration. In Chapter 8, discussion about the conclusions, contributions to original knowledge and recommendations for future work are discussed. A schematic overview of the structure of the thesis is presented in Figure 1.1. The chapter details are:

Chapter 1 - Introduction: General introduction covers the problem of water pollution by heavy metals, discuss zeolites as adsorbent materials for their removal. The idea of zeolite synthesis from coal fly ash (CFA) is introduced.

Chapter 2, 3 and 4 – Literature review: These chapter contains the literature review of the three topics that are crucially important for this thesis: water treatment, zeolites, magnetic adsorbents.

Chapter 2 – Water treatment: Overview of water pollution and water treatment technologies, including flotation, membrane technologies, ion exchange and adsorption. Materials that are commonly used in water treatment are discussed. This chapter also overviews water pollution problem in mining industry, focusing on Canadian mining sector, and discussing specific metal ions selected for this work.

Chapter 3 – Zeolite: Zeolite types, different synthesis methods and coal fly ash (CFA) use as a raw material for zeolite synthesis are described. Furthermore, use of CFA derived zeolites (CFAZ) in water treatment is reviewed for both single and mixed ions systems.

Chapter 4 – Magnetic adsorbents: This chapter overviews magnetically modified adsorbents, particularly, magnetic zeolites and their use in water treatment from heavy metals.

Magnetic separation technology that can be applied for zeolite extraction from treated water is described. Additionally, the regeneration, reuse and disposal of zeolites are covered in Chapter 4.

Chapter 5 – Experimental methods: A detailed description of materials, experimental methods, and characterization techniques used in this thesis.

Chapter 6 – Zeolite synthesis and characterization: This chapter represents the results of the synthesis of a) non-magnetic LTA zeolite (LTAZ) and CFA zeolite (CFAZ); b) magnetic LTA zeolite (M-LTAZ) and magnetic CFA zeolite (M-CFAZ).

Chapter 7 – Adsorption experiments: Results of batch adsorption of non-magnetic (LTAZ, CFAZ) and magnetic zeolites (M-LTAZ, M-CFAZ), adsorption in continuous flow system using magnetic zeolites (M-LTAZ, M-CFAZ) and extraction of magnetic zeolites using magnetic separation technology. Additionally, this chapter covers results of M-LTAZ and M-CFAZ regeneration after adsorption of metal ions.

Chapter 8 - Conclusions, Contributions and Future work: A discussion of results, contributions to original knowledge and recommendations for future work.

Appendix A - Different adsorption isotherm models.

Appendix B - Absolute adsorption capacities of different zeolites synthesized from CFA for heavy metal ions remediation.

Appendix C – SEM-EDS results of synthesized M-CFAZ showing map scans and point IDs.

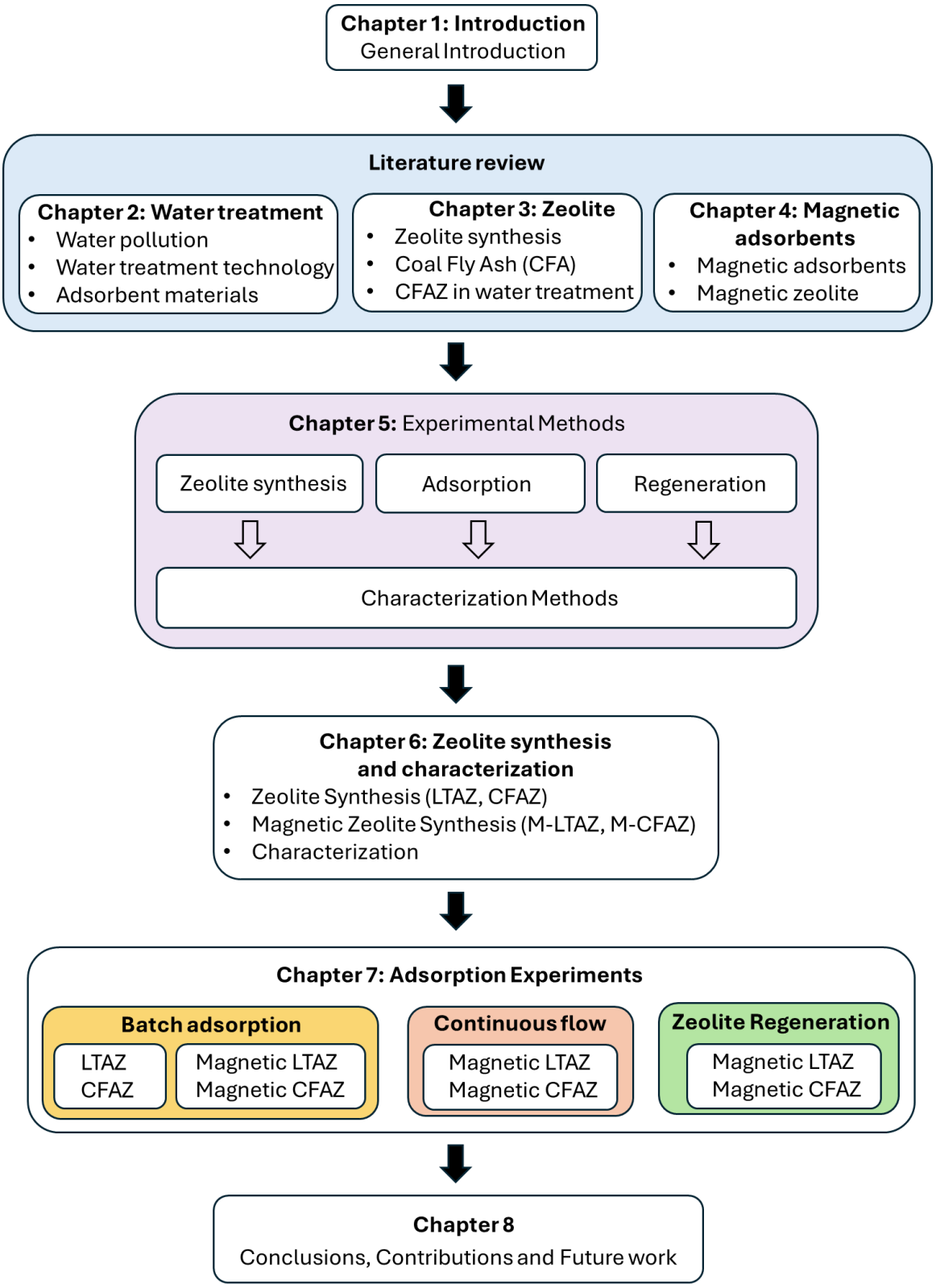

Figure 1.1 - Flowsheet of the thesis structure.

1.4 Publications

The following manuscripts were published based on the results of this thesis.

- The following manuscript was published in the journal "*Canadian Metallurgical Quarterly" and covers the majority of literature review presented in Chapter 3.*

S. Buzukashvili, R. Sommerville, N. A. Rowson, K. E. Waters (2024) An overview of zeolites synthesised from coal fly ash and their potential for extracting heavy metals from industrial wastewater, Canadian Metallurgical Quarterly, 63:1, 130-152.

- The following manuscript was published in the journal "Crystals" and covers the description of magnetic zeolite synthesis procedure from LTA zeolite and its application in single ions adsorption experiments, covered in Chapter 5 Section 5.2, and Chapter 7, Section 7.1 and 7.3.

Buzukashvili, S.; Hu, W.; Sommerville, R.; Brooks, O.; Kökkılıç, O.; Rowson, N.A.; Ouzilleau, P.; Waters, K.E. Magnetic Zeolite: Synthesis and Copper Adsorption Followed by Magnetic Separation from Treated Water. Crystals 2023, 13, 1369.

- The following manuscript was published in the journal Minerals Engineering and covers the majority of the results presented in Chapter 7, Sections 7.2, 7.4, and 7.5.

Buzukashvili, S.; Sommerville, R.; Hu, W.; Brooks, O.; Kökkılıç, O.; Ouzilleau, P.; Rowson, N.A.; Waters, K.E. Zeolite synthesis from coal fly ash and its application to heavy metals remediation from water contaminated with Pb, Cu, Zn and Ni ions. Minerals Engineering 2024, 209, 108619.

- The following manuscript was published in the journal JCIS Open and covers the majority of the results presented in Chapter 7, Sections 7.6 and 7.7.

Buzukashvili, S.; Sommerville, R.; Hu, W.; Brooks, O.; Kökkılıç, O.; Ouzilleau, P.; Rowson, N.A.; Waters, K.E. Exploring efficiency and regeneration of magnetic zeolite synthesized from coal fly ash for water treatment applications. JCIS Open 2025, 17, 100127.

1.5 Contribution of Authors

The contribution of authors adheres to the CRediT (Contributor Roles Taxonomy) guidelines and is detailed for experimental and results chapters in the thesis (Chapters 3, 5, 6, and 7). Chapters 1, 2, 4 and 8 wholly attributed to S. Buzukashvili.

Sofi Buzukashvili: Conceptualization, Formal analysis, Investigation, Methodology, Writing – original draft, Writing – review & editing. **Roberto Sommerville**: Conceptualization, Formal analysis, Investigation, Methodology, Writing – review & editing. **Weiqing Hu**: Formal analysis, Investigation. **Oliver Brooks**: Formal analysis, Investigation, Methodology. **Ozan Kökkılıç**: Formal analysis, Investigation, Methodology, Writing – review & editing. **Philippe Ouzilleau**: Methodology, Resources, Writing – review & editing. **Neil A. Rowson**: Conceptualization, Methodology, Writing – review & editing. **Kristian E. Waters**: Conceptualization, Methodology, Resources, Writing — review & editing, Supervision, Project administration, Funding acquisition.

S. Buzukashvili also express her gratitude to Dr. Shiva Mohammadi-Jam, Dzmitry Pashkevich, Ronghao Li and Tian Zhao for their assistance and help with experiments and data analysis.

Chapter 2
Water Treatment

2.1 Introduction

Water is an irreplaceable and essential resource [6,47]. In recent years, global urbanization has led to increased demand and rapid expansion in the agricultural and industrial sectors [48,49]. Global water demand has increased sixfold over the last century and continues to grow at about 1% annually, driven by rising populations and expanding economies [50]. This increased demand can pose significant risks such as water scarcity, which impacts food and energy security and can lead to conflicts [51]. Consequently, reducing water scarcity aligns with the Sustainable Development Goal (SDG) on clean water and sanitation [51]. With the added pressure of climate change threatening water supplies, there is a heightened need to balance the competing demands of humans and the environment [50,51].

Water stress is measured by comparing human water use — such as water abstraction or consumption — to the amount of water resources available in the environment [52]. This measure is used in the globally recognized SDG indicator 6.4.2 on water stress, which specifically tracks water abstraction as a form of water use [53]. Environmentally available water resources are calculated by deducting the environmental flows needed to sustain ecosystem integrity in aquatic systems such as streams, rivers, wetlands, riparian zones, and estuaries from the total available water resources. This approach helps in understanding the balance between human demand and ecological preservation [52].

2.2 Water pollution

In recent years, global urbanization led to increased demand and rapid expansion in agricultural and industrial sectors [48]. Many industries generate significant volumes of polluted wastewater that requires treatment and management systems to minimize environmental harm and comply with legal standards [6,48,54-56]. The nature and volume of generated wastewater varies significantly across industries, largely depending on the specific type of processing involved [48,57]. The most common contaminants in industrial water include chemicals, heavy

metals, organic constituents, soils, pesticides, pharmaceuticals, and other industrial by-products [6,58,59]. Numerous research has been dedicated to develop alternative solutions targeting three key areas: (a) detecting contaminants in water intended for human consumption, (b) assessing the risks these contaminants pose to public and environmental health, and (c) proposing new water treatment technologies [60].

Wastewater is generally classified into two main categories: sewage wastewater that includes discharge from domestic activities and non-sewage wastewater combining wastewater produced from commercial activities, such as agricultural or industrial wastewater [61]. Industrial wastewater refers to water discharged from various commercial activities, including manufacturing processes and cleaning operations [62]. The nature and volume of generated wastewater varies significantly across industries, largely depending on the specific type of processing involved [48,57]. The most common contaminants in industrial water include chemicals, heavy metals, organic constituents, soils, pesticides, pharmaceuticals and other industrial by-products [6,58,59]. In this work, the focus is on the non-sewage, industrial wastewater coming from the mining industry with a high concentration of heavy metals. However, the same type of contaminants can be present in wastewater coming from other industries, such as chemical or textile manufacturing. Examples of major pollutants found in wastewater coming from common industries can be found in Table 2.1

Table 2.1 – Common industries producing bulk wastewater and their major pollutants. Adapted from Manasa et al. [63].

Type of industry	**Pollutant type**
Food industry	Organic materials
Textile industry	Color, polyvinyl alcohol detergents
Thermal power plant	Sulphur and nitrogen oxides
Nuclear power plant	Transuranic elements
Pulp and paper industry	Organic halides and inorganic compounds
Pharmaceutical industry	Bulk drugs and pharmaceutical ingredients
Petroleum industries	Lubricants and hydrocarbons
Chemical industries	Lead, mercury and nitrogen compounds
Mining industries	Metal ions, suspended solids from precipitation of the rocks

Heavy metals are considered to be one of the most dangerous groups of pollutants as they are toxic, carcinogenic and not biodegradable; they are typically defined as metals with a density exceeding 5 g/cm^3 [11,59,64]. Heavy metals can be divided into three groups, including toxic metals (such as Hg, Cr, Pb, Zn, Cu, Ni, Cd, As, Co, Sn, etc.), precious metals (such as Pd, Pt, Ag, Au, Ru, etc.) and radionuclides (such as U, Th, Ra, Am) [11,65-67]. They are considered as one of the most dangerous groups of pollutants because they are not biodegradable and tend to accumulate in living organisms [12,68]. Furthermore, conventional wastewater treatment methods might be challenging to apply to heavy metals removal due to their high stability and solubility [68]. Heavy metals pollute the environment through wastewater originating through many sources including metal plating facilities, mining operations, agriculture, fertiliser production, tanneries, batteries, paper industries and pesticides, battery manufacturing, textile printing, and leather industries [12,13]. Among the most hazardous industries that produce the large volumes of wastewater contaminated by heavy metals are chemical, food and diary, textile, petrochemical, and mining industries [59,69]. Examples of typical heavy metals found in wastewater and their main sources are presented in Table 2.2.

Table 2.2 – Typical heavy metals existing in wastewater and their sources, in addition to the health issues caused by improper quantities and the permitted amounts in drinking water based on the world health organization (WHO) recommendations. Adapted from Qasem et al. [11].

Heavy metal	**Main sources** [70,71]	**Health impact** [72-76]	**Permitted amounts (µg)** [70]
Cadmium (Cd)	Batteries, paints, steel industry, plastic industries, metal refineries, and corroded galvanized pipes.	Bones, liver, kidneys, lungs, testes, brain, immunological system, and cardiovascular system.	3
Mercury (Hg)	Electrolytic production of chlorine and caustic soda, runoff from landfills and agriculture, electrical appliances, industrial and control instruments, laboratory apparatus, and refineries.	Brain, lungs, kidneys, liver, immunological system, cardiovascular system, endocrine, and reproductive system.	6
Lead (Pb)	Lead-based batteries, solder, alloys, cable sheathing pigments, rust inhibitors, ammunition, glazes, and plastic stabilizers.	Bones, liver, kidneys, brain, lungs, spleen, immunological system, hematological system, cardiovascular system, and reproductive system.	10
Arsenic (As)	Electronics and glass production.	Skin, lungs, brain, kidneys, metabolic system, cardiovascular	10

Heavy metal	**Main sources** [70,71]	**Health impact** [72-76]	**Permitted amounts (µg)** [70]
		system, immunological system, and endocrine.	
Chromium (Cr)	Steel and pulp mills and tanneries.	Skin, lungs, kidneys, liver, brain, pancreas, testes, gastrointestinal system, and reproductive system.	50
Nickel (Ni)	Stainless steel and nickel alloy production.	Lung, kidney, gastrointestinal distress, pulmonary fibrosis, and skin.	70
Copper (Cu)	Corroded plumbing systems, electronic and cables industry.	Liver, brain, kidneys, cornea, gastrointestinal system, lungs, immunological system, and hematological system.	2000
Zinc (Zn)	Brass coating, rubber products, some cosmetics, and aerosol deodorants.	Stomach cramps, skin irritations, vomiting, nausea, and anemia, and convulsions.	3000

It is essential to treat wastewater contaminated with heavy metal ions before releasing it into the environment [13,59,69]. An overview of different methods used for water contaminated by heavy metals is presented in the following section.

2.3 Water treatment technologies

The growing concerns over heavy metal pollution and its effects on human health and the environment have accelerated the development of affordable and sustainable remediation technologies [77]. These technologies include membrane filtration, ion-exchange, adsorption, chemical precipitation, and electrocoagulation among others [58,64,77] and are summarized in Figure 2.1.

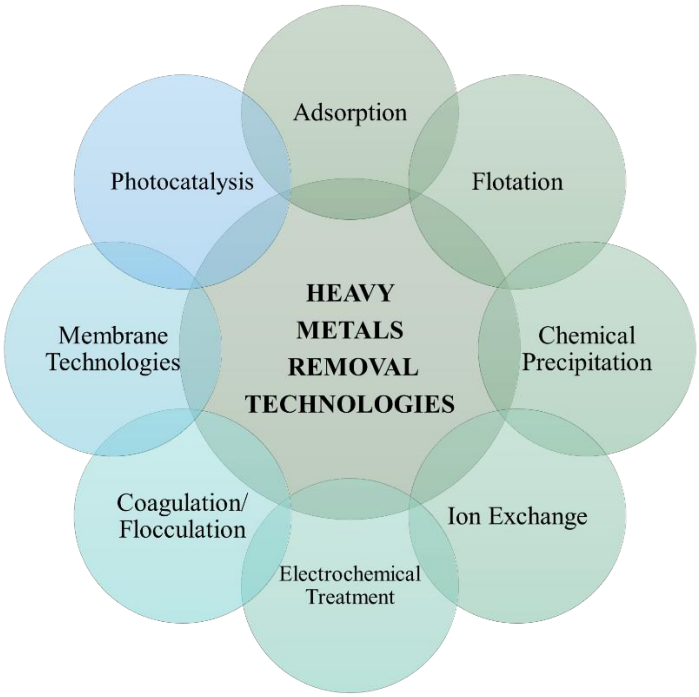

Figure 2.1 - Water treatment technologies to remove heavy metals from wastewater.

Conventional methods to remove heavy metal from wastewater include ion exchange, membrane filtration, and chemical precipitation. While these methods have their benefits, they also have several drawbacks, including high costs, incomplete removal of certain ions, increased operational expenses, among others [78]. For example, the membrane filtration process is an effective method, but it has significant initial costs [79], and the ion exchange method is considered less effective in highly concentrated metal solutions [78]. Recently, alternative wastewater treatment methods such as photocatalysis, electrochemical treatments, and adsorption have gained significant attention [78]. A more detailed overview of water treatment technologies is provided in the following sections.

2.3.1 Photocatalysis

Photocatalysis has emerged as an innovative and advanced method for removing heavy metal ions from water [78,80]. Photocatalytic processes utilize semiconductors such as TiO_2, ZnO, ZnS among others known for their photocatalytic activities [81,82]. These materials, known for their strong oxidizing properties, have the ability to break heavy metal complexes, releasing the metal ions [78]. This, as well as their ability to oxidize and degrade organic compounds, makes them highly effective in purifying water by targeting both metallic and organic pollutants, thereby enhancing the overall efficiency of the treatment process [78].

The basic mechanism of photocatalysis involves the following steps: (I) light absorption to generate electron-hole pairs; (II) separation of excited charges; (III) transfer of electrons and holes to the surface of photocatalysts; and (IV) utilization of charges on the surface for redox reactions [83]. The general mechanism of heterogeneous photocatalysis is shown in Figure 2.2.

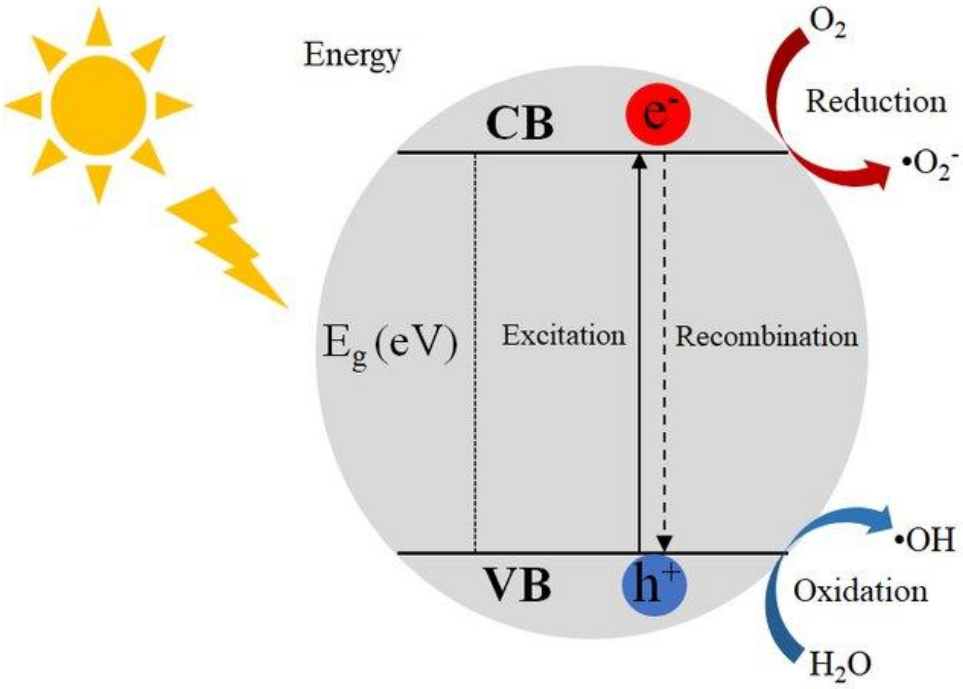

Figure 2.2 - General mechanism of the heterogeneous photocatalysis. Photocatalyst being irradiated with a light source of an energy equal to or higher than its band gap energy. Abbreviations VB and CB state for valence band and conduction band, respectively. Adapted from de Macedo et al. [84].

2.3.2 Flotation

Flotation is a method which originated from the froth flotation process, one of the most commonly used separation techniques in mineral processing. This method involves generating tiny air bubbles smaller than 0.1 mm to remove heavy metals from water [85]. Recently, ion flotation has gained significant attention among the various flotation processes [11].

Ion flotation involves the addition of surfactants or collectors to remove surface-inactive ions from aqueous solutions, usually with an ion having a charge opposite to that of the metal ion to be removed [86,87]. Ion flotation is often used to remove metal ions from solutions with low concentrations of heavy metals, which can originate from various industrial processes such as metal industries semiconductor manufacturing, and mining operations [87,88]. A schematic of the ion flotation process is illustrated in Figure 2.3.

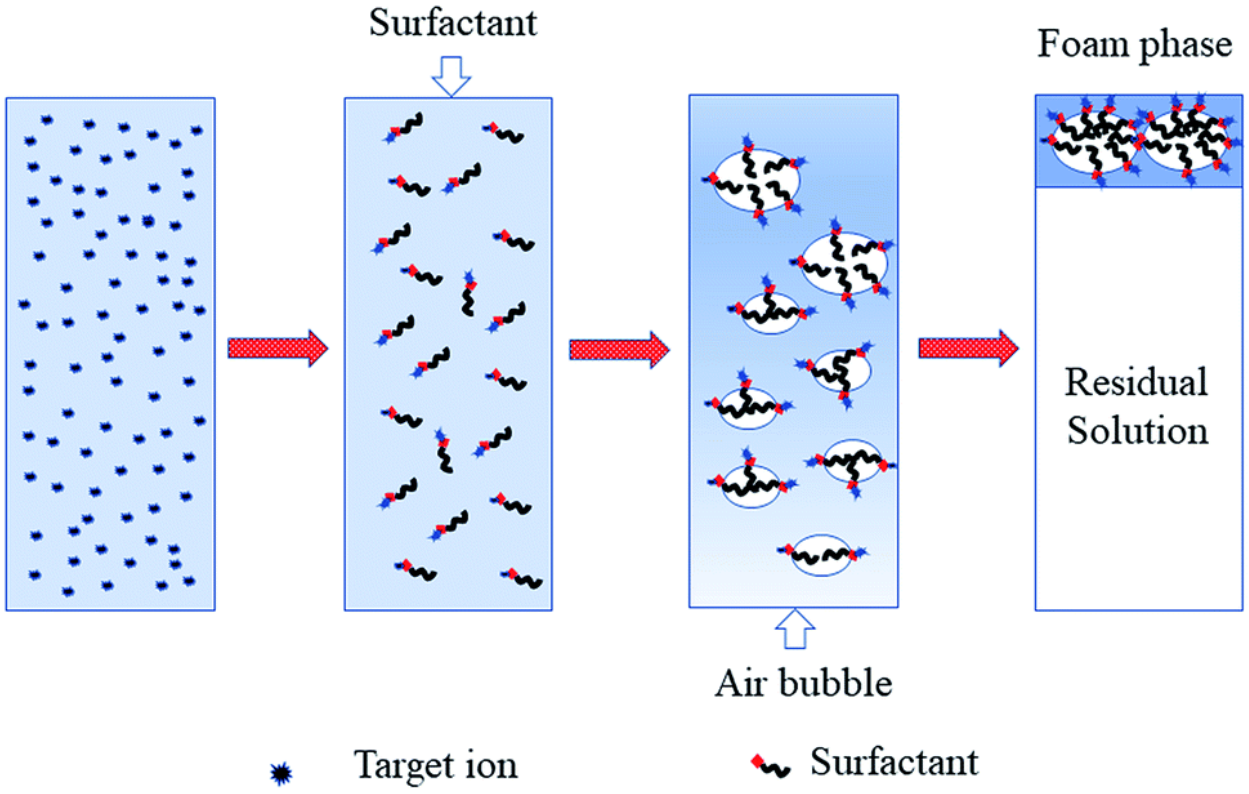

Figure 2.3 - Schematic of the overall process of ion flotation. Adapted from Chang et al. [89].

2.3.3 Chemical precipitation

Chemical precipitation utilizes a chemical compound that is added to wastewater to initiate a chemical reaction with particles changing them into solid-state that can be separated later. Agents such as caustic soda, lime, and limestone are commonly used to transform dissolved heavy metals into insoluble forms such as hydroxides, carbonates, or sulfides, so they can be then recovered. While the chemical precipitation method is cost-effective and simple, it produces a significant amount of sludge, presenting disposal challenges and being less effective when contaminant concentrations are very low [78,90]. A schematic of chemical precipitation used in heavy metal ions removal from water is shown in Figure 2.4.

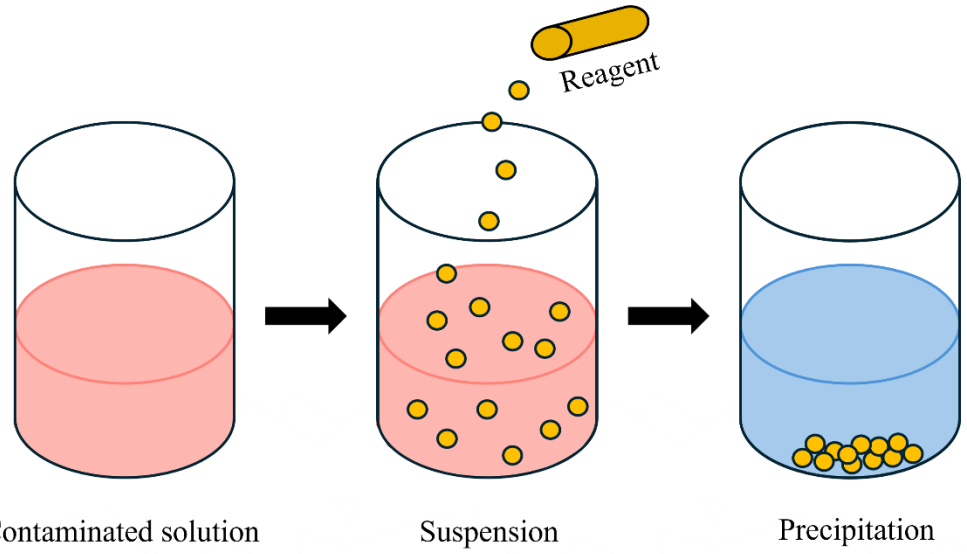

Figure 2.4 - Schematic diagram showing chemical precipitation for removal of heavy metal ions.

2.3.4 Ion exchange

The ion exchange method is a reversible chemical reaction that replaces undesirable metal ions with harmless, environmentally friendly ones [91]. Ion exchange leverages the properties of dissolved impurities in ionic form. This process involves the temporary capture of ions and their subsequent replacement with ions from solution. Ion exchange can be used for various purposes such as softening, deionizing, de-alkalizing, or disinfecting water. A variety of materials, including zeolites, synthetic organic resins, and others, can serve as exchange mediums in water purification processes [11]. A schematic of ion exchange method is shown in Figure 2.5.

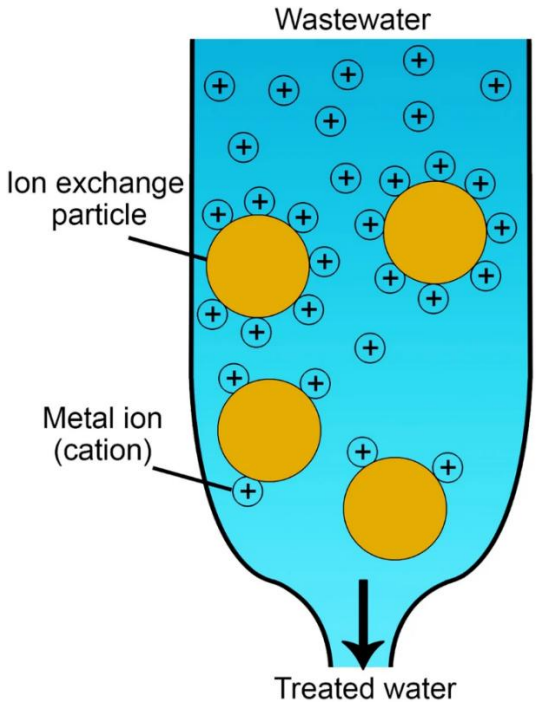

Figure 2.5 - Schematic diagram showing ion exchange for removal of heavy metal ions. Reproduced from Qasem et al. [11].

2.3.5 Electrochemical treatment

Electrochemical processes used in wastewater treatment are termed electrocoagulation. Electrocoagulation typically occurs through electrochemical reactions at the anode and cathode, but reactions within the solution itself also play a crucial role in the overall process [92]. The process involves applying a direct current to metallic electrodes (anode and cathode) immersed in wastewater, initiating two main electrochemical reactions. At the anode, cations such as Fe^{2+} or Al^{3+} are released into the solution, while at the cathode, water is reduced to hydrogen gas (bubbles) and hydroxide ions (OH^-). When cations are introduced during the electrocoagulation they destabilize the colloidal solution, as colloidal particles in wastewater, that are typically negatively charged, causing the particles to aggregate and form larger entities known as flocs. These flocs, due to their increased size, can then be easily separated from the water by sedimentation and flotation, aided by the electrogenerated bubbles [92]. A schematic sketch of the electrocoagulation process is shown in Figure 2.6.

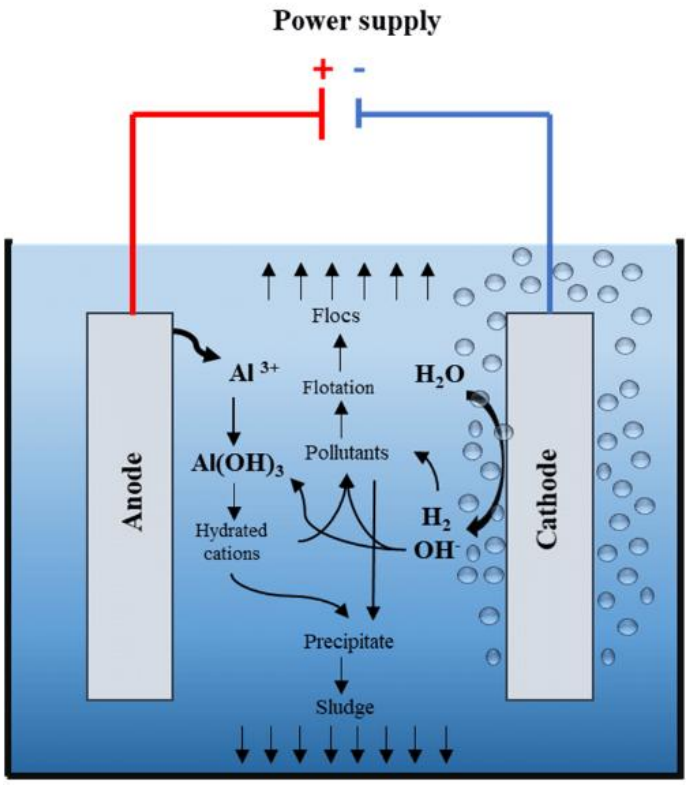

Figure 2.6 - A schematic sketch of the electrocoagulation process. Reproduced from Almukdad et al. [93].

2.3.6 Coagulation/Flocculation

Coagulation and flocculation are processes that enhance the aggregation and removal of suspended solids and dissolved contaminants from water. These methods are notably simple and cost-effective technique for the removal of organic and inorganic compounds as well as colloidal particles from wastewater [94].

Flocculation can occur naturally, as with microalgal cells that produce flocculating chemicals, or be induced by adding flocculating agents [95]. This process results in the agglomeration of destabilized particles into larger particles that settle out of the suspension by sedimentation [96]. Coagulation involves adding substances such as aluminum sulfate or ferric salts to wastewater in a mixing chamber, that enhance particle collisions and reduce opposing forces. Consequently, large agglomerates (flocs) are formed and can be removed efficiently through filtration or sedimentation processes [94]. The dosage of coagulants generally varies with the turbidity and Total Organic

Carbon (TOC) levels in the water, with higher levels requiring greater doses to effectively reduce contaminants [96]. Coagulant aid polymers and/or acid may also be added to enhance the coagulation process. Generally, higher TOC and/or higher turbidity levels require higher coagulant dosages. The removal of metal effluents from water waste can also be done by combining coagulation-flocculation with other techniques. The schematic of the general coagulation/flocculation process is shown in Figure 2.7.

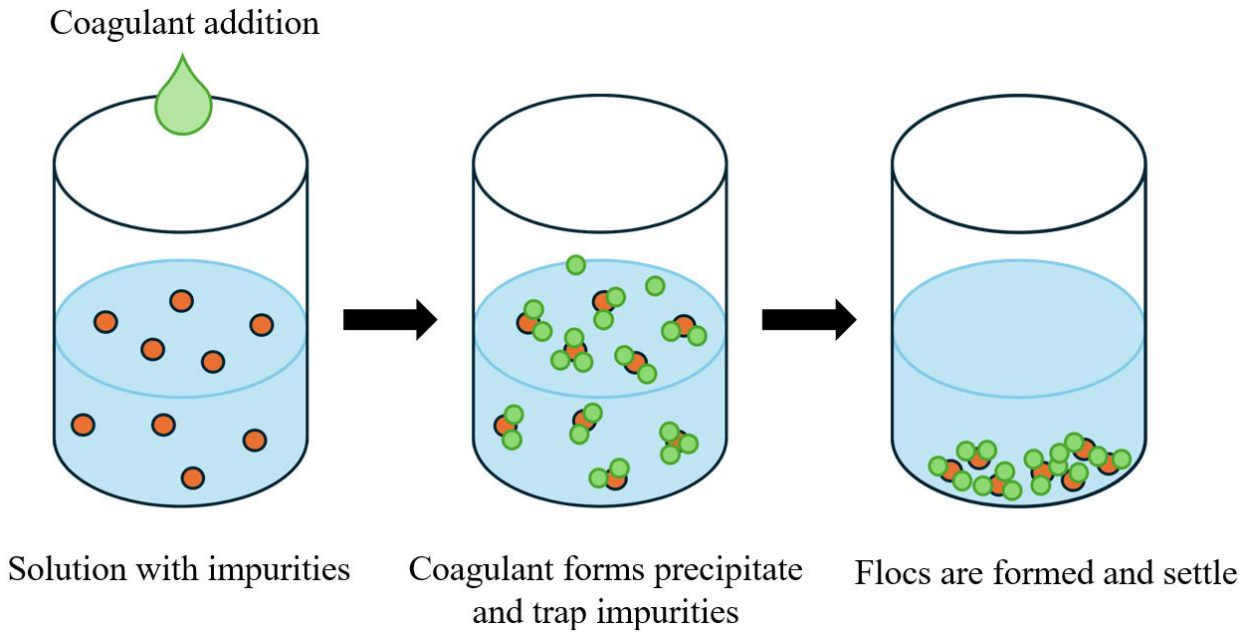

Figure 2.7 - Schematic of water purification via coagulation/flocculation process.

2.3.7 Membrane technologies

Membrane filtration separation technologies are the most widely used method for separation, with the driving force of the process being hydraulic pressure. The four main techniques employed in these processes are Reverse Osmosis (RO), Microfiltration (MF), Ultrafiltration (UF), and Nanofiltration (NF). These methods effectively separate substances based on various particle sizes and molecular weights [78]. The key difference among the techniques is in the size of the membrane pores, and varying pressure requirements. Thus, membrane technologies are categorized based on their capacity to filter out particles and solutes of different sizes, with each technique tailored to specific separation needs [97]. Various types of porous and thin film composite (TFC) membranes are utilized in wastewater treatment. [98]. The efficiency of metal removal in membrane processes

is significantly affected by the pore size of the membrane and the presence of charged groups on its surface [99]. These factors determine how effectively the membrane can trap and filter metal ions from a solution. An example of a schematic of membrane water treatment system is shown in Figure 2.8.

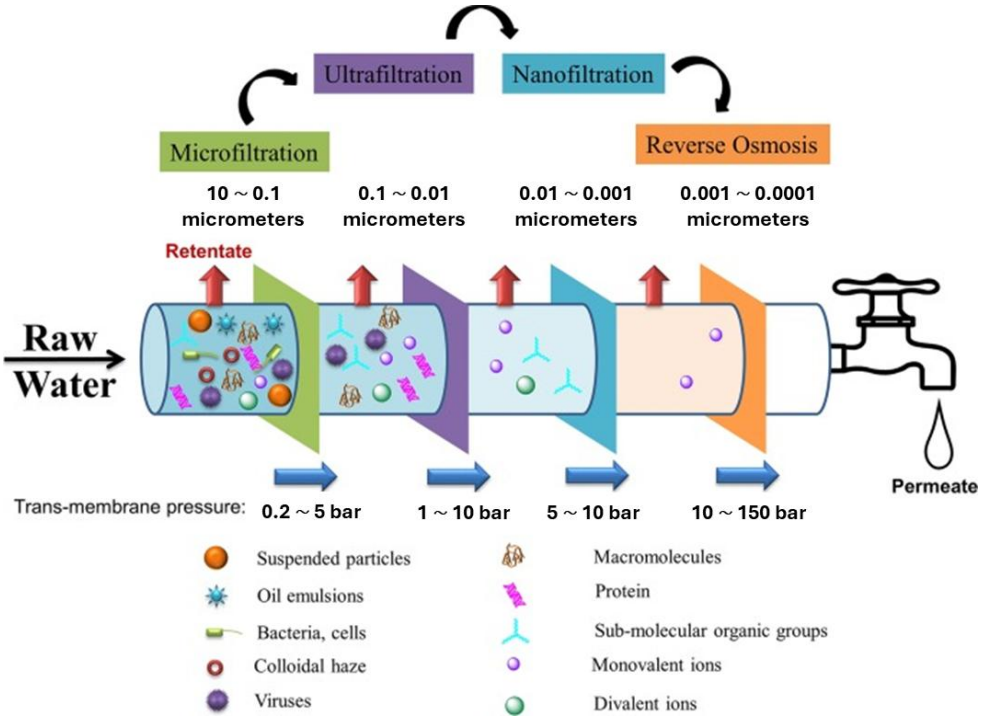

Figure 2.8 - Schematics of membrane water treatment system. Reproduced from Liao et al. [100].

2.3.8 Adsorption

As other methods present notable drawbacks, including the generation of large quantities of sludge, poor quality of treated water, high disposal costs among others, adsorption is a potentially more effective approach for wastewater treatment [101-103]. Adsorption is often considered the most effective method due to its high efficiency for removing low but still toxic concentrations of heavy metals [12,13,104]. Adsorption provides flexibility in design, high-quality treated effluent, low cost, it is reversible, and the adsorbent can be regenerated [13,105,106]. Cost efficiency is an important parameter and should be taken into consideration when using adsorbents to extract heavy metals from wastewater. Widely used adsorbents such as silica gel, activated carbon, and alumina, though

effective, can be expensive on a large scale, while synthesized adsorbents can be more cost-effective [102].

Adsorption involves the accumulation of substances at an interface, which can be liquid-liquid, gas-liquid, gas-solid, or liquid-solid [107-109]. The substance being adsorbed is called the adsorbate, while the material on which adsorption occurs is known as the adsorbent [108,110]. The adsorption mechanism is influenced by the physicochemical properties of the adsorbent and heavy metals, as well as operating conditions such as temperature, adsorbent amount, pH, adsorption time, and initial metal ion concentration[11,111-113]. The porosity of adsorbent material is an important factor as it indicates the available space on the adsorbent material [78,114]. The schematic illustration of heavy metal ions adsorption is shown in Figure 2.9.

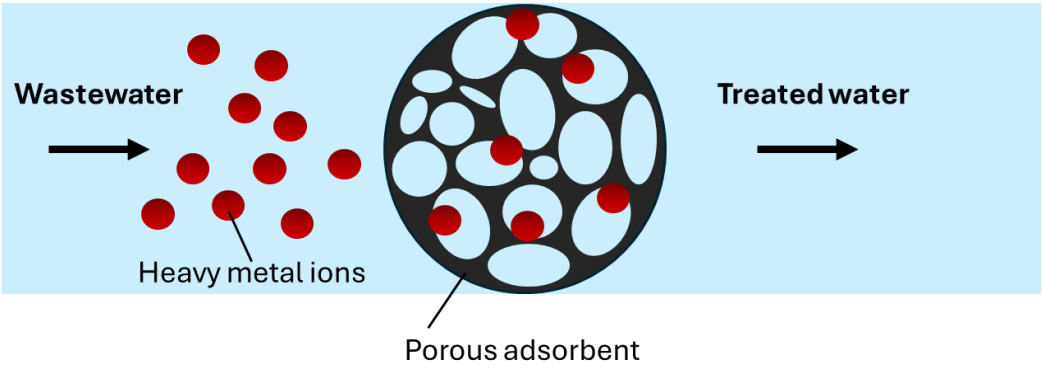

Figure 2.9 - The schematic adsorption process as a wastewater treatment.

The use of adsorption in wastewater treatment dates back to the late 19th century, with the first patent for an activated carbon filter was registered by Ostrejko in 1900 [109]. While activated carbon has subsequently been widely used for water purification due to its high surface area and porosity, it has disadvantages including high cost, low selectivity, and challenges in regeneration [115]. Given these limitations, many researchers have explored alternative types of adsorbents, showing significant advancements in enhancing the adsorption capabilities of newly designed adsorbents over the past decades [109]. Common adsorbents used in wastewater treatment include carbon-based adsorbents (activated carbons (ACs), carbon nanotubes (CNTs), and graphene), mineral adsorbents (zeolites, silica, and clays), magnetic adsorbents (modified adsorbents that host

magnetic nanoparticles), metal-organic frameworks adsorbents (where metal ions form strong bonds with organic linkers), among others [11].

A critical innovation in adsorbents development was the development and integration of nanotechnology, enabling the synthesis of nanoscale materials with unique properties such as high surface area, tunable pore size and shape, and functional groups [109,116]. Widely studied nanomaterials for adsorption include carbon nanotubes, graphene, metal oxides, metal-organic frameworks, zeolites, and magnetic nanoparticles, which show promise for future applications due to their distinctive morphological and structural properties [117].

To design effective adsorbents and adsorption systems, understanding the adsorption mechanism is of utmost importance [118,119]. Isotherm modeling is a reliable technique for predicting adsorption mechanisms and examining the relationship between adsorbents and heavy metals under equilibrium conditions [119]. This topic will be further covered in more details in the following section.

2.3.8.1 Adsorption models

Numerous sorption isotherm models have been effectively utilized to analyze experimental data, providing insights into the interactions between pollutants and adsorbents [78,120]. The thermodynamic equilibrium relationship between adsorbate and adsorbent at constant temperatures can be described by adsorption models, which are classified based on the number of parameters into one-parameter, two-parameter, and three-parameter models [119,121]. By investigating the adsorption kinetics, including time and solute feeding rate, the pathway, mechanism, and performance of the adsorption process can be assessed, helping to determine the sorbent's potential and efficiency [78]. For ease of access, the different adsorption isotherms and parameters of each isotherm are presented in Appendix A. While various models are discussed in this section, it is important to consider that in the field of water treatment, the two-parameter models, Langmuir and Freundlich isotherms, are used in most of the published research.

The Langmuir isotherm is one of the earliest proposed models that assumes monolayer coverage of adsorbent on homogeneous adsorbate surface with each molecule sorbing onto the surface having equal sorption activation energy [122]. The Langmuir model has been shown suitable for

describing chemisorption processes involving ionic or covalent chemical bonds between the adsorbent and adsorbate [123].

The Langmuir model can be expressed as follows [120]:

$$q_e = \frac{Q_{sat} K_L C_e}{1 + K_L C_e} \quad (2.1)$$

where Q_{sat} is the monolayer adsorption capacity, mg/g; K_L is the Langmuir constant related to the adsorption capacity, which obeys the free adsorption energy, L/mg. The linear form of Equation (2.1) is presented as follows:

$$\frac{C_e}{q_e} = \frac{1}{q_m K_L} + \frac{1}{q_m} C_e \quad (2.2)$$

When adsorption involves the formation of multiple layers of adsorbate molecules on a heterogeneous surface of the adsorbent, the process can be described using the Freundlich adsorption model which is mathematically described as follows [120].

$$q_e = K_f C_e^{\frac{1}{n}} \quad (2.3)$$

where K_f is the Freundlich constant related to the adsorption capacity, L/g; and n is the adsorption intensity, describing the heterogeneity of the adsorbate sites.

2.4 Water Pollution in the Mining Industry

Historically, metal mining has been crucial for sustaining life in both developed and emerging nations, contributing to economy and technological advancements, and is expected to continue in the future [124,125]. Mining takes place in diverse hydrological settings, from the arid regions of central Australia, to the tropical zones, and the sub-arctic climates of Canada [126]. However, the extraction and purification of mineral resources require large volumes of water, which are subsequently released into the environment after use [66]. The mining industry faces significant challenges in achieving environmental sustainability, particularly in terms of water usage and waste management [66,127]. Mining wastewater usually contains elevated levels of toxic organic pollutants such as flotation reagents and inorganic pollutants such as metal ions, which normally

exceed the World Health Organization (WHO) discharge limits [128,129]. If released into water, they can impact aquatic life and human health [130-132]. Additionally, mining wastewater is typically highly acidic due to the high concentrations of sulfates and metals present in the water, and contains a large amount of suspended solids [133,134]. Thus, discharging mining wastewater into the environment can contaminate water resources and adversely impact living organisms, including humans, aquatic animals, and plants [135,136]. Historically, mine tailings were often discharged into nearby surface water bodies without treatment, which created significant environmental liabilities and incurs high remediation and reclamation costs [137]. Currently, in most countries, water discharge from mine sites is regulated with specific limits on pollutant concentrations and total volume. To mitigate potential environmental risks, many mining companies monitor the water discharged from their sites and comply with regulations requiring pollution prevention measures [128,138]. Given the remote locations of many mining projects, which lack the necessary infrastructure and workforce for large-scale treatment facilities, there is a growing need for simple, efficient, and sustainable wastewater treatment methods to minimize environmental impacts.

Wastewater coming from the mining industry will vary significantly from mine to mine, with potential effects on both hydrology and water quality throughout a mine's lifecycle [126]. Additionally, due to the low-grade ores, mining operations generate vast amounts of waste, and disposing of this waste in open pits can lead to significant landscape and environmental degradation [139-141]. Thus, to mitigate the risks of negative water impacts, the mining industry employs a variety of water management strategies. This substantial variability within the sector presents challenges in accurately quantifying the water footprint of mining operations and mineral commodities. As a result, the considerable variability within the mining industry presents numerous challenges in accurately measuring the water footprint of mining operations and mineral commodities [126] and innovation is crucial in the mining industry for addressing growing social and environmental concerns from the public and regulatory bodies [66,142,143].

Water use in mineral processing depends on the recovery method for valuable minerals, which can be categorized as wet or dry methods [126]. Dry processing techniques, such as air cyclones, ore sorting, electrostatic separation, dry grinding and dry magnetic separation, are limited to niche

applications due to issues including dust generation and lower recovery efficiency [144]. In contrast, wet processing methods such as flotation, leaching, wet grinding and gravity separation are more prevalent due to higher efficiency and easier transport of solids. Water in these processes mainly ends up in products or tailings, with recovery and recycling through thickening and filtration being key to reducing external water usage. The extent of water recovery from tailings depends on the long-term waste management strategy [145,146]. Tailings can be stored in dams, backfilled into mines, dry-stacked [147], or discharged into rivers or marine environments [148]. Among the various methods, storing tailings in dam structures or natural depressions near the mine site is the most prevalent worldwide [126]. However, storage of tailings not only requires a significant amount of land but also has the potential of causing river and air pollution [132]. Over the past 100 years of data, there is a 1.2% failure rate for tailings dams due to reasons including the overtopping, piping, foundation problems, slope instability, structural defects, or poor management practices [126,149]. Some of the examples of tragic mining tailings dams include gold and copper mine Mount Polley, British Columbia, Canada in 2014 and Córrego do Feijão iron ore dam collapse in Brumadinho, Brazil, 2019.

(a) (b)

Figure 2.10 – Mine Polley mine disaster: The contents of a tailings pond are pictured flowing down the Hazeltine Creek into Quesnel Lake near the town of Likely, B.C. on August, 5, 2014 [150] (a); An aerial view after a tailings dam collapsed near Brumadinho, Brazil [151] (b).

Common methods for mining wastewater treatment include membrane filtration, coagulation/flocculation, chemical precipitation, adsorption, and ion exchange among others [81,126,152-156]. Technology choices and configurations in the mining industry are

determined by site-specific conditions, which can differ even when the same mineral is extracted. Factors such as the chemical composition of the mine rock, the quality of wastewater, available space, and the volume of water treated necessitate customized solutions from companies specializing in mining water treatment, as there is no one-size-fits-all approach [157]. Furthermore, most commercially used methods do not sufficiently remove all elements in wastewater to the required concentrations. This has driven continuous research and development in wastewater treatment systems. Additionally, some treatment systems have high maintenance costs, high energy consumption, and slow treatment processes. Therefore, there is a need for cost-effective and efficient treatment systems that can produce high-quality effluent and reduce environmental pollution [66].

2.4.1 Wastewater in the Canadian Mining Industry

Canada's mining industry is one of the largest in the world, producing more than 60 minerals and metals, including gold, potash, copper, nickel, aluminium, and others, at almost 200 mines [158]. In 2021, the minerals and metals sector contributed 5% of Canada's total gross domestic product (GDP) [158].

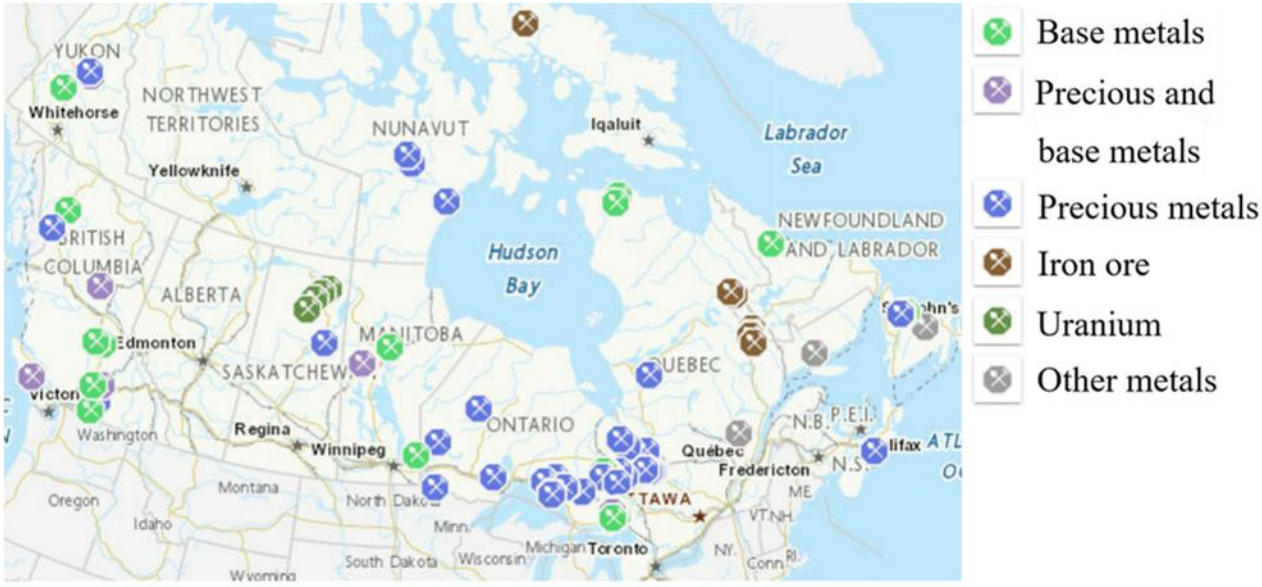

Figure 2.11 – Canadian metal mines; atlas.gc.ca (2024). Accessed on August 20, 2024.

Mining is a significant industrial activity in Canada and is expected to become increasingly important as global demand continues to grow [159]. Wastewater management in Canada is achieved through collaborations among federal, provincial, and local governments [160]. Given the substantial variations among mines, most companies are likely to adhere to specific national regulations, which could influence the industry's developmental path [161].

The Fisheries Act is the primary federal legislation for managing and protecting Canada's fisheries resources [162]. The Metal and Diamond Mining Effluent Regulations aim to safeguard Canada's lakes and rivers by imposing strict limits on the quality of effluent discharged by metal and diamond mines. These regulations permit the release of effluent into waters frequented by fish and specified locations under subsection 36(3) of the Fisheries Act. Effluent must meet concentration-based limits for various pollutants, including arsenic, copper, cyanide, lead, nickel, zinc, suspended solids, radium 226, and un-ionized ammonia. Additionally, the effluent must have a pH within a specified range and must not be acutely lethal. The regulations mandate effluent testing, reporting, and Environmental Effects Monitoring studies.

Detailed information on the maximum authorized concentration in discharged water in Canada for metals investigated in this work is provided in Table 2.3.

Table 2.3 – The maximum authorized heavy metal ion concentration in mining effluent set by the Canadian government [163].

Metal	**Maximum authorized monthly mean concentration, mg/L**	**Maximum authorized concentration in a grab sample, mg/L**
Copper	0.30	0.60
Lead	0.20	0.40
Nickel	0.50	1.00
Zinc	0.50	1.00

2.4.2. Discussion on selected metal ions

In this work the focus is on the removal of copper (Cu), nickel (Ni), zinc (Zn) and lead (Pb) ions from wastewater. These metals are commonly found in mining wastewater due to their widespread use and natural presence in mineral deposits. Mining and ore processing activities often release

these metals into the environment, where they can become major pollutants. Exposure to elevated levels of Cu, Zn, Ni, and Pb can result in severe health issues, so it is essential to effectively remove these metals from wastewater to safeguard public health. Many research efforts are focused on enhancing the efficiency and cost-effectiveness and sustainable of technologies for removing these metals from industrial wastewater.

The following sections provide a detailed overview on each of the heavy metal investigated in this thesis, their potential hazard and a short review of some of the recent studies on their removal from water.

2.4.2.1 Copper

Copper is one of the most valuable and prevalent metals used in many industries, including metal finishing, electroplating, plastics, and etching [59,164-167]. The escalating copper pollution in global water resources presents a significant threat to both human health and aquatic ecosystems as it is a toxic heavy metal due to its high hazardous effects [165,168]. Copper can cause numerous health issues in humans, including vomiting, convulsions, and cramps [169]. Reported copper concentrations in wastewater span from 2.5 mg/L to as high as 10,000 mg/L [170]. Considering the potential environmental and health risks associated with copper-contaminated wastewater, it should be treated before discharging [166,171,172].

Copper is a transition metal that is abundantly found in nature and ranks as the third most widely used metal after iron and aluminum [173]. Copper exists in various forms, such as Cu(0) (metal), Cu(I) (cuprous ion), and Cu(II) (copper ion), with Cu(II) being the most toxic and prevalent in the environment [170]. Cu(II) is extensively utilized in industries such as electroplating, paints and dyes, petroleum refining, fertilizer production, mining and metallurgy, explosives manufacturing, pesticides, and steel production [170,174]. Excessive copper exposure can lead to acute gastrointestinal problems, liver enzyme system inactivation, and motor disorders in some individuals suffering from copper overdose [175,176]. The presence of Cu(II) in the global aqueous environment has been increasing and is recognized as a significant heavy metal contaminant due to its associated health risks [170,176,177]. According to the U.S. Environmental Protection Agency (EPA) and the World Health Organization (WHO), the maximum allowed Cu(II) concentration in drinking water is 1.3 mg/L and 3 mg/L, respectively [170,173].

Different materials have been investigated for Cu removal from water and different mechanisms can be applied [170]. Some of the recent results of different adsorbents capacities for Cu ions are shown in Table 2.4. For a more detailed review of methods used for Cu(II) removal from wastewater, readers are referred to Liu et al. [170].

Table 2.4 – Adsorption capacities of different adsorbents for copper.

Adsorbent material	**Adsorption capacity, mg/g**	**Reference**
Chitin	2.8	Boulaiche et al. [178]
Fe_2O_3-carbon foam	3.8	Lee et al. [179]
Herbaceous peat	4.8	Gündoğan et al. [180]
Lemon peel	13.2	Meseldzija et al. [152]
Clinoptilolite	13.6	Doula et al. [181]
Shells of wheat	17.4	Aydın et al. [182]
Diatomite	27.6	Gaballah et al. [183]
Chitosan nanoparticles	35.5	Yuwei et al. [184]
Tea waste + dolomite	38.1	Albadarin et al. [185]
NaP1 Zeolite	51.0	Alvarez-Ayuso et al. [186]
Coal Fly Ash (CFA) Zeolite	56	He et al. [187]
CFA Zeolite	96.0	Sireesha et al. [188]
Carbonized Zeolite/Chitosan Composite	111.4	Hidayat et al. [189]
Functionalized multi-walled carbon nanotubes	118.4	Gupta et al. [190]
Facial composite adsorbent	176.3	Awual et al. [191]
Poly(Acrylic Acid/Chestnut Shell Pigment) Hydrogel	200.0	Zhang et al. [192]

2.4.2.2 Nickel

Ni is a silvery-white transition metal that exists in diverse mineral forms [193]. Ni ions are a common contaminant in polluted wastewater, known for its high toxicity and carcinogenic characteristics [194]. Humans can be exposed to nickel through consumption of food, water, or inhalation of air which can cause brain damage, along with serious lung and kidney problems [194-196]. The U.S. Environmental Protection Agency (EPA), the Agency for Toxic Substances and Disease Registry (ATSDR), and the World Health Organization (WHO) recommend maximum acceptable concentrations for nickel in drinking water at 0.02 mg/L [197,198]. Different methods can be used for Ni removal from water, however as this work focuses on adsorption technique, a synopsis of recent studies investigating Ni(II) adsorption by a variety of different materials are presented in Table 2.5. For further information on different methods of Ni removal from wastewater, readers are referred to Coman et al. [199] and Raval et al. [197].

Table 2.5 – Adsorption capacities of different adsorbents for nickel.

Adsorbent material	**Adsorption capacity, mg/g**	**Reference**
Clinoptilolite	3.3	Argun [200]
Rice husk ash (RHA)	6.5	Srivastava et al. [201]
Natural zeolite	8.7	Coruh etl a. [202]
Husk of Lathyrus sativus	15.7	Panda et al. [203]
Bentonite	19.9	Katsou et al. [204]
Graphene oxide	38.6	Najafi et al. [205]
Zeolite A	47.0	He et al. [3]
Activated charcoal	99.0	Choksi et al. [206]
Protonated rice bran	102.0	Zafar et al. [207]
Chitosan coated PVC beads	120.5	Popuri et al. [208]
Jordan natural zeolite	153.8	Alabbad et al. [209]
Calcium alginate	310.4	Vijaya et al. [210]

2.4.2.3 Zinc

Zinc is the third most utilized nonferrous metal, following aluminum and copper [211]. Zinc is an essential trace element for humans, however, high concentrations can cause significant health issues, such as stomach cramps, vomiting, skin irritations, anemia, and nausea and can be harmful to aquatic life [166,212,213]. The remediation of zinc in wastewater is of particular concern due to its highly toxic and persistent nature. Recommended safe limits by WHO in drinking water are below 3 mg/L, and the WHO recommended safe limits in wastewater is 2–5 mg/L [166,214]. Zinc can cause contamination of soil, water, and food chains [215,216]. Some of the recent results of different adsorbents capacities for Zn ions are shown in Table 2.6.

Table 2.6 – Adsorption capacities of different adsorbents for zinc.

Adsorbent material	**Adsorption capacity, mg/g**	**Reference**
NaP1 Zeolite	33	Alvarez-Ayuso et al. [186]
Powdered waste sludge	168	Zwain et al. [217]
Raw bentonite (25 °C, pH 6.5)	73.5	Zhang et al. [218]
Wheat bran	16.4	Dupont et al. [219]
Black gram husk	39.99	Saeed et al. [220]
NaP Zeolite	37	Zhang et al.[221]
Zeolite A	220	Izidoro et al. [222]

2.4.2.4 Lead

Lead is one of the most common heavy metals in wastewater, and poses a considerable threat to vegetation and wildlife, severely disrupting entire ecosystems due to its extreme toxicity [223,224]. In addition to these environmental concerns, it also presents serious risks to human health as it is not biodegradable and can accumulate in body tissues, causing brain dysfunction and severe kidney disease [13,224].

Lead is commonly extracted from galena (PbS; lead sulfide) and occurs in its +2 oxidation state (Pb(II)) in wastewater streams [225]. The WHO and Guidelines for Canadian Drinking Water

Quality set the permissible level of Pb(II) in drinking water at 0.01 mg/L [226]. Some of the recent results of different adsorbents capacities for Pb ions are shown in Table 2.7.

Table 2.7 – Lead adsorption capacities of different adsorbents

Adsorbent material	**Adsorption capacity, mg/g**	**Reference**
Rice husk activated carbon	492.0	Zhang et al. [227]
Zeolite A	556	Jangkorn et al. [228]
Nitrogen- and phosphorusenriched biochar	723.6	Fan et al. [229]
Zeolite Na-X zeolite	457	Ge et al. [230]
Powdered activated carbon	232.5	Kharrazi et al. [231]
Cashew nut shell (CNS)	17.8	Senthil Kumar [232]
Montmorillonite	31.1	Sarı et al. [233]
K-type Zeolite (FA48)	56	Kobayashi et al. [234]
Zeolite-NaX at 303 K	14.2	Pandey et al. [235]

2.4.2.5 Mixed ions solutions containing Cu, Ni, Zn and Pb

While single-ion systems provide important information on maximum adsorption capacity of selected adsorbents for specific metal ions, mixed-ion systems are closer to a real-world scenario, where wastewater typically contains various metal contaminants.

To date, no papers have been found on wastewater treatment that contains only Pb, Cu, Zn, and Ni ions. Several studies have focused on specific water compositions, where metal ions were removed using ultrafiltration and microflotation [236], coagulation-flocculation [237] and solar photocatalytic removal [238]. This indicates that no studies have investigated the adsorption of these metal ions in mixed ion systems. The absence of research on wastewater remediation containing only Pb, Cu, Zn, and Ni ions underscores the importance of investigating the adsorption of these metal ions in mixed ion systems, as these metals are among common contaminants.

2.5 Circular Economy of Water

Circular Economy (CE) is a concept developed in the 1970s that proposes a shift from the linear economy (LE), i.e. "extraction-production-disposal" to the concept of retains and recovers as much value as possible from resources by reusing, repairing, refurbishing, remanufacturing, repurposing, or recycling products and materials [239-241]. However, only in the past decade has the concept of CE gained significant popularity and been widely discussed in numerous publications [242]. Currently it is implemented by various governments around the world, including those of the European Union, the USA, Canada, China, and other countries, to address industrial environmental concerns and promote sustainability [243-245].

The circular economy has been proposed as an effective concept for sustainable water management, recognizing water as a vital resource, product, and service essential for agriculture, industry, electricity generation, and urban and recreational activities [246-248]. The concept of circular economy and sustainability in the mining industry, particularly regarding the use of water, focuses on reducing waste, maximizing resource efficiency, and minimizing environmental impact.

In mining operations, water is a critical resource used in various processes, from mineral processing to dust suppression. A general waster flowsheet in a typical mineral processing plant can be seen in Figure 2.12. The circular economy approach encourages the treatment and recycling of process water, allowing it to be reused in other mining operations or safely discharged back into the environment. For example, water recovered from the concentrator can be recycled and combined with a specific amount of fresh water for internal reuse, while water from the tailings pond can also be recycled in a process known as external reuse [249]. The extent to which resource recovery motivates mine water reuse is influenced by the concentration of valuable components, the complexity of selective extraction processes along with their water requirements, and the costs associated with treatment [157].

By adopting circular economy principles, mining operations can significantly reduce their environmental footprint, enhance operational efficiencies, and contribute to sustainable development goals. This approach not only supports compliance with increasingly strict

environmental regulations but also helps in building a positive corporate image and securing social license to operate.

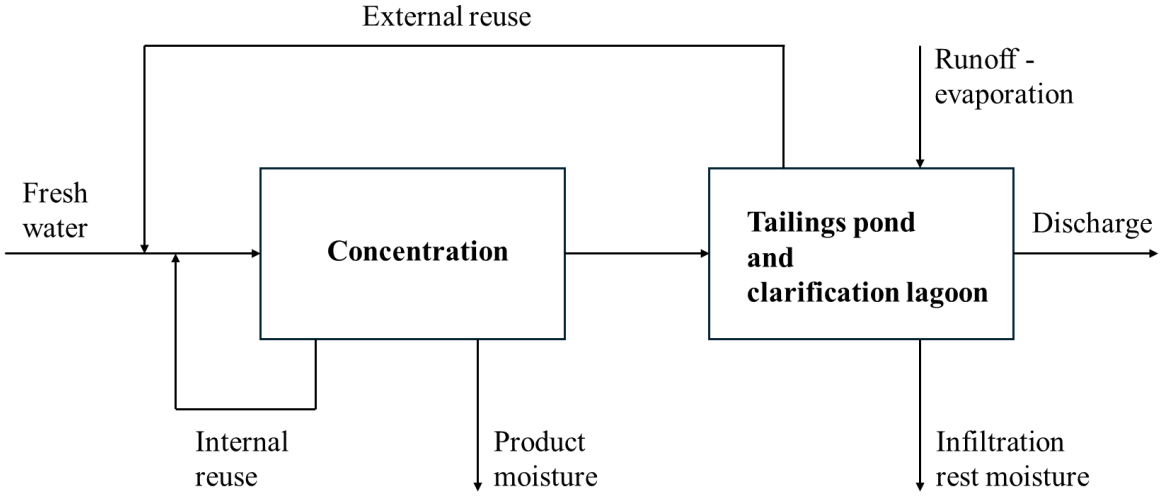

Figure 2.12 - A general waster flowsheet in a typical mineral processing plant. Adapted from Broman et al. [250].

2.6 Adsorbent Materials

2.6.1 Overview

Over the past 70 years, extensive research has been conducted on solid material adsorbents, revealing a wide variety of natural and manufactured adsorbents, each demonstrating different levels of adsorption performance [251]. Ideally, an adsorbent material should have a high internal volume that is accessible to the components being removed from the aqueous media [252]. Adsorption relies on the physical and chemical interactions between the adsorbent material and the contaminants [253]. Various adsorbent materials have been developed and utilized for water treatment, each with unique properties and applications. Common adsorbent materials include activated carbon, zeolites, silica gels, and carbon molecular sieves, among others [254]. Each type of adsorbent possesses distinct characteristics, such as pore size and metallic or non-metallic nature, which play a significant role in the adsorption process [255,256]. The choice of adsorbent material depends on its specific characteristics and the operational conditions in which it will be

used [257]. The selection of adsorbent materials for water treatment depends on the specific contaminants present, the desired treatment efficiency, and economic considerations.

2.6.2 Zeolites in wastewater treatment

Zeolites are widely used in diverse applications, including the removal of heavy metals from wastewater. Zeolites are often considered a low-cost adsorbent for heavy metal remediation due to limitations and high cost of other popular adsorbents such as activated carbon, alumina, and silica [13,258]. They have unique ion exchange and adsorption properties, high porosity and thermal stability and as such are highly suitable for water treatment processes [259-261].

Zeolites are crystalline aluminosilicates that possess unique physicochemical properties, such as cation exchange capacity, large surface area, molecular sieving, catalysis, and sorption [22,262-264] and have diverse applications as commercial adsorbents and catalysts [264-266]. Natural zeolites are porous, hydrated aluminosilicate minerals that are formed hydrothermally [22,267]. Despite their unique properties, the potential of natural zeolites is constrained by the limitations posed by their microstructures and surface chemistry [268,269]. However, synthesized zeolites can be designed to have a specific composition, structure, and properties [270-273]. All this makes synthetic zeolites a compelling material for water remediation from heavy metal ions.

Zeolites, their synthesis, and use in water treatment will be described in depth in Chapter 3.

2.7 Summary

This literature review chapter is a comprehensive examination of various aspects related to water pollution and wastewater management, focusing particularly on the remediation of heavy metals. An in-depth overview is provided on various water treatment technologies, including photocatalysis, flotation, ion exchange, and adsorption, among others. Special attention is given to the mining industry wastewater contaminated with heavy metals. The review investigates the use of various existing adsorbent materials for their efficiency of the removal of Cu, Ni, Zn and Pb ions from single ions solutions. Additionally, the review identified a gap in the existing research, noting that no studies have investigated the adsorption of the particular mixed metal ions system (Cu, Ni, Zn, Pb) by adsorption method.

The chapter further explores the concept of the circular economy of water, emphasizing the importance of sustainable water management practices. It gives a brief overview of existing adsorbent materials and emphasize zeolites as a promising material for heavy metals removal from wastewater.

In conclusion, this chapter highlighting the need for effective solutions to address the removal of mixed heavy metal ions from wastewater. The use of zeolite as an adsorbent in this work is motivated based on its promising potential and sustainability, aiming to contribute valuable insights and advancements in the field of wastewater remediation.

Chapter 3
Zeolites

3.1 Overview

This chapter focuses on zeolites synthesis from coal fly ash (CFA) - the industrial by-product of coal combustion in thermal power plants and their applications in wastewater treatment for the extraction of heavy metal ions. Due to their toxicity and carcinogenic properties, heavy metal ions are among the most dangerous pollutants, posing an increasing threat to humans and other living organisms [274]. This chapter of the thesis covers recent scientific literature, focused on using CFA-derived zeolites to remove Ni, Hg, Mn, Cu, Zn, Cd, Pb, Cr, and Co from aqueous solutions. The results described in many papers cited in this chapter show CFA zeolite as promising adsorbent for industrial wastewater treatment operations. Furthermore, the large variety of possible synthetic zeolites provides a route for energy-efficient, pollutant-specific remediation of industrial heavy metals.

3.2 Zeolites

3.2.1 The History of Zeolites

The knowledge of zeolites dates from 1756 when they were first mentioned by Swedish mineralogist Axel Fredrik Cronstedt [275]. Zeolite research progressed for centuries, and by the mid-1930s, researchers had published the ion exchange, adsorption, molecular sieve, and structural properties of zeolite minerals [276]. The next big step was when Cambridge University chemist Richard Barrer began his work with zeolite adsorption and synthesis in the mid-1930s to 1940s [276]. Barrer presented the first classification of zeolites in 1945 based on their molecular size [277] and the first definitive technique for the synthesis of zeolites in 1948 [278]. His pioneering work in adsorption and synthesis began the era of synthetic zeolites [276,279]. Currently, 256 natural and synthetic zeolite framework types are present in the database of zeolite structures by the International Zeolite Association (IZA) [280].

Zeolites possess strong mechanical properties, thermal stability and high sorption capacity. Additionally, they may slightly adjust the pH of a soil or aqueous system [281]. Due to their catalytic properties, zeolites are widely used in the field of heterogeneous catalysis [282], as essential catalysts [263]. Zeolites are also used in many industrial processes and play a role in many large scale industrial applications [263]. Other zeolite applications are ion exchange, separation, adsorption, host/guest chemistry, microelectronic devices, optics, medicine, and membranes [263,283,284]. Though zeolites' primary use is in catalytic processes, zeolites are promising materials for sustainable development and energy conservation [263,282]. Additionally, natural and modified zeolites are low-cost due to their high availability in many parts of the world and are environmentally safe to use [281].

3.2.2 Zeolite Types

Zeolites are made of a framework of $[SiO_4]^{4-}$ and $[AlO_4]^{5-}$ tetrahedral linked at the corners by shared oxygen atoms that form a three-dimensional network with numerous voids and open spaces [285-287]. These voids are the source of many unique zeolite properties, including the selectivity of molecules in adsorption process, and catalytic properties [288].

Ideal aluminosilicate zeolites are characterized as crystallised solids with a three-dimensional and regular framework structure formed by linked TO_4 tetrahedra, where each oxygen being shared between two T elements, with T = Si, Al [289]. An example of TO_4 units building LTA and FAU type zeolite is shown in Figure 3.1.

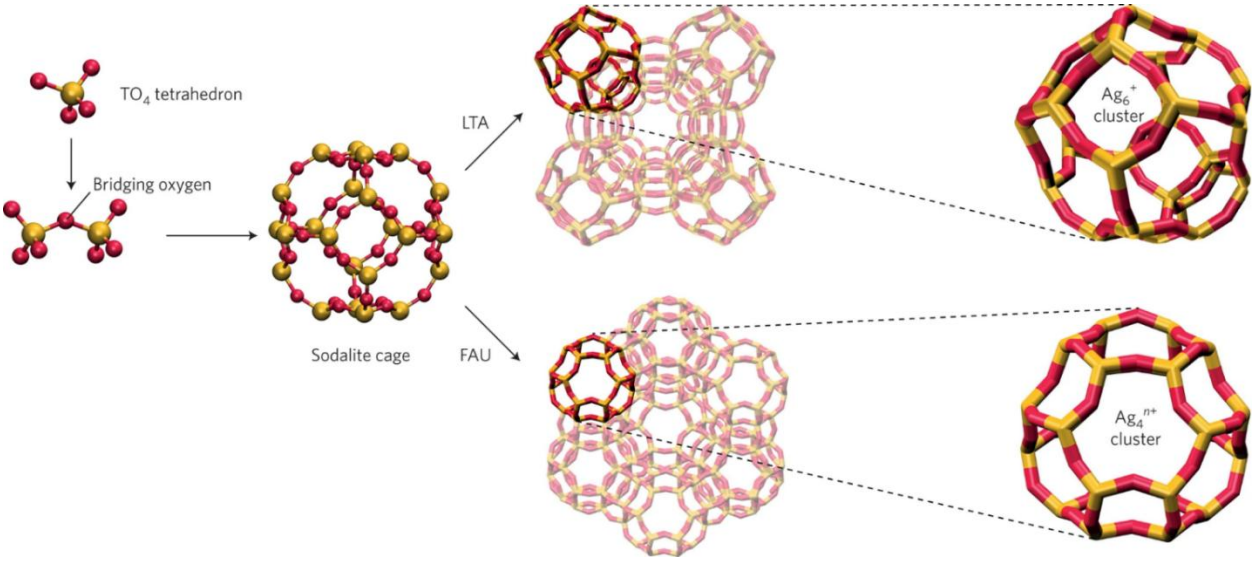

Figure 3.1 - Structures of LTA and FAU zeolites, including their sodalite cages and the way they are connected via the secondary building units (double 4-ring for LTA and double 6-ring for FAU), as well as their respective encapsulated Ag clusters; that is, a Ag_6^+ cluster in LTA and a Ag_4^{n+} cluster in FAU. Reproduced from Weckhuysen [290].

Zeolite frameworks can be broken down into rings of different sizes, which correspond to the pore opening windows. Based on their maximum pore size, zeolites are categorized as small-pore (8-ring), medium-pore (10-ring), large-pore (12-ring), and extra-large-pore zeolites (>12-ring) [291]. The zeolite framework's negative charge is usually compensated by extra-framework mono-or di-valent cations, which can be exchanged for other cations [291]. The pore structure of zeolite depends on their type [292]. Examples of different zeolite structures and their respective pore sizes of commonly used zeolites are given in Figure 3.2 [291].

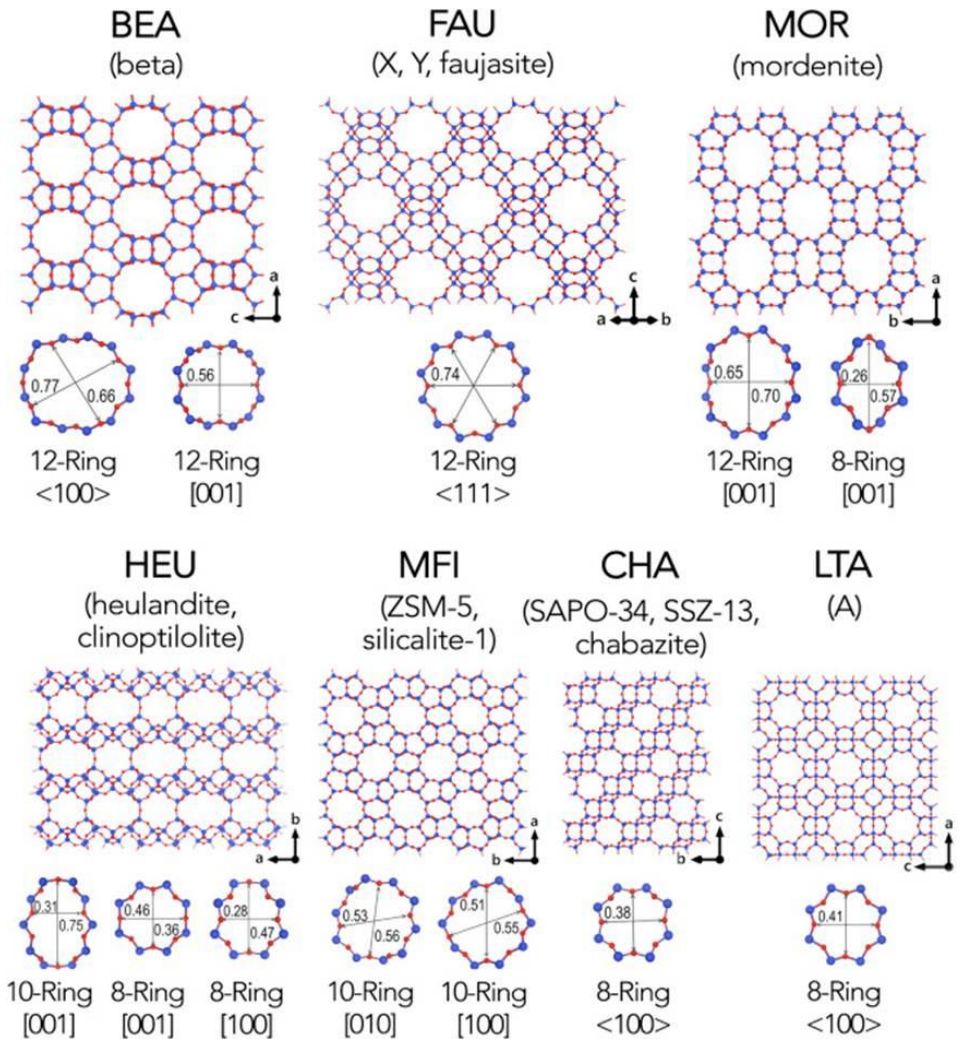

Figure 3.2 - A selection of widely used Zeolite Framework Types, with their International Zeolite Association (IZA) three-letter code (in bold). Examples of zeolites in each category, pore size (in nm), and direction are given. The ball-stick models represent T atoms with blue spheres and red spheres represent oxygen atoms. Reproduced from Li et al. [291]. Data accessed July 2024.

3.2.2.1 Natural Zeolites

The regular formula of natural zeolites is $M_{x/n}[(AlO_2)_x \cdot (SiO_2)_y] \cdot wH_2O$ [293] where M is an alkali or alkaline-earth cation, *n* is the cation charge, *w* is the number of water molecules per unit cell, *x* and *y* comprise the total number of tetrahedra per unit cell; the ratio *y*/*x* usually has values ranging from 1 to ∞ [294,295].

Natural zeolites are porous, hydrated aluminosilicate minerals [296]. They form hydrothermally when hot water reacts with volcanic ash or lava [267]. These materials possess unique physicochemical properties, such as cation exchange capacity, large surface area, molecular sieving, catalysis, and sorption [297-300]. Currently, there are more than 45 natural zeolite types known [301], with the more common forms being chabazite, erionite, mordenite, and clinoptilolite [276,302].

Natural zeolites' unique physical and chemical properties make them useful in a wide range of applications including wastewater treatment [303], agriculture [304], fertilisers [305], aquaculture [304], animal health [306], animal nourishment [307], gas separation [308,309], solar refrigeration [309], gas cleaning [310], deodorisation [296], solid electrolytes [311], construction materials [312], and cleanup of radioactive wastes [303,313]. Natural zeolites used for environmental applications have received more attention from researchers due to their relative low cost [281], unique properties and broad worldwide occurrence [296]. In 2020 the worldwide mine production of zeolite was 1.1 million tons according to the United States Geological Survey (USGS) [314].

Although natural zeolites' features make them useful for a wide variety of purposes, their applications are limited by their microstructures and surface chemistry [269,293]. It is possible to control zeolite porosity, surface chemistry, and structure by various modification methods [269], including physical and chemical modification [269,293,315]. Natural and modified zeolites' sorption capacity cannot compete with synthetic zeolites with designed composition, structure, and properties [315].

The focus of this overview is on synthetic rather than natural or modified zeolites. For a detailed description of natural zeolites' structures, physicochemical properties, and uses, readers are referred to Wang et al. [296]. For an in depth review on modified zeolites, readers are referred to Kuhl et al. [293], Shi et al. [269] and Karge et al. [316].

3.2.2.2 Synthetic Zeolites

The broad range of zeolite applications results from the various morphologies, pore sizes, and channel types [317,318]. As such, there is value in developing synthetic approaches to control crystal size and zeolite morphology [318,319]. In laboratory conditions, it is possible to emulate the natural

process to form a zeolite [24]. Furthermore, zeolites can be synthesised with desired chemical properties and pore size [24]. There are multiple methods for zeolite synthesis [320], a selection of which will be covered in Section 3.3 of this chapter.

Among the most popular types of zeolites, are Zeolite A, Zeolite X,Y and ZSM Zeolite types [321]. Representative zeolite frameworks of zeolite A, zeolite Y, zeolite L and ZSM-5 zeolite can be seen in Figure 3.3.

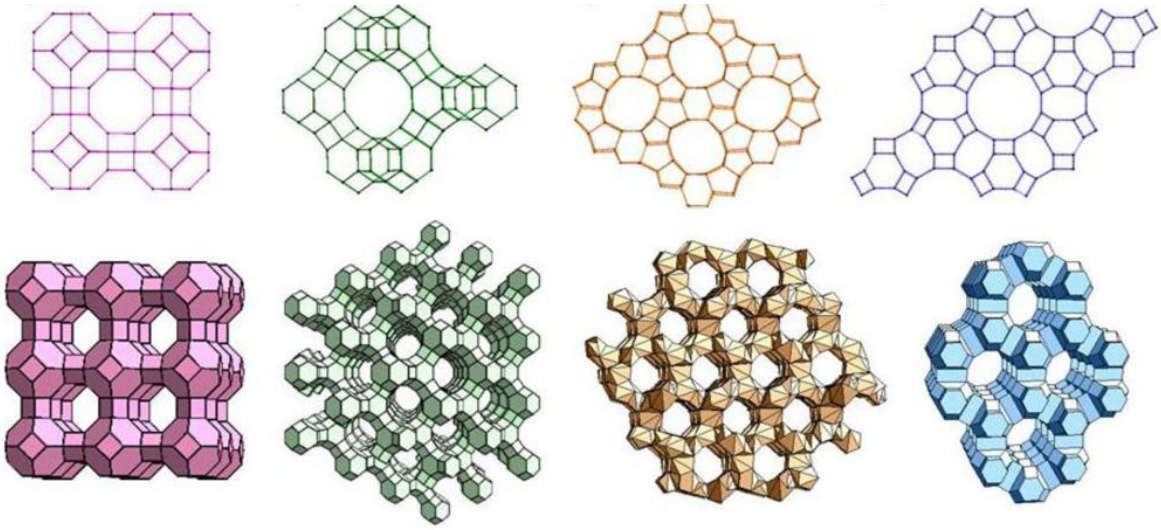

(a) (b) (c) (d)

Figure 3.3 - Representative zeolite frameworks, (with pore openings). (a) zeolite A (3D, 4.2 Å); (b) zeolite Y (3D, 7.4 Å); (c) Zeolite L (1D, 7.1 Å); (d) ZSM-5 (silicalite) (2D, 5.3 × 5.6 Å, 5.1 × 5.5 Å) D—dimensions of channel system. Reproduced from Zheng et al. [322]

In this work, synthesized zeolites belong to type A zeolite. Zeolite A is a synthetic zeolite, also referred to as Linde Type A (LTA), zeolite 4A (due to the 4 Å pore size), or zeolite Na-A (due to the counterbalancing Na^+) [18,323,324]. Zeolite A has a cubic structure and its typical chemical formula would be [321]:

$$| Na_{12} (H_2O)_{27} | [Al_{12} Si_{12} O_{48}] \quad 3.1$$

Equation 3.1 can be expanded to include information about the pore structure:

$$|Na_{12} (H_2O)_{27} | [Al_{12} Si_{12} O_{48}]_h\{3 [4^6]\}_p\{0 [4^6 6^8] / 3 [4^{12} 6^8 8^6] <100> (0.41)\} \quad 3.2$$

This emphasizes that the zeolite structure is three-dimensional, constructed by linking double 4-rings as composite building units. The pore description reveals the presence of sodalite cages and a three-dimensional channel system containing α-cavities. The channels run parallel to the [100] directions ([100], [010], and [001]), with an effective width of 0.41 nm [325]. The described structure can be seen in Figure 3.4.

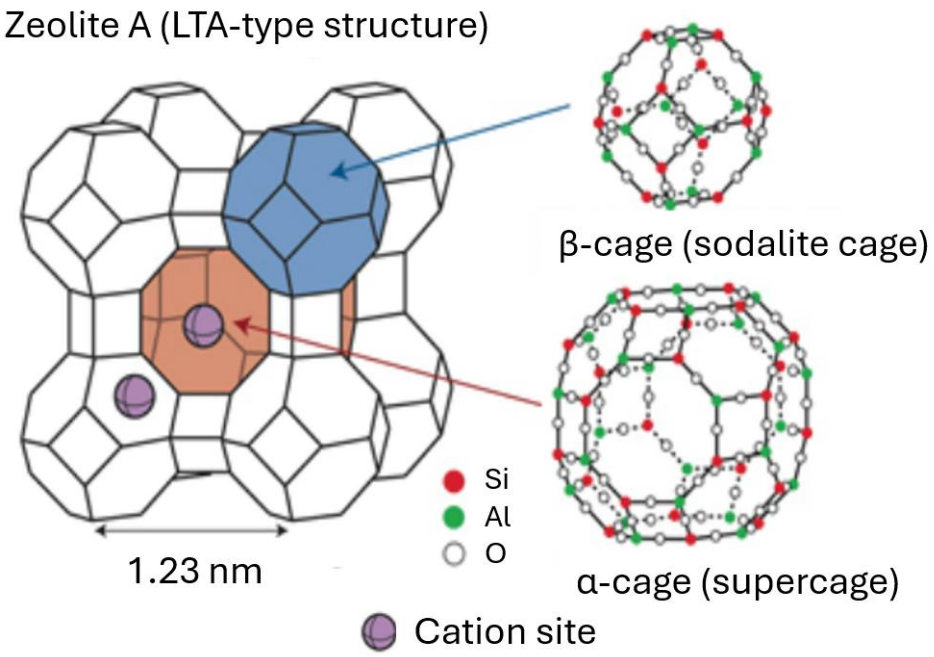

Figure 3.4 - Features of the pores in zeolite A (LTA): the sodalite cage ($[4^6 6^8]$), the *a*-cavity ($[4^{12} 6^8 8^6]$), the 3-dimensional channel system, and the 8-ring defining the 0.41nm effective channel width. Adapted from Petrov and Michalev [321].

All synthesis reactions require appropriate equipment, clean substrates and energy, all of which affect the economics and use of synthetic zeolites versus natural zeolites [24]. Despite this, the variety of zeolite-dependent processes is high, leading many researchers to search for sustainable, less expensive, and cleaner synthetic zeolites [16,296]. One of the most popular uses for synthetic zeolites is heterogeneous catalysis in various traditional and emerging catalytic processes [326]. Similarly, synthetic zeolites are also used for manufacturing membranes to process radioactive solutions [327] and the promotion of direct gasoline synthesis from syngas [328].

Environmental aspects of production currently take centre stage, leading to a trend for using natural or waste raw materials for zeolite synthesis [24].

3.3 Zeolite Synthesis

For zeolite synthesis a source of Si and Al is required [329]. The synthesis process often utilises one of the following methods: hydrothermal [330], solvothermal [331,332] or ionothermal [333,334]. For all of these processes, there are three necessary steps for zeolite formation [335]: supersaturation, nucleation, and crystal growth [316,336]. For a better understanding of the underlying mechanisms of zeolite formation, the concept of crystallization and nucleation theory are discussed in Section 3.3.1.

3.3.1 Nucleation theory and crystal growth

Crystallization from solution typically follows sequential steps: nucleation dictated by the solution's composition, followed by the growth of nuclei to larger sizes through the incorporation of particles from the solution [337-339].

Nucleation is a critical initial step in the formation of crystals from a solution serving as the precursor to the growth phase of crystallization [340]. The theoretical framework for nucleation is often described by Classical Nucleation Theory (CNT) first developed by Volmer and Weber [341], which posits that the formation of an aggregate of atoms or molecules, or critical nucleus, requires overcoming an energy barrier [342,343]. The nucleation process can be categorized into homogeneous and heterogeneous nucleation [344-346]. Homogeneous nucleation occurs uniformly throughout the parent phase, typically in highly supersaturated solutions where no preferential nucleation sites exist. Heterogeneous nucleation occurs at interfaces such as beaker walls, impurities, or pre-existing surfaces, often requiring lower supersaturation levels due to the reduced energy barrier for nucleation at these sites [346-348].

Crystallization involves the incorporation of molecules or ions into the expanding crystal lattice. This process is influenced by multiple factors, such as diffusion, temperature, and supersaturation [347,349]. The interaction between nucleation and growth affects the final size, morphology, and purity of the crystals [349,350].

Zeolites, as aluminosilicate minerals, exhibit a well-defined crystalline structure that imparts its unique properties such as adsorption or ion-exchange [351]. The crystallization of zeolites involves a series of complex hydrothermal processes, typically starting with the preparation of a gel containing sources of silica, alumina, alkali, and water. The gel is then subjected to elevated temperatures and pressures, promoting nucleation and subsequent zeolite's crystal growth [19,330,347].

Generalised mechanism for zeolite synthesis are summarized by Cundy and Cox [352] as a phase transition that occurs when a critical volume of a semi-ordered gel network transforms into a sufficiently well-ordered structure, creating a viable growth center from which the crystal lattice can expand. This is shown schematically in Figure 3.5.

Nucleation does not start immediately after mixing the necessary reagents for zeolite synthesis. There is a resting period described by Equation 3.3:

$$\tau = t_r + t_n + t_g \qquad 3.3$$

where τ is the nucleation induction period, t_r is the equilibration time for reagents to reach temperature and silicate and aluminate ion distribution, t_n is time taken for a stable nucleus to form, and t_g is time taken for said nucleus to grow to a detectable size [353].

However, a review of the literature on the nucleation process of type A zeolite, which is the focus of this work, reveals disagreement regarding the details of the nucleation process [352].

Crystal growth in zeolites is influenced by various factors, including the chemical composition of the gel, temperature, and time [354]. In zeolite synthesis, controlling the crystal size and morphology is crucial for optimizing their application-specific properties [355], thus understanding the nucleation and crystallization behavior of zeolites is crucial for tailoring their properties for specific applications [352]. Factors, such as temperature, pressure, chemical composition and ratio of reagents, equilibration period and others can affect the zeolite synthesis process [353]. For example, finer particle size in the final product is achieved when a large number of nuclei are present in the solution before crystal growth begins [352,356]. To increase crystallization rate, temperature should be increased, as higher temperatures accelerate crystal growth [18,357]. At the same time, the nucleation rate is inversely proportional to temperature [357]. Additionally, at high

temperature, dissolution of CFA is better [356,358]. These factors are discussed further in the next section.

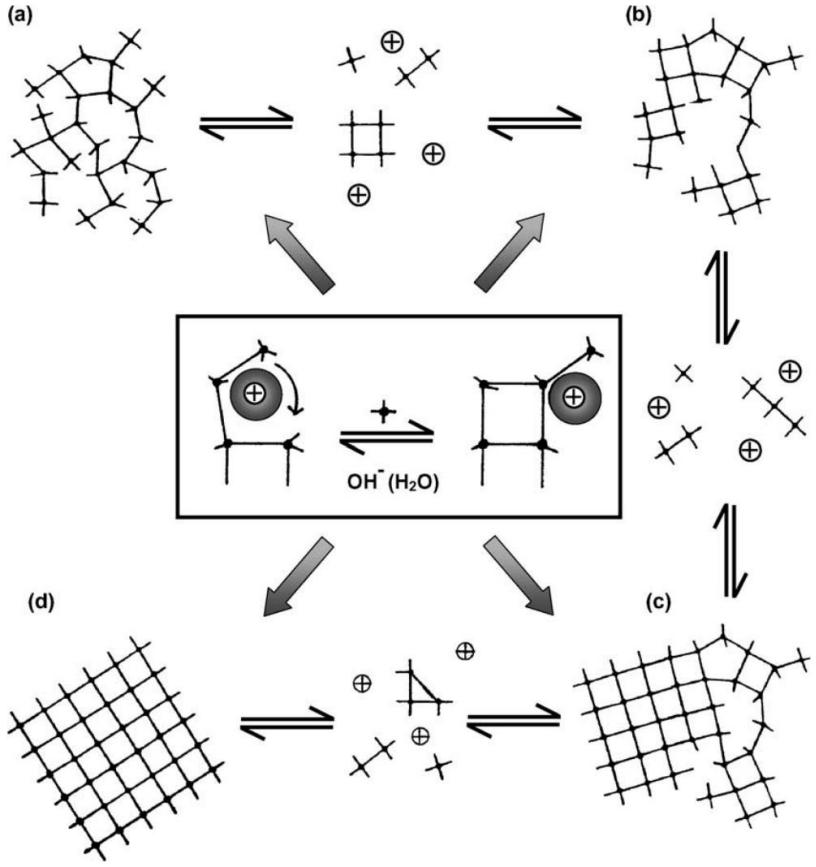

Figure 3.5 - A generalised mechanism for zeolite synthesis. A fragment or domain of amorphous material (a) equilibrates with solution species (anions and cations) to develop elements of local order (b). In due course, the equilibration process leads to an area of sufficient order for a periodic structure to become established—i.e. nucleation has occurred (c). The same equilibration reactions (Si,Al-O-Si,Al bond-making and bondbreaking) then allow the nascent crystal to grow and the amorphous areas to dissolve (d). The self-assembly process is mediated by the associated solvated cations, which act as coordination centres (templates) for the construction of the framework (central insert). These transformations most usually take place via a bulk solution phase, but may occur within a solvated layer at the surface of a "dry" solid (apparent solid-phase transformation). Reproduced from Cundy and Cox [352].

3.3.2 Zeolite synthesis methods

Hydrothermal synthesis is one of the most common approaches for zeolite synthesis [330,359]. For a review of developments in hydrothermal chemistry from 1845 to 1937, readers are referred to Rabenau et al. [360]. For a review of zeolite hydrothermal synthesis in the second half of the twentieth century, see Cundy and Cox [352]. It involves heating aqueous solutions of silica and alumina in an alkaline environment, commonly in sealed vessels to create autogenous pressure as the temperature rises. Structure-directing templates such as organic molecules and specific cations can also be included to control which form of zeolite is produced [335].

The zeolite crystal morphology produced using the hydrothermal method depends on [18,361-363]:

-the pH of the reaction mixture;

-process temperature and pressure;

-equilibration period and reaction time;

-reaction mixture composition, including structure-directing cations;

-any pretreatment applied.

Cundy and Cox [352] proposed a mechanism describing zeolite synthesis, which is currently the accepted model for these reactions. In brief, the model describes the equilibrium systems between an amorphous gel phase and the alkaline solution, which are conjugated to the ordered phase, the zeolite. The authors provide a detailed thermodynamic and kinetic treatment of the various reactions involved in zeolite synthesis, summarised as [352]:

-amorphous material reaches equilibrium with anions and cations in solution

-a small area of local order forms (nucleation)

-this area of local order grows consuming anions and cations from solution

-the amorphous phase and solution maintain equilibrium, thus dissolving the amorphous phase.

Based on this model, the main parameters which control the synthesis process are temperature, alkalinity, Si/Al ratio, cation content, and time [359]. Additionally, the model gives a quantitative

description of the effect of temperature on Al–Si dissolution and reaction rate. Finally, the model points at a strong relationship between solution alkalinity and nucleation rate. Ostwald's rule of successive transformations describes how the early forming and potentially meta-stable phases (such as zeolites A, X, or P) can be replaced by more stable structures (such as sodalite) as time progresses [23,352]. This is especially important in more alkaline systems where the increased hydroxide concentration accelerates the dissolution of meta-stable zeolites [330,364]. For a detailed view on zeolite frameworks and their properties, readers are referred to the International Zeolite Association (IZA) [280]. For a detailed synopsis of hydrothermal technology, including verified protocols for acquiring specific zeolite frameworks, see Byrappa and Yoshimura [365].

Research on zeolite synthesis from fly ash is rapidly gaining momentum due to the environmental benefits of redirecting this abundant waste material [288]. The remainder of this chapter will focus on zeolites generated from coal fly ash.

3.3.3 Coal fly ash (CFA)

Coal has been used as a fuel since at least ancient Greek and Roman times [288]. Coal was formed millions of years ago from deposited vegetable matter that over time has been transformed by geological processes to a carbon-rich coal [288,366]. Coal is currently the most widely distributed fossil fuel worldwide and is used by many countries to produce electricity [32,367]. The industrial combustion by-product of pulverised coal in coal-fired power stations is called coal fly ash (CFA) [303], produced at 1200–1700°C from the various inorganic and organic constituents of the feed coal and generated today in large quantities [33,34]. Consequently, CFA is a mineral waste and recognised as an environmental pollutant and a waste product [34].

Of relevant note is the UN Climate Change Conference (UKCOP26) which was held November 2021. During UKCOP26 the reduction of global coal production by 2040 was proposed [368]. However, some of the world's biggest coal-dependent countries, including India, China and the USA, did not support this statement. As such, CFA is expected to be a relevant environmental pollutant for decades to come, adding to the already present billions of tons of stockpiled fly ash [36].

CFA comprises the following minerals: quartz, mullite, hematite and magnetite, carbon, and a prevalent phase of amorphous aluminosilicate [369,370]. Although these constituents are common to CFAs of all types, CFA chemistry is determined by the type of coal used [34]. Thus, more than 300 individual minerals and 188 mineral groups have been identified in different CFAs [371], and some certain critical elements such as rare earth elements (REE) [372-374]. Approximately 750 million tonnes of CFA is generated globally per year [34], and this number continues to increase with the growth in power demand [375]. CFA finds use in various applications. The most significant is in cement and concrete manufacturing, due to the considerable SiO_2 and Al_2O_3 content and its pozzolanic properties [303,376]. For a review of CFA applications in the construction industry, including cement and concrete production, readers are referred to Kelechi et al. [377]. However, this application is limited to the demand for building materials [378]. For a detailed review of CFA used in the removal of both inorganic and organic pollutants, including heavy metals, dyes, pesticides, pharmaceuticals wastes and other pollutants readers are referred to a review paper by Singh et al. [379]. Additionally, Mushtaq et al. [380] looked at the potential applications of CFA as a photocatalyst, Fenton catalyst, membrane filter, and adsorbent in wastewater treatment.

CFA's use has significant economic and environmental implications and has become an increasing concern [381,382]. This massive amount of CFA industrial waste could cause significant environmental, ecological problems if not appropriately remediated [383] and may cause health issues [375], including chronic bronchitis, asthma, premature death, and lung cancer [359]. The forecast predicts power generation capacity to double in the next 30 years [384]. Even though many countries are moving away from using fossil fuels for energy, the historical volume of CFA and ash ponds are still an issue and can cause severe environmental problems, especially groundwater pollution [385].

Due to the high costs associated with CFA disposal, researchers have been investigating various promising methods to utilize CFA, including the production of new materials, thus reducing the use of natural resources [386]. The glass phase in CFA exhibits high solubility in alkaline solutions making it particularly well-suited for zeolite synthesis [39,40,387]. Zeolite synthesis has received a lot of interest as they may be synthesised from CFA using a relatively cheap and fast conversion process [34,303,381,388]. This topic is further discussed in Section 3.3.4. For a detailed breakdown

of CFA production and utilisation by country as of 2019, see Gollakota et al. [389] with the production and utilisation of fly ash by a selection of countries being given in Figure 3.6 [389].

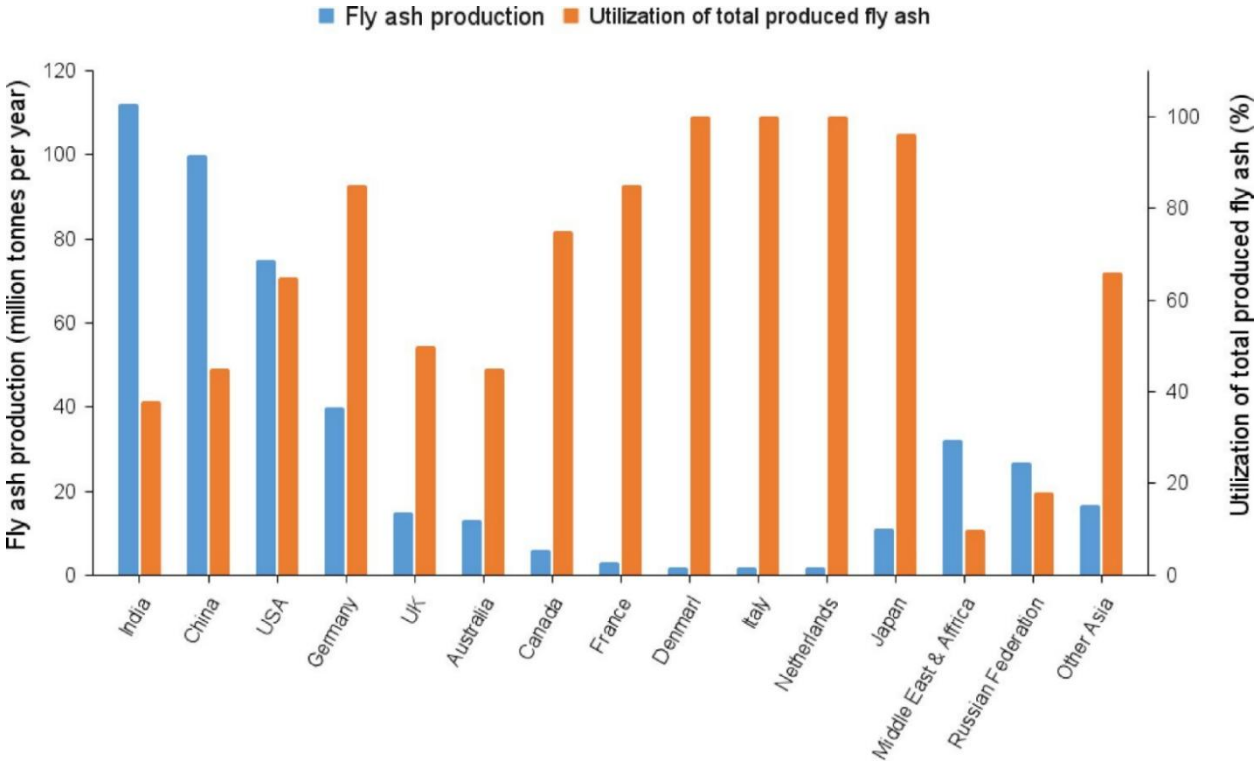

Figure 3.6 - Fly ash production (million tonnes/year) and the utilisation of the produced fly ash for different countries, adapted from Gollakota et al. [389], data accessed in 2019.

3.3.4 Zeolite synthesis from CFA

Since the pioneering work by Holler and Wirsching [390], many researchers have synthesised different types of zeolites from fly ash [303]. Numerous methods have been proposed [391], varying the process by employing different alkaline solutions, alkaline agents' molarity, solution/solid ratio, temperature, time of reaction, pressure, and incubation type [33]. A few examples of zeolites synthesised from CFA include: Na–P1 [392], zeolite A [104,393], zeolite X [394,395] and zeolite ZSM-5 [396]. One major issue of zeolite synthesis from CFA is the large volume of potentially toxic coal-derived substances [104,397,398]. Toxicity in this instance is essentially of two forms.

One form is due to the presence of heavy metals (Ni, Cd, Sb, As, Cr, Pb, etc.) generally found in fly ash. These metals do not degrade in biological systems and accumulate [399].

A number of methods are being proposed for extracting heavy metals from CFA. For example, Sahoo et al. [400] reviewed several hydrometallurgical methods developed for the recovery of metals from CFA. Similarly, Weibel et al. [401] investigated the extraction of heavy metals using hydrochloric acid and sodium chloride solution. Additionally, Leelarungroj et al. [402] looked into leaching mechanisms of As, Cr, Pb, and Zn from cement and fly ash stabilised soils. Readers are referred to Meer and Nazir [403] for a more thorough review of the methods used to remove heavy metals from fly ash, including leaching, biological processes, and other techniques.

Another form of toxicity is a result of the fly ash's particle size (3–5 μm). Particles of this size can reach the pulmonary region of the human lungs and embed into them. Without a mechanism to clear these particles, they accumulate and act as cumulative poisons [404]. Furthermore, any submicron particles can penetrate deeper into the lungs and deposit on alveolar walls. Due to the high surface area in alveoli, metals can efficiently transfer to the blood plasma. Finally, the remaining particles (40–73% by mass), being mostly silica, may cause silicosis, a form of pulmonary fibrosis [404].

As previously mentioned, CFA can be used as a feed stock in a range of applications, including the construction industry and wastewater treatment. The functionality of CFA in these applications can be improved and diversified through beneficiation of CFA into five streams: cenospheres, carbon concentrate, magnetic concentrate, fine products and coarse products [329]. Cenospheres are hollow ceramic spheres with a relative density <1 formed during the combustion process. These have applications as low-density fillers, and as a substrate for value added products. The carbon concentrate can be used as a high surface area substrate or adsorbent with lower cost and performance than activated carbon or reused as fuel [353]. The magnetic fraction can be used where functional products with magnetic properties are desired, or as a filler, especially where high density or electromagnetic shielding properties are required. This fraction is also enriched in trace elements and comprises finer particles. The remaining material can be screened to produce a fine and coarse product. The coarse material, rich in Al and Si, with a reduced concentration of other metals, can be used as an inert aggregate or filler and is a prime candidate for zeolite

synthesis [353]. Numerous researchers have examined the use of CFA for zeolite synthesis since it is rich in crystalline aluminosilicates [405].

In large-scale synthetic zeolite production, common feedstocks include silica gel, sodium hydroxide (NaOH), aluminum salts, clay minerals, silicate group minerals, and fly ash [18,353,406,407]. The amorphous nature of the aluminosilicate glass that is prevalent in CFA and is the most readily soluble the makes it particularly suitable for zeolite synthesis [353,408,409]. During the synthesis process, CFA is partially dissolved forming a rich aluminum and silicon solution, from which zeolites can crystallize [353].

Zeolites can be synthesised under various conditions; however, the most widely used zeolite synthesis methods from fly ash are the hydrothermal and the fusion methods [33,410]. These two methods can be combined with microwave-assisted reactions to further control the reaction rate and zeolite morphology. Studies of zeolite synthesis with microwave-assisted heating showed significantly shorter synthesis times compared to conventional heating [378,411]. The control of experimental parameters and increased rate of formation afforded by microwave-assisted heating led to the development of various zeolites for extracting heavy metals from water. For example, Mishra and Tiwari [412] compared the adsorption of Cu^{2+}, Co^{2+}, and Ni^{2+} to fresh CFA. They found that the synthetic zeolite had a higher capacity than fly ash – the source material. Similarly, Hui et al. [104] investigated the performance and selectivity sequence of mixed heavy metal ions in an aqueous solution. This study compared zeolite A prepared from fly ash to commercial zeolite A, and residual products recycled from fly ash. They found that the Langmuir isotherm well described the equilibrium data and showed the affinity order: $Cu^{2+} > Cr^{3+} > Zn^{2+} > Co^{2+} > Ni^{2+}$.

In conjunction with the development of synthetic methods for making zeolites, research has been carried out on the potential applications of zeolites synthesised from fly ash [303]. The Al(III)/Si(IV) ratio in zeolite structure accounts for the high cation exchange capacity (CEC) of some of these zeolites, including NaP1, 4A, X, KM, F, chabazite, herschellite, and faujasite [303]. The use of these materials as molecular sieves for gas purification was investigated by Querol et al. [413] and Srinivasan et al. [414].

In contrast with these hydrothermal methods, Park et al. [415] developed a technique of thermally treating CFA with a base and a salt. The cooled products were crushed and washed to remove

unreacted bases and salts. The authors suggest the structure-directing nature of the chosen salts play a significant role in the zeolites formed, as indicated by the predominance of cancrinite produced by a NaOH-KNO_3 process, compared to sodalite in a NaOH-$NaNO_3$ process. The molten salt method is limited by high temperature requirements, long activation periods, and a low selectivity for high CEC zeolites [34]. The method has not been widely investigated by other authors. For further information, readers are referred to work on dry or molten-salt conversion by Berkgaut and Singer [392] and Park et al. [415].

The following sections detail recent studies that have utilised the most popular synthesis methods for synthesising zeolites from CFA.

3.3.4.1 Hydrothermal synthesis method

In the late twentieth century, a variety of hydrothermal activation methods for synthesising different zeolites from coal fly ash were proposed [288,378,408,416].

Most of the proposed approaches control the dissolution of the Al–Si amorphous phase present in the CFA using hot alkaline solutions, mainly NaOH and KOH. Figure 3.7 describes the steps, namely a leaching process, which produces a supersaturated solution from which zeolites can be precipitated (crystallization), following the hydrothermal synthesis routes described in Section 3.3.2.

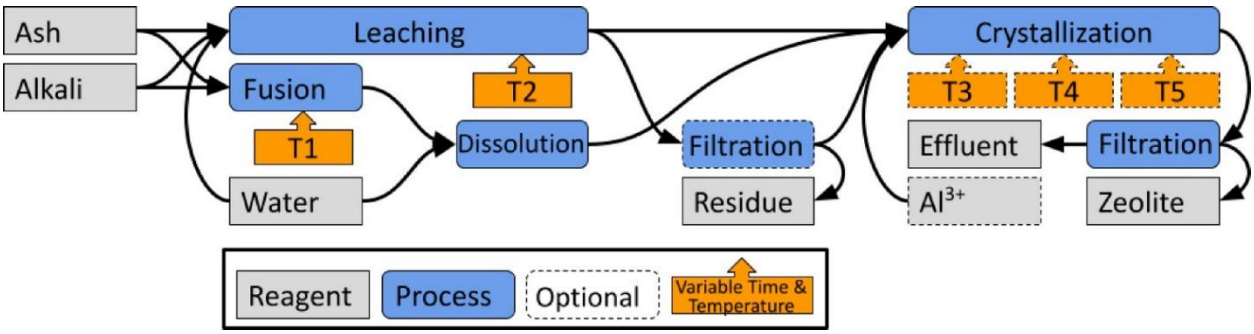

Figure 3.7 - Unit operations in hydrothermal synthesis of zeolites from CFA.

Zeolite synthesis is highly sensitive to initial conditions, such as nucleation rate, source material and activation solution/source material ratio, and leads to significant variations in synthesis results. Blissett et al. [34] showed that up to 13 different zeolite types can be synthesised from the same

CFA sample, by controlling these parameters. In general, they found that high activation temperatures (Figure 3.7 T2) and alkaline conditions (200°C and 5 M NaOH) led to low CEC zeolite formation. Conversely, lower temperature and alkalinity (<150°C and 0.5–3 M) led to the formation of high CEC zeolites [34].

This distinction between low and high-temperature synthesis leads to process economics issues, as the low CEC morphologies are prevalent when the rate is increased by heating. As such, an important issue for commercial zeolite production is how to speed up the production of the desired species [34]. Therefore, a faster synthesis process is preferable, one that sidesteps the expensive, high-temperature process, limiting the achievable morphologies [104,417]. However, Hui and Chao [356] successfully synthesised zeolite A by heating the crystallization solution to 90°C to encourage nucleation (T3 in Figure 3.7), which was followed by a temperature increase to 95°C (T4 in Figure 3.7) to promote crystal growth [359]. Other authors used microwave-assisted heating to promote crystal growth after a conventionally heated nucleation period [418]. This process produced zeolite A faster than a conventionally heated crystallization process [418]. Querol et al. [419] reported using microwave-assisted and conventional methods with similar yields and zeolite types, while the activation time required for microwave-assisted synthesis was significantly reduced: 30 min instead of the conventional 24–48 h. Kim and Lee [418] and Tanaka et al. [420] also used microwave-assisted heating, combining it with two-step silica extraction, and reported the production of high-quality zeolite A.

Hydrothermal methods easily dissolve the amorphous Si and Al content of CFA, but crystalline material such as quartz and mullite will not readily dissolve, and will remain as an impurity in the finished zeolite product [421].

One approach to improve zeolite purity is to filter out undissolved CFA between the dissolution and crystallization steps. Hollman et al. [422] proposed a two-stage hydrothermal method. The first step aims to obtain a Si-rich solution by dissolving Si from CFA by dissolution in NaOH. This is then filtered to remove undissolved fly ash, and stop zeolite formation. Thus, in Figure 3.7, the leaching and crystallization steps take place separately. The second step is to adjust the Si:Al molar ratio through the addition of an Al source such as sodium aluminate [423-425]. Zeolite can then be crystallized under static conditions during hydrothermal treatment at <100°C [395,426,427].

For the leaching process, a variety of authors [356,422,428] used 2 M NaOH at 90–100°C, with solids loadings of 40–400 g CFA/L. Kim and Lee [418] investigated 1–5 M NaOH for leaching, followed by filtering, dilution, and adjustment of Si/Al ratio and NaOH concentration prior to crystallization. These experiments were compared to microwave-assisted leaching, which was found to increase the yield of Si and Al in the leachate, from 10 and 10% respectively through hydrothermal extraction to 35 and 20% using microwave-assisted extraction.

These leachates can then be used to crystallize zeolites through hydrothermal methods, with Hollman et al. [422] producing zeolite P, X, and A with sodalite through control of the Si/Al ratio (2:1, 1.8:1, and 1.2:1) and duration of crystallization (48, 48, and 67 h). Fukui et al. [428] altered the Si/Al ratio by adding rice husk ash (RHA) prior to the crystallization step. RHA is rich in Si, and this caused the Si/Al ratio to increase, resulting in the synthesis of phillipsite and sodalite, rather than zeolite A, X, and P which have a significantly higher Al content. Hui and Chao [356] added an aluminium solution to their leachate before ageing it for 30 min at RTP. (Figure 3.7 T3). The solution was heated in two stages, firstly for 1.5 h at 80–90°C (Figure 3.7 T4) to allow nucleation to occur, and then to a higher temperature of 90–95°C (Figure 3.7 T5) to encourage crystal growth and inhibit nucleation. This produced highly crystalline zeolites with a narrow particle distribution using a 30 min ageing step, a 90 min nucleation step at 90°C, and a 60 min crystal growth step at 95°C.

The fusion method was proposed by Shigemoto and Hayashi [429] to improve product purity. This approach's novelty was in introducing an alkaline fusion stage before the conventional zeolite synthesis [421]. In Figure 3.7 this is represented by the Fusion and dissolution steps which replace the leaching step. The main two differences of the fusion method compared to the classical hydrothermal method are:

-mixing and grinding CFA with a solid alkali in a ratio of 1:1.2 before heating to 500–550°C [421,429], for 1–2 h [392] (Figure 3.7 T1);

-grinding or crushing the cooled fusion product, and dissolving in water, distilled water, or seawater [33].

Molina and Poole [421] compared the cation exchange capacities (CEC) of zeolites formed through conventional hydrothermal methods, and alkaline fusion methods at a variety of NaOH:CFA ratios. The authors concluded that the CEC of zeolites produced with an alkaline fusion step were higher than those produced through the hydrothermal method alone. The authors also concluded that the optimum NaOH:CFA ratio was 1.2:1, with lower ratios producing less crystalline zeolite X, and higher ratios producing a mixture of zeolite X and sodalite, or sodalite alone.

After the fusion process, the CFA has been converted to water-soluble species such as sodium aluminosilicate and sodium silicate [324,392,409,430]. This fusion product is broken up and then dissolved. Commonly, this dissolution occurs at room temperature and pressure overnight, or for 12–24 h [392,409,421,430]. In lieu of distilled water, seawater can be used to reduce material and energy costs, reduce consumption of potentially potable water, and to benefit from the presence of NaCl which can aid the crystallisation process [352,431]. Berkgaut and Singer [392] studied the effect of an ageing step, where the solution is kept at room temperature for 12 h prior to hydrothermal crystallization at 100°C. The unaged sample produced zeolite P whilst the aged sample produced zeolite X.

After the dissolution process, zeolite crystallization can be performed using methods similar to the hydrothermal methods described earlier. Work by Belviso et al. [409] showed that the use of seawater as a dissolution medium lowered subsequent temperatures required to crystallize zeolites, and Ca and Mg were sequestered during the crystallization process of zeolite X. This supports the idea that cations perform a structure-directing role during zeolite synthesis.

Izidoro et al. [222] were able to achieve complete conversion of CFA into zeolite A or X by varying the crystallization conditions. Complete conversion was confirmed by the lack of mullite or quartz in XRD analysis, and a lack of other materials in SEM images. During the dissolution process, the authors altered the solid/liquid ratio, and during the crystallization process the authors altered the Si:Al ratio with additional sodium aluminate, and varied the duration of the crystallization process to produce either zeolite X or zeolite A. Zeolite X was produced with a lower solid loading, less additional Al, and longer crystallization time compared to conditions required to produce zeolite A.

In conclusion, the most significant variables in the alkaline fusion method are:

-NaOH:CFA ratio has an optimum value of 1.2:1; other ratios will produce zeolties but the CEC may be lowered.

-Solids loading during the 'dissolution' step will affect the pH of the solution, and concentration of Si and Al.

-Choice of solvent. Using seawater provides NaCl to assist crystallization, and other structure-directing cations.

-Si/Al ratios, temperatures and durations applied during the crystallization phases are relevant here, similar to the hydrothermal method.

Ayele et al. [432], Shigemoto et al. [429], and Kumar et al. [433] investigated the topic of synthesis by fusion. Further improvements on the base method have been proposed by Ozdemir et al. [375], who follow the **A**lkaline **F**usion with the **U**ltrasonic-assisted synthesis **M**ethod (AFUM). This shortened the time required to synthesise zeolite X.

3.4 CFA derived Zeolite Applications in Water Treatment

As mentioned in Chapter 2, heavy metals are considered to be one of the most dangerous groups of pollutants [12] because they are not biodegradable and tend to accumulate in living organisms [434]. Furthermore, conventional wastewater treatment methods might be challenging to apply to heavy metals removal due to their high stability and solubility [434]. Heavy metals pollute the environment through wastewater originating through many sources including metal plating facilities, mining operations, agriculture, fertiliser production, tanneries, batteries, paper industries and pesticides, battery manufacturing, textile printing, and leather industries [12,13].

There are various methods available to reduce heavy metal concentrations in wastewater, including: chemical precipitation [435-437], ion exchange [438,439], photocatalysis [81], electrocoagulation [440,441], electrochemical treatment [442], adsorption [443], membrane filtration [444], reverse osmosis [445,446], bioadsorbents [67,447], coagulation and flocculation [448], flotation [13,397], solvent extraction [398] among others [6,13].

Adsorption is often considered the most effective method due to its high efficiency for removing low but still toxic concentrations heavy metals [12,13,104]. Adsorption provides flexibility in design, high-quality treated effluent; it is reversible, and the adsorbent can afterwards be regenerated [13,105,106].

Zeolites are often considered a low-cost adsorbent for heavy metal remediation due to limitations and high cost of other popular adsorbents such as activated carbon, alumina, and silica [13,258]. Zeolites have unique ion exchange and adsorption properties, high porosity and thermal stability and as such are highly suitable for water treatment processes [259-261].

Furthermore, their net negative charge is balanced by the exchangeable cation, which has been demonstrated with Pb, Cd, Zn, Fe, Cu, and Mn ions [28,449]. These ions are of specific interest due to their detrimental environmental and health impacts [449].

For a review of natural and modified zeolites remediation of various chemical pollutants from water and wastewater, see Wang and Peng [296]. For a review of surfactant modified zeolites used for the removal of heavy metals from water, readers are referred to Jimenez-Castaneda et al. [450], Erdem et al. [451], and Blanchard et al. [452].

As this chapter is aiming at focusing specific heavy metals and their mixtures, the following section will contrast studies on single cation remediation and compare them to mixed-species studies. Publications from the 1990s to 2024 are described, all of which investigated metal ion adsorption onto zeolites synthesised from coal fly ash. The results of these studies are presented in this section and summarised in Appendix B1-B9 for single-ion systems and Appendix B10 for mixed-ion systems.

3.4.1 Nickel

When considering Ni remediation from single cation solutions, He et al. [3] showed that A-type CFA synthesised zeolite can achieve efficiencies of up to 94% removal of Ni^{2+} ions from solution with calculated adsorption capacity of 47 mg/g from 100 mg/L Ni^{2+}. Similarly, Zhang et al. [453] demonstrated that zeolite X can achieve up to 95% nickel removal with a capacity of 16 mg/g.

Sireesha et al. [188] modified CFA with zeolite (FA-Z) and investigated its efficiency in Ni and Cd ions removal from aqueous solutions in both single and mixed-ion system. Thus for Ni^{2+} the maximum adsorption capacity was found to be 61 mg/g and for Cu^{2+} 96 mg/g or 99% and 97%, respectively. The efficiency of FA-Z in removing Ni^{2+} and Cu^{2+} in mixed ion solution and in real effluent was found at ~60% and ~95%, respectively. Furthermore, Sireesha et al. [188] investigated both batch and column systems, and column system was identified as a more sufficient method. They also investigated the desorption of metal ions from the zeolite surface using H_2SO_4.

Other studies focused on mixtures of heavy metal ions, including Ni. These studies have shown that Ni adsorption efficiency is low in the presence of other metal ions. As such, Visa et al. [454] investigated the efficiency of novel zeolitic materials (ZCET40 and ZDs40) synthesised from fly ash for the removal of Cd^{2+}, Ni^{2+}, Cu^{2+}, Zn^{2+}, Pb^{2+} from single and mixed-ions synthetic solutions. It was shown that Ni is poorly adsorbed by both type of zeolites as long as other ions remain in solution due to the competitive mechanisms of heavy metals for the similar adsorption sites on the zeolite.

Similarly, Hui et al. [104] synthesised pure and chamfered-edge type 4A zeolites prepared from CFA, and studied them for the adsorption of mixed metal ions (Co^{2+}, Cr^{3+}, Cu^{2+}, Zn^{2+}, and Ni^{2+}) solutions. The highest equilibrium sorption was obtained for Cu at 50 mg/g, which decreased to 42 mg/g for Cr^{3+}, 31 mg/g for Zn^{2+}, 14 mg/g for Co^{2+}, and 9 mg/g for Ni^{2+}. Similarly, for commercial zeolite 4A, the greatest equilibrium sorption capacity obtained was, in mg/g, 53 (Cu^{2+}), 45 (Cr^{3+}), 32 (Zn^{2+}), 12 (Co^{2+}), and 8 (Ni^{2+}).

Additionally, He et al. [187] studied the maximum adsorption capacities of CFA zeolite prepared using the fusion method. This study worked with single and mixed cations in aqueous solutions focusing on Pb, Cu, Cd, Ni, and Mn ions. It reported that the absolute Ni^{2+} adsorption capacity is 34 mg/g for a single ion system and 16 mg/g in a multi-ion system with an adsorption efficiency of 85 ± 0.5% in a multi-ion system. In this work, it was indicated that the main factor impacting the selectivity adsorption was the hydrolysis constant.

Alvarez-Ayuso et al. [455] investigated the sorption behaviour of natural (clinoptilolite) and synthetic (NaP1) zeolites for Cr^{3+}, Ni^{2+}, Zn^{2+}, Cu^{2+} and Cd^{2+} from wastewater. Maximum adsorption capacities achieved were, in mg/g, 44 (Cr), 20 (Ni), 33 (Zn), 51 (Cu), 51 (Cd) and

4 (Cr), 2 (Ni), 3 (Zn), 6 (Cu), 5 (Cd) for synthetic and natural zeolites, respectively. The sorption capacities shown by the synthetic zeolites were approximately 10 times greater than those shown by natural zeolite also investigated in this study. This could be explained by a higher H^+ exchange capacity and higher cation exchange capacity of synthesised zeolites.

In summary, Ni ions are adsorbed well by multiple zeolite types, although they have reduced removal efficiencies in multi-ion solutions. Some of this effect could be attributed to competition with other species in solution. Furthermore, a significant effect on removal efficiency could be observed due to pH. Consequently, controlling for pH during remediation of multi-ion systems is a significant factor in achieving a given removal efficiency.

3.4.2 Copper

Wang et al. [410] compared zeolite A and zeolite X synthesised from CFA for Cu^{2+} ion removal from a Cu-Zn multi-ion system. In this study, zeolite A showed a maximum adsorption capacity of 38 mg/g for Cu^{2+} and 30 mg/g for Zn^{2+}. For zeolite X, the amount of Cu^{2+} adsorbed was 29, and 22 mg/g for Zn^{2+}.

He et al. [187] established a maximum adsorption capacity for Cu at 56 mg/g from a single-ion solution and 33 mg/g from a Pb, Mn, Ni, Cu, Cd system with an efficiency of $95 \pm 0.7\%$. Additionally, Hui et al. [104] showed that pure and chamfered-edge zeolite 4A prepared from CFA had adsorbed 50 mg/g of Cu^{2+} a multi-species solution containing of Co^{2+}, Cr^{3+}, Cu^{2+}, Zn^{2+}, and Ni^{2+}.

Wang et al. [456] also used CFA derived zeolite for the removal of Cu^{2+}, Pb^{2+} and Cd^{2+} from water. The maximum adsorption capacity shown in this study was 10 mg/g for Cu^{2+}, 1 mg/g for Pb^{2+} and 0.3 mg/g for Cd^{2+}. Thus, the order of selectivity for metal ions in their study was $Cu^{2+} > Pb^{2+} > Cd^{2+}$.

Wu et al. [457] investigated Cu^{2+} and Cd^{2+} adsorption by zeolite synthesised from hydrothermally treated CFA. For each experiment, a set of 50–500 mg/L metal concentration were prepared and 1 g/L of adsorbent was added. The pH was 6.0 ± 0.2 for all solutions. The sorption capacity of the

synthesised zeolite at equilibrium was calculated to be 71 and 83 mg/g for Cu^{2+} and Cd^{2+}, respectively.

Yang et al. [458] compared CFA synthesised zeolite A with CFA synthesised zeolite modified with Fe_3O_4 (MFZ) for Cu removal from water. The adsorption capacity of synthesised zeolites was found to be around 50 mg/g. Similarly, Wang et al. [459] used magnetic zeolite P synthesised from low-grade fly ash for the removal of Cu^{2+} and Pb^{2+} ions from a multi-ion aqueous solution. The saturation adsorption capacity of Cu^{2+} ions by magnetic zeolite P (synthesised from low-grade fly ash with iron oxide) and synthesised non-magnetic zeolite P were 25 and 30 mg/g, respectively. For Pb^{2+} adsorption by the non-magnetic zeolite was higher than the magnetic (28 mg/g and 20 mg/g, respectively). Even though the adsorption capacity of magnetic zeolite was lower than of non-magnetic, the induction of magnetic particles may make recovery of the used zeolite from wastewater easier by leveraging its magnetic properties.

Huiping et al. [460] investigated the ability of zeolite synthesised from CFA to adsorb Cu^{2+} ions. XRD results showed that the synthesised material has basic structural unit of microporous zeolite molecular sieves, and consist of zeolite 4A and zeolite X The maximum adsorption capacity at pH 5 and sorbent dosage of 4 g/L ranged from 69 mg/g at 20°C to 141 mg/g at 50°C.

3.4.3 Zinc

A novel method for metal ion adsorption from sewage using NaP zeolite synthesised from stage-treated CFA was proposed by Zhang et al. [221]. The study investigated the synthesis of NaP, NaP-AMP (2-amino-methyl-propyl alcohol), NaP-PEG (polyethylene glycol), NaP-CyOH (cyclohexanol) zeolites and their use in Zn^{2+} adsorption. NaP, NaP-AMP, NaP-PEG zeolites showed the adsorption capacity and removal of 37 mg/g (91.4%), 39 mg/g (96.8%) 35 mg/g (88%), respectively. NaP-CyOH zeolite showed the highest adsorption capacity of 40 mg/g and the removal of 99.9% due to it having the largest surface area of 80 m^2/g vs 27 m^2/g (NaP zeolite), 29 m^2/g (NaP-AMP zeolite) and 24 m^2/g (NaP-PEG zeolite).

Izidoro et al. [222] investigated zeolites X (ZXJL) and A (ZAJL) synthesised from CFA for Cd^{2+} and Zn^{2+} remediation. The study used several CFA source materials for synthesising the zeolites

and measured their capacity and efficiency both from single and multi-ion systems. The maximum adsorption capacity for Zn^{2+} ions in a single ion solution varied from 156 (ZXJL) to 185 mg/g (ZAJL) and for Cd^{2+} from 205 (ZXJL) to 220 mg/g (ZAJL). For a two ion system, the adsorption capacities for zeolite X ranged from 58 to 70 mg/g for Zn^{2+} and from 60 to 72 mg/g for Cd^{2+}. For zeolite A, the values ranged from 89 to 90 mg/g for Zn^{2+} and from 174 to 195 mg/g for Cd^{2+} ions. Comparing the adsorption results of Cd^{2+} and Zn^{2+} ions between one and two ion solutions indicated that Cd and Zn adsorption percentages were strongly affected by the presence of competitor ions on zeolite X, while zeolite A still reached high adsorption percentages in the presence of the competing ions. In general, Cd^{2+} removal was more affected by the presence of Zn due to the preference for Zn^{2+} ions by the pure zeolites [222].

3.4.4 Lead

He et al. [187] used CFA derived zeolite prepared using the fusion method, achieving capacities of 66 mg/g for Pb in single cation solutions and 45 mg/g in multiple-species solutions of Pb, Cu, Cd, Ni, and Mn ions with an efficiency of 93%.

Jangkorn et al. [228] synthesised Zeolite A from CFA (ZCF) and bagasse fly ash (ZBG) using alkaline fusion method followed by hydrothermal synthesis. Additionally, they investigated adsorption capacity of ZCF and ZBG for Pb ions removal and both showed 100% efficiency. Thus, the maximum adsorption capacity of ZCF was found 556 mg/g at pH 5 while the Pb ion concentration was 200 mg/L.

Kobayashi et al. [234] used a novel K-type zeolite synthesised from CFA for Pb^{2+} adsorption from aqueous solutions. The maximum adsorption capacity of the zeolite they synthesised was 20 mg/g meaning that 76% of Pb ions were removed from a solution with an initial concentration of 50 mg/L. At the same time, the effect of coexisting ions on the adsorption capability of Pb^{2+} was investigated for Mg^{2+}, K^{+}, Ca^{2+}, Ni^{+}, Cu^{2+}, Zn^{2+}, Sr^{2+}, and Cd^{2+} as the components of the two-cation solution. The adsorption capacity of other metal ions was significantly lower than that of Pb^{2+}, meaning that the synthesised K-type FA48 zeolite exhibited selectivity for Pb^{2+} adsorption from the investigated mixed solution. This can be explained by several factors, such as metal ions

difference in charge density and hydrated ion radius, and the accessibility of the active sites of natural FA48 [234], similarly to the results presented in other studies [461,462].

Zeolites synthesised from low-calcium LCZ and high-calcium HCZ fly ash were investigated for the removal of Zn^{2+}, Cu^{2+}, Cd^{2+}, and Pb^{2+} from aqueous solutions by Ji et al. [463]. The maximum adsorption capacities in mg/g obtained for the removal of Zn^{2+}, Cu^{2+}, Cd^{2+}, and Pb^{2+}, were 156 (Zn2+), 198 (Cu), 124 (Cd), and 186 (Pb) mg/g for LCZ and 154 (Zn), 183 (Cu), 119 (Cd), and 192 (Pb) mg/g for HCZ, respectively. This study showed that both low and high calcium coal fly ash have potential as effective adsorbents for the simultaneous removal of Zn^{2+}, Cu^{2+}, Cd^{2+}, and Pb^{2+} from an aqueous solution. However, if selectivity is required, these zeolites are not suitable.

Qiu et al. [464] synthesised zeolites from fly ash for multi-ion heavy metal solutions of Cd, Cu, Mn, Ni, Pb and Zn adsorption using municipal solid waste incineration fly ash by microwave-assisted hydrothermal treatment. The results showed that the adsorption capacity followed the order of Pb > Cu > Zn > Mn ≈ Ni > Cd. It was shown that with an increase in zeolite content, the adsorption of all metal ions improved as well. The highest adsorption capacity shown in this study, in mg/g, was 50 (Pb), 28 (Cu), 20 (Zn), 15 (Mn), 14 (Ni), 11 (Cd).

The adsorption of Cu^{2+}, Pb^{2+}, Zn^{2+}, and Mn^{2+} using zeolites synthesised from Brazilian fly ash was studied by Nascimento et al. [465]. Their results showed that the maximum adsorption capacity of synthesised zeolite was, in mg/g, 195 (Pb), 77 (Cu), 60 (Mn), 59 (Zn). The adsorption increased up to 25 times compared to the original ash. The preferred order observed for adsorption was Pb > Cu > Mn ≥ Zn, meaning that synthesised zeolite is selective for Pb. Based on this study, part of the sorption properties of these ions are due to ion exchange with the zeolite. Specifically, Pb appears to preferentially replace exchangeable cations (mainly sodium and calcium) in the zeolite compared to Cu, Mn and Zn. The zeolite's preference for Pb ions might be attributed to due to its lower dehydration energy and smaller hydrated radius [187,466].

Joseph et al. [467] investigated simultaneous removal of Cd^{2+}, Co^{2+}, Cu^{2+}, Pb^{2+}, and Zn^{2+} ions from aqueous solutions via adsorption onto FAU-type zeolites synthesised from CFA. The results showed that in the presence of competing ions, the FAU zeolite sample CFZ10-68 simultaneously removed heavy metals from aqueous solution in the order $Pb^{2+} > Cu^{2+} > Cd^{2+} > Zn^{2+} > Co^{2+}$. The maximum adsorption capacity was found for Pb^{2+} 110 mg/g and for Co^{2+} 12 mg/g.

Similarly, Bai et al. [468] synthesised X-type zeolite from combination of CFA oil shale ash (OSA) using the alkaline fusion hydrothermal method and investigated its use in water treatment from Cd^{2+}, Cr^{3+}, Cu^{2+}, Pb^{2+}, and Zn^{2+}. The study showed that the removal efficiency of the heavy metals increases with an increase in the amount of added adsorbent. Furthermore, the selectivity sequence was in following order: $Pb^{2+} > Cr^{3+} > Cu^{2+} > Zn^{2+} > Cd^{2+}$ with the maximum adsorption capacity of 112 mg/g (Pb^{2+}), 62 mg/g (Cr^{3+}), 54 mg/g (Cu^{2+}), 45 mg/g (Zn^{2+}) and 38 mg/g (Cd^{2+}). This result agrees with the order of the ionic radius of the metal ions [468].

Koshlak [469] investigated zeolite synthesized from CFA by alkaline fusion method and its applications in removing Ni^{2+}, Cd^{2+} and Pb^{2+}. The maximum adsorption capacity of the investigated zeolite was calculated as 2.68 mmol/g (555.3 mg/g) for Pb, 1.54 mmol/g (90.4 mg/g) for Cs, and 1.3 mmol/g (76.3 mg/g) for Ni.

Lastly, Li et al. [470] used a one-step hydrothermal method to synthesize a zeolite-calcium silicate hydrate composite from CFA with co-activation of $Ca(OH)_2$-NaOH. They investigated the material's adsorption capacities for single ion solutions of Pb^{2+}, Ni^{2+}, Cd^{2+}, Zn^{2+}, Cu^{2+} and Cr^{3+}. The maximum adsorption capacities were respectively found to be 409 mg/g (Pb^{2+}), 222 mg/g (Ni^{2+}), 148 mg/g (Cd^{2+}), 93 mg/g (Zn^{2+}), 101 mg/g (Cu^{2+}) and 157 mg/g (Cr^{3+}) at the pH of 4.5. At the same time, for mixed-ion system, the adsorption capacities were 122 mg/g (Pb^{2+}), 71 mg/g (Cr^{3+}), 34 mg/g (Cu^{2+}), 28 mg/g (Zn^{2+}), 10 mg/g (Cd^{2+}) and 5 mg/g (Ni^{2+}). Thus, the adsorption selectivity order was found as $Pb^{2+} > Cr^{3+} > Cu^{2+} > Zn^{2+} > Cd^{2+} > Ni^{2+}$. Such difference can be explained by the competitive adsorption driven by differences in the metal ions properties, including ionic radius, hydration energy, and charge density.

3.4.5 Cadmium

Li et al. [471] presented a novel microwave assisted digestion, and alkali fusion assisted hydrothermal method for synthesising zeolite from CFA for Cd^{2+} ion remediation. The synthesised zeolite was identified as faujasite and showed an efficiency of 99% and a maximum adsorption capacity of 87 mg/g.

Yao et al. [472] used a one-step synthesis of zeolite from fly ash using the mechanochemical method. Obtained P1 zeolite type was tested for Cd^{2+} removal and the adsorption capacity was found as 131 mg/g at pH= 5.

Remenarova et al. [473] used zeolitic materials ZM1 and ZM3 (synthesised by hydrothermal alternation from CFA with 1 and 3 M NaOH, respectively) for Cd^{2+} ion removal from aqueous solutions. The maximum adsorption capacities were calculated from Langmuir isotherms to be ~696 μmol/g (78 mg/g) for ZM1 and ~1,160 μmol/g (130 mg/g) for ZM3.

3.4.6 Other metals (Cr, Hg, Co, Mn)

3.4.6.1 Chromium

In addition to Cr adsorption investigated by Alvarez-Ayuso et al. [455] mentioned in Section 3.4.1, Wu et al. [474] investigated the ability of 14 zeolites synthesised from different fly ashes to remove Cr^{3+} from an aqueous solution. The maximum adsorption capacity of 51 mg/g was obtained at pH 4 ± 0.1 for high calcium Wujin F zeolite. Compared with the NaP1 zeolite, the small pore size of the hydroxysodalite of the Wujin F zeolite would promote selective sorption of chromium by hindering the sorption of relatively large ionic radius elements (Ca^{2+}, Mg^{2+}, Na^{+}, K^{+}, with Ca^{2+} and Na^{+} the most abundant ions in solution).

Ghasemi et al. [475] used CFA synthesised NA-P1 type zeolites modified with Ammonyx KP (KP) and Hexamethylenediamine (HDTMA) modified zeolites for the removal of Cr^{6+} from aqueous solutions. The maximum adsorption capacities of zeolites synthesised in this study were 49 and 338 mg/g for KP-Na-P1 and HDTMA-Na-P1, respectively.

Furthermore, Liu and Cheng [476] investigated CFA based P zeolite for adsorption of Cr^{3+}, Ni^{2+}, and Co^{2+} with the results showing the selectivity sequence of $Cr^{3+} > Co^{2+} > Ni^{2+}$. Thus, at elevated temperature (338.15 K) using 0.1 g of synthesized zeolite in 25 mL solution volume, a maximum removal rate of 98% was achieved for Cr^{3+} at the initial concentration of 300 mg/L, while for Ni^{2+} and Co^{2+} with the initial ion concentrations of 150 mg/L removal rates exceeding 85%.

3.4.6.2 Mercury

Attari et al. [477] compared the removal efficiency of Linde Type A zeolite synthesised from CFA and a commercial-grade activated carbon for mercury adsorption. Both adsorbents showed a similar equilibrium value close to 95% under the same experimental conditions with the maximum adsorption capacity of the zeolite being 0.4 mg/g.

A modified approach was attempted by Tauanov et al. [478] using coal fly ash-derived zeolites doped with silver nanoparticles. Their research showed that this nano-composite approach could remove 99% of Hg^{2+} in 1 day while fly ash derived zeolite without doping achieved only 91.3% efficiency after 14 days. The adsorption capacity of the zeolite and Ag-nanocomposite in 10 mg/L Hg^{2+} solution at pH 2.0 was measured to be 0.4 and 6 mg/g, respectively. Overall, while CFA derived zeolites are effective Hg adsorbents, composite approaches are showing higher efficiencies. That was explained as a difference in adsorption mechanisms by Tauanov et al. [478]. The dominating mechanism of mercury uptake in zeolite is physical adsorption, whereas in the investigated Ag nanocomposites it is a combination of adsorption, redox reaction producing Hg^0, and amalgamation [478].

Kobayashi et al. [234] synthesised K-type zeolite using CFA by hydrothermal treatment of CFA at different intervals. Representative samples of FA48 has shown the highest adsorption efficiency for Hg^{2+} ions, indicating that the hydrothermal treatment time is important to enhance the adsorption capability of K-type zeolite. Additionally, the desorption process was investigated, showing that approximately 70% of Hg^{2+} ions could be desorbed using a sodium hydroxide solution.

3.4.6.3 Cobalt

Lee et al. [479] studied the adsorption of cobalt ions on zeolites synthesised from CFA. The results showed that maximum adsorption capacity for Z-C1 synthesised zeolites was 94 mg/g.

As mentioned in Section 3.4.1, Hui et al. [480] investigated adsorption capacities of zeolite A prepared from fly ash in solutions with the presence of Cu^{2+}, Cr^{3+}, Zn^{2+}, Co^{2+}, Ni^{2+} ions. The maximum adsorption capacity for Co^{2+} was found to be 14 mg/g and the selectivity sequence was

in the following order $Cu^{2+} > Cr^{3+} > Zn^{2+} > Co^{2+} > Ni^{2+}$. Similarly, Joseph et al. [481] investigated simultaneous removal of Cd^{2+}, Co^{2+}, Cu^{2+}, Pb^{2+}, and Zn^{2+} ions from aqueous solutions via adsorption on FAU-type zeolites synthesised from CFA. In this study, the selectivity sequence was in following order $Pb^{2+} > Cu^{2+} > Cd^{2+} > Zn^{2+} > Co^{2+}$ with the adsorption capacity 12 mg/g for Co^{2+} ions.

3.4.6.4 Manganese

He et al. [187] studied the adsorption capacities of CFA zeolite in single and mixed-species aqueous solutions. In this study, the maximum adsorption capacities for Mn were established at 31 mg/g for a single species system and 15 mg/g for a five species system with an efficiency of 78 ± 0.7% for manganese in the Pb, Mn, Ni, Cu, Cd system.

Additionally, mixed-ions solutions were investigated by Qiu et al. [464] and Nascimento et al. [465]. The study by Nascimento et al. [465] showed that the preferred order observed for adsorption of Cu^{2+}, Pb^{2+}, Zn^{2+}, and Mn^{2+} using zeolites synthesised from Brazilian fly ash was Pb > Cu > Mn ≥ Zn, with maximum adsorption capacity for Mn 60 mg/g. Qiu et al. [464] used synthesised CFA zeolite for Cd, Cu, Mn, Ni, Pb and Zn adsorption. The results showed that the adsorption capacity followed the order of Pb > Cu > Zn > Mn ≈ Ni > Cd. The maximum adsorption capacity for Mn ions was found 15 mg/g.

3.4.7 Mixed ions solutions

While single-ion systems give us important information on maximum adsorption capacity of selected zeolites for specific metal ions, mixed-ion systems are closer to a real-world scenario, where wastewater typically contains various metal contaminants.

In Sections 3.4.1–3.4.6 research works examined CFA zeolites adsorption capacities for heavy metal ions in both single and mixed-species systems were described. For the readers' convenience, studies on single and mixed-ion systems are available separately in Appendix B1-B10, where single-ion systems are presented in Appendix B1-9 and mixed-ions combined in Appendix B10 .

To better correlate the adsorption selectivity in mixed-ion systems, the maximum adsorption capacities of different CFA zeolites are summarized in Appendix B10. For example, it can be seen from research by Visa et al. [454], He et al. [187], Joseph et al. [481], Qiu et al. [464], Nascimento et al. [465], Bai et al. [468] and Li et al. [470], that the adsorption capacity of different zeolites for Pb ions is greater than for other metal ions that are present in the system. At the same time, the maximum adsorption for Cu ions are greater than for Pb in studies by Wang et al. [459], Wang et al. [456] and Ji et al. [463].

The reasons for a certain selectivity order of metal ions uptake, however, have not yet been given a definitive explanation in the literature. Therefore, more research in this field will assist in comprehending the relationship between synthesised zeolite and other experimental parameters and metals selectivity sequence.

3.5 Summary

Natural zeolites are a well-known group of minerals with good mechanical and thermal properties and high sorption capacity. They are widely used in the field of heterogeneous catalysis and have many other industrial applications. However, due to the limited variety of natural zeolite microstructures and surface chemistry, synthetic zeolites often outperform natural zeolites. The sorption capacity of synthetic zeolites using various synthesis methods with designed chemical properties and pore size has been the subject of many studies. CFA is the waste product of one of the most widely used electricity production processes worldwide, so productively utilising CFA can alleviate environmental impacts. Furthermore, zeolites synthesised from CFA could be an alternative to other, more expensive adsorbents.

Due to the superior adsorption capacities achieved by synthetic zeolites, they are a promising material for water treatment applications, including heavy metal remediation. Unique ion exchange and adsorption properties, high porosity, and thermal stability make zeolites suitable for water treatment processes. Water is an essential resource, pollution of which is one of the leading causes of water shortages worldwide. The diversion of a waste stream such as a CFA to an ecologically beneficial process is likely to be important in the coming years. There are numerous researchers investigating CFA-synthesised zeolite-based water remediation processes. However, in most studies, researchers investigated zeolite adsorption capacity in a batch process. While it shows the

ability of the investigated zeolites to be efficiently applied water remediation, investigations of continuous processes would be of significant interest and value because to the industrial wastewater streams require a continuous system.

Zeolites synthesised from CFA have been demonstrated as being effective heavy metal adsorbents for heavy metal ions both from single and multi-cation solutions. While these zeolites' carrying capacity is comparable or better than commercial products, care should be taken to tailor the adsorbent to the ions that require remediation. As has been detailed in this overview, the type of synthesised zeolite plays a significant role in the adsorption process both in single and mixed-ion solutions. Furthermore, in mixed ion solutions, the selectivity order is affected by zeolite choice, a feature that could be leveraged to mitigate the effects of competition in such systems. However, currently, there seems to be no explicit reason in the literature as to why specific zeolites and their characteristics result in a specific selectivity order. Consequently, further research could provide a better explanation for the relationship between zeolite choice and the selectivity series. Such a model could then be utilised in the rational design of synthetic zeolites for specific remediation targets.

The synthesis of magnetic CFA zeolites would further enhance the sustainability of the water treatment process by enabling their extraction from treated water using magnetic fields.

Chapter 4
Magnetic Adsorbents

4.1 Introduction

Magnetic adsorbents are a new class of adsorbents wherein a primary adsorbent material is combined with magnetic particles composed of elemental metal or their oxides, such as magnetite (Fe_3O_4), maghemite (γ-Fe_2O_3), cobalt ferrite ($CoFe_2O_4$), nickel ferrite ($NiFe_2O_4$) among others [45,46,482,483]. In recent years, magnetic materials have been widely used in biology cell separation, wastewater treatment, coal desulfurization, mineral exploitation, catalysis, heavy metal removal, dye removal, biomedical applications, drug delivery, cancer therapy, solid phase extraction [45,46,484-488]. Magnetic adsorbents play an important role in the development of innovative and future-oriented water purification technologies. Moreover, they can be removed from wastewater using an applied magnetic field [45,46,482,483]. The use of a magnetic field generated by permanent magnets or superconducting coils for separation is used in many fields, including mining, solid state chemistry, biochemistry and medical research [488]. Additionally, they possess extraordinary surface charge and redox activity characteristics [489,490].

Most magnetic adsorbents are endowed with superparamagnetic properties, however, magnetite (Fe_3O_4, or iron oxide) is the most frequently used [491,492]. Fine magnetite particles (smaller than 25 nm) possess superparamagnetic properties, high chemical stability, large surface area, high magnetic coercivity, low toxicity and are often used to make a variety of magnetic adsorbents [43,493-495]. The physical and magnetic properties of iron oxides are presented in Table 4.1.

Table 4.1 – The physical and magnetic properties of iron oxides. Adapted from Liosis et al. [496].

Molecular Formula	**α-Fe_2O_3**	**Fe_3O_4**	**γ-Fe_2O_3**
Density (g/cm3)	5.26	5.18	4.87
Melting point (K)	1623.15	1856.15-1870.15	-
Hardness	6.50	5.50	5.00

Molecular Formula	**α-Fe_2O_3**	**Fe_3O_4**	**γ-Fe_2O_3**
Type of magnetism	Paramagnetic above its Curie temperature ($T_C \approx 956$ K), ferromagnetic below. At the Morin temperature ($T_M \sim 260$ K) undergoes a phase transition to an antiferromagnetic state [497,498].	Ferromagnetic	Ferromagnetic
Crystallographic system	Rhombohedral	Cubic	Cubic

Nanomaterials include the nanoscale particles, developed from organic or inorganic components that have high potential to adsorb pollutants due to their small size, high porosity, and active surface binding capacity [484]. Nanotechnology has significantly advanced the development of adsorption methods over the past decade, leading to substantial improvements in efficiency and effectiveness. The incorporation of nanomaterials has enabled the creation of adsorbents with enhanced surface areas, increased reactivity, and greater selectivity for specific pollutants, thereby revolutionizing the field of water treatment [496]. These properties allow iron oxide nanoparticles to be used as an adsorbent itself [499-501], however, the main problem remains the recycling of nanoparticles due to their size [502,503]. The mechanism and kinetics of adsorption in this case will depend on several parameters, including surface morphology and the magnetic behavior of the adsorbents [11]. The interaction between nanoparticles and adsorbents, as well as the formation and aggregation of nanoparticles, is influenced by their physicochemical properties, including magnetic, mechanical, optical, and electrical characteristics [496,504,505]. They can also be easily separated from aqueous solutions using a magnetic field [506,507]. A schematic illustration of the concept of magnetic adsorbents application and their removal is illustrated in Figure 4.1.

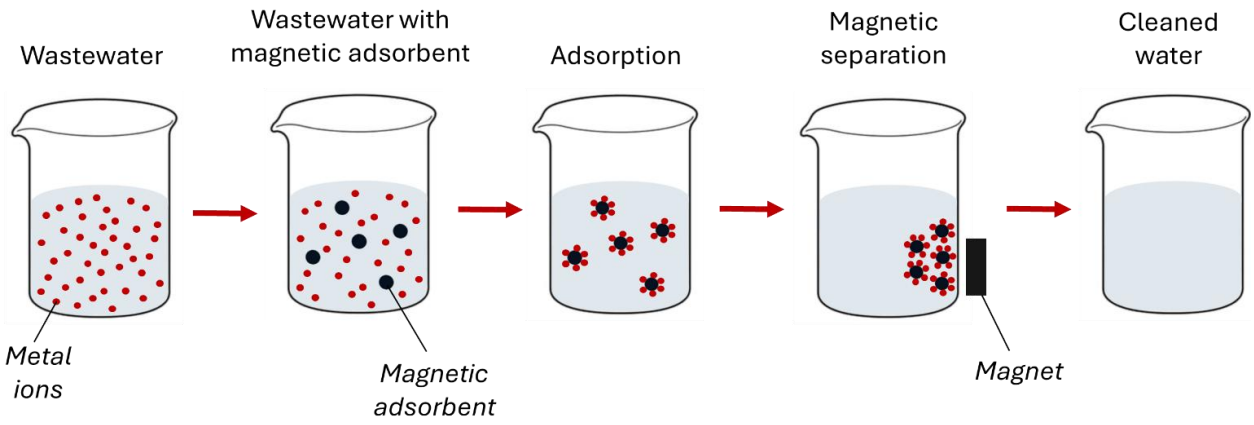

Figure 4.1 - A schematic image of adsorption by magnetic adsorbent followed by magnetic separation.

In recent years, the development of magnetic adsorbents has focused on enhancing their adsorption capacity, selectivity, and reusability. This involves tailoring the surface chemistry and morphology of the adsorbents to improve interactions with specific pollutants, such as heavy metals, dyes, and organic compounds. The preparation of each adsorbent must be specifically tailored for the removal of individual pollutants using the adsorption method [496]. For a detailed review of the use of magnetic adsorbents in the removal of other pollutants readers are referred to Mehta et al. [45], Ali et al. [484], and Liosis et al. [496].

4.2 Magnetic Zeolites

While zeolites have been demonstrated to be an effective material for water treatment, the separation of fine zeolite particles after the adsorption process is a significant challenge [43,508,509]. The separation of fine zeolite particles following the adsorption process remains a considerable challenge since the effectiveness of conventional methods in removing such fine particles from treated water can often be limited [510]. One promising method to overcome these limitations and effectively remove fine particles from water is the synthesis of magnetic zeolite composites [43,511]. Due to the magnetic properties of such composites, they can be separated from aqueous systems by the application of a magnetic field [43,511]. Various methods have been studied for magnetic zeolite synthesis; however up until now the synthesis of magnetic zeolites can be only achieved by using nano-scale particles [511]. By binding iron oxide nanoparticles with a zeolite,

the zeolite takes on iron oxide properties such as superparamagnetism, while remaining or even improving their adsorption capacity [512]. Furthermore, magnetic zeolite composites can be regenerated for further reuse, making them an asset in water treatment applications due to their sustainable characteristics [43,489,513,514].

Numerous researchers have explored the modification of zeolites to incorporate magnetic properties focusing on its potential to remove heavy metals from water [43,515-517]. The subsequent subsections 4.2.1 and 4.2.2 offer an overview of recent studies on magnetic zeolites used for single ions and mixed ions, respectively.

4.2.1 Magnetic Zeolites Use for Adsorption of Heavy Metals in Single Ions Systems

Praipipat et al. [518] investigated the potential of different type A zeolites synthesized from sugarcane bagasse fly ash and modified with iron (III) oxide to remove Pb from water. The study demonstrated that the addition of iron (III) oxide-hydroxide to the studied zeolites improved its efficiency for lead removal in both powder and bead forms. The adsorption capacity was found to be 666.67 mg/g for zeolite A sugarcane bagasse fly ash powder mixed iron(III) oxide-hydroxide (ZBF), 555.56 mg/g for zeolite A sugarcane bagasse fly ash powder mixed iron(III) oxide-hydroxide beads (ZBFB), and 625.00 mg/g for zeolite A sugarcane bagasse fly ash beads coated with iron(III) oxide-hydroxide (ZBBF). Similarly, Yuan et al. [519] investigated synthesized magnetic zeolite X composites by addition of Fe_3O_4 suspension in the hydrothermal synthesis process for the Pb^{2+} adsorption. The results showed that the products have an X zeolite crystal structure and present superparamagnetic properties with the saturation magnetization value of the product being approximately 3.7 emu/g. The maximum adsorption capacity of the synthesized magnetic zeolite was found to be 196.8 mg/g.

Yang et al. [520] synthesized magnetic fly ash-based zeolites and investigated its use for the adsorption of Cu^{2+} ions. The maximum saturated adsorption capacity of the studied magnetic zeolite for Cu^{2+} ions was found to be 48.99 mg/g, which is close to the fly ash derived non-magnetic zeolite A adsorption capacity of 50.5 mg/g.

Attia et al. [521] modified natural zeolite with iron oxide and investigated the obtained magnetic zeolite for As removal. The saturation adsorption capacity of arsenic onto non-magnetic zeolite

used in this study was measured to be 5.46 mg/g at a pH 2.5, while for the magnetically modified zeolite it reached 19.4 mg/g.

4.2.2 Magnetic Zeolites Use for Adsorption of Heavy Metals in Mixed-Ion Systems

Oliveira et al. [516] investigated NaY zeolite:iron oxides composite for the adsorption of Cr^{3+}, Cu^{2+} and Zn^{2+} from aqueous solution. The composites were prepared by using NaY zeolite:iron oxides weight ratio of 3:1 and showed good chemical resistance in a wide pH range (5–11).
The adsorption tests indicated that the presence of iron oxide in the composite does not affect the adsorption capacity. The adsorption capacity of magnetic zeolite was found to be 49, 87 and 114 mg/g for Cr^{3+}, Cu^{2+} and Zn^{2+}, respectively.

Boycheva et al. [522] synthesized Na-X type nanocrystalline zeolite from coal fly ash (CFAZ) by ultrasonic-assisted double stage fusion-hydrothermal alkaline conversion of lignite coal fly ash. CFAZ was modified with magnetic nanoparticles (MNP-CFAZ) by adding pre-synthesized magnetic nanoparticles between the synthesis stages. The resulting magnetic CFA zeolite was investigated for its adsorption capacity for Cd^{2+} and Pb^{2+} ions removal from aqueous solutions. The highest adsorption capacities of zeolites were found at the pH range of 5–7 for Cd ions and pH 3–5 for Pb ions. The maximum adsorption capacity for Cd ions was found to be 170.1 mg/g and 163.7 mg/g when using the Langmuir linear model for CFAZ and MNP-CFAZ, respectively.
Wang et al. [459] investigated magnetic zeolite P synthesized from low-grade fly ash via a hydrothermal synthesis method for Cu^{2+} and Pb^{2+} ions adsorption. The saturation adsorption capacity of Cu^{2+} and Pb^{2+} ions was shown to be 29.85 mg/g and 27.50 mg/g for synthesized Zeolite P and 25.20 mg/g and 20.38 mg/g for Magnetic Zeolite P. Additionally, the VSM study confirmed that the saturation magnetization of synthesized zeolite was 11.99 emu/g, indicating that magnetic zeolite has sufficiently magnetic property to be attracted by a permanent magnet after water treatment.

Liu et al. [515] synthesized magnetic zeolite NaA by applying a hydrothermal method. Magnetic zeolite NaA was prepared by adding Fe_3O_4 to the reactants before the crystallization phase. The study showed that the magnetic susceptibility of zeolite NaA increased with an increase in the amount of Fe_3O_4 loading. Moreover, the adsorption results indicated that the addition of Fe_3O_4 did not significantly decrease the adsorption capacity of Zeolite NaA for Cu^{2+} and Pb^{2+}. Thus, the

removal capacity for Cu^{2+} and Pb^{2+} has a slight decrease from 2.35 to 2.28 mmol/g and from 2.42 to 2.32 mmol/g, respectively, with an increase of Fe_3O_4 loading from 0 to 4.7 wt%. Thus, the adsorption capacity at 4.7 wt% Fe_3O_4 was calculated to be 144.9 mg/g and 480.7 mg/g for Cu^{2+} and Pb^{2+}, respectively. The results showed that the synthesized magnetic zeolite NaA is suitable for the removal of some heavy metal and then would be able to be removed by a magnetic separation process.

Faghihian et al. [523] prepared magnetic zeolite nanocomposite (MZNC) from nanozeolite A and iron oxide and investigated its efficiency at removing of Cs^+ and Sr^{2+} from aqueous solutions. The VSM results showed the saturation magnetization of synthesized zeolite to be 19.50 emu, meaning that it can be attracted by a application of magnetic field. The adsorption capacity of MZNC for Cs^+ and Sr^{2+} was 1.691 (224.7 mg/g) and 2.024 meq/g (88.7 mg/g), respectively. Comparing to micro-crystalline zeolite composite, the nanocomposite showed a 21.9% and 18.4% increase in adsorption of Cs^+ and Sr^{2+}, respectively.

Overall, the results of the use of magnetic zeolites for metal ions adsorption from both single and multi-ion systems indicate that they can be competitive to non-magnetic zeolites. Furthermore, the presence of magnetic particles does significantly affect their adsorption capacity. Several studies showed that synthesized magnetic zeolites have the advantage of being separated from aqueous solutions by applying a magnetic field due to their stable magnetic properties. Magnetic zeolite attracted by magnet illustrated in different studies is shown in Figure 4.2.

Additionally, although the magnetic properties of the synthesized magnetic zeolite were measured using VSM and visualized through magnet attraction in the studies described above, none of them reported the actual application of magnetic separation technology after adsorption experiments. This gap is addressed by the current work. Studies described in this section are summarized in Table 4.2.

(a) (b)

Figure 4.2 - Magnetic zeolite attracted by magnet in different studies: (a) Oliveira et al. [516], and (b) Faghihian et al. [523].

Table 4.2 – Different magnetic zeolites used for heavy metal ions removal from single and mixed ion solutions.

Zeolite type	**Metal ion**	**Adsorption capacity, mg/g**	**Reference**
Single ion system			
Zeolite A sugarcane bagasse fly ash powder mixed iron(III) oxide-hydroxide (ZBF)	Pb^{2+}	666.67	Praipipat et al. [518]
Zeolite A sugarcane bagasse fly ash powder mixed iron(III) oxide-hydroxide beads (ZBFB)	Pb^{2+}	555.56	
Zeolite A sugarcane bagasse fly ash beads	Pb^{2+}	625.00	

Zeolite type	**Metal ion**	**Adsorption capacity, mg/g**	**Reference**
coated iron(III) oxide-hydroxide (ZBBF)			
Zeolite X composites by addition of Fe3O4	Pb^{2+}	196.80	Yuan et al. [519]
Magnetic fly ash-based zeolites	Cu^{2+}	48.99	Yang et al. [520]
Natural zeolite with iron oxide	As	19.4	Attia et al. [521]
Mixed ion systems			
NaY zeolite:iron oxides composite	Cr^{3+}	49	Oliveira et al. [516]
	Cu^{2+}	87	
	Zn^{2+}	114	
Na-X type nanocrystalline zeolite from coal fly	Cd^{2+}	170.1	Boycheva et al. [522]
	Pb^{2+}	125	
Magnetic zeolite P synthesized from low-grade fly ash	Cu^{2+}	29.85	Wang et al. [459]
	Pb^{2+}	20.38	
Magnetic zeolite NaA	Cu^{2+}	144.9 (2.28 mmol/g)	Liu et al. [515]
	Pb^{2+}	480.7 (2.32 mmol/g)	
Nanozeolite A and iron oxide	Cs^{+}	224.7 (1.691 meq/g)	Faghihian et al. [523]
	Sr^{2+}	88.7 (2.024 meq/g)	

4.3 Magnetic Separation

Magnetic separation is a fundamental technique in mineral processing that utilizes the force induced by a magnetic field to differentiate and separate mineral particles based on their magnetic

properties [524,525]. Magnetic separators are utilized to separate minerals into magnetic and non-magnetic fractions [526].

The driving force of magnetic separation is the difference in magnetic susceptibility of materials, that describes how much a material can become magnetized or how readily a material can develop a magnetic moment when exposed to such a field in the presence of an external magnetic field, indicating its capacity to concentrate magnetic lines of force within itself [524,527].

Magnetic susceptibility (χ) can be found as the ratio of the intensity of magnetization (M) produced in the material over the applied magnetic field that produces the magnetization (H) [526]:

$$\chi=\frac{M}{H} \qquad 4.1$$

For paramagnetic materials, χ is a small positive constant, and for diamagnetic materials it is a much smaller negative constant [526].

Materials can be broadly categorized into ferromagnetic, paramagnetic and diamagnetic materials [527,528].

Ferromagnetic materials can be magnetized and exhibit strong magnetic properties since they have unpaired electrons whose magnetic fields align easily and retain their magnetization even after an external magnetic field is removed, a phenomenon known as hysteresis. These materials are characterized by easy magnetization up to a saturation point and include magnetite, iron, cobalt, nickel, and certain rare-earth elements, among others [527].

Paramagnetic materials are weakly attracted to externally applied magnetic fields and do not retain magnetism once the external field is removed, exhibiting a small positive internal induced magnetic field. Paramagnetism appears due to the presence of unpaired electrons in the material. Examples of paramagnetic materials include aluminum, lithium, and others.

Diamagnetic materials are repelled by magnetic fields, moving toward areas of lower magnetic intensity. Diamagnetic minerals include quartz, calcite, barite, diamond, and others. Despite the common reference to these substances as "nonmagnetic," they do exhibit weak magnetic properties due to the small forces involved in their repulsion from magnetic fields. In mineral processing, for magnetic separation technology, diamagnetic minerals are considered nonmagnetic products because they are not attracted by a magnetic field. Paramagnetic minerals, on the other hand, are

classified as magnetic when the magnetic field is sufficiently strong. However, if the magnetic force is not strong enough, paramagnetic minerals may also be referred to as nonmagnetic [526]. Thus, paramagnetic materials require high intensity magnetic separators to separate the magnetic product, whereas ferromagnetic materials are recovered in low-intensity magnetic separators.

To measure the magnetic properties a variety of techniques can be used, including VSM [529,530], fractionation with a magnetic separator [531], Frantz isodynamic separator [532] and others [533]. VSM is specifically designed to capture the variation of the magnetic properties of a material as a function of applied magnetic field strength, but is expensive equipment and require skilled operators, making them predominantly available in research environments [526]. This technique involves suspending a small amount of material from a rod that oscillates at a specific amplitude, frequency, and phase. The material is exposed to uniform magnetic fields of varying strengths. Distortions in the magnetic field caused by the sample are measured using detection coils. The magnetic moment of the sample is then converted to magnetization by dividing by the sample's volume. This data is plotted against the applied magnetic field strength to analyze the material's magnetic properties, as illustrated in Figure 4.3.

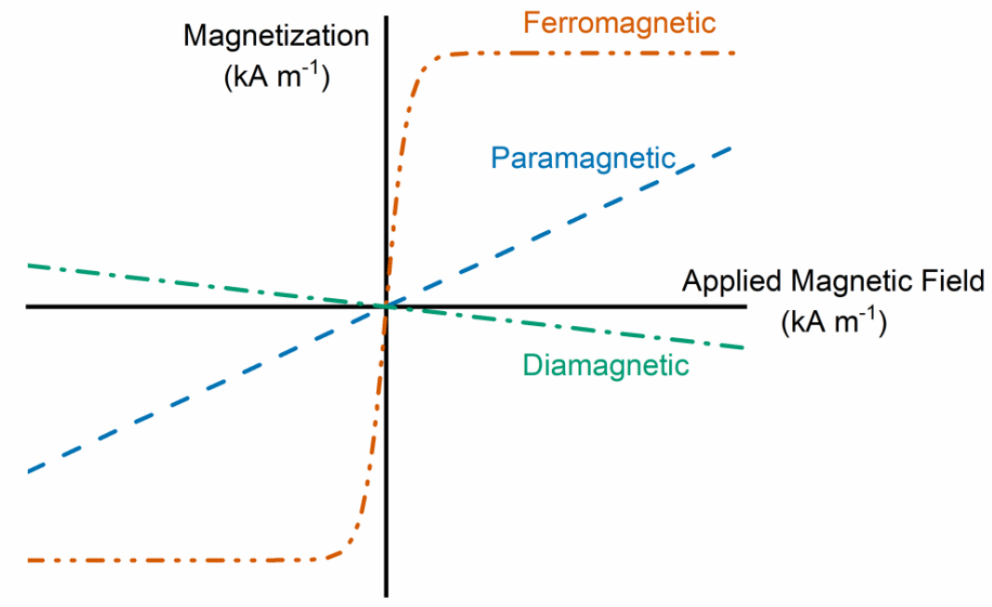

Figure 4.3 - Typical magnetization versus applied magnetic field strength trends for diamagnetic, paramagnetic and ferromagnetic materials. Reproduced from Marion (2020) [534].

Magnetic flux density, also known as magnetic induction, is measured by the number of magnetic force lines passing through a unit area of a material, represented as B. The unit of measurement for magnetic induction is the Tesla (T) [526].

The magnetization (M, A/m) of a material refers to the induced magnetization within the material, which can also be described as the volumetric density of induced magnetic dipoles. The relationship between magnetic induction (B), field intensity (H), and magnetization (M) is expressed by Equation 4.2:

$$B=\mu_0(H+M) \quad 4.2$$

where μ_0 is the permeability of free space and has the value of $4\pi\times10^{-7}$ NA^{-2}.

The magnetizing force that induces lines of force through a material is known as the field intensity, or H-field (A/m) [535].

In air and water, magnetization (M) is extremely low. Thus, for mineral processing purposes may be simplified to Equation 4.3:

$$B=\mu_0 H \quad 4.3$$

Thus, the field intensity (H) is directly proportional to the induced flux density (B).

The magnetic separation equipment used in this thesis are briefly described in the following section. For a more detailed discussion on magnetic separation techniques, readers are referred to Wills and Finch [526], Svoboda and Fujita [536], and Svoboda [530].

The magnetic separator's function is based on the balance between magnetic force and other forces, such as fluid drag or gravity, depending on the particle size. The effectiveness of a magnetic separator depends on factors such as the strength of the applied magnetic field, the magnetic field gradient, the particle size and magnetic susceptibility of both the particles and the fluid medium.

When considered only in the x-direction, the magnetic force exerted on a particle in a magnetic separator can be expressed by Equation 4.4:

$$F_x=V(\chi_p-\chi_f)H\frac{dB}{dx} \quad 4.4$$

Where F_x is the magnetic force on the particle (N), V is the particle volume (m^3), H is the applied magnetic field strength ($A\cdot m^{-1}$), χ_p is the magnetic susceptibility of the particle, χ_f is the magnetic susceptibility of the fluid and dB/dx is the magnetic field gradient ($T\cdot m^{-1}$).

The magnetic force will exceed competing forces within a certain particle size range, determined by the mineral's magnetic susceptibility. Minerals with higher magnetic susceptibility can be recovered across a broader range of particle sizes [526]. Oberteuffer et al. [537] demonstrated that the particle size range where magnetic force is dominant spans from approximately 5 micrometers to 1 millimeter.

4.3.1 Wet Magnetic Test Chute

A wet magnetic test chute is a lab-scale tool used for magnetic separation testing. As shown in Figure 4.4, it consists of an inclined surface placed above a permanent magnet, down which a mineral slurry is fed. Minerals with high magnetic susceptibility are attracted to the magnetic field and adhere to the surface, while those that are not attracted continue with the slurry and are collected as non-magnetics product at the bottom.

To enhance the magnetic force on the particles and thus improve the recovery of minerals with lower magnetic susceptibility, or to mitigate the effects of fluid drag and gravity on fine and coarse particles respectively, the permanent magnet in the device can be replaced with a magnet of higher field strength. For example, substituting an iron-based magnet with a rare-earth (RE) magnet can achieve these enhancements.

Figure 4.4 - Laboratory wet magnetic test chute.

4.3.2 Wet High Intensity Magnetic Separator (WHIMS)

The development of continuous wet high-intensity magnetic separators (WHIMS) [538] was the most significant advancement in the field of magnetic separation [526] that was developed to reach high magnitude field gradients [536,539]. In WHIMS, a matrix made of ferromagnetic material is placed in a high-intensity magnetic field created by an electromagnet. This setup generates numerous sites with high field gradients, allowing for the capture of particles with low magnetization and particle size. For industrial-scale continuous flow experiments, a high-gradient magnetic separation (HGMS) system operating in a carousel configuration, similar to the Jones WHIMS, can be employed [526]. The principle of HGMS operation is illustrated in Figure 4.5.

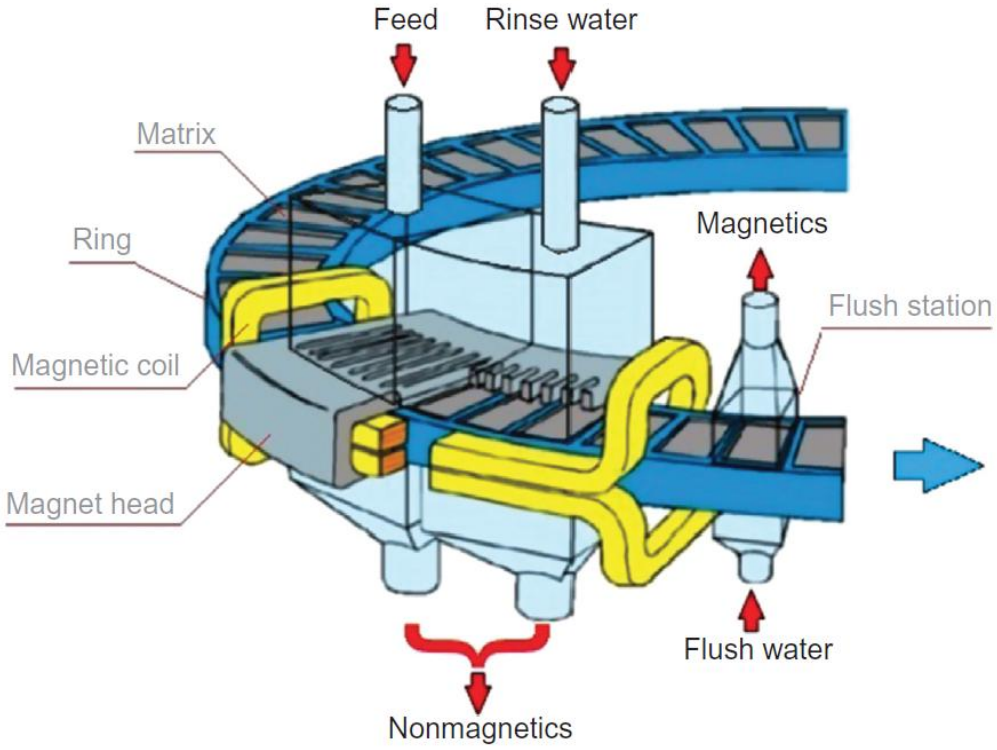

Figure 4.5 - Metso HGMS operating principle (Courtesy Metso). Reproduced from Wills and Finch [526].

4.4 Regeneration, Reuse and Disposal of Zeolite

One of the key advantages of magnetic zeolite is its potential for recovery after extraction, allowing ease of water cleaning and the ability to be employed in multiple cycles of water treatment. The effectiveness of reused zeolites depends on the regeneration method and the nature of the contaminants. Studies have shown that while regenerated zeolites can maintain substantial

adsorption capacity, their performance may gradually decrease over time. The regenerated magnetic zeolite is promising for multiple reuses in subsequent water treatment cycles, thereby enhancing the sustainability of the process.

Regeneration of magnetic zeolite was reported using NaCl [42], NaOH and HCl solutions [526], NaCl solutions [540-542], thermal regeneration [540], and regeneration by pyrolysis [543]. All these studies successfully cleaned magnetic zeolites and reused them in several cycles of water treatment.

The most widely used methods for regenerating adsorbents are photocatalytic processes, biological treatments, chemical methods, and thermal techniques [544,545]. The reusability of nanocomposite zeolite depends on the type of zeolite and the contaminants in the water. Regeneration processes are affected by variety of parameters including pH, conductivity, and temperature, which is also time-consuming [544]. Additionally, the process can be costly due to the cost of chemicals or energy. Thus, it is important to find optimal conditions for effective regeneration of magnetic zeolites. This topic requires further investigation due to limited research in this area. For a more detailed review on magnetic zeolite nanocomposites use for removing heavy metals, organic pollutants, and emerging contaminants from water, Sossou et al. [544] is a suggested resource.

When exhausted, metal-loaded zeolites can be incorporated into construction materials including concrete production [546-548]. It has been shown in several studies that zeolites not only add structural properties but also immobilizes heavy metals, preventing environmental leaching [548,549]. Thus, the use of magnetic zeolite in water treatment, along with its subsequent regeneration and reuse, potentially streamlines the recycling and repurposing of the used zeolite, thereby mitigating environmental impacts.

4.5 Summary

The literature review in Chapter 4 highlighted recent developments in water treatment technology using magnetic adsorbents materials. It has been shown that magnetic adsorbents can be effective for the removal of heavy metal contaminants from water and have high adsorption yields. This chapter also covers magnetic separation technology, which offers an efficient method for separating magnetic adsorbents from treated water. This chapter also discuss the possibility of

regeneration, reuse, and disposal of magnetic zeolites extracted from treated water, underlining the importance of sustainability in water treatment processes.

The review covers the use of magnetic zeolite in water treatment and their efficiency for heavy metals removal. Furthermore, their use in water purification gives a significant advantage as a low-cost, ease to synthesize, and the ability to be separated from water by application of magnetic field and then to be used again.

In conclusion, the literature review identifies a knowledge gap in the synthesis of magnetic zeolites from CFA and their application in the removal of heavy metal ions from water. This gap highlights the need for further research and innovation in the synthesis of magnetic zeolites and their subsequent recovery, which forms the motivation for the current thesis.

Chapter 5
Experimental Methods

5.1 Introduction

This chapter details the experimental methods employed throughout the thesis, presenting the procedures in the same sequence as the results and discussion chapters.

5.2 Materials and Methods

5.2.1 Zeolite synthesis

5.2.1.1 LTA zeolite synthesized from laboratory grade chemicals

Linde Type A (LTA) zeolite (Si(50), Al(50)) was synthesized using the method described in *Verified Syntheses of Zeolitic Materials* [550]. For the synthesis, sodium hydroxide (Thermo Fisher Scientific Inc., Waltham, MA, USA, >99% NaOH), sodium aluminate (Fisher Scientific, NaO_2:Al_2O_3:$3H_2O$), sodium metasilicate (Thermo Fisher Scientific Inc., Waltham, MA, USA, Na_2SiO_3:$5H_2O$) and reverse osmosis (RO) water were used.

First, ~0.72 g of sodium hydroxide was dissolved in 80 mL of RO water and then divided into two equal volumes in polypropylene bottles. After that, one-half of the solution was gently mixed with ~8.26 g of sodium aluminate in a capped polypropylene bottle until fully dissolved. Next, the remaining half of the sodium hydroxide solution was mixed with ~15.48 g of sodium metasilicate and mixed in a sealed bottle until fully dissolved. Subsequently, the silicate solution was quickly poured into the aluminate solution, forming a thick gel. The bottle was then shaken until the gel homogenized. Afterward, the sealed bottle was placed into an oven for 4 h at 99 ± 1 °C. In the next step, the bottle was extracted from the oven and allowed to cool to room temperature, and then the contents of the bottle were washed out using RO water and filtered using a pressure filter (OFI Testing Equipment, Inc., Houston, TX, USA). The wet solid product was dried overnight at ~60°C, and then the dried product was weighed using a precision balance (Mettler AJ100 Analytical balance, Gemini, Apeldoorn, The Netherlands). A graphical representation of the described synthesis process can be seen in Figure 5.1. To investigate the synthesized material crystal

structure, it was analyzed using X-ray diffraction (XRD), and the obtained pattern or diffractogram was compared with the data from the Crystallography Open Database (COD).

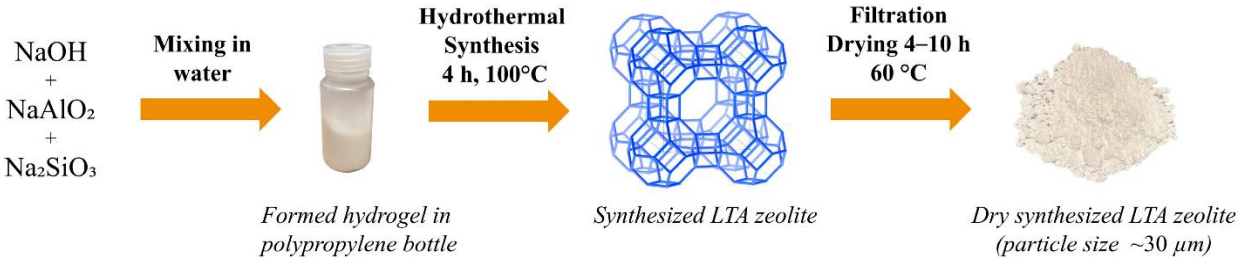

Figure 5.1 - Graphical representation of the process of LTA zeolite synthesis used in this work. The image of the LTA zeolite framework (viewed along [100] direction) is adapted from the website of the International Zeolite Association (IZA). Pictures of hydrogel in a polypropylene bottle and dry synthesized LTA zeolite were taken during the experiments.

5.2.1.2 CFA synthesized zeolites

The CFA used in the zeolite synthesis was a byproduct of Rocktron's beneficiation process [329]: CFA was subjected to sink/float density separation using water to remove a cenosphere concentrate, comprising of hollow spheres, froth flotation to produce a carbon enriched product, magnetic separation to produce a stream rich in maghemite and hematite, and size classification to separate a fine "Alpha" product suitable for use as a substitute for pozzolanic material in cement. The coarse "Delta" product comprised primarily aluminosilicates, and formed a low value, high volume product with limited applications beyond use as an aggregate.

This coarse product was used as the feedstock for the zeolite synthesis process, which involved two stages: microwave-assisted fusion, and hydrothermal crystallisation. For microwave-assisted fusion, 67.66 g of "Delta" ash product was mixed with 2 M of NaOH pellets (Analytical grade, Fisher Scientific, UK) and heated in a custom nickel vessel in a 700 W microwave on full power for 5 min, mixed whilst hot, using nickel spatulas and microwaved for a further 5 min. This fused product was then coarsely crushed in a pestle and mortar, and mixed with 1 L of distilled water and agitated with an overhead stirrer at 300 rpm for 10 min to produce 895–920 mL of leachate rich in Si and Al. The undissolved material was filtered out using a sintered glass buchner funnel. For the hydrothermal crystallisation step, 12 g of sodium aluminate (technical grade, Sigma-Aldrich) and 35 g of NaCl were added to 900 mL of leachate. The solution was heated in a conical

flask on hotplate with feedback temperature control and agitated with a magnetic stir bar. The solution was heated to 90 °C for 2 h, and then for a further 3 h at 95 °C after which the zeolite was separated from the solution by filtration using a sintered glass Buchner funnel and washed with distilled water. For a more detailed discussion of this synthesis method readers are referred to Sommerville (2017) [353].

5.2.1.3 Iron Oxide Nanoparticles:Zeolite Composite

To synthesize magnetic LTA or CFA zeolite (M-LTAZ and M−CFAZ, respectively), non-magnetic zeolite powder was mixed with magnetite nanopowder and a novel high-temperature colloidal polyvinyl alcohol (PVA) solution.

To prepare the PVA solution, a glass flask was used to add 1 g boric acid (crystalline, Thermo Fisher Scientific Inc., U.S.A.) and 0.1 g copper (II) sulfate (anhydrous, Sigma-Aldrich, U.S.A.) in 40 mL reverse osmosis (RO) water. This catalytic mixture was stirred using a magnetic stirrer for 15 min at 70 °C until the complete dissolution of both polymerisation catalysts. After that, 300 mL of tetrahydrofurfuryl acid (THFA) (Sigma-Aldrich, U.S.A.) and 40 g polyvinyl acetate (Sigma-Aldrich, U.S.A.) were added into the flask in an IKA RV 10 rotary evaporator (IKA, U.S.A.) for 3 h at 180 rpm, 70 °C and 0.95 bar. Consequently, all traces of water were removed from the solution using a vacuum oven (VWR, U.S.A.) at 90 °C for 2 h. The colloidal PVA solution was cooled to room temperature, for use in the subsequent magnetic zeolite synthesis.

5.2.1.3.1 Different iron oxide loadings in magnetic LTA zeolite synthesis process

To synthesize the magnetic LTA zeolite with different iron oxide loadings, 10 g of LTA zeolite was mixed with a set amount (0.1 g, 0.5 g, 1 g, and 2 g) of 50–100 nm iron oxide nanopowder (Iron (II, III) oxide, Sigma-Aldrich, USA) followed by the addition of 20 mL of colloidal PVA solution. The solution was then sonicated using Sonics Vibra-Cell VC 50 (Sonics & Materials Inc., Newtown, CT, USA) for 15 min in a glass beaker, after which reverse osmosis (RO) water was added to form a hydrogel. The hydrogel was then dried in a Thermolyne FB1415M Compact Benchtop Muffle Furnace (Thermo Fisher Scientific, USA) for 2 h at 160 °C in a polytetrafluoroethylene (PTFE) container to bond iron oxide nanoparticles and CFAZ together through PVA cross-linking. After that, the obtained material was cooled to room temperature and then transferred into a ceramic container and heated in the air in the muffle furnace for 2 h at 400°C

to cure and carbonize the PVA cross-linking. The final obtained material was then cooled to room temperature and milled to a very fine powder using a monomill (Pulverisette 6 planetary monomill, Fritsch, Idar-Oberstein, Germany) for 5 min set at 500 rpm.

5.2.1.3.2 Magnetic CFA zeolite synthesis

To prepare the M−CFAZ, 5 g of CFAZ was mixed with 0.05 g of 50–100 nm magnetite nanopowder (Iron (II, III) oxide, Sigma Aldrich, U.S.A.) and then 15 mL of PVA solution was added. The solution was then sonicated using Sonics Vibra-Cell VC 50 (Sonics & Materials Inc., U.S.A.) for 15 min in a glass beaker, after which RO water was added to form a hydrogel. The hydrogel was then dried in a muffle furnace for 2 h at 160 °C in a polytetrafluoroethylene (PTFE) container to bond nano-magnetite and CFAZ together through PVA crosslinking. The obtained material was subsequently cooled to room temperature, transferred into a ceramic container and heated in air in a muffle furnace for 2 h at 400 °C to cure and carbonised the PVA crosslinking. The final obtained material was then cooled to room temperature and milled to a fine powder using a monomill (Pulverisette 6 planetary monomill, Fritsch, Idar-Oberstein, Germany) for 5 min at 500 rpm.

5.2.2 Magnetic separation

To separate M−CFAZ from the non-magnetic fraction after synthesis and to confirm that the synthesized magnetic zeolite can be removed from solution, a jaw type wet high intensity magnetic separator (WHIMS) (Bunting, UK) was used. The working parameters of WHIMS in this study were: 12 A, 184 V, 1.4 T. After the solution was slowly poured into the WHIMS funnel, non-magnetic particles pass through, and magnetic particles remain inside the metal matrix. Non-magnetic particles were collected in a container under WHIMS and the magnetic particles were washed out after the WHIMS was turned off. The described process is summarized in a schematic diagram in Figure 5.2.

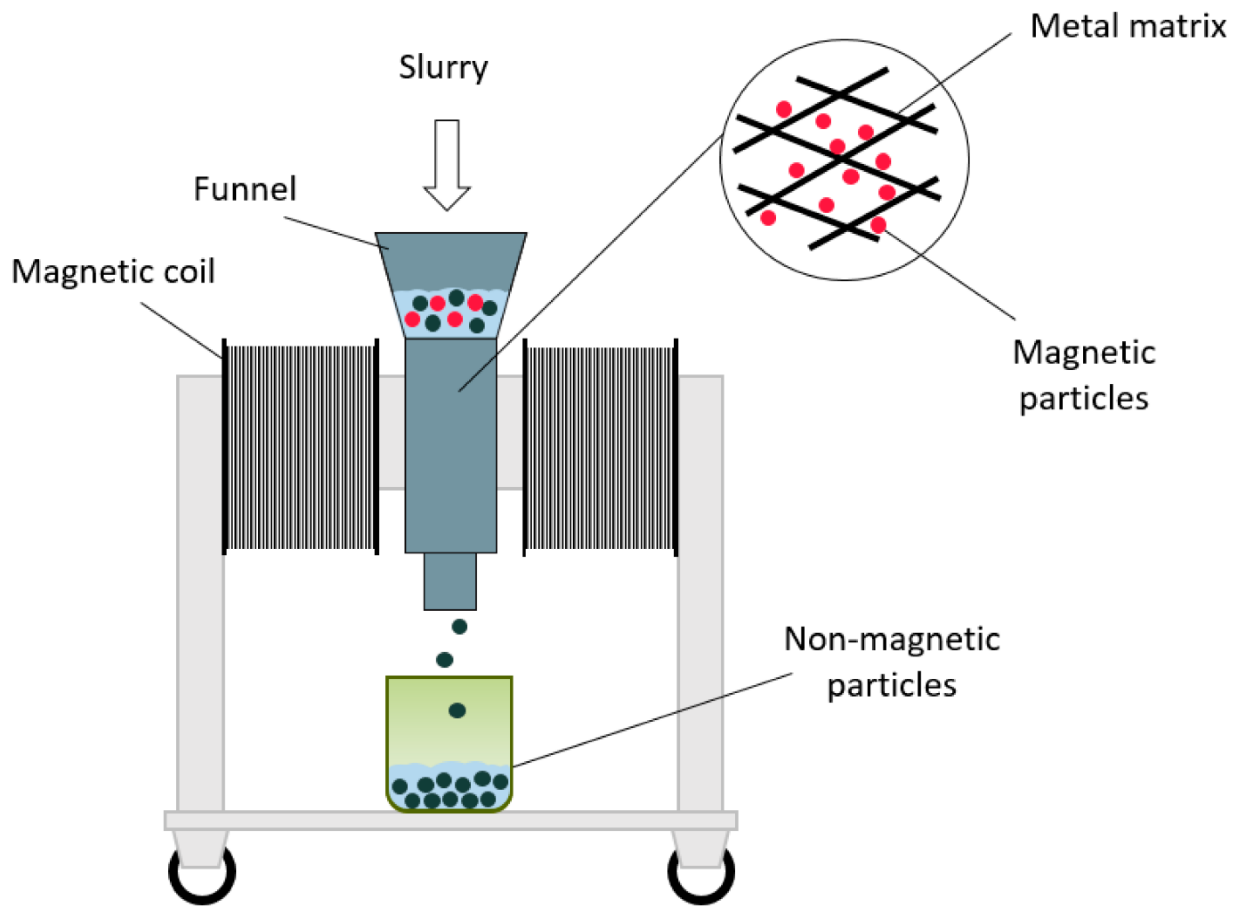

Figure 5.2 - Schematic diagram of high-intensity electromagnetic separator (WHIMS) used for the extraction of magnetic zeolite.

5.2.3 Adsorption experiments

Adsorption experiments were carried out to investigate adsorption kinetics and quantify the adsorption capacity of the investigated zeolites.

5.2.3.1 Solution preparation

Synthetic solutions containing Cu^{2+}, Zn^{2+}, Ni^{2+}, Pb^{2+} ions were prepared using analytical reagent grade chemicals by preparing stock solutions which were then diluted using RO water to the desired concentrations. Cu^{2+}, Zn^{2+}, Ni^{2+}, Pb^{2+} solutions were prepared using copper(II) nitrate trihydrate, 99% (Thermo Fisher Scientific, U.S.A.), zinc nitrate hexahydrate (98% Thermo Fisher

Scientific, U.S.A.), nickel(II) nitrate hexahydrate (99% Thermo Fisher Scientific, U.S.A.), and lead(II) nitrate (99% Thermo Fisher Scientific, U.S.A.), respectively. Tests were conducted in single-ion solutions for each metal and with mixed-ions solutions where all four metal ions were present. The initial metal concentration prepared was 300 mg/L for both single and mixed ions solutions. Experiments were conducted at pH 5.5–6, at room temperature without temperature control and the stirring speed was set at 400 rpm. The pH of the solutions was measured before and after adsorption. A control experiment was conducted at the same pH where no zeolite was added. This resulted in no precipitation or change in metal concentration.

5.2.3.2 Batch adsorption experiments

Unless otherwise stated, all adsorption experiments were conducted using 0.1 g zeolite in 100 mL of solution in 200 mL glass beakers positioned on an orbital shaker (New Brunswick Scientific Co., Canada) and covered with parafilm when using magnetic zeolite. Once the zeolite was introduced to the solution, periodic samples were taken from the solution using a syringe and filtered using 0.1 μm filter (MilliporeSigma, Germany), preventing any further adsorption. Metal ion concentrations of these filtered samples was measured using inductively coupled plasma optical emission spectroscopy (ICP-OES) using a Thermo Scientific iCAP 6000 series ICP Spectrometer (USA). Each experiment was conducted in triplicate and a control experiment with no addition of zeolite in solution was performed to confirm that there is no precipitation or change in metal concentration without zeolite in the system. The results are reported as average values with error bars denoting ± 95% confidence interval. A schematic representation of batch adsorption experiments is presented in Figure 5.3.

To extract M−CFAZ from solution after batch adsorption experiments, a lab scale WHIMS was used with the working parameters of WHIMS at 12 A, 184 V, 1.4 T. After the treated solution passed through WHIMS, it was collected into a clean beaker and analyzed using ICP-OES.

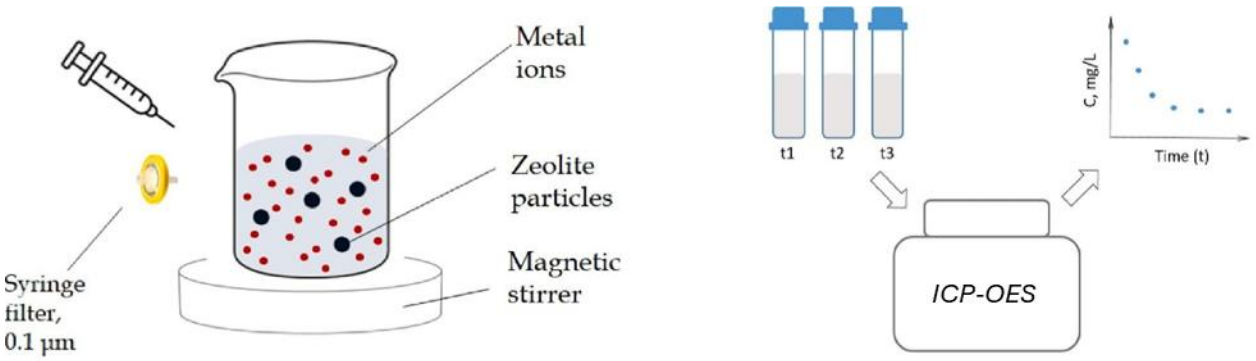

(a) (b)

Figure 5.3 - Schematic representation of batch adsorption – (a) known quantity of zeolite is homogenously mixed in a metal ions solutions on a magnetic stirrer. Supernatant samples are than periodically taken using a syringe and a 0.1 µm filter, stopping the adsorption in the sample; (b) periodic samples are then analyzed using inductively coupled plasma optical emission spectroscopy (ICP-OES) to measure residual metal ions concentration in solution. The residual concentration over time represents the progress of the adsorption reaction.

5.2.3.3 Continuous flow adsorption experiments

For the continuous flow system, the design shown in Figure 5.4 was utilized. The process begins with the contaminated solution being pumped from Beaker 1 using Pump 1 into the Beaker 2. Here, magnetic zeolite particles are introduced, and a mechanical stirrer set at 400 rpm ensures thorough mixing. Simultaneously, the treated solution is pumped out from Beaker 2 by Pump 2 which is set to the same volumetric flow rate as Pump 1, such that the volume in Beaker 2 remains constant. The solution pumped from Beaker 2 will contain magnetic zeolite particles, so before discharge it is pumped directly through the WHIMS. During these experiments the WHIMS was operated at 12 A and 184 V generating a magnetic field of 1.4 T.

After passing through the WHIMS, the treated solution free of zeolite particles was collected into a Beaker 3 below the WHIMS. Finally, based on the desired final metal ions concentration in solution, the solution from Beaker 3 can be either discharged or reintroduced for another cycle of water treatment with the addition of new magnetic zeolite by using Pump 3 to pump solution back into the cycle. Samples of solution were taken over time from Beakers 1-3 to monitor the change

of metal ion concentration over time. Experiments were repeated at different pump speeds and with a different amount of added zeolite and treated solution to investigate how the amount of zeolite and the retention time would affect the adsorption kinetics. All experiments were conducted in triplicate and error bars on the graphs in the Results section represent ± 95% confidence interval.

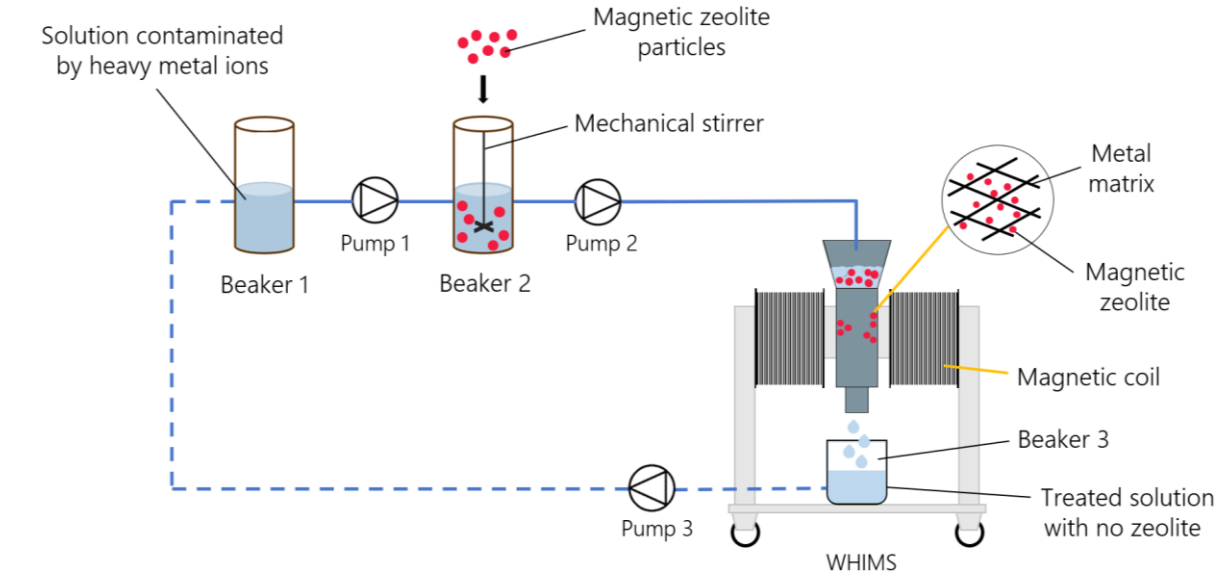

(a)

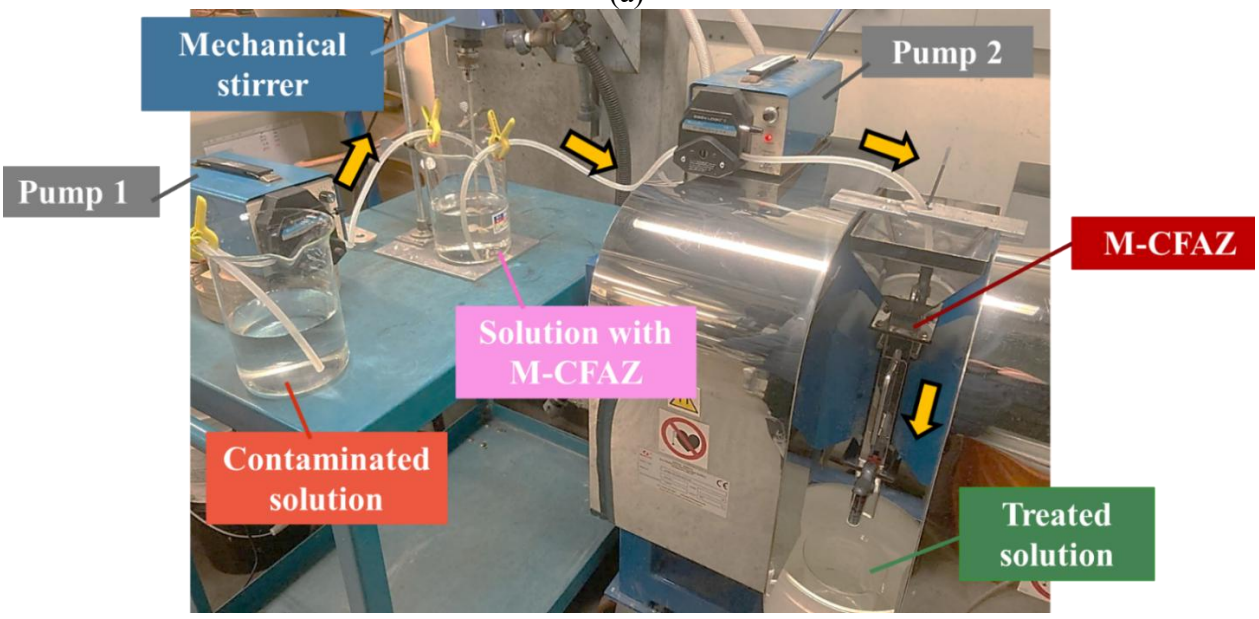

(b)

Figure 5.4 - Continuous flow experimental design for water treatment using magnetic zeolite where treated solution goes directly into WHIMS: (a) schematic, (b)photo of the setup utilized for the experiments.

5.2.4 Desorption experiments

Figure 5.5 illustrates a schematic of metal ion (represented by the red colored circles) desorption from magnetic zeolite (represented by the black colored circles). The metal-laden zeolite is placed in a saturated NaCl solution that forces ion exchange to start. The center of the image details the mechanism of ion action facilitated by the high concentration of Na^+ in the solution, where Na^+ ions (represented by the green circles) from the solution displace metal ions from the zeolite surface. That process ideally results in the complete replacement of metal ions by Na^+ ions from the solution, indicating the cleansing of metal ions from the zeolite's surface. This process illustrates the regeneration of the magnetic zeolite for potential reuse.

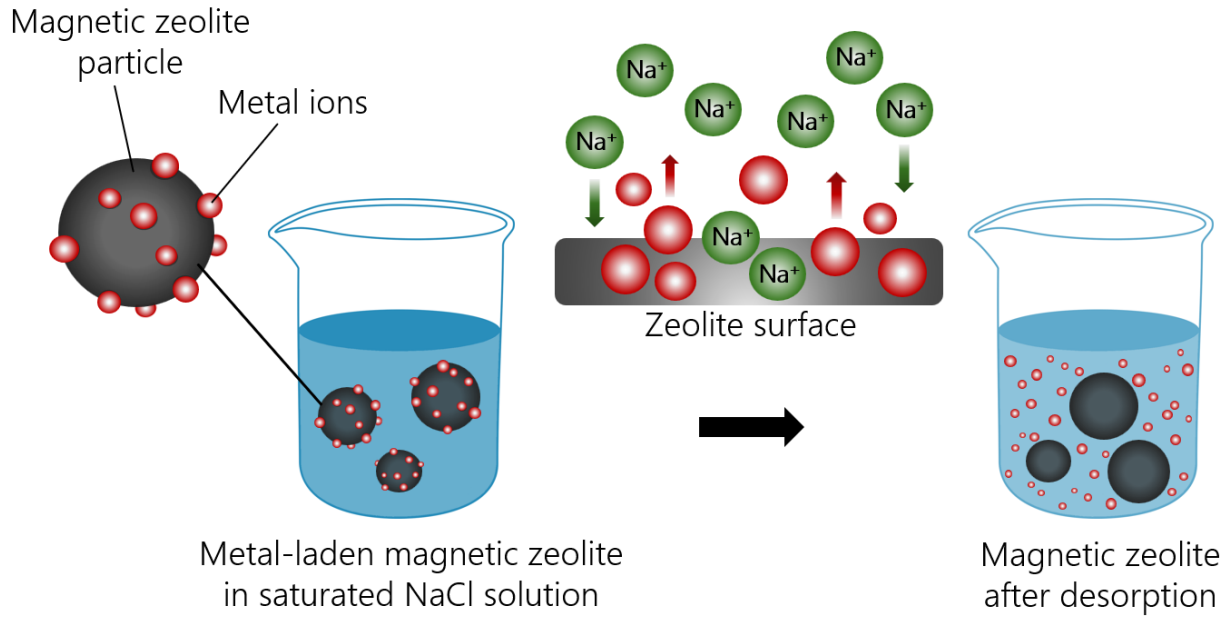

Figure 5.5 - Schematic illustration of desorption of metal ions (Pb^{2+}, Cu^{2+}, $Zn^{2+}$and Ni^{2+}) from magnetic zeolite by to ion exchange with Na^+ ions in saturated sodium chloride (NaCl) solution.

To prepare saturated NaCl solutions, 36 g NaCl (anhydrous, Sigma-Aldrich, USA) was diluted in 100 mL RO water. For desorption experiments, 100 mL of saturated NaCl solution was mixed with 0.1 g dried zeolite powder after the adsorption experiments and stirred using a mechanical stirrer at room temperature. Samples were taken over time and analyzed using ICP-OES, to compare the concentration of metal ions in solution before and after desorption. Additionally, the zeolite was

analyzed after adsorption and desorption experiments using SEM-EDS to compare the weight % of metals in the sample before and after desorption.

5.3 Characterization methods

The zeolites were characterized via several techniques, including X-ray diffraction (XRD), Scanning electron microscopy (SEM), Energy-dispersive X-ray spectroscopy (EDS), X-ray photoelectron spectrometer (XPS), Brunauer-Emmett-Teller (BET) technique, and particle size analysis (PSA). Solution concentrations were measured at the Inductively Coupled Plasma Optical Emission spectroscopy (ICP-OES). To measure the magnetic properties of synthesized zeolites, a vibrating-sample magnetometer (VSM) was used.

5.3.1 XRD

XRD patterns were recorded using Bruker D2 phaser (Bruker, Germany) with the LYNXEYE XE-T, Cu, Kα, (λ = 1.5418 Å) X-ray source and operating conditions of 30 kV and 10 mA. The diffraction angle (2θ) was measured in the range of 5–70°. Diffraction patterns were analyzed using MAUD Java Program.

XRD exploits Bragg's law that can be expressed as:

$$\lambda = 2d \sin \theta \qquad 5.1$$

Where λ – wavelength (nm), d - lattice spacing (Å), θ - angle of incidence.

When analyzing sample using XRD, an X-ray of known wavelength λ is directed at a crystalline sample. A detector positioned at an angle 2θ from the X-ray source measures the intensity of the X-rays emitted from the sample, as illustrated in Figure 5.5. At certain values of θ, constructive interference occurs with the X-rays leaving the sample, leading to a significant increase in the intensity measured by the detector [551].

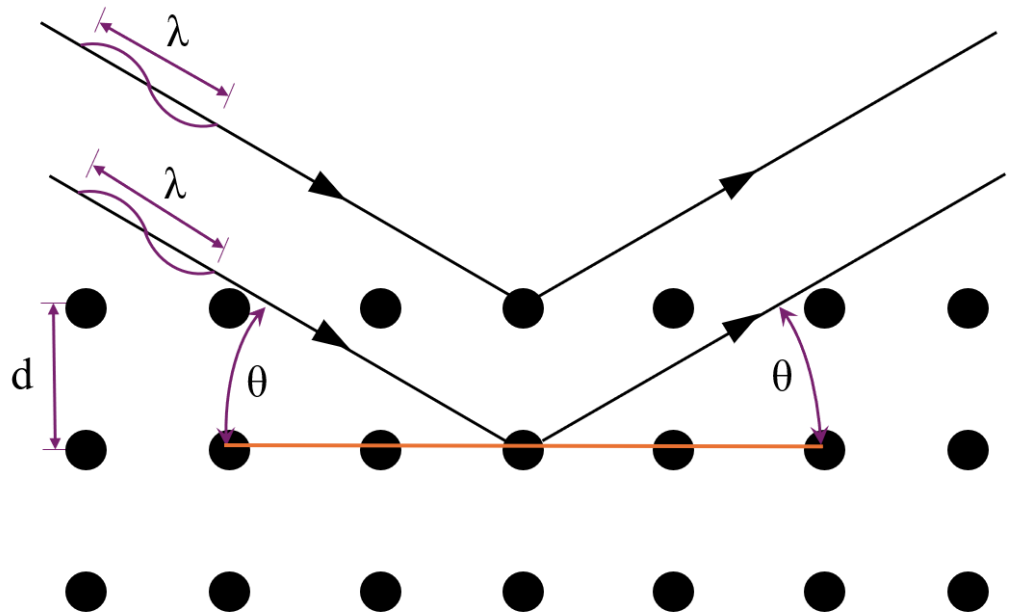

Figure 5.6 - XRD Principles of Operation. The diagram shows two parallel beams of X-rays incident on a crystal lattice. The X-rays are represented by black lines with arrows indicating the direction of the rays, where λ represents wavelength (nm), and θ is the angle of incidence. The black dots in the diagram represent the atoms in the crystal lattice, and the orange horizontal line indicates the plane of atoms within the crystal. The distance between planes is denoted by d lattice spacing (Å).

5.3.2 SEM

SEM was conducted using a SU3500 SEM (Hitachi, Japan) equipped with an 80 mm^2 X-MaxN Silicon Drift energy dispersive spectrometer (EDS) detector (Oxford Instruments, UK). The collected data were analyzed using AZtec software (Oxford Instruments, UK) to identify elements present in the samples.

SEM operates by directing an electron beam at a sample in a raster pattern. When the electron beam hits the sample, it displaces electrons from the sample, which can be emitted as secondary electrons. The secondary electrons possess low energy and are unable to travel far before being absorbed, which makes secondary electrons particularly well-suited for analyzing the topography of a sample, as only those originating from the surface can escape.

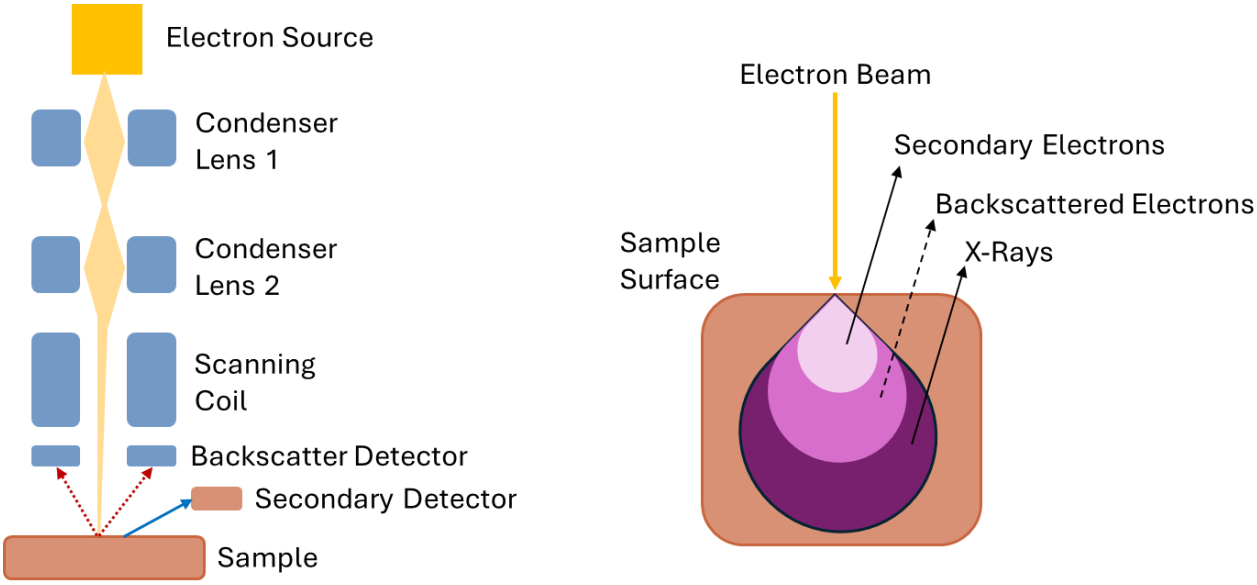

Figure 5.7 - Scanning Electron Microscopy Principles of Operation.

5.3.3 XPS

The X-ray photoelectron spectrometer (XPS) used in this study was a Thermo Scientific K-Alpha monochromatic X-ray photoelectron spectrometer (Thermo Fisher Scientific Inc., U.S.A.). It was quipped with an Al Kα X-ray source (1486.6 eV, 0.834 nm), ultrahigh vacuum chamber (10—— 9 Torr) and microfocused monochromator. The analysis consisted of an elemental survey from 0 to 1350 eV and high-resolution scans with a pass energy of 1 and 0.1 eV respectively. The analyses were conducted on 3 target points for each sample using a spot size of 400 μm. Zeolite samples were dried overnight in an oven at ~ 60 °C and then were kept in a desiccator prior to analysis. Experimental results were analyzed using Avantage Data System software (Thermo Fisher Scientific Inc., U.S.A.).

In XPS, the sample is irradiated with soft X-rays (energies lower than ~6 keV) and the kinetic energy of the emitted electrons is analyzed as is shown in Figure 5.7. The emitted photoelectron, resulting from the complete transfer of X-ray energy to a core level electron, has its energy measured to determine the elemental composition and chemical state of the material's surface [552].

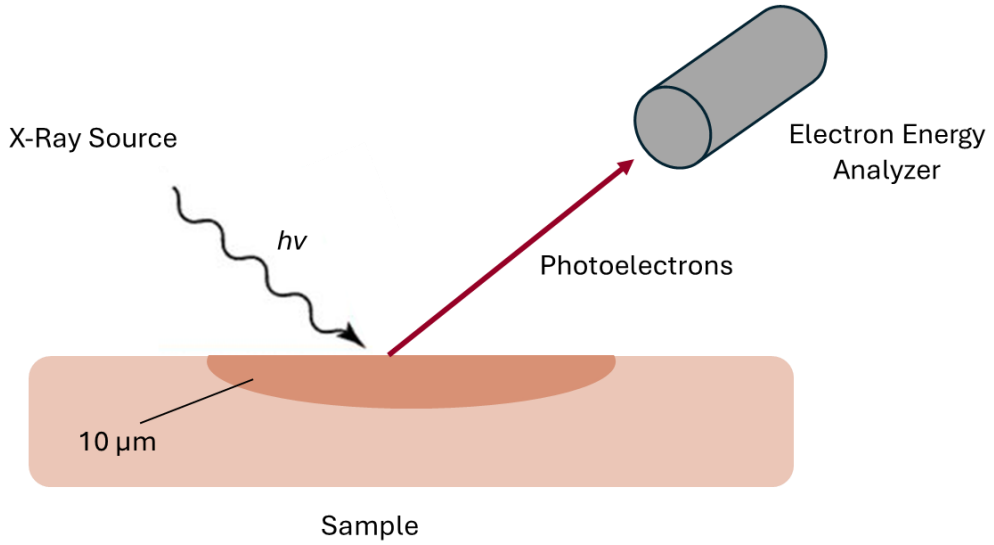

Figure 5.8 – XPS principles of operation.

5.3.4 Particle size analysis

PSA was performed using an LA-920 particle size analyzer (Horiba, Japan). Particles suspended in a solution will diffract light, with smaller particles causing greater diffraction than larger ones. The particle size distribution can be determined by passing a suspension through a laser beam, as illustrated in Figure 5.8. By measuring the scattering of the light, the particle size distribution can be assessed. It is important to note that this method is sensitive to anisotropic particles [526].

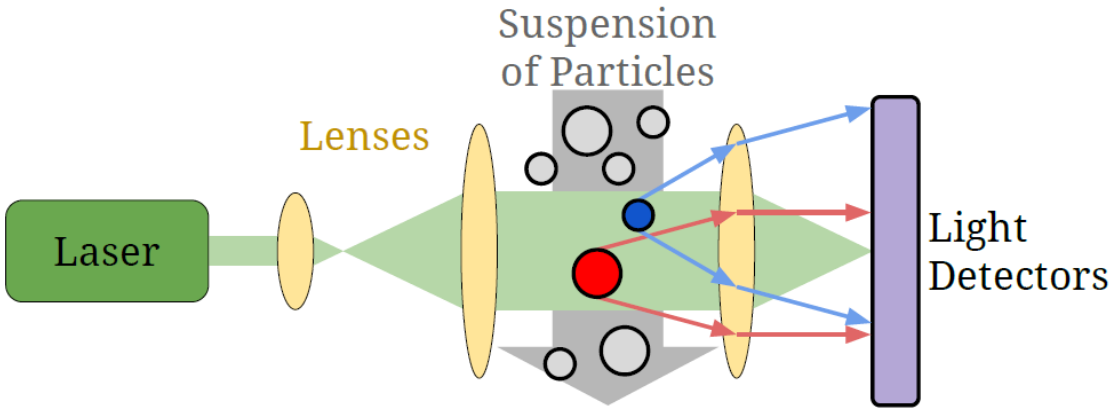

Figure 5.9 - Use of laser diffraction in PSD analysis [353].

5.3.5 Specific surface area (BET)

Specific surface area and adsorption average pore diameter were measured using the nitrogen Brunauer-Emmett-Teller (N2-BET) technique on a TriStar II Plus surface area and porosity analyzer (Micromeritics, U.S.A.).

To measure specific surface area, samples have to be dried under a flow of inert gas or in a vacuum atmosphere to remove any contaminants from the surface. Then, the sample is cooled to cryogenic temperatures, allowing a probe gas to physically adsorb onto its surface. The volume of the adsorbed probe gas is measured to ascertain the amount needed to cover the sample's surface. The Brunauer, Emmett, and Teller (BET) theory is then applied to the adsorption data to calculate the specific surface area, which is reported in units of area per mass of the sample (m^2/g).

5.3.6 ICP-OES

Solution samples taken over time were analyzed ICP-OES using a Thermo Scientific iCAP 6000 series ICP Spectrometer (USA) to measure residual metal ion concentrations. Solution samples were diluted with 4% nitric acid prior to measurements.

The principle of ICP-OES relies on the ability of atoms and ions to absorb energy, causing their electrons to transition from the ground state to an excited state. For the analysis, a liquid sample is converted into an aerosol and ionized by a plasma at 10,000K [553]. The ions are excited to higher energy states and subsequently emit photons as they return to the ground state. Each element has a unique emission spectrum at specific wavelengths, which allows for its identification [553,554]. Schematic of a basic ICP-OES system is shown in Figure 5.9.

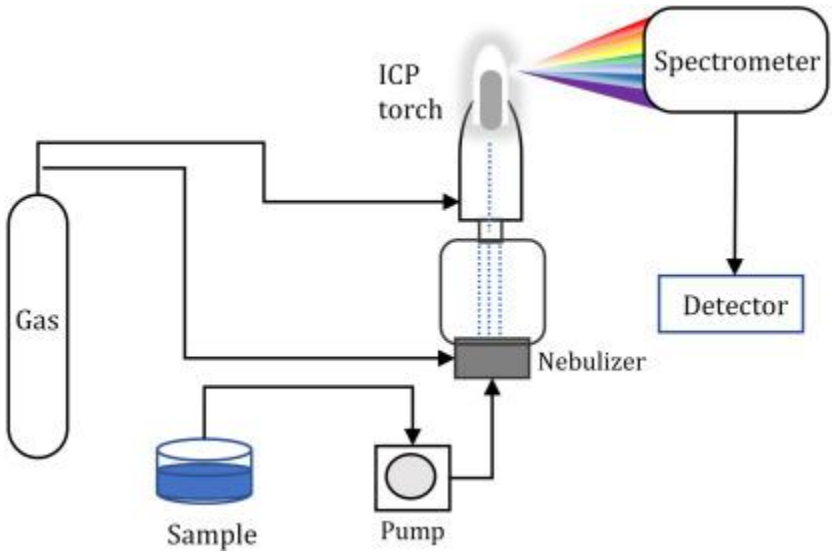

Figure 5.10 - Schematic of a basic ICP-OES system. Reproduced from [553].

5.3.7 VSM

A Lakeshore 8600 Series (Lake Shore Cryotronics, Inc., Westerville, OH, USA) vibrating-sample magnetometer (VSM) was used to measure the magnetic properties of pure zeolites and the synthesized composite magnetic zeolites. Powder samples were loaded in Kel-F powder sample holders and measured at room temperature from 0 to +1.9 T, +1.9 to −1.9 T, and −1.9 T to +1.9T.

Chapter 6
Zeolite Synthesis and Characterization

6.1 Introduction

This chapter covers experimental results of zeolite synthesis and characterization, including non-magnetic and magnetic zeolites.

Unless stated otherwise, with the aim of simplifying their names, the synthesized materials will be referred to as follows: pure synthesized LTA zeolite – LTAZ. Magnetic composites of LTA zeolite with the mixed ratio of 10 g of LTAZ and 0.1 g, 0.5 g, 1 g, and 2g of iron oxide nanoparticles - MZ0.1, MZ0.5, MZ1, and MZ2, respectively. After finding suitable conditions for magnetic modification, magnetic LTAZ is further called M-LTAZ. Zeolite synthesized from coal fly ash will be called CFAZ, and magnetic composite of CFAZ and iron oxide composite at the ratio 10:1 – M-CFAZ.

6.2 Non-magnetic zeolites

6.2.1 LTA Zeolite

Figures 6.1 and 6.2 shows the SEM and EDS images of synthesized zeolite, revealing its cubic particles, which is common for LTA zeolite [555-557], and that it mainly consists of Si, Al, and Na, which are the main elements of zeolites.

PSA and BET characterization revealed the surface area of LTAZ of 425 m^2/g and particle size (d_{90}) of 30 μm.

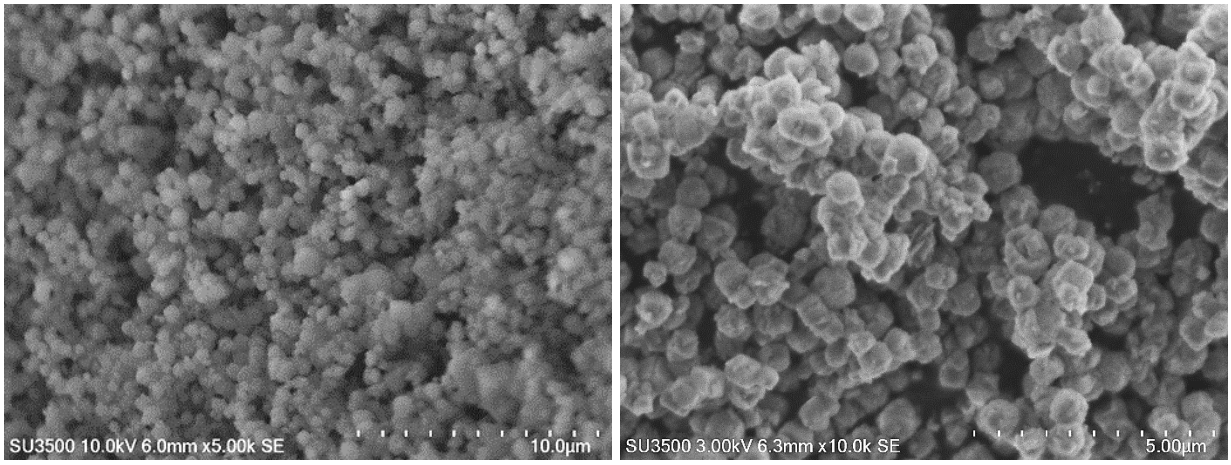

(a) (b)

Figure 6.1 – SEM of synthetic LTA zeolite at different magnifications: (a) 5.00k; (b) 10.00k.

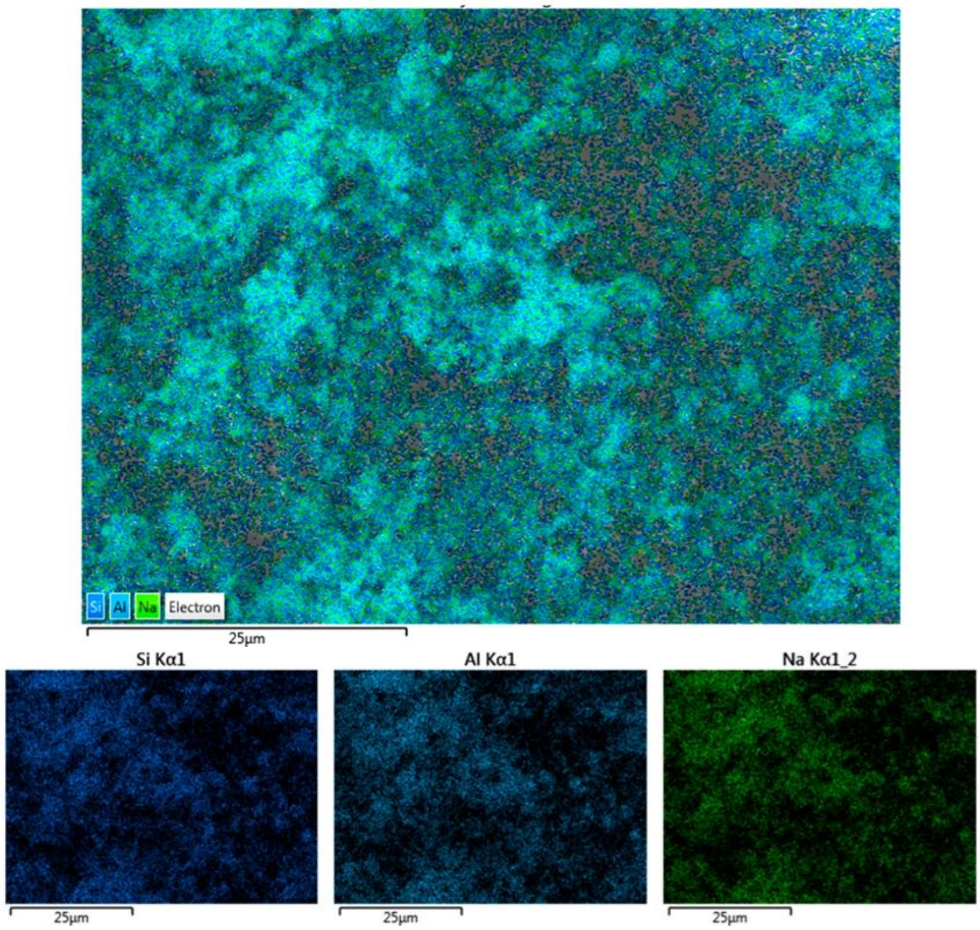

Figure 6.2 - EDS image of synthesized zeolite A indicating the presence of Si, Al, and Na in the sample.

6.2.2 CFA Zeolite

For a deeper insight into the structure and composition of CFAZ, SEM and EDS analysis were conducted. These techniques allow for a detailed examination of the surface morphology of the sample, as well as the identification of its elemental composition.

The SEM images obtained at different magnifications are shown in Figure 6.3, revealing that CFAZ consists primarily of chamfered-edged cubes, consistent with the crystal structure of type A zeolite [558,559].

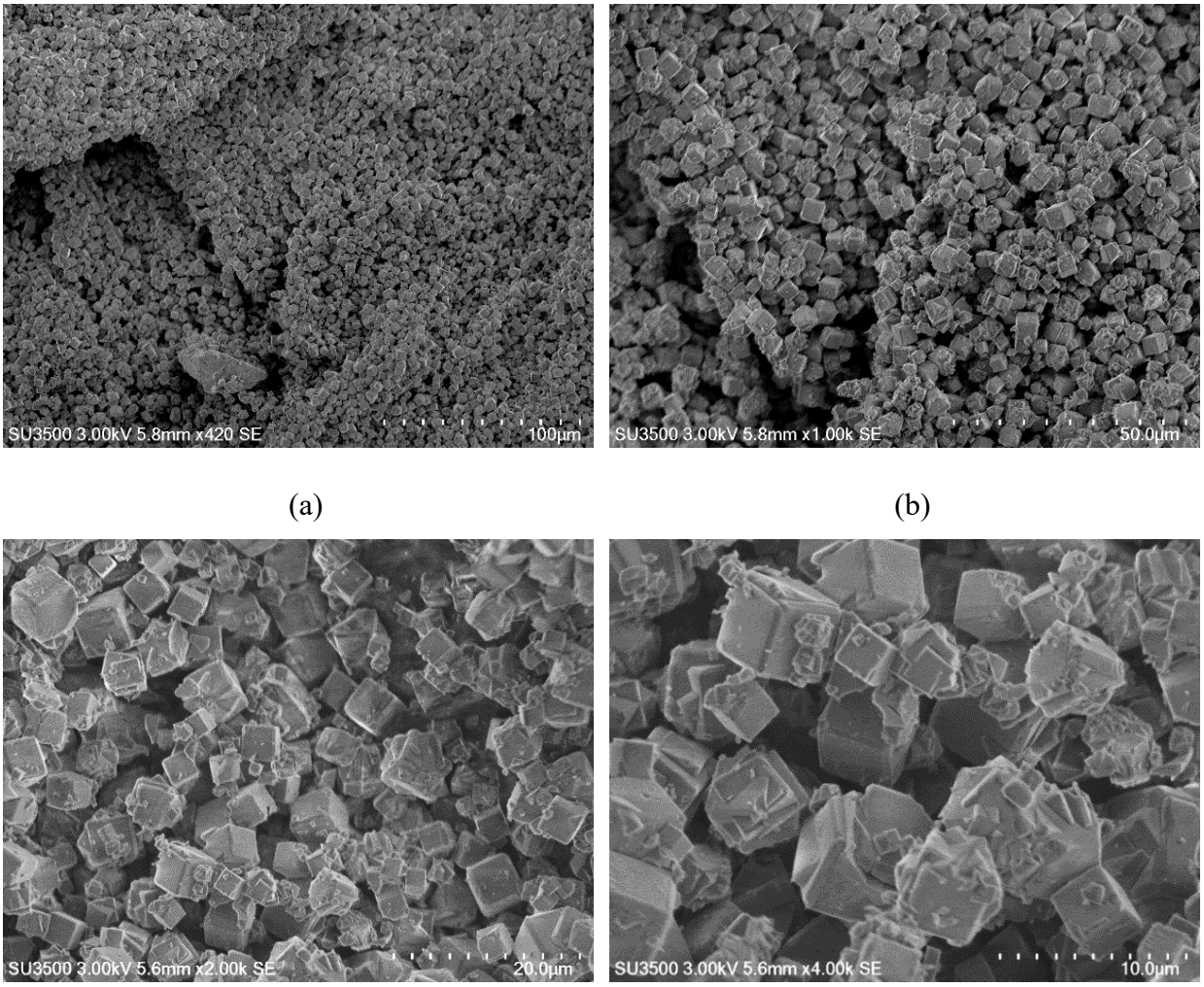

Figure 6.3 – SEM images of CFAZ at magnifications of (a) 400, (b) 1.00k, (c) 2.00k and (d) 4.00k demonstrating a morphology typical for type A (LTA) zeolite.

The EDS mapping analysis in Figure 6.4 shows clear indications for the presence of Na, Si, and Al which are the main zeolite constituents. Additionally, trace amounts of Ca and K originating from the initial CFA used for zeolite synthesis were identified in the sample.

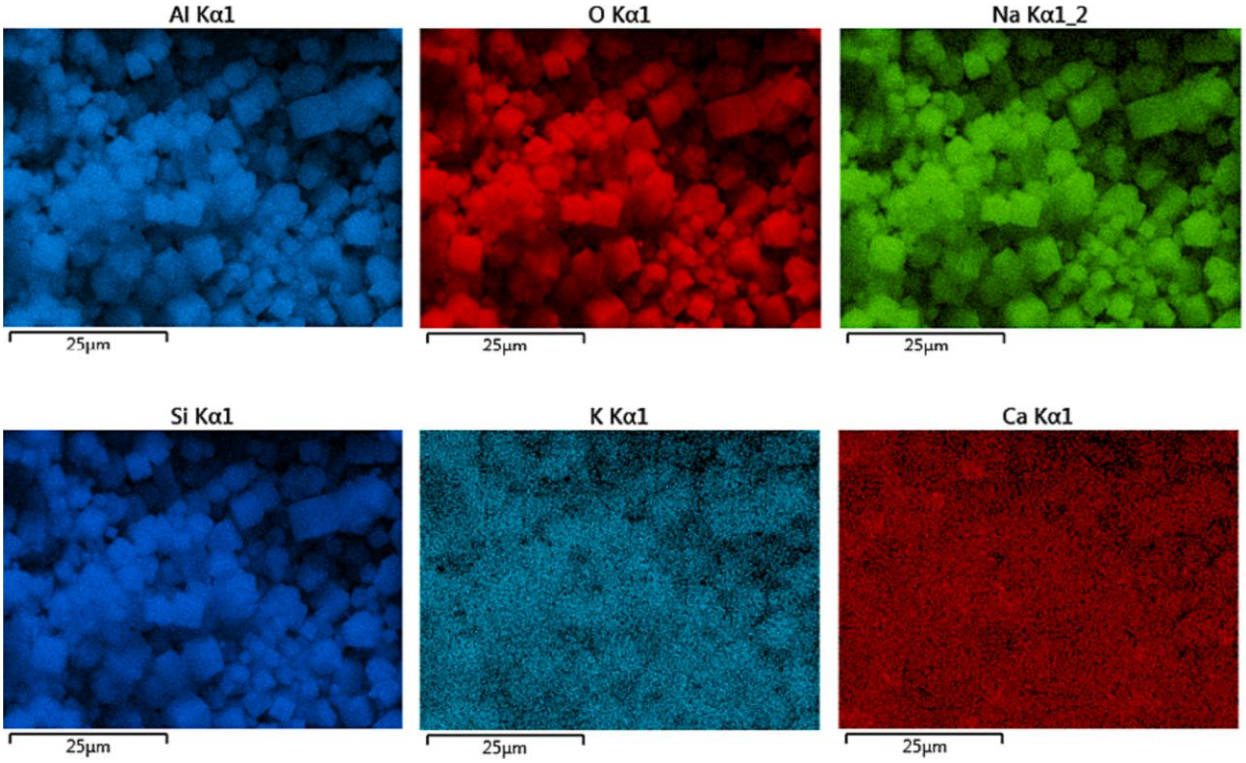

Figure 6.4 - Element mapping-EDS of the area on CFAZ containing Al, O, Na, Si, K, Ca.

PSA and BET characterization revealed the surface area of CFAZ of 70 m^2/g and particle size (d_{90}) of 22 µm.

To characterize LTAZ and CFAZ, dry powder XRD diffractograms were acquired and compared to reference LTA zeolite (type A zeolite) peak positions from the Database of Zeolite Structures. The results are shown in Figure 6.5 and they indicate that both LTAZ and CFAZ exhibit comparable intensities and peak positions to the reference LTA zeolite indicating that both zeolites are also type A or LTA zeolites.

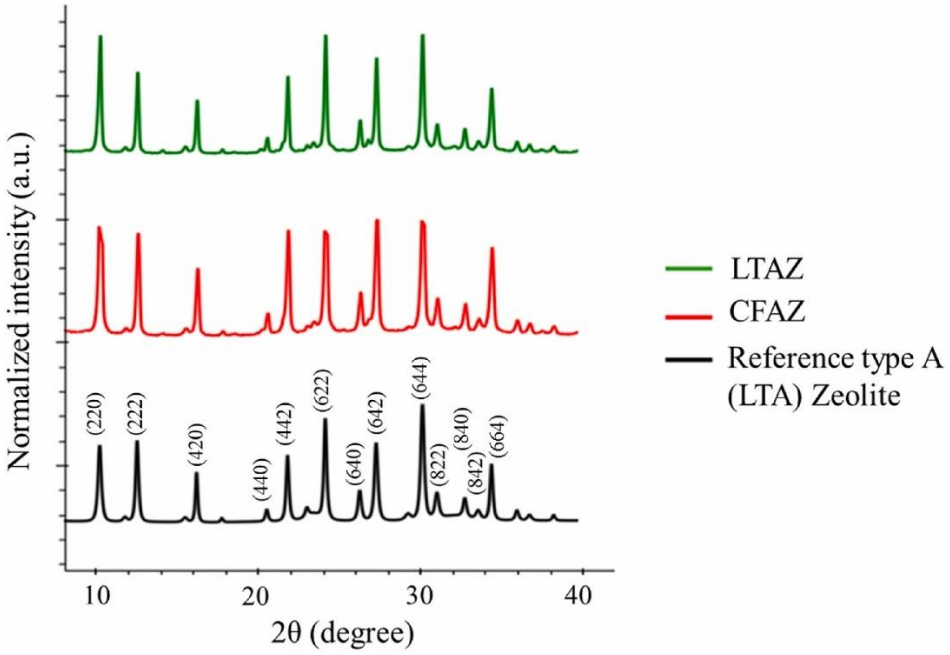

Figure 6.5 – XRD diffractograms of synthesized zeolites LTAZ and CFAZ compared with a reference XRD patterns of type A (LTA) zeolite [280,560], confirming that synthesized zeolites are LTA type zeolites.

6.3 Magnetic Zeolites

6.3.1 Magnetic LTA Zeolite

Magnetic LTAZ:iron oxide composites were synthesized with different iron oxide loadings to investigate how the amount of added iron oxide would affect adsorption capacity of synthesized zeolite and to find suitable conditions for magnetic zeolite synthesis for the purpose of this research. The synthesized zeolites were characterized using XRD, and the acquired diffractograms were compared with each other and with a reference comprising LTA zeolite and iron oxide. It can be seen from Figure 6.6 that the pure zeolite diffractogram has the same peak positions and similar intensities as the reference LTA zeolite. Furthermore, it can be seen that MZ0.1–MZ1 have peaks corresponding to the positions of iron oxide reference peaks at 18.31° and 35.47° (2θ). Additionally, it is observed that with an increase in the number of added iron oxide nanoparticles to the synthesis process, the peak intensities also increase, i.e., MZ1 has higher peaks than MZ0.5 and MZ0.1.

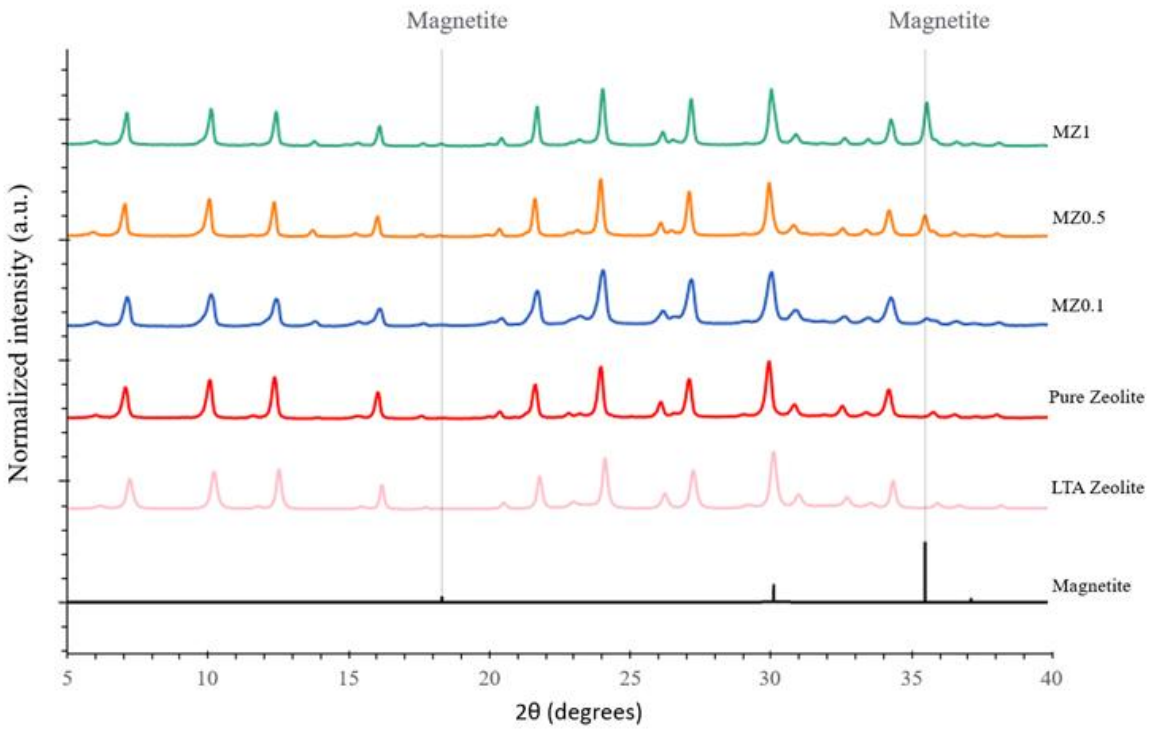

Figure 6.6 – XRD patterns of synthesized zeolites (LTAZ, MZ0.1, MZ0.5 and MZ1) compared to reference XRD patterns of LTA zeolite and magnetite.

Figure 6.7 shows SEM image of M-LTAZ showing that morphology of magnetic zeolite did not change compared to non-magnetic LTAZ shown in Figure 6.1.

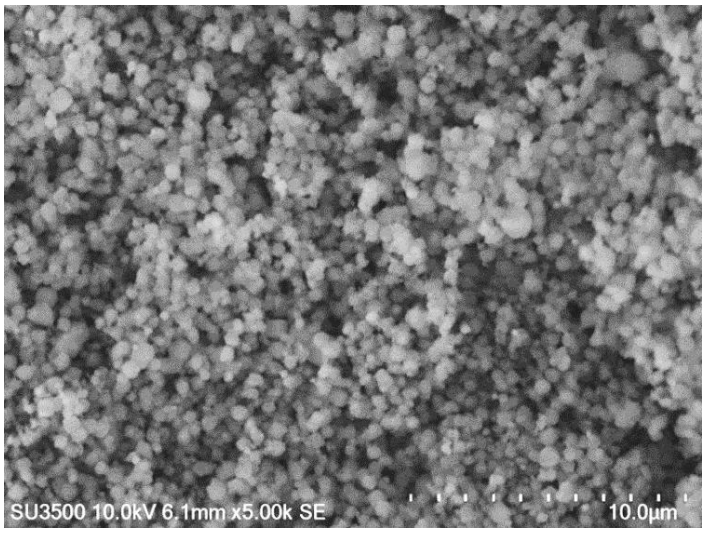

Figure 6.7 – SEM image of M-LTAZ.

The results of surface area and particle size measurements are presented in Table 6.1.

Table 6.1 – Surface characterization of synthesized zeolites

Adsorbent material	**Iron oxide nanoparticles added to the synthesis process, g**	**Surface area, m^2/g**	**Particle size d_{80}, µm**
LTAZ	0	425	30
MZ0.1	0.1	296	58
MZ0.5	0.5	280	64
MZ1	1	253	62

The results of the Vibrating Sample Magnetometry (VSM) characterization of LTAZ compared to synthesized magnetic zeolites MZ1 and MZ2 and to the iron oxide nano-particles are shown in Figure 6.8. The pure zeolite is slightly diamagnetic and appears as a flat line in Figure 6.8a, but the diamagnetic trend can be seen more clearly in Figure 6.8b. Figure 6.8c shows a very small hysteresis for the iron oxide nanoparticles, MZ1, and MZ2. The results show that the iron oxide nanoparticles exhibit superparamagnetic properties, and as the slightly diamagnetic zeolite is combined with the iron oxide nanoparticles in increasing quantities, the saturation magnetization decreases. The saturation magnetization is highest for the pure iron oxide nanoparticles, lower for MZ2, with the lower zeolite content, and lower still for the MZ1, which has the highest zeolite content.

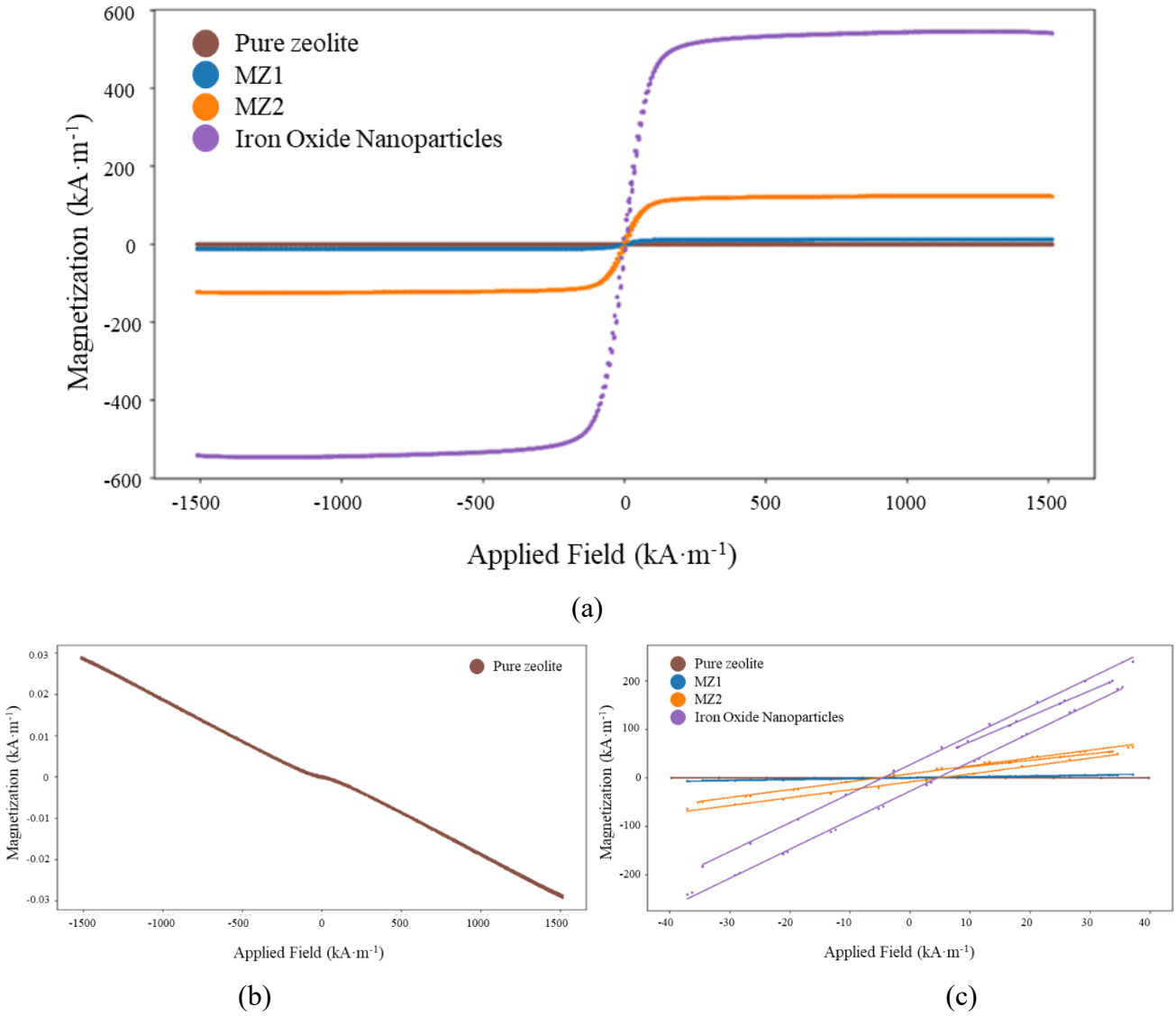

Figure 6.8 - Vibrating Sample Magnetometry comparison of: (a) pure zeolite, MZ1, MZ2 and iron oxide nanoparticles; (b) Pure zeolite with scaled Y-axis, highlighting slightly diamagnetic properties; (c) All samples, zoomed in between -50 and +50 kA m^{-1}, showing very slight hysteresis.

Synthesized magnetic LTA zeolites were investigated for Cu removal from water as described in Section 7.3. The results shown that there is no significant difference in adsorption capacity of magnetic zeolites with different iron oxide loadings. Thus, for further magnetic CFA zeolite synthesis 10:0.1 loadings were investigated.

6.3.2 Magnetic CFA Zeolite

M-CFAZ was successfully synthesized in multiple batches. Figure 6.9 shows dried M-CFAZ (a) and its ability to be attracted and attach to a low intensity magnet (b).

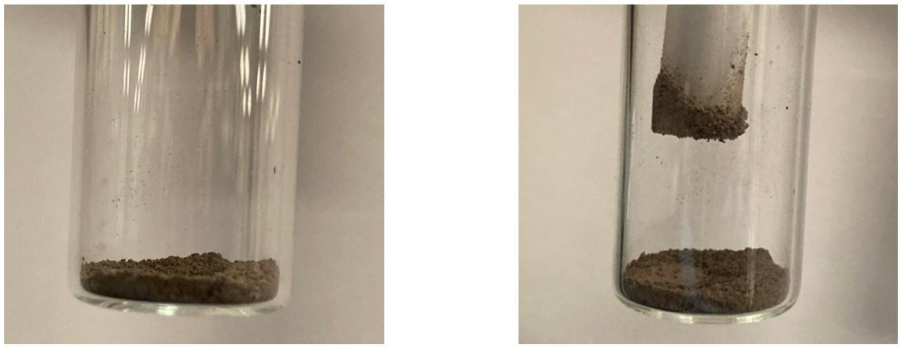

(a) (b)

Figure 6.9 – Synthesized (a) M-CFAZ; (b) M-CFAZ attached to the low intensity magnet.

SEM images of M-CFAZ microstructure at different magnifications are shown in Figure 6.10. Figure 6.11 shows the SEM-EDS analysis confirming the presence of iron (red color) in the synthesized composite zeolite material. More SEM-EDS scans of magnetic zeolite particles are presented in Appendix C.

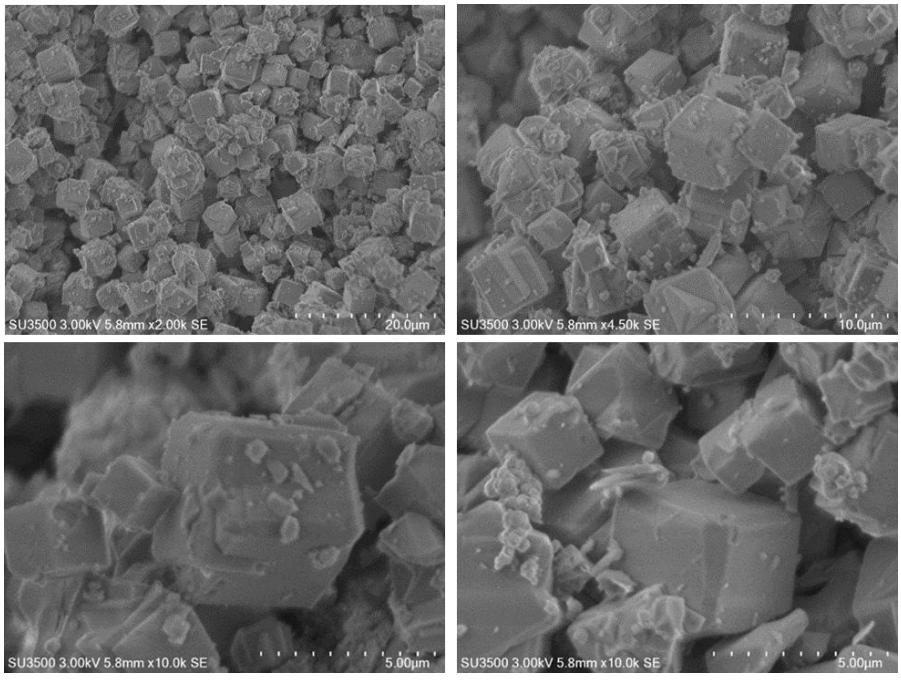

Figure 6.10 – SEM images of M-CFAZ at different magnifications.

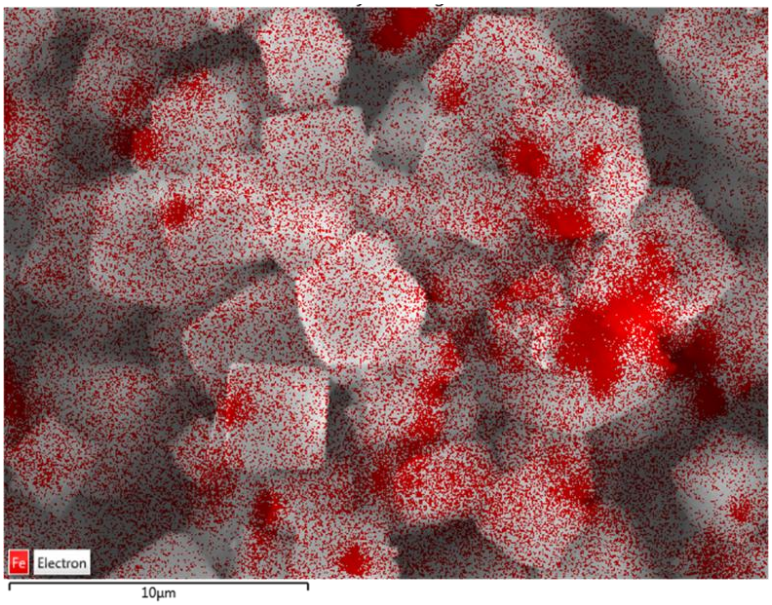

Figure 6.11 - Element mapping-EDS results of the M-CFAZ indicating the presence of iron in the synthesized composite material.

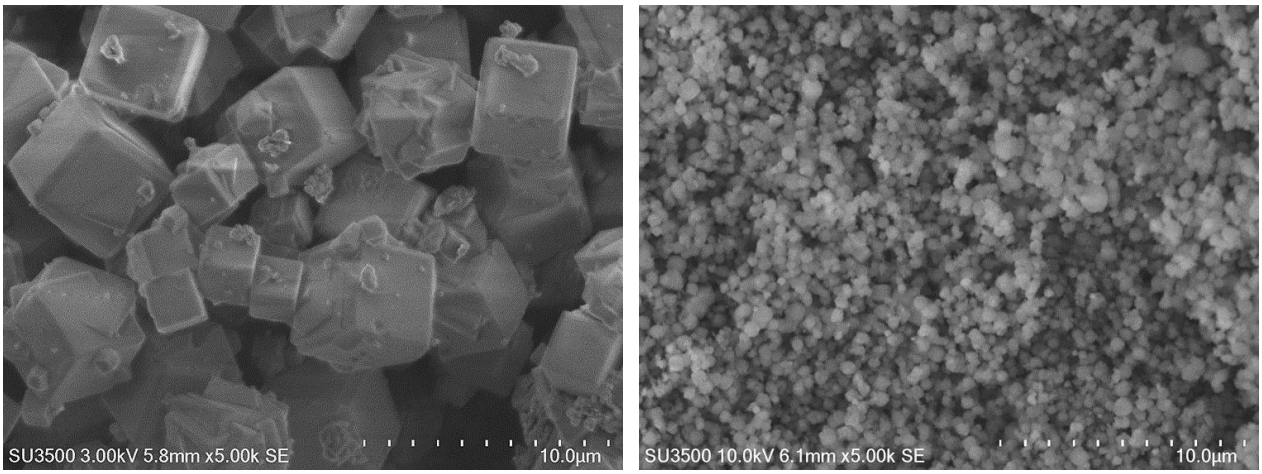

(a) (b)

Figure 6.12 – SEM images of (a) M-CFAZ and (b) M-LTAZ.

The results of M-CFAZ and M-LTAZ SEM comparison at the scale of 10 µm are shown in Figure 6.12. As can be seen from the images, the particles are cubically shaped, which is common for zeolite type A, further confirming previous results from XRD analysis.

Additionally, Figure 6.12 demonstrates that the M-CFAZ (a) has a larger particle size compared to M-LTAZ (b) in the SEM-analyzed areas of the sample. In addition to that, surface area characterization (BET) was conducted on both M-CFAZ and M-LTAZ. The results shown in Table 6.2 indicate that M-CFAZ has a smaller surface area, meaning that there are fewer available sites for adsorption per unit mass.

Table 6.2 – Surface characterization of synthesized magnetic zeolites.

	Surface area, m^2/g	**Adsorption average pore diameter, Å**
M-CFAZ	2.5	79
M-LTAZ	296	29

The VSM characterization of CFAZ with the addition of 1 g nano-magnetite (CFAZ-M1) and 0.1 g nano-magnetite (CFAZ-M2) are compared to nano-magnetite and shown in Figure 6,13a. CFAZ with the addition of 0.1 nano-magnetite appears as the almost flat line in Figure 6,13a, CFAZ with the addition of 1 g nano-magnetite (M-CFAZ or CFAZ-1) shows larger magnetic response, and nano magnetite exhibits superparamagnetic properties. All samples, zoomed in between -40 and +40 kA m^{-1} are shown in Figures 6,13b-d.

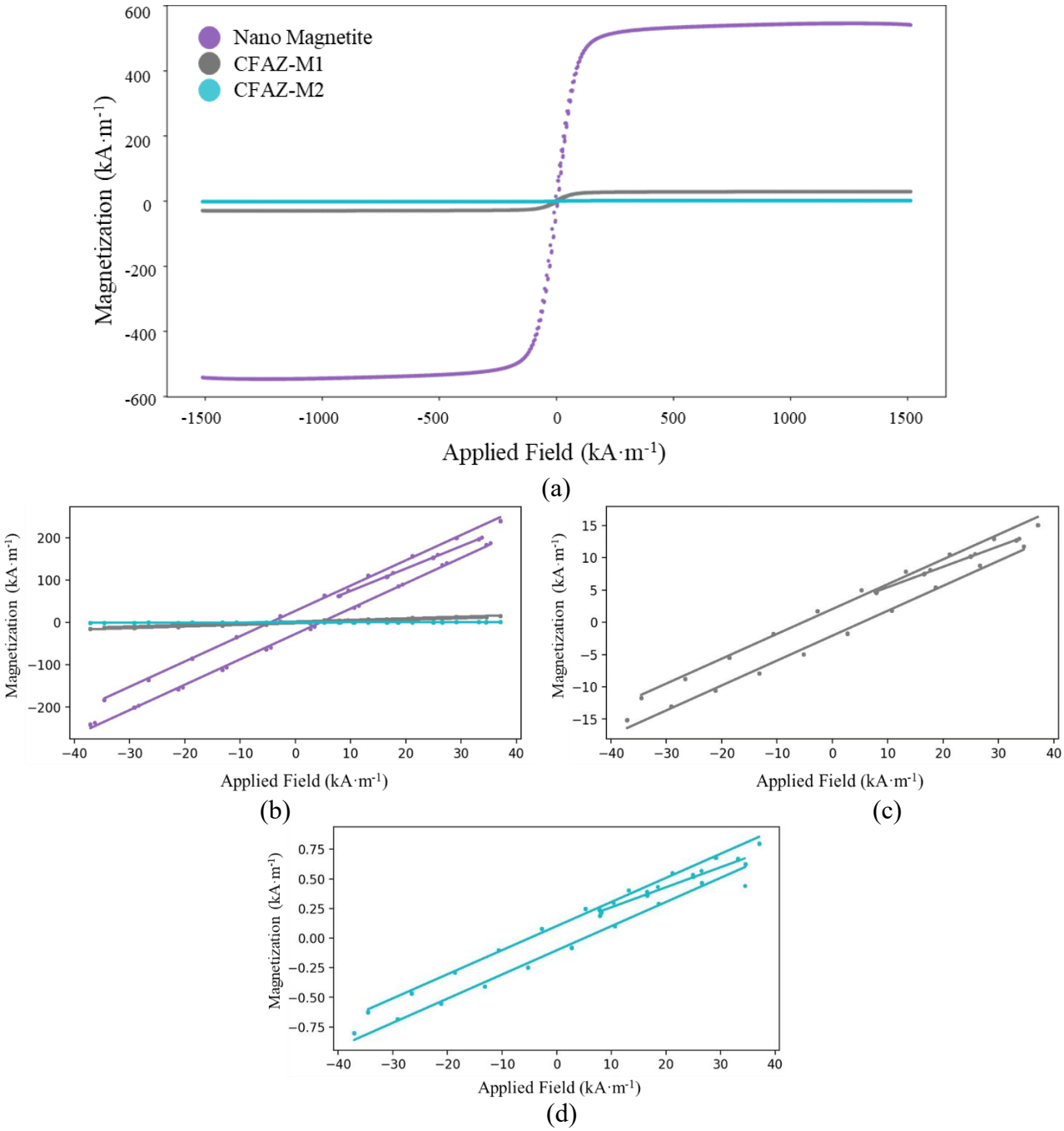

Figure 6.13 – Vibrating Sample Magnetometry comparison of CFAZ-M1, CFAZ-M2 and nano-magnetite showing slight paramagnetic properties of: CFAZ-M2 and superparamagnetic properties of CFAZ-M1 or M-CFAZ (a), all samples zoomed in between -40 and +40 kA m^{-1} (b), CFAZ with the addition of 1 g nano-magnetite – CFAZ-M1 (c) and CFAZ with the addition of 0.1 g nano-magnetite - CFAZ-M2 (d).

6.4 Summary

This chapter showed the results of LTA and CFA zeolite synthesis and their characterization and further modification of these zeolite into magnetic zeolite composites M-LTAZ and M-CFAZ.

XRD results showed that both synthesized LTAZ and CFAZ have similar crystalline structure that is also corresponding to type A (LTA) zeolite from the reference database. SEM results in this chapter show the cubic morphology of zeolite particles, typical for zeolite type A.

Magnetic zeolite composites were successfully synthesized using novel method by binding iron oxide nanoparticles to zeolite using PVA solution. Magnetic zeolite composites were synthesized at different loadings of iron oxide nanoparticles. The XRD, SEM, and VSM characterization results confirm the presence of iron in the synthesized magnetic zeolite. Furthermore, they demonstrate that the magnetic properties of the composite are enhanced with the increased addition of iron oxide.

Surface area and particle size analysis revealed that LTAZ exhibits a higher surface area and smaller particle size compared to CFAZ. Additionally, the surface area decreases following magnetic modification, whereas particle size increases for both M-LTAZ and M-CFAZ. These results are summarized in Table 6.3.

Table 6.3 – Surface characterization of synthesized zeolites.

	Surface area, m^2/g	**Particle size d_{90}, µm**
LTAZ	425	30
M-LTAZ	296	58
CFAZ	70	22
M-CFAZ	2.5	110

Chapter 7
Adsorption Experiments

7.1 Introduction

This chapter shows the results of heavy metals removal from water using LTAZ, CFAZ, M-LTAZ and M-CFAZ. Zeolites were also characterized after adsorption to confirm the presence of adsorbed metal ions.

7.2 Adsorption Experiments using Non-Magnetic Zeolites

7.2.1 CFA Zeolite

Figures 7.1a and 7.1b illustrate that there were notable differences in both the kinetics and equilibrium concentrations across the studied metal ions. The Pb ions were rapidly and completely adsorbed within 1 minute, whereas Cu reached an equilibrium concentration of 52 mg/L after approximately 24 hours. A similar time period is required for Zn ions to equilibrate at 123 mg/L, while Ni required approximately 90 hours to reach the equilibrium concentration of 170 mg/L. Based on these results, the adsorption capacity of CFAZ for Cu, Zn and Ni were estimated to be 248 mg/g (3.5 mg/m^2), 177 mg/g (2.5 mg/m^2) and 130 mg/g (1.9 mg/m^2), respectively. To determine the maximum adsorption capacity of CFAZ for Pb ions, an additional experiment was performed with a higher concentration of Pb ions. At an initial concentration of 1000 mg/L, Pb reached equilibrium at 507 mg/L after 1 hour. Based on this an adsorption capacity of CFAZ for Pb was calculated to be 493 mg/g (7 mg/m^2). The results of kinetics study and calculated maximum adsorption capacities of CFAZ for single ions adsorption can be found in Table 7.1.

By comparing the obtained results with the most effective CFA zeolite previously reported in literature and described in Section 2.4.2 for the investigated metal ions, it was observed that the CFA zeolite synthesized in this work demonstrates higher or comparable adsorption capacities to those reported in the literature. The data used for the comparison is represented in Table 7.1 and the outcomes are illustrated in Figure 7.1c.

The amount of adsorbed metal in mg of metal per g of zeolite was calculated using Equation 7.1:

$$Q = \frac{C_0 - C_e}{m} \times V \qquad 7.1$$

where Q is adsorption capacity (mg/g), V is solution volume (L), m is the adsorbent dosage (g), C_0 and C_e are the initial concentrations of metal ions in solution and after the adsorption process, respectively (mg/L).

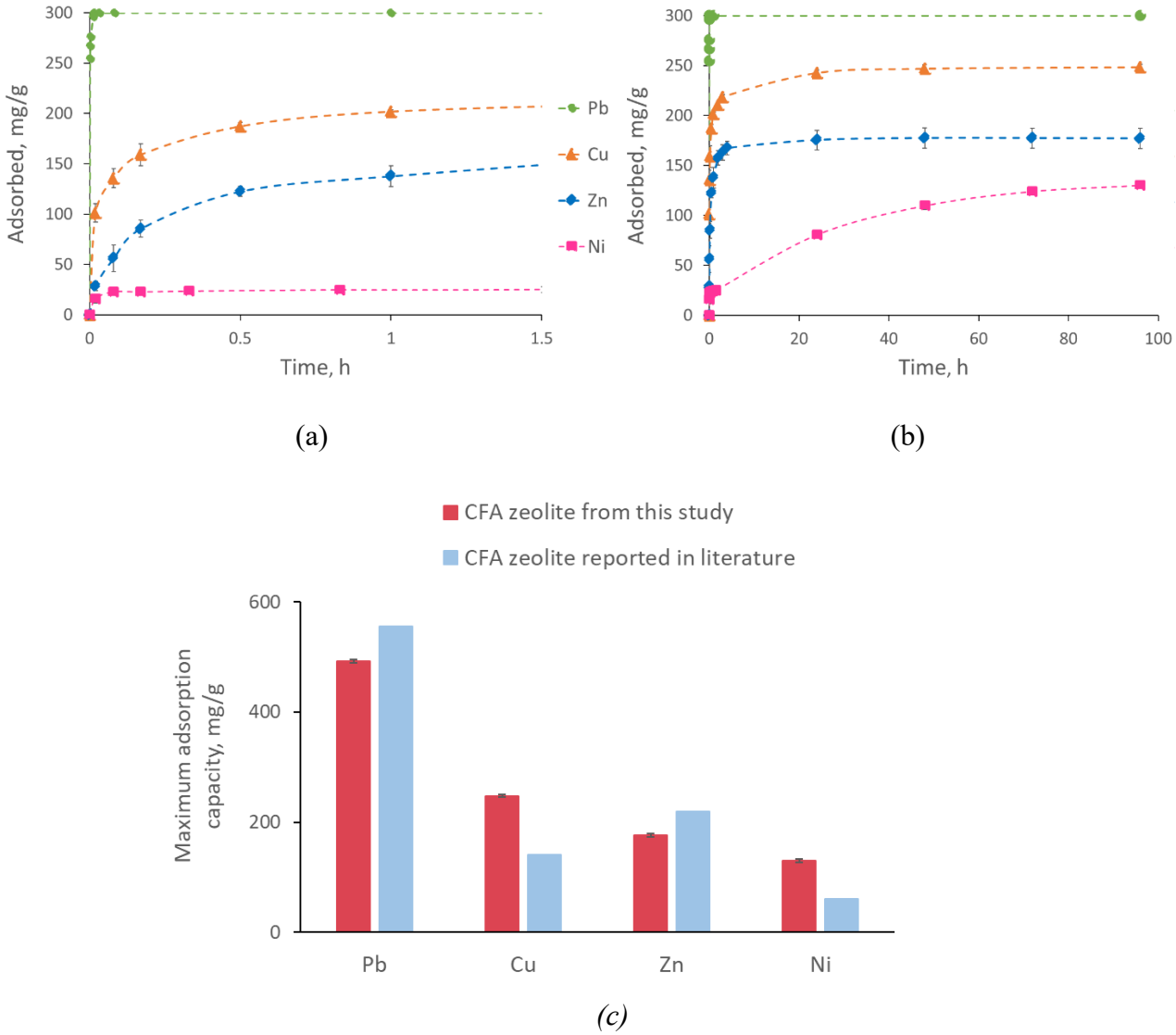

Figure 7.1 – Adsorption kinetics of single ions systems of Pb^{2+}, Cu^{2+}, Zn^{2+} and Ni^{2+} on CFAZ over (a) 1.5 hours and (b) 96 hours; (c) A comparison of maximum adsorption capacities of CFAZ and top performers CFA derived zeolites reported in literature *[3,188,221,222,410,561-563]*.

Table 7.1 – Comparison of maximum adsorption capacities of CFA synthesized zeolite in single ion systems.

Metal ion	Adsorption capacity, mg/g	References
Pb	493±4	*This study*
	556	Jangkorn et al. [564]
	409	Li et al. [563]
	66	Wang et al. [410]
Cu	248±3	*This study*
	96	Sireesha et al. [188]
	69–141	Song et al. [561]
	71	Wu et al. [562]
Zn	177±10	*This study*
	220	Izidoro et al. [222]
	205	Izidoro et al. [222]
	40	Zhang et al. [221]
Ni	130±2	*This study*
	61	Sireesha et al. [188]
	47	He et al. [3]
	34	He et al. [3]

Adsorption experiments were also carried out under the same conditions in mixed ion systems with the same metal ions. The initial concentration of each metal ion in solution was 300 mg/L and a volume of 100 mL, while the quantity of CFAZ was varied between 0.1 g (Figure 7.2a) and 0.4 g (Figure 7.2b, 7.2c).

The results revealed a similar trend to the one observed in single ion adsorption experiments with a rapid Pb adsorption, and gradually decreasing concentration for Cu, Zn and Ni. Specifically, for the experiment with 0.1 g zeolite, within the first hour of the adsorption experiments, Pb and Cu attained equilibrium concentrations of 24 and 206 mg/L, respectively, while no noticeable

adsorption was observed for Ni and Zn. Moreover, it was observed that the equilibrium concentration was consistently greater for Pb and Cu when compared to single ion adsorption experiments. In the experiment with 0.4 g zeolite and 100 mL of mixed ions solution, Pb ions were rapidly adsorbed within 3 minutes, Cu equilibrated at 4 mg/L after approximately 4 hours, Zn equilibrated at a concentration of 72 mg/L after 90 hours, whereas the Ni concentration did not change from the initial one over time. Based on these experiments, the adsorption capacity of CFAZ for mixed ions was calculated as 276 mg/g (3.9 mg/m^2), 94 mg/g (1.3 mg/m^2) for Pb and Cu ions and no adsorption was achieved for Zn and Ni ions, when 0.1g of CFAZ was added. Similarly, when 0.4 g CFAZ was added into the same system, the adsorption capacity was calculated as 300 mg/g (4.3 mg/m^2), 296 mg/g (4.2 mg/m^2) and 228 mg/g (3.3 mg/m^2) for Pb, Cu and Zn ions, respectively. No adsorption was observed for Ni ions.

The reason for the observed selectivity order of $Pb^{2+} > Cu^{2+} > Zn^{2+} > Ni^{2+}$ may be due to a variety of factors, including molar weight, ionic radius, hydration enthalpies, hydration radii, and solubility of the cations [363,410]. Additionally, the zeolite framework structure, such as the pore size and the amount of exchangeable Na ions bonded to zeolite framework will be an important factor [565]. For example, the smallest ions should be adsorbed faster and in larger quantities due to their ability to pass through the micropores and channels [451]. The hydration radii of the investigated metal ions are 4.01 Å, 4.04 Å, 4.19 Å, 4.30 Å for Pb^{2+}, Ni^{2+}, Cu^{2+} and Zn^{2+}, respectively [566]. Therefore, according to the hydration radii, Pb ions should be adsorbed faster then other ions which is in line with the findings of this study. However, the suggested selectivity order based on the hydration radii, should be $Pb^{2+} > Ni^{2+} > Cu^{2+} > Zn^{2+}$ which is different from the observed experimental selectivity order of $Pb^{2+} > Cu^{2+} > Zn^{2+} > Ni^{2+}$. The difference in the series may be indicative of the complexity of the process and the possibility that other mechanisms could be contributing to the removal of heavy metals from solution [363].

A comparison of mixed ions adsorption in the systems with the addition of 0.1 g and 0.4 g CFAZ, showed that an increase in the amount of added zeolite leads to faster adsorption kinetics and enhances the adsorption capacity for metal ions. Thus, with the increase of zeolite dosage, better and faster adsorption could be achieved. The results described in this section are summarized in Table 7.2.

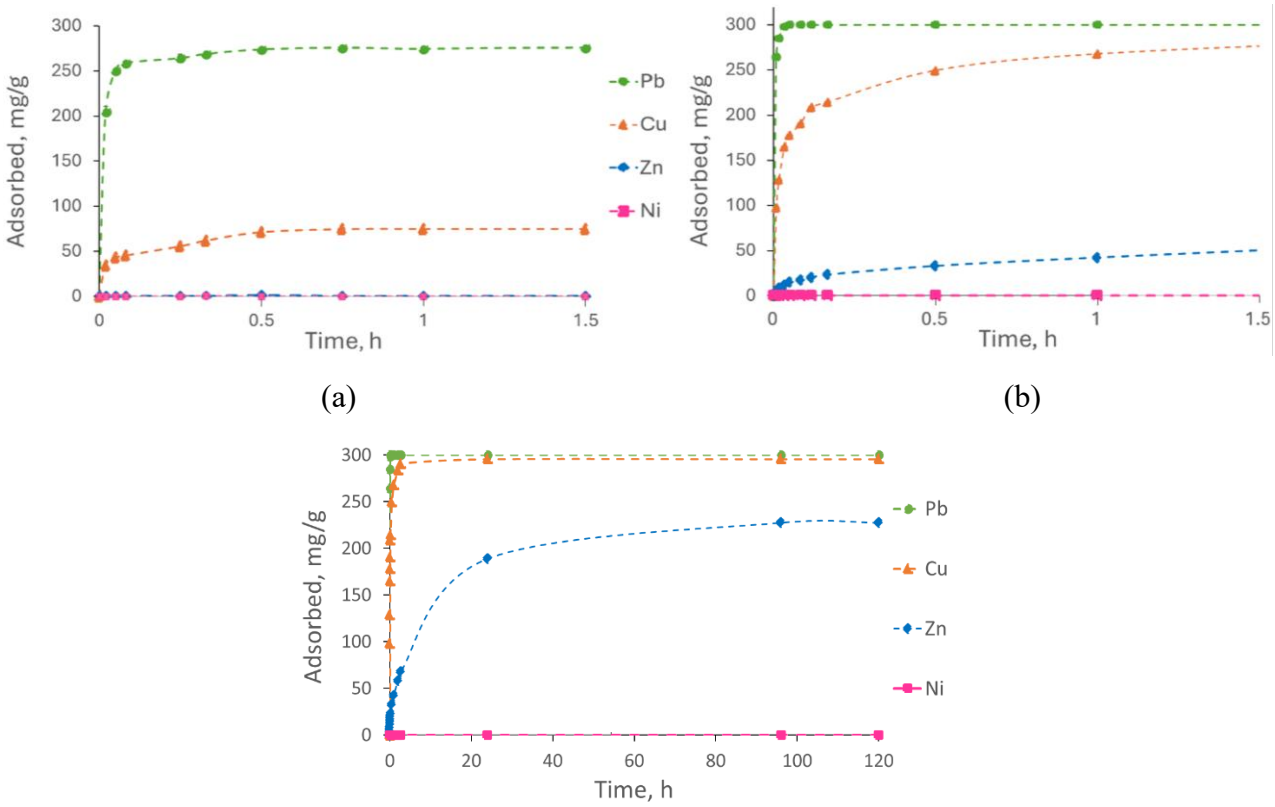

Figure 7.2 – Adsorption kinetics of a mixed ion solution comprised of 300 mg/L Pb^{2+}, Cu^{2+}, Zn^{2+} and Ni^{2+} with 0.1 g in (a) 1.5 hours and (b) 0.4 g CFAZ in 1.5 hours and (c) 0.4 g in 100 hours.

Table 7.2 – Experimental results on adsorption capacity of CFAZ for selected metal ion systems for single and mixed ions systems at the constant solution volume of 100 mL and pH 6.

Metal ion	**Initial concentration, mg/L**	**Equilibrium concentration, mg/L**	**Adsorbed, mg/g**	**Adsorbed, mg/m²**	**Adsorbent Dosage, g/L**
Single ions					
Pb	1000	507	493±4	7.0	1
Cu	300	52	248±3	3.5	1
Zn	300	123	177±10	2.5	1
Ni	300	170	130±2	1.9	1

Metal ion	**Initial concentration, mg/L**	**Equilibrium concentration, mg/L**	**Adsorbed, mg/g**	**Adsorbed, mg/m²**	**Adsorbent Dosage, g/L**
Mixed ions (low CFAZ dosage)					
Pb	300	24	276±1.3	3.9	1
Cu	300	206	94±2	1.3	1
Zn	300	300	0	0	1
Ni	300	300	0	0	1
Mixed ions (high CFAZ dosage)					
Pb	300	0	300±0	4.3	4
Cu	300	4	296±1	4.2	4
Zn	300	72	228±1	3.3	4
Ni	300	300	0	0	4

To provide a point of comparison between CFAZ and other adsorbents Langmuir and Freundlich adsorption models were fit to the experimental data and adsorption parameters derived are summarized in Table 7.3.

The Langmuir model assumes that adsorption takes place through the formation of a monolayer of adsorbate molecules on the homogeneous surface of the adsorbent. It can be described by the following equation [567,568]:

$$q_e = \frac{Q_{sat} K_L C_e}{1 + K_L C_e} \qquad 7.2$$

where Q_{sat} is the monolayer adsorption capacity, mg/g; K_L—Langmuir constant related to adsorption capacity obeyed by the free adsorption energy, L/mg. The linear form of Equation (7.2) is presented as follows [568]:

$$\frac{C_e}{q_e} = \frac{1}{q_m K_L} + \frac{1}{q_m} C \qquad 7.3$$

When adsorption involves the formation of multiple layers of adsorbate molecules on a heterogeneous surface of the adsorbent, the process can be described by the Freundlich adsorption model that is described mathematically as [567,568]:

$$q_e = K_f C_e^{1/n} \qquad 7.4$$

where K_f is the Freundlich constant related to the adsorption capacity, L/g; n—adsorption intensity, describing the heterogeneity of the adsorbate sites.

Figures 7.3-7.6 show Langmuir nonlinear, Langmuir linear and Freundlich adsorption isotherm fits for Pb^{2+}, Cu^{2+}, Zn^{2+} and Ni^{2+} single ion adsorption onto CFAZ. The isotherm parameters are listed in Table 7.3. As can be seen, the correlation coefficient (R^2) for all the investigated models is >0.99.

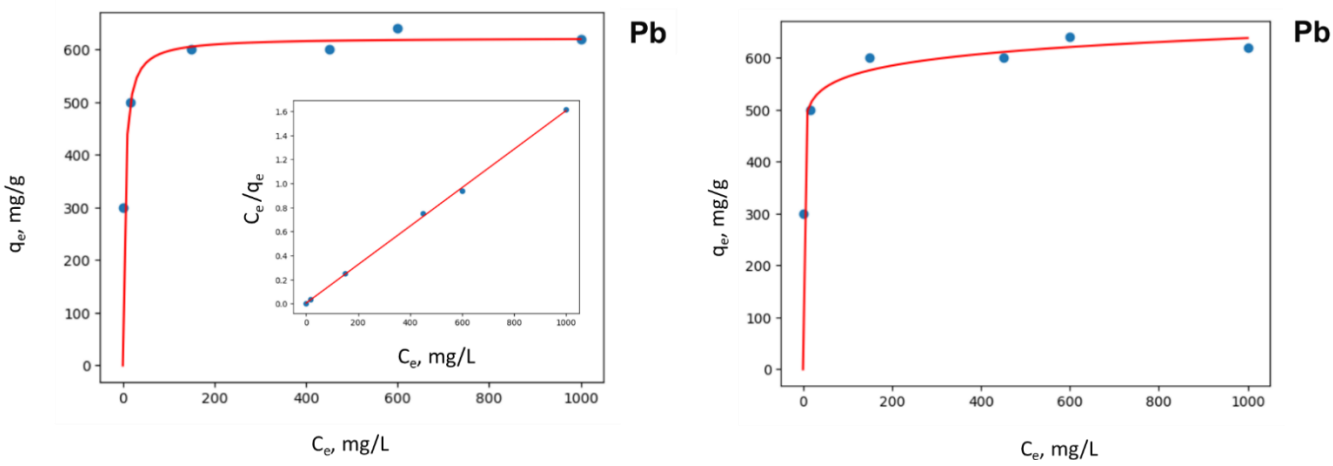

(a) *(b)*

Figure 7.3 - Adsorption isotherms of Pb^{2+} fit to: (a) Langmuir non-linear and linear models; (b) Freundlich model.

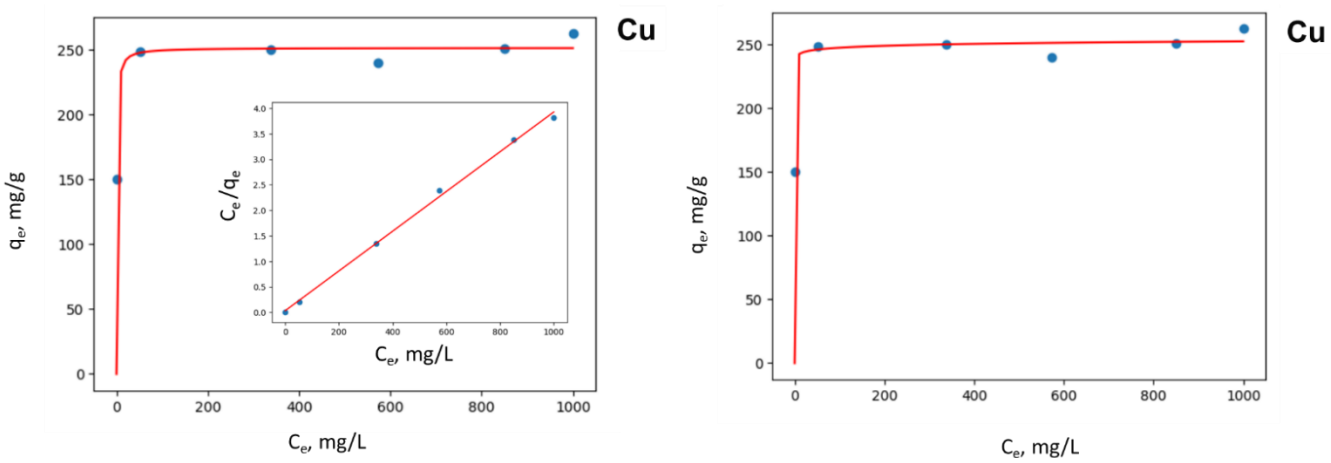

(a) *(b)*

Figure 7.4 - Adsorption isotherms of Cu^{2+} fit to: (a) Langmuir non-linear and linear models; (b) Freundlich model.

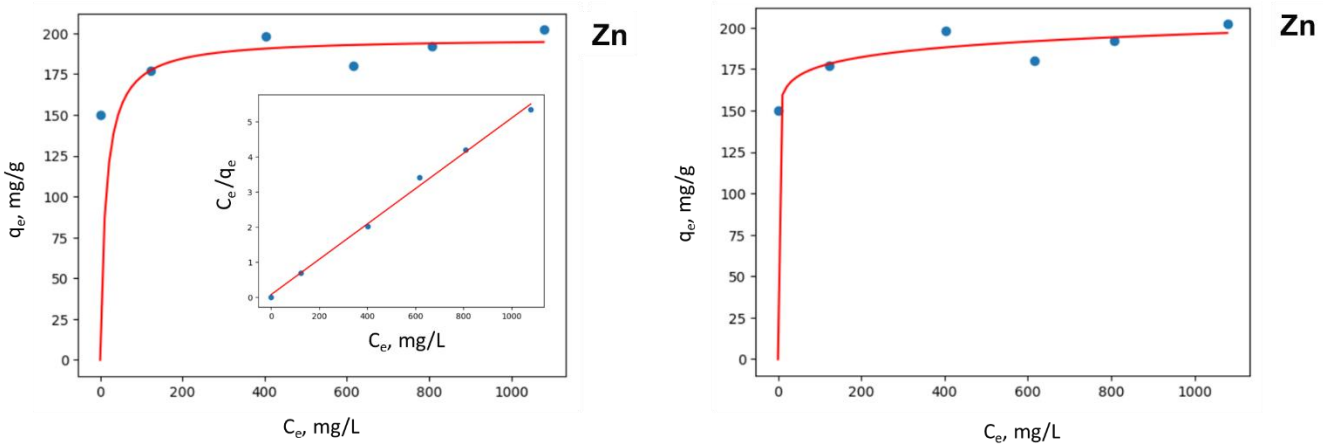

(a) *(b)*

Figure 7.5 - Adsorption isotherms of Zn^{2+} fit to: (a) Langmuir non-linear and linear models; (b) Freundlich model.

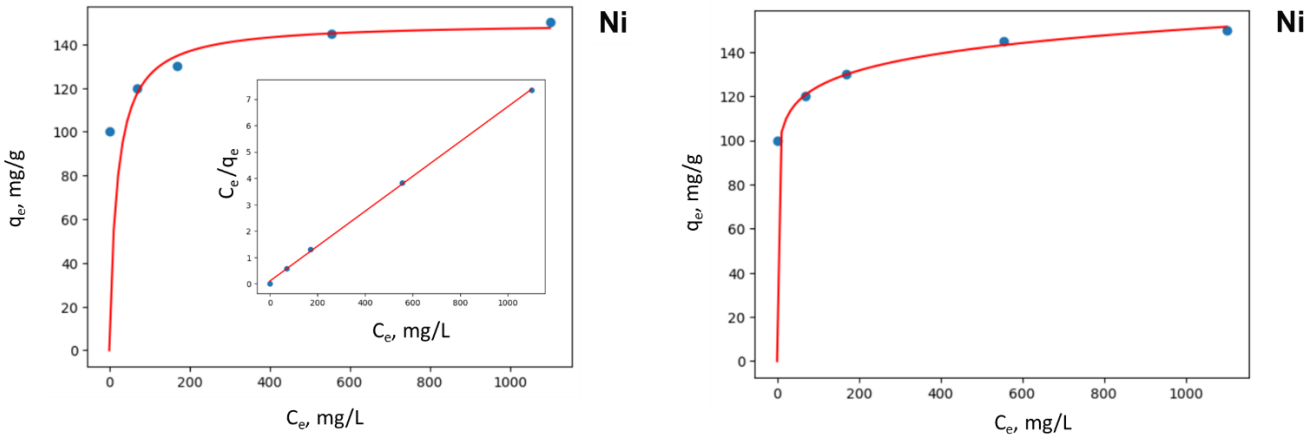

(a) *(b)*

Figure 7.6 - Adsorption isotherms of Ni^{2+} fit to: (a) Langmuir non-linear and linear models; (b) Freundlich model.

Table 7.3 – Isotherm parameters for different models obtained from the adsorption of heavy metals in single ion systems for adsorption of Pb^{2+}, Cu^{2+}, Zn^{2+} and Ni^{2+} ions on CFAZ.

Thermodynamic Model	**Model parameters**	**Pb adsorption**	**Cu adsorption**	**Zn adsorption**	**Ni adsorption**
Langmuir nonlinear model	Q_{sat}, mg/g	622	251	197	150
	K_L, L/mg	0.23	1.27	0.07	0.05
	R^2	0.997	0.995	0.991	0.998
Langmuir linear model	Q_{sat}, mg/g	624	257	199	151
	K_L, L/mg	3.64	8.96	15.39	16.12
	R^2	0.998	0.998	0.995	0.999
Freundlich	K_f, mg/g	425	237	142	85
	n	16	115	21	12
	R^2	0.997	0.996	0.991	0.999

7.2.2 Characterization of CFAZ after adsorption

CFAZ samples were analyzed after the adsorption of a mixed ion solution of Cu^{2+}, Zn^{2+}, Ni^{2+}, Pb^{2+} using SEM and SEM-EDS. The SEM image presented in Figure 7.7 was obtained using a magnification of 1.00k times to allow a wider field of view.

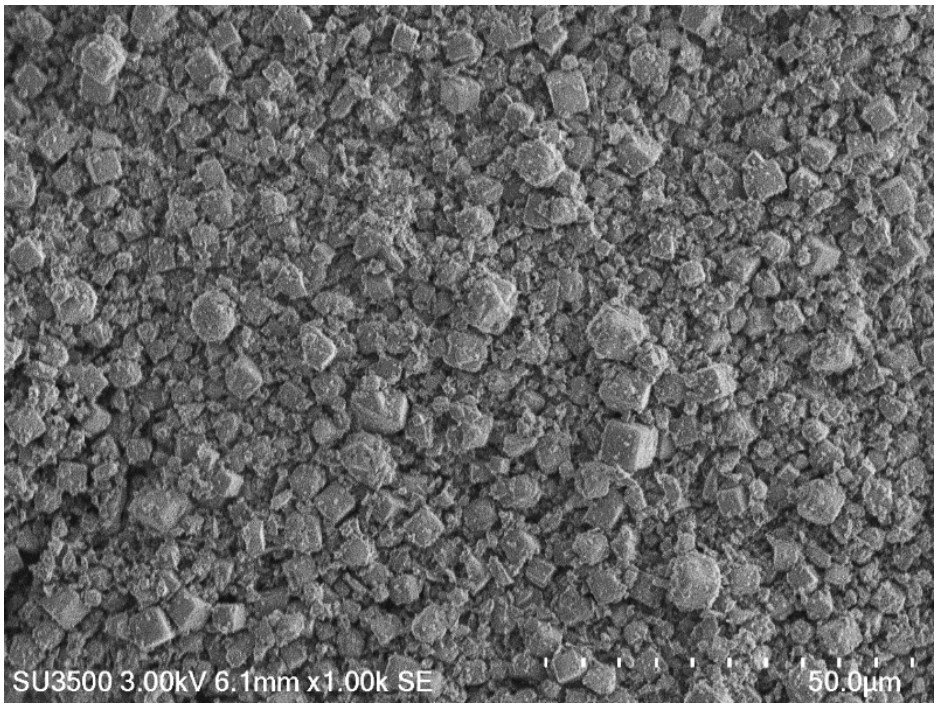

Figure 7.7 - SEM image of CFAZ sample after the adsorption experiments with mixed ions solution that contained Cu^{2+}, Zn^{2+}, Ni^{2+}, Pb^{2+}.

The results of the EDS mapping analysis are presented in Figure 7.8, which clearly indicates the presence of Pb, Cu, and Zn in the samples, while Ni was not detected.

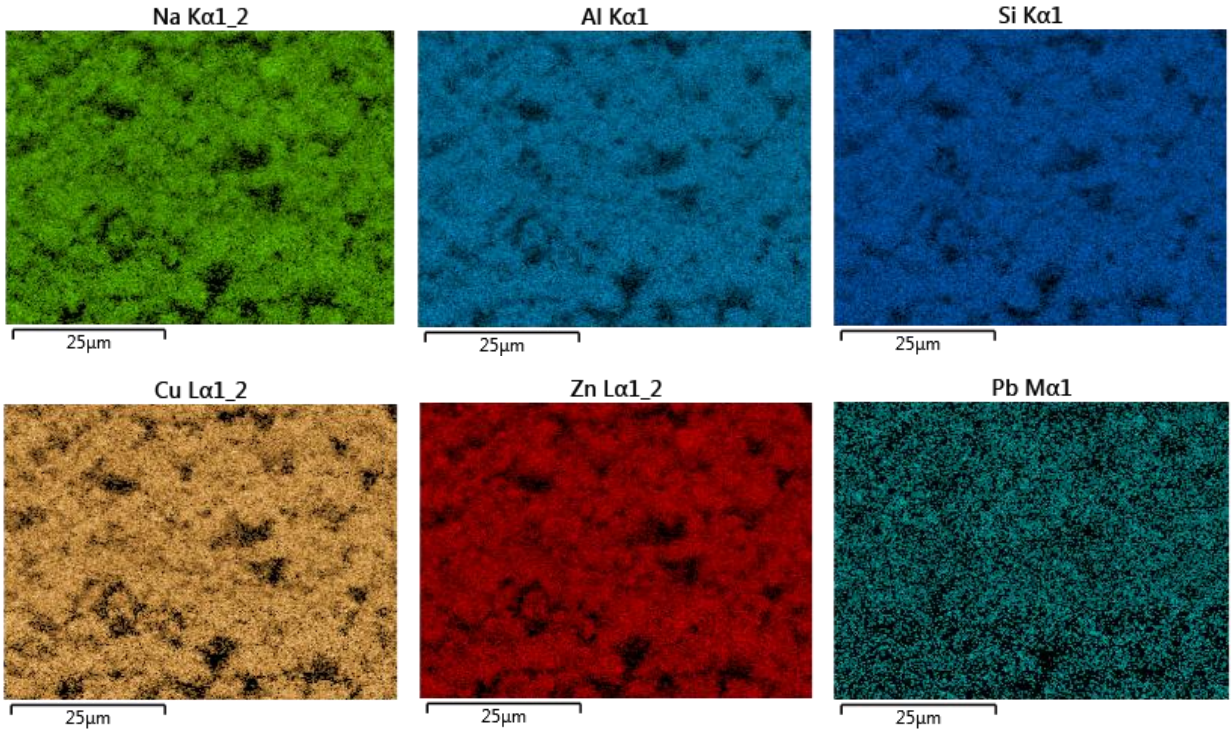

Figure 7.8 - Element mapping-EDS results of the CFAZ sample after the adsorption of metal ions, which includes Na, Al, and Si, as previously measured in CFAZ before adsorption, and the adsorbed metal ions of Pb, Cu, and Zn.

XPS experiments were conducted on CFAZ samples before and after adsorption of single metal ions (Cu^{2+}, Zn^{2+}, Ni^{2+} and Pb^{2+}). The obtained results are presented in Figure 7.9, indicating that the Na peaks vanish after the adsorption of metal ions, and specific metal peaks are observed in each experiment. These findings suggest an ion exchange mechanism for selected heavy metals adsorption by CFAZ.

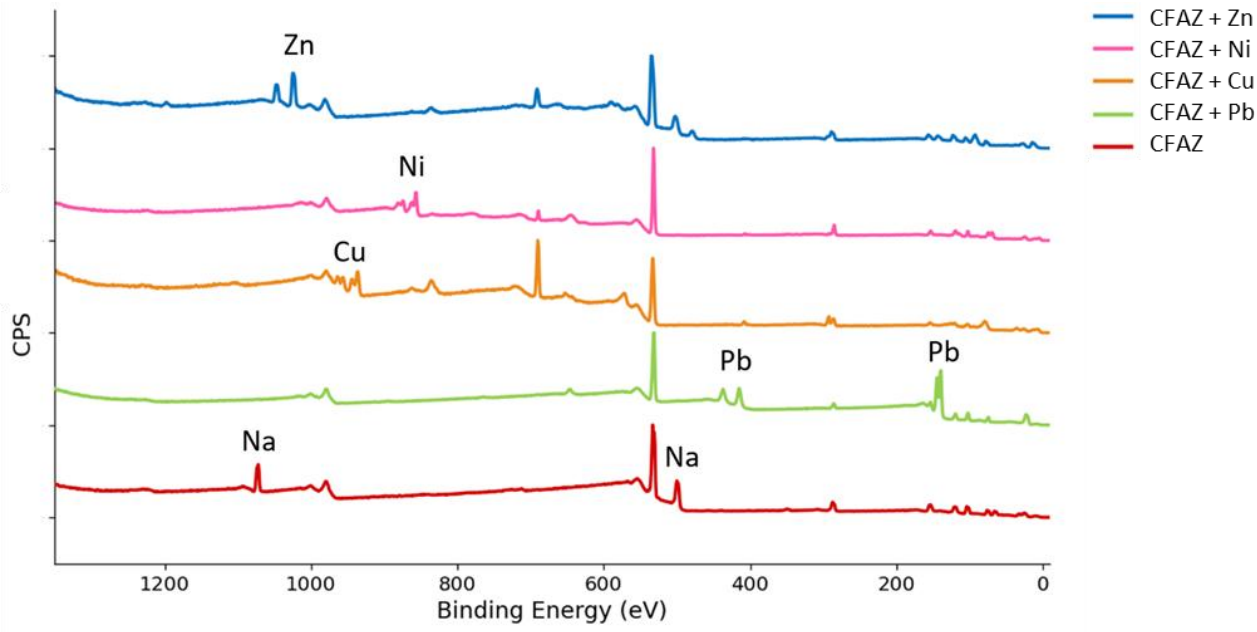

Figure 7.9 - XPS spectra of CFAZ before adsorption (represented by red color) and after adsorption of single metal ions (CFA after Zn ions adsorption is represented by the blue color spectra, Ni - pink, Cu - orange, and Pb - green). Each spectra exhibits a peak position that corresponds to the adsorbed metal ion. When compared to the CFAZ spectrum before adsorption, the Na peaks are absent from all other spectra, indicating that it was replaced by other metals.

7.2.3 Comparison of Adsorption Performance of LTA and CFA Zeolite

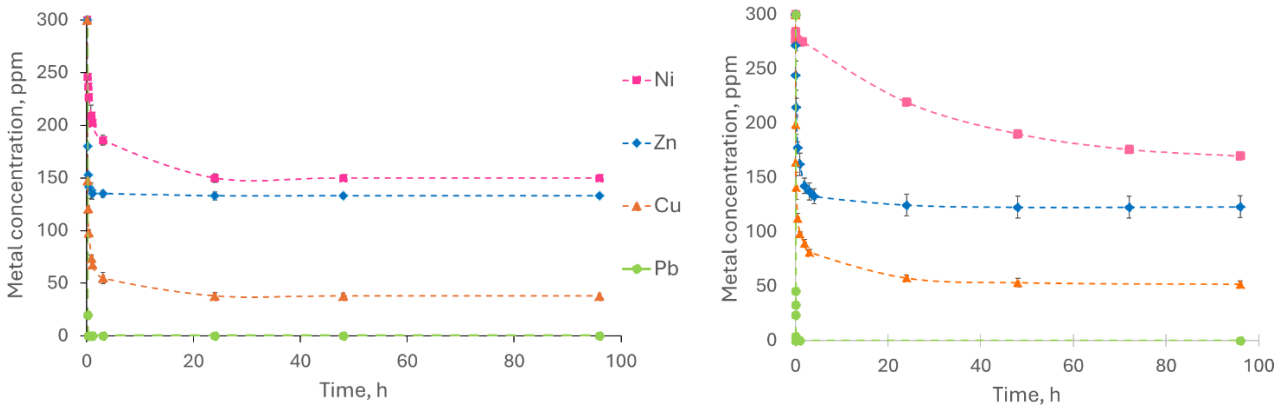

Figure 7.10 - Adsorption kinetics of single ions adsorption of Pb^{2+}, Cu^{2+}, Zn^{2+} and Ni^{2+} over 96 h on (a) LTA zeolite and (b) CFA zeolite.

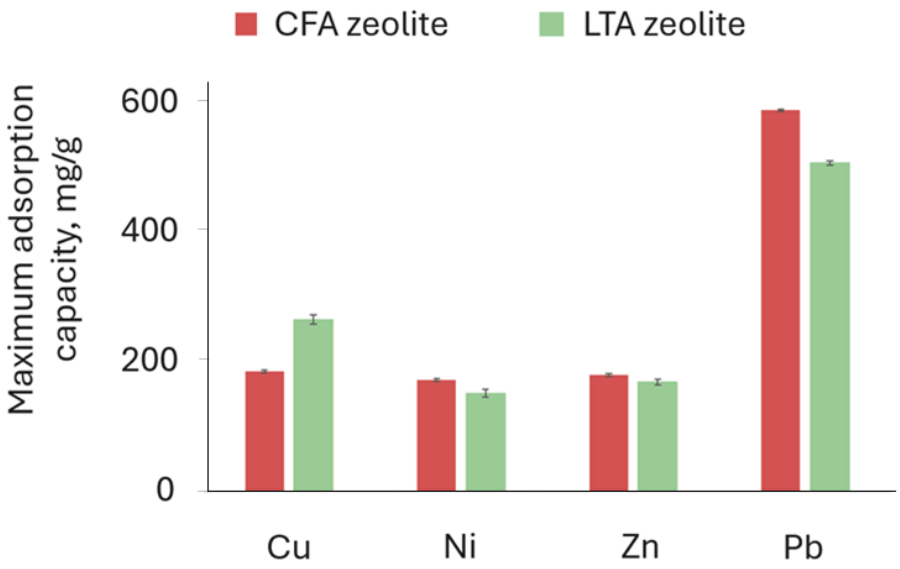

Figure 7.11 – Comparison of maximum adsorption capacities of CFA and LTA zeolites in single ions systems.

The results of metal ion removal by non-magnetic zeolites investigated in this work show that both zeolites were shown to be highly effective at adsorbing heavy metals. The findings indicate that the CFAZ adsorption performance for selected metal ions does not significantly differ from LTAZ.

Furthermore, findings demonstrate excellent adsorption efficiency when compared to other CFA-synthesized zeolites reported in the literature.

The adsorption experiments were conducted for both single and mixed ion systems, and the results revealed a consistent pattern of sorption selectivity between the investigated metal ions. Specifically, the selectivity order of $Pb^{2+} > Cu^{2+} > Zn^{2+} > Ni^{2+}$ was established.

Additionally, the results shown in Figure 7.9 suggest an ion exchange mechanism for metal ion removal by CFAZ.

7.3 Adsorption with Magnetic Zeolites

7.3.1 Magnetic LTA Zeolite

7.3.1.1 Cu adsorption by M-LTAZ with different iron oxide loadings

By varying the iron oxide nanoparticles' loading, different magnetic zeolites were synthesized and subsequently investigated for their Cu adsorption capacity. The experiments demonstrated the efficiency of all synthesized magnetic zeolites in removing Cu ions.

During adsorption experiments, it is expected that Cu concentration in prepared solution will gradually decrease over time, as the zeolite adsorbs metal ions. Eventually, the concentration should reach equilibrium, where it no longer changes over time. The equilibrium concentration is used to calculate adsorbed fraction q_e (mg/g) as was shown in Equation 7.1

Figure 7.12 illustrates that there were notable differences in both the kinetics and equilibrium concentrations across the studied zeolites. For pure zeolite, the equilibrium concentration of Cu^{2+} ions was found to be 38 ppm. When comparing magnetic zeolites MZ0.1, MZ0.5 and MZ1, the adsorption capacity decreased as the proportion of iron oxide nanoparticles increased. Thus, MZ0.1 equilibrated at 149 ppm, MZ0.5 at a similar concentration of 147 ppm and MZ1 at a lower concentration of 130 ppm. The results mentioned above are shown with ± 95% confidence interval. A more evident comparison of the obtained results can be seen in Figure 7.13.

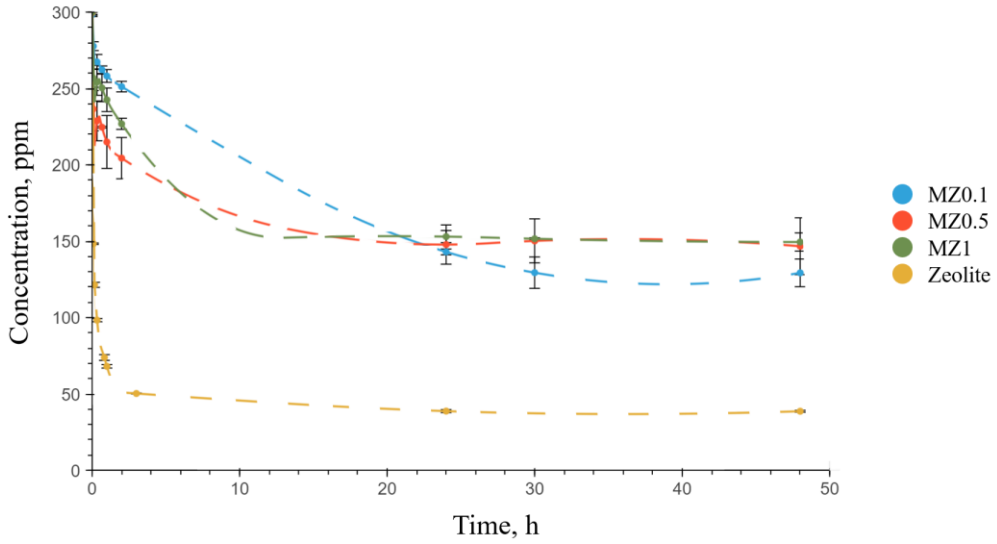

Figure 7.12 - Adsorption of Cu^{2+} ions by different synthesized zeolites.

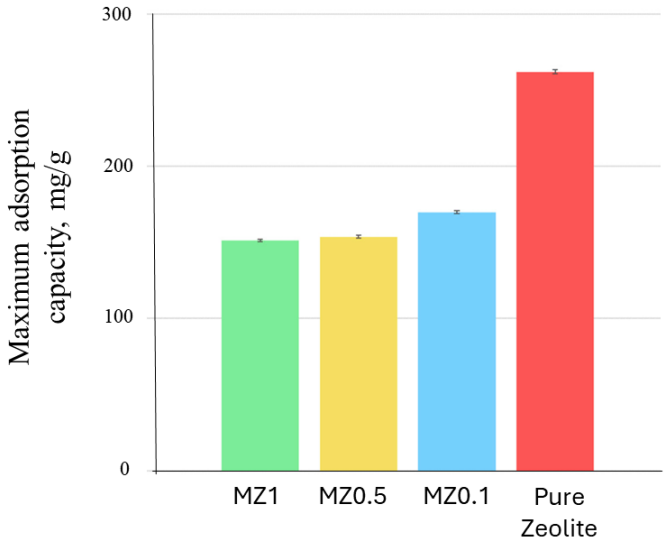

Figure 7.13 - Comparison of adsorption capacities of different zeolites used in this study for Cu^{2+} ions.

Based on these adsorption experiments and on previously measured surface area of the used zeolites, maximum adsorption capacity was calculated for all the investigated zeolite in mg/g and in mg/m^2. The results are summarized in Table 7.4.

Table 7.4 – Calculated maximum adsorption capacities for Cu^{2+} ions for synthesized zeolites used in this study.

Adsorbent material	**Adsorption capacity, mg/g**	**Adsorption capacity, mg/m²**	**Adsorbed Cu, %**
Iron oxide nanoparticles	0	0	0
LTA zeolite	262	0.6	87
MZ-0.1	170	2.9	57
MZ-0.5	154	2.4	51
MZ-1	151	2.4	50

To better understand the underlying process of Cu removal from water, adsorption models were investigated. Langmuir and Freundlich adsorption models were fit to the experimental data and adsorption parameters derived. Similar to section 7.2.1, the results were fit using Langmuir and Freundlich models, using Equations 7.2-7.4. Figures 7.14-7.17 show Langmuir nonlinear, Langmuir linear and Freundlich adsorption isotherms fit for Cu^{2+} adsorption on all synthesized zeolites.

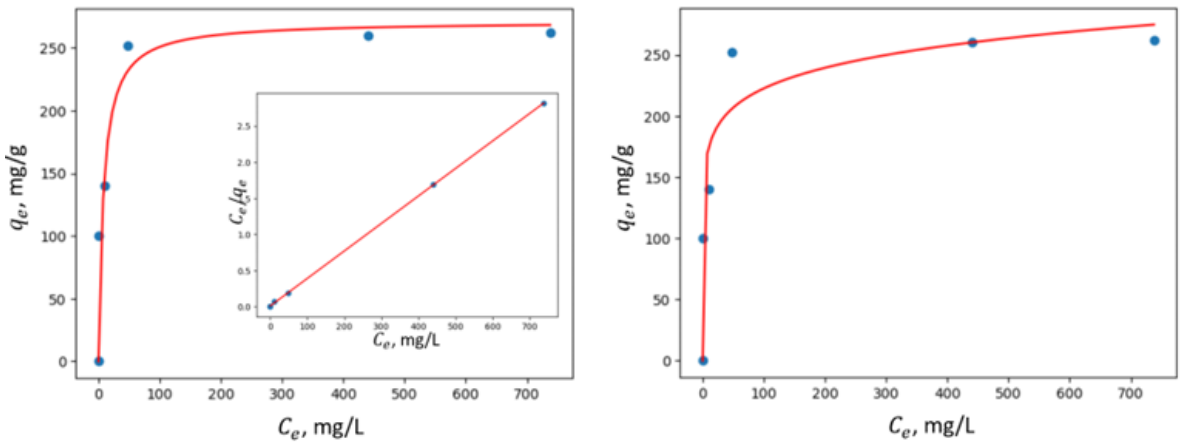

(a) *(b)*

Figure 7.14 - Adsorption isotherms of Cu2+ adsorption on pure zeolite fit to: (a) Langmuir non-linear and linear models; (b) Freundlich model.

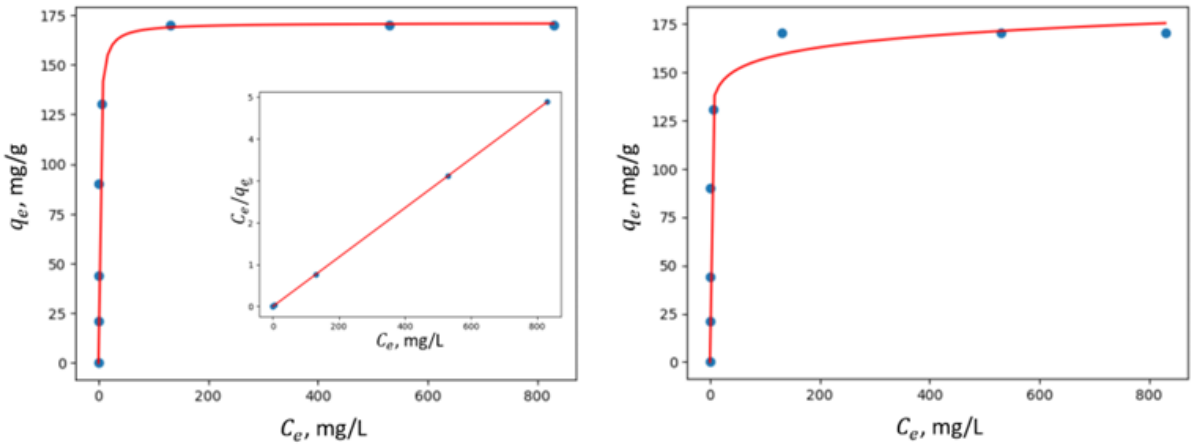

(a) *(b)*

Figure 7.15 - Adsorption isotherms of Cu^{2+} adsorption on MZ0.1 fit to: (a) Langmuir nonlinear and linear models; (b) Freundlich model.

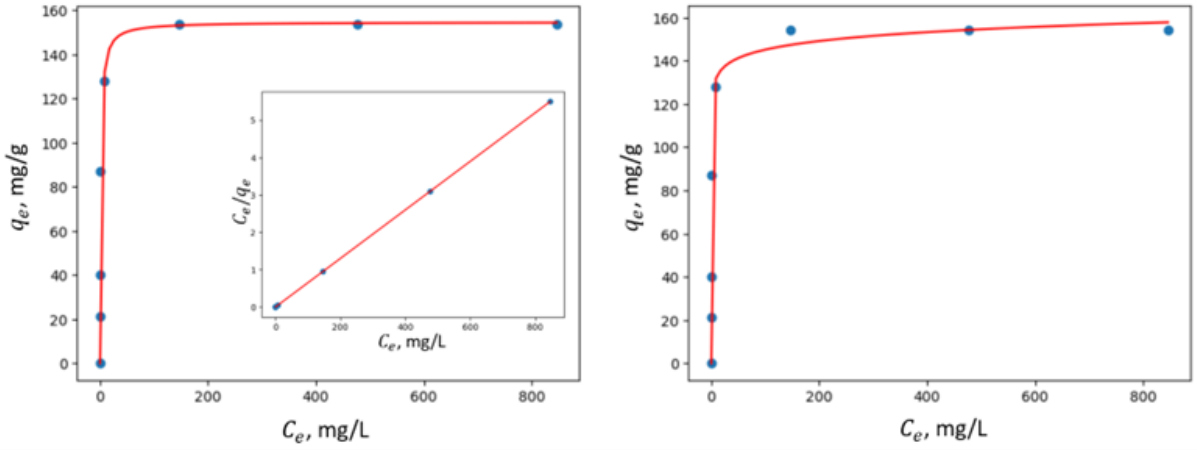

(a) *(b)*

Figure 7.16 - Adsorption isotherms of Cu^{2+} adsorption on MZ0.5 fit to: (a) Langmuir nonlinear and linear models; (b) Freundlich model.

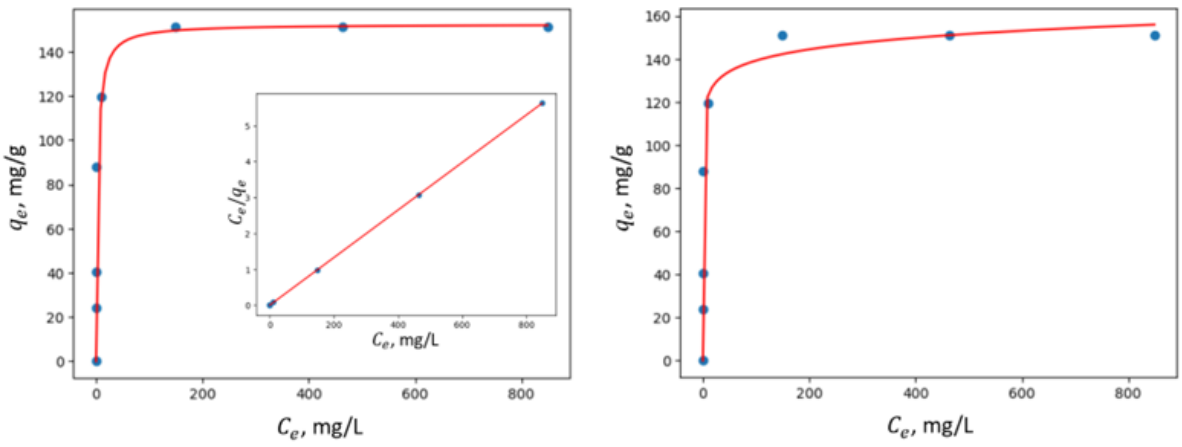

(a) *(b)*

Figure 7.17 - Adsorption isotherms of Cu^{2+} adsorption on MZ1 fit to: (a) Langmuir nonlinear and linear models; (b) Freundlich model.

The summary of the applied models and the results obtained for their parameters, including the corresponding values for the correlation coefficients R^2 are provided in Table 7.5.

Table 7.5 – Results from the thermodynamic model studies of the experimental isotherms for adsorption of Cu^{2+} ions.

Thermodynamic model	**Model parameters**	**Pure zeolite**	**MZ-0.1**	**MZ-0.5**	**MZ-1**
Langmuir nonlinear model	Q_{sat}, mg/g	271.1	171.0	155.0	152.4
	K_L, L/mg	0.12	0.57	0.68	0.35
	R^2	0.866	0.800	0.738	0.761
Langmuir linear model	Q_{sat}, mg/g	0.35	3.4	3.9	2.1
	K_L, L/mg	262.7	170.1	154.1	151.1
	R^2	1	1	0.975	0.996
Freundlich	K_f, mg/g	137.0	123.4	118.5	109.1
	n	9.5	19.2	21.8	18.9
	R^2	0.768	0.697	0.608	0.626

In all studied zeolites, the Langmuir linear model exhibits a higher correlation coefficient R^2, suggesting that adsorption predominantly occurs via the formation of a monolayer of adsorbate molecules on the homogeneous surface of the investigated adsorbents.

7.3.2 Characterization of zeolites after adsorption

High-resolution XPS survey spectra were collected and compared for zeolite samples before and after adsorption and compared to a baseline of pure zeolite, as shown in Figure 14. The analysis confirmed the presence of Cu ions on the surface of MZ samples tested after adsorption experiments. Furthermore, Fe peaks were detected for some of the MZ zeolites, even though the intensity of these peaks is low. Thus, Figure 14 shows peaks for Cu 2p3 at 935.3 eV, Na 1s at 1072.9 eV and Fe 2p at 711.4 eV. Moreover, it is evident that before adsorption, Na peaks are present in all zeolite samples. However, after adsorption and reaching the maximum adsorption capacity, Cu peaks emerge, while Na peaks vanish. These findings suggest an ion exchange mechanism for Cu adsorption by the zeolites.

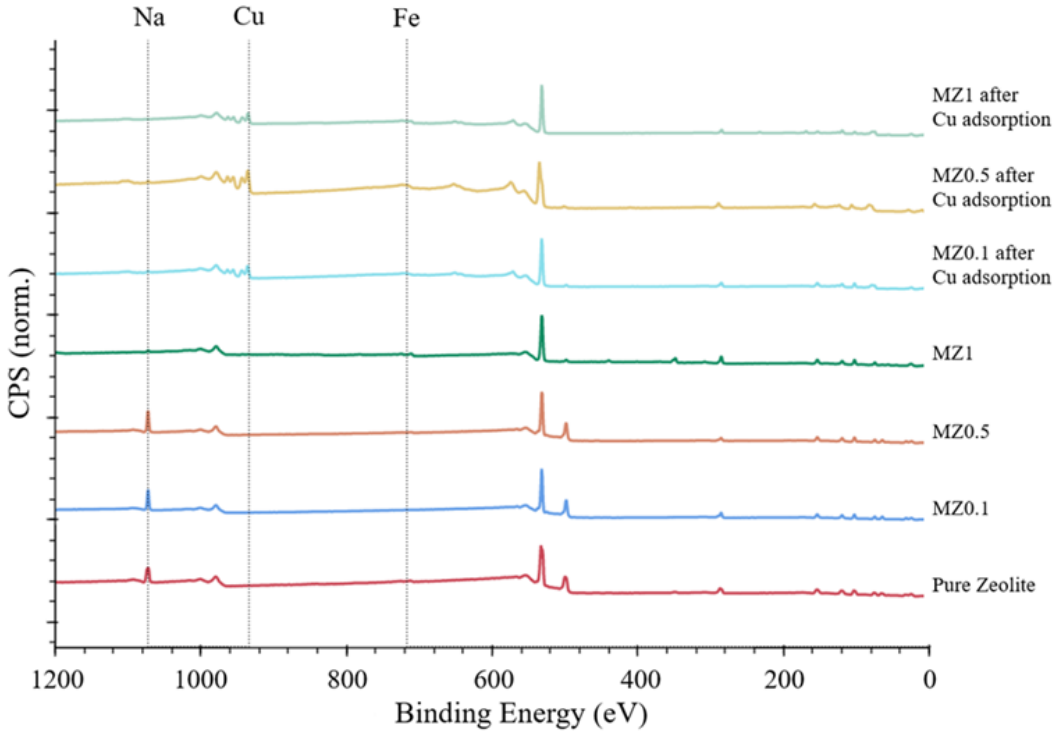

Figure 7.18 - XPS spectra comparison of LTAZ and MZ0.1-MZ1 before and after Cu^{2+} ions adsorption.

To further investigate the magnetic zeolites and their adsorption performance for Cu ions, SEM-EDS experiments were performed. SEM images were taken at 5.00k magnification and a low voltage of 10.0 kV of pure zeolite and MZ1. The results presented in Figure 7.19 indicates that the synthesized zeolites used in this study have cubic morphology typical for LTA zeolites same as was shown in Chapter 6.

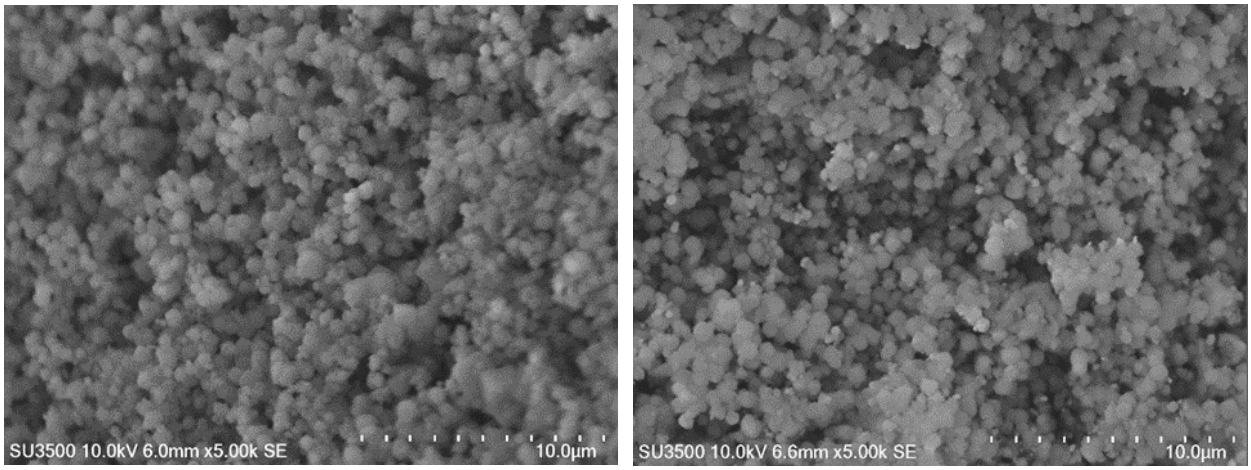

(a) (b)

Figure 7.19 - SEM of: (a) pure zeolite; (b) MZ 10:1

Figure 7.20 shows the comparison of SEM-EDS images of MZ before and after Cu adsorption. It can be seen that the MZ sample before adsorption indicates the presence of iron (represented by red areas). Furthermore, after Cu adsorption there is presence of both Fe and Cu. This result further confirms that magnetic synthesized zeolites adsorbed Cu from investigated solutions. Similar SEM-EDS scans were made on MZ0.1 and MZ0.5 samples and showed similar results, indicating the presence of both Cu and Fe after adsorption experiments.

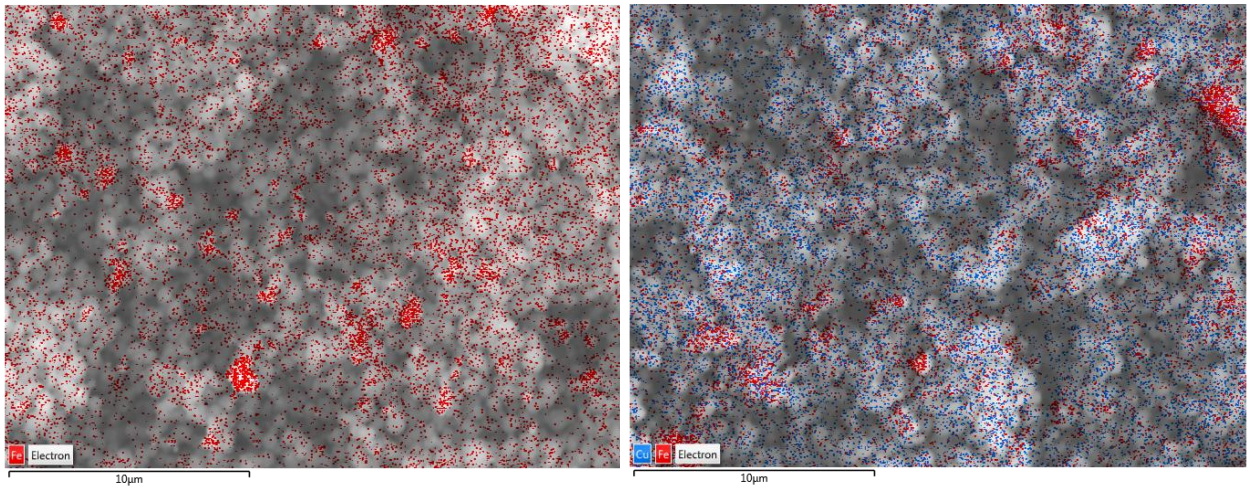

(a) (b)

Figure 7.20 - EDS of MZ1 (a) before adsorption; (b) after adsorption. Red areas correspond to Fe and blue areas correspond to Cu in the analyzed samples.

To confirm these results, EDS spectra were obtained using AZtec software. The results can be found in Figure 7.21, indicating the presence of Cu ions in MZ samples after the adsorption process. Furthermore, Na peaks were present in MZ0.1-MZ1 and were no longer present in the same samples after Cu adsorption, suggesting an ion exchange mechanism. Additionally, in MZ0.5 and MZ1 an Fe peak was observed before and after adsorption. These results correspond well with the previous experimental data obtained by different characterization techniques used in this work.

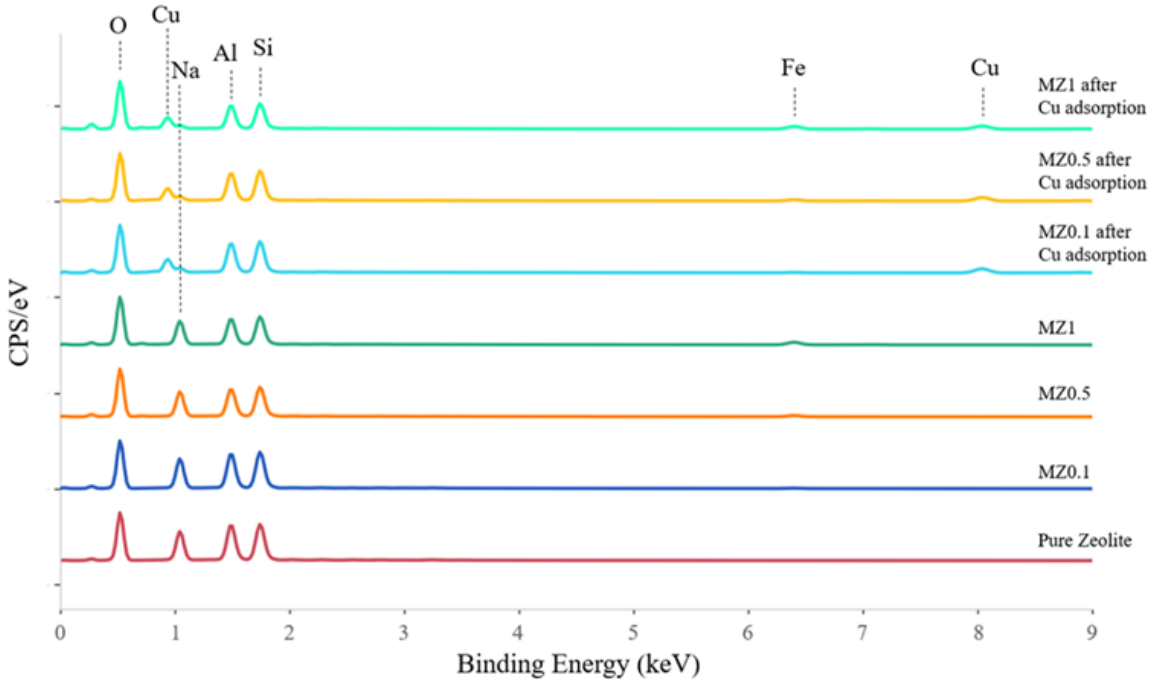

Figure 7.21 - EDS results comparing MZ used in this study before and after adsorption of Cu^{2+} ions and baseline of pure synthetic LTA zeolite (red line).

7.3.3 Extraction of magnetic zeolite from treated water using WHIMS

To remove the magnetic zeolite from the suspension after the adsorption process equilibrated, WHIMS was used. The treated solution containing the magnetic zeolite was introduced into the WHIMS, where the magnetic zeolite became trapped within the metal matrix of WHIMS, while the rest liquid passed through and was collected in a clean beaker. Figure 18 shows a photo of the treated solution after adsorption with the presence of magnetic zeolite that caused reddish color on the left, and the purified transparent solution devoid of zeolite particles on the right. The results indicate that only one cycle of magnetic zeolite extraction using WHIMS is required for the used amount of adsorbent and solution.

Figure 7.22 - Treated solution with magnetic zeolite particles (left bottle) and after extraction of magnetic zeolite using WHIMS (right bottle).

7.4 Adsorption with magnetic CFA Zeolite

To compare the adsorption capacities of the CFAZ and M-CFAZ, adsorption experiments were performed following the same protocol for mixed ions systems containing Pb^{2+}, Cu^{2+}, Zn^{2+} and Ni^{2+} ions. The results of these experiments are shown in Figure 7.23a,b. It can be seen that the same selectivity order is observed, with Pb adsorbing rapidly and Cu slightly slower. The rate of adsorption over the first 1.5 hours can be seen in Figure 7.23a, while a longer observation time that is presented in Figure 7.23b allows the equilibrium concentration for each metal to be determined. Additionally, it was found that a small amount of Zn^{2+} and Ni^{2+} ions were also adsorbed by M-CFAZ. Thus, the maximum adsorption capacity for selected metal ions was calculated to be 261 mg/g, 109 mg/g, 45 mg/g and 42 mg/g for Pb, Cu, Zn and Ni ions, respectively. The comparison of adsorption capacities of selected metal ions by CFAZ and M-CFAZ is shown in Figure 7.24.

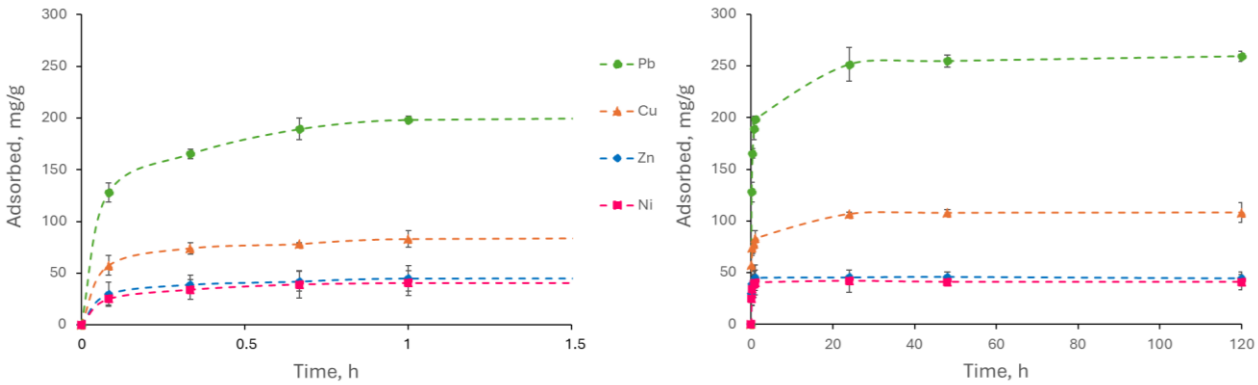

(a) (b)

Figure 7.23 – Adsorption kinetics of a mixed ion solution comprised of 300 mg/L Pb^{2+}, Cu^{2+}, Zn^{2+} and Ni^{2+} with 0.1 g M-CFAZ in (a) 1.5 hours and (b) 120 hours.

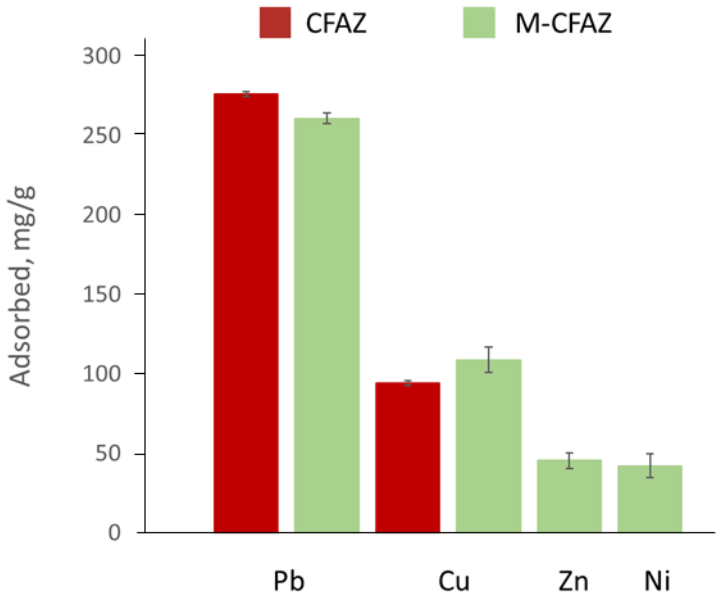

Figure 7.24 – A comparison of maximum adsorption capacities of CFAZ and M-CFAZ used in this study for mixed ions system in mg/g.

A comparative analysis of the adsorption kinetics and capacities of CFAZ and M-CFAZ revealed similar performances for Pb^{2+} and Cu^{2+} ions. Notably, the magnetic zeolite demonstrated the additional capacity to adsorb Zn^{2+} and Ni^{2+}, which was not observed in the non-magnetic CFA

zeolite, which could be attributed to partial metal ions adsorption onto the carbonized binder, which is a highly oxygenated graphenic structure. This suggests that M-CFAZ not only retains the adsorption properties of CFAZ, but also improves it. In summary, this indicates that M-CFAZ can be considered as an efficient adsorbent for the removal of heavy metals from contaminated water.

Figure 7.25 demonstrates the comparison of XPS spectra of pure zeolite, magnetic zeolite and magnetic zeolite after adsorption. It can be seen that a low amount of nano-magnetite added to the synthesis process was not detected by XPS. However, the results of SEM-EDS shown in Figure 7.26 confirm the presence of Fe and the presence of the adsorbed Pb, Cu, Zn and Ni in the M-CFAZ.

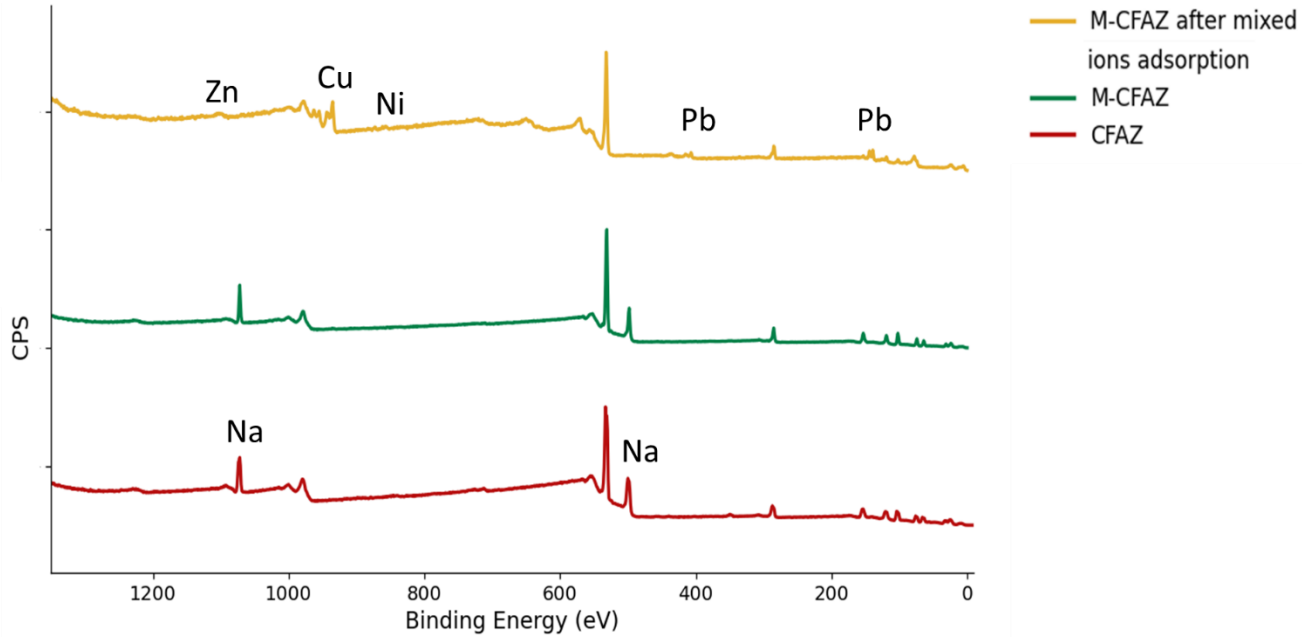

Figure 7.25 - XPS spectra of CFAZ before adsorption (represented by red color), M-CFAZ (green color) and M-CFAZ after adsorption of mixed metal ions. CFAZ and M-CFAZ have similar spectra, while M-CFAZ after adsorption experiments exhibits a peak position that corresponds to the adsorbed metal ion. More evident peaks can be seen for Pb and Cu ions and less obvious for Ni and Zn as the less amount of Ni and Zn ions were adsorbed. Similar to CFAZ adsorption, Na peaks are absent from after adsorption spectra, indicating that it was replaced by other metals.

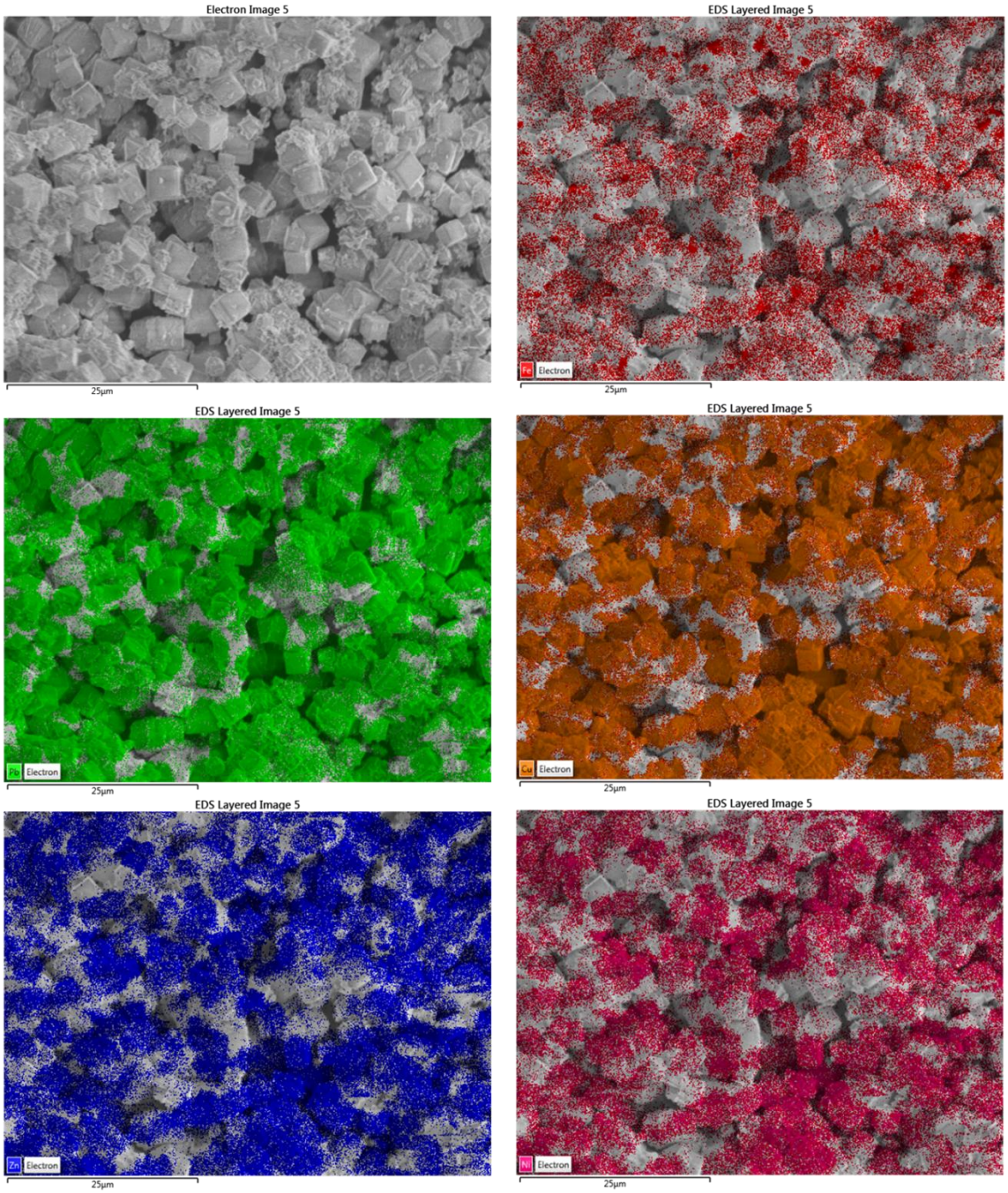

Figure 7.26 - Element mapping-EDS results of the M-CFAZ after the adsorption of mixed ions. It can be seen that the results indicate the presence of Fe (red color, top right image) confirming that synthesized contains iron. Other images show the indication of Pb (green), Cu (orange), Zn (blue) and Ni (pink) confirming that these metal ions were adsorbed by M-CFAZ.

To remove M-CFAZ from the treated solution, it was passed through the WHIMS, where magnetic particles became trapped within the metal matrix of WHIMS, while the rest passed through and were collected in a clean beaker. Figure 7.27 shows a photo of the treated solution with the presence of M-CFAZ which caused the darker color on the left, and the purified solution after it was passed through the WHIMS on the right. The results indicate that only one pass of magnetic zeolite extraction is required for the amount of adsorbent and solution used in this study.

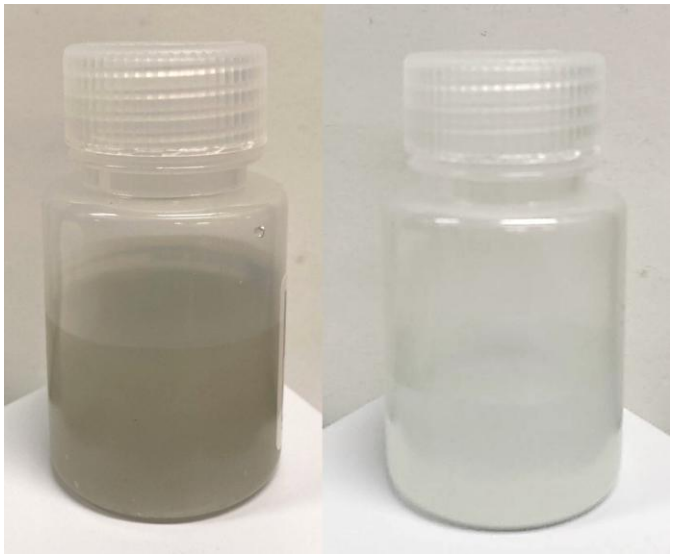

Figure 7.27 - Treated solution with magnetic zeolite particles (left) and after extraction of magnetic zeolite using WHIMS (right).

7.5 Adsorption in a Continuous Flow System

7.5.1 M-LTAZ Use at Different Flow Rates

First, the adsorption performance of M-LTAZ in a continuous flow system was compared at flow rates of 4 L/h (Experiment A) and 8 L/h (Experiment B). The parameters of Experiments A and B are summarized in Table 7.6 and the results are presented in Figures 7.28 and 7.29. Figure 7.28 illustrates the adsorption kinetics of investigated metal ions (Pb, Cu, Zn and Ni) over time, with each metal represented by a distinct color. All experiments were conducted in triplicate and error bars on the graphs represent ± 95% confidence interval.

Table 7.6 – Parameters of the experiments with continuous flow with M-LTAZ

Parameter	**Value (Experiment A)**	**Value (Experiment B)**
Zeolite dosage	1.5 g/L	1.5 g/L
Solution volume	3 L	3 L
Solution flow speed	4 L/h	8 L/h
Retention time	40 min	20 min
Number of cycles	3	4

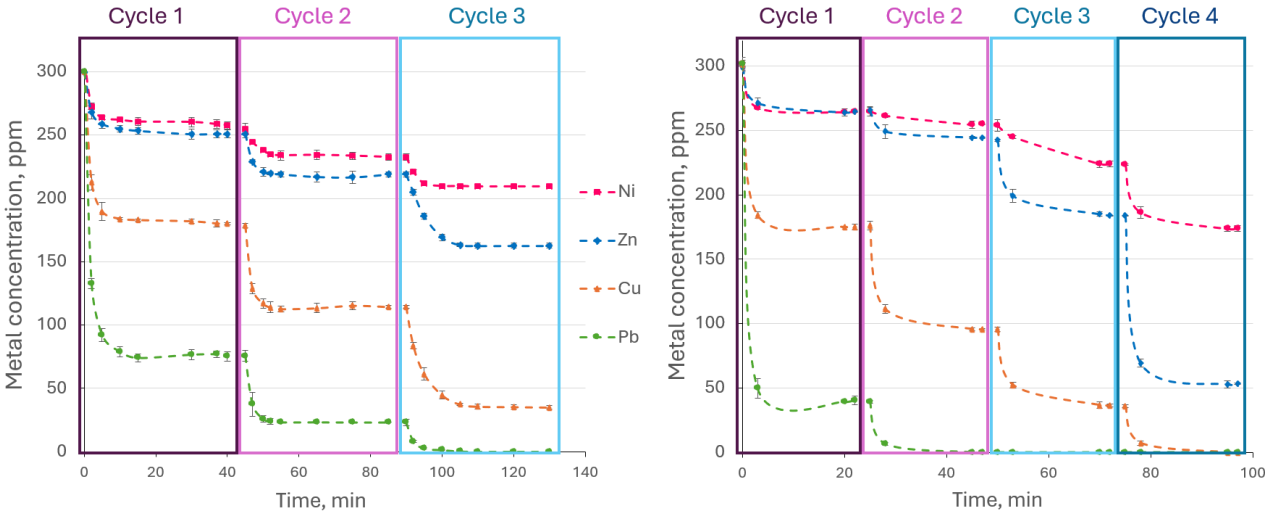

(a) (b)

Figure 7.28 - Decrease of metal concentration in solution over time at a flow rate of 4 L/h (a) and 8 L/h (b) with M-LTAZ dosage of 1.5 g/L.

Figure 7.28 illustrates the decrease of the metal ion concentrations over time for a flow speed of 4 L/h during 3 cycles of adsorption (a) and 8 L/h during 4 cycles of adsorption (b). The initial concentration of all ions in solution was 300 ppm in both cases. In Experiment A with a slower flow speed and longer retention time (40 min per cycle), after 3 cycles, the final concentration of metal ions in solution was found to be 0 ppm for Pb, 35 ppm for Cu, 163 ppm for Zn and 209 ppm for Ni. Previous work on the use of magnetic zeolite synthesized from CFA used in adsorption of same metal ions in batch experiments in Section 7.2.3 showed the following selectivity order of Pb>Cu>Zn>Ni, also indicating that metal ions compete for the spots available on the zeolite

surface. The results observed in Figure 7.28a show the same adsorption selectivity order. Based on these findings, it can be estimated that in the 4th cycle all Cu will be removed and more Zn than Ni will be adsorbed by M-LTAZ.

When comparing this with Experiment B (Figure 7.28b), where the flow rate was twice as fast (8 L/h) and therefore retention time was 20 min, even though the adsorption selectivity and kinetics pattern are similar to Experiment A, the kinetics and adsorption rate shown are different. Thus, after 4 cycles, the final concentration of metal ions in solution was found to be 0 ppm for Pb and Cu, 53 ppm for Zn and 174 ppm for Ni.

It can be seen from Figures 7.28a and 7.28b that the effectiveness of the adsorption varies by metal, with efficient Pb and Cu removal within 3-4 cycles. The initial fast phase in the adsorption kinetics for all metals suggests a high affinity or of active sites in the zeolite at the beginning of the process, which decreases as these sites are occupied over time. Furthermore, the flow rate does not significantly affect adsorption kinetics as metal ions reached equilibrium after approximately 20 minutes at the slower flow rate (Figure 7.28a). The differences observed between the two graphs underline the importance of optimizing adsorption conditions to enhance the removal efficiency of specific metal ions from solutions.

In the observed adsorption kinetics results, there is an inverse relationship between the adsorption of Pb ions and the other metal ions (Cu, Zn and Ni). This relationship can be attributed to competitive adsorption, where multiple metal ions in a solution compete for the limited available adsorption sites on the adsorbent.

The observed data suggest that when a significant amount of Pb is adsorbed, the adsorption of other metal ions such as Ni, Zn, and Cu is comparatively reduced within the same cycle. Conversely, when less Pb is adsorbed, there is an increase in the adsorption rates of Cu and other metals. This phenomenon can be explained by the competitive adsorption dynamics in multi-ion systems.

By using Equation 7.1 the adsorbed mass of metal per g of zeolite can be calculated for each metal during each cycle. The results for both flow rates are represented in Figure 7.29:

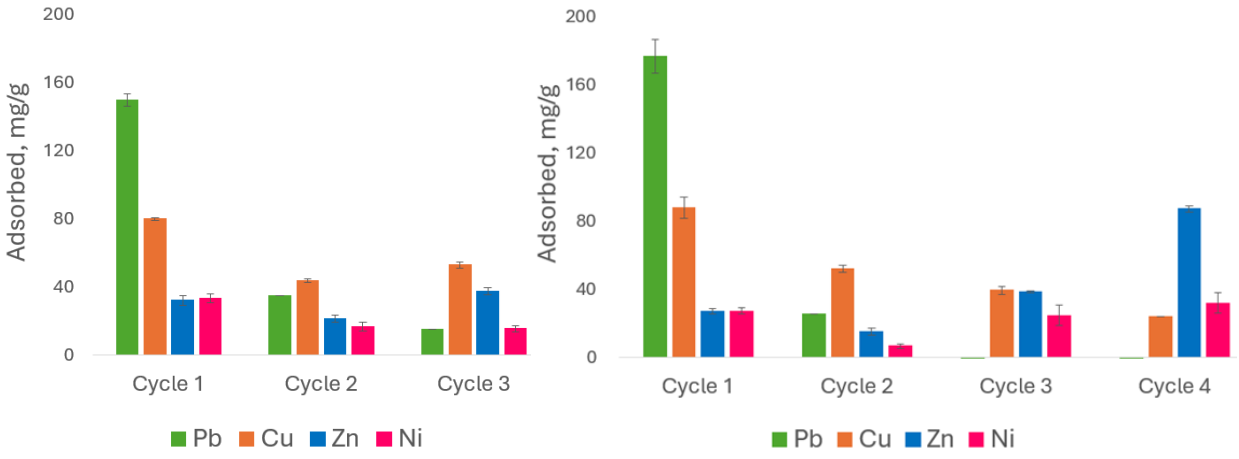

(a) (b)

Figure 7.29 - The amount of adsorbed metal per cycle at a flow rate of (a) 4 L/h and (b) 8 L/h and M-LTAZ dosage of 1.5 g/L.

As can be seen for both M-CFAZ and M-LTAZ, in the 1st cycle the highest degree of adsorption is for Pb, followed by Cu, then smaller amounts of Zn and Ni. While in the 2nd cycle, Cu is the most adsorbed metal (in absolute values), followed by Pb, Zn and Ni. In the 3rd cycle Cu was once again the highest adsorbed metal, and no Pb or trace amounts of Pb were adsorbed, while Zn is adsorbed faster than Ni. Finally, in Figure 7.29b, when no Pb is present, first Cu ions are removed completely, then Zn removal increases significantly, and approximately the same amount of Ni is removed as in previous cycle, following the selectivity order of Pb>Cu>Zn>Ni.

7.5.2 M-LTAZ and M-CFAZ comparison

To compare M-LTAZ and M-CFAZ adsorption performance in the continuous flow system with equivalent parameters, experiments with a flow speed of 8 L/h and zeolite dosage of 0.5 g/L were conducted. The lower dosage was chosen to investigate the adsorption capacity of zeolites. All parameters used in the experiments described in this section are provided in Table 7.7.

Table 7.7 – Parameters of the experiment with continuous flow comparing performance of M-CFAZ and M-LTAZ with the identical parameters.

Parameter	**Value**
Zeolite dosage	0.5 g/L
Solution volume	1 L
Solution flow speed	8 L/h
Retention time	7.5 min
Number of cycles	5

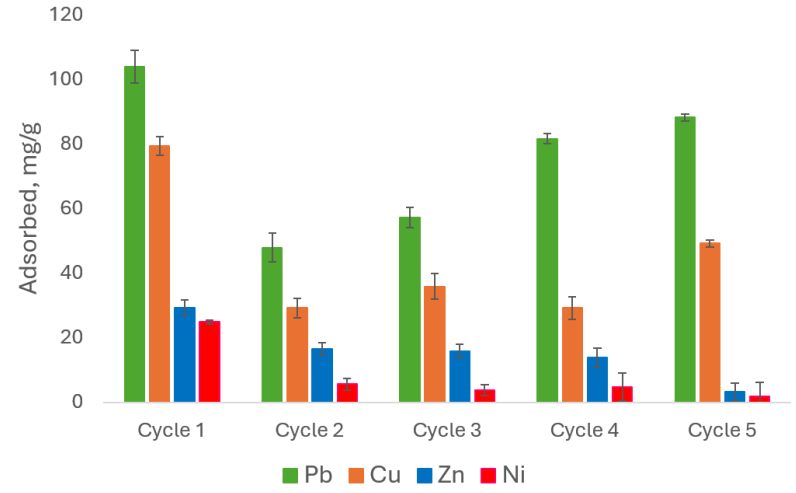

(a)

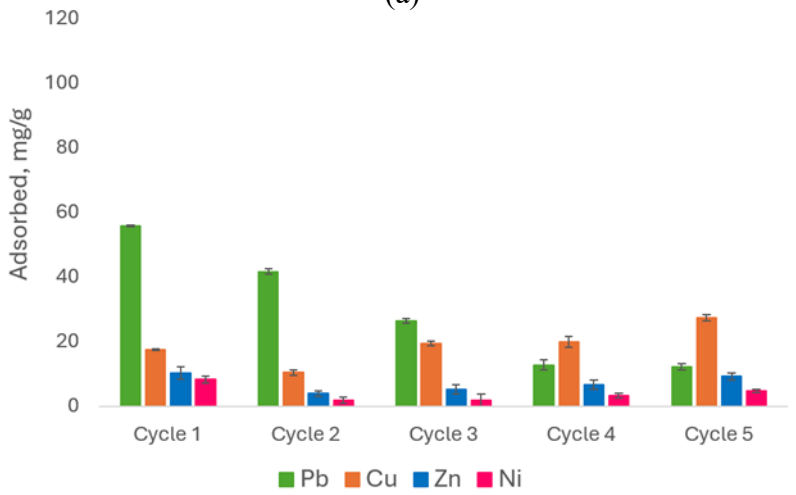

(b)

Figure 7.30 – The amount of adsorbed metal per cycle at a flow rate of 8 L/h and zeolite dosage of 0.5 g/L by (a) M-CFA zeolite and (b) M-LTA zeolite. The results are presented over five cycles.

The results show significantly higher adsorption capacities for Pb across all cycles and followed by Cu, Zn and Ni. The pattern of metal adsorption of M-LTAZ (Figure 7.30b) is similar to M-CFAZ, however, the overall adsorption capacities are generally lower compared to those in Figure 7.30a. The results indicate changes in the competition dynamics among the metal ions or alterations in the adsorbent properties and underline the influence of experimental conditions on the adsorption capacities and kinetics of different metals. This analysis can inform future studies aimed at optimizing adsorbent materials for the effective removal of specific metal ions from contaminated environments.

7.6 Regeneration of Zeolites

SEM-EDS analysis was performed on M-CFAZ and M-LTAZ after adsorption of heavy metal ions and after their subsequent desorption in NaCl solution. EDS scans of M-CFAZ (Figure 7.31) and M-LTAZ (Figure 7.32) show elements detected in the sample after desorption. Particularly, for both samples Al and Si are present (the main elements in zeolites), Na and Cl (due to the NaCl solution), Fe (indicates that the zeolite sample is still magnetic) and Cu (indicating that it was not desorbed completely from the sample). EDS analysis of the weight % of elements found in the sample was extracted from Aztec software and is presented in Figure 7.33.

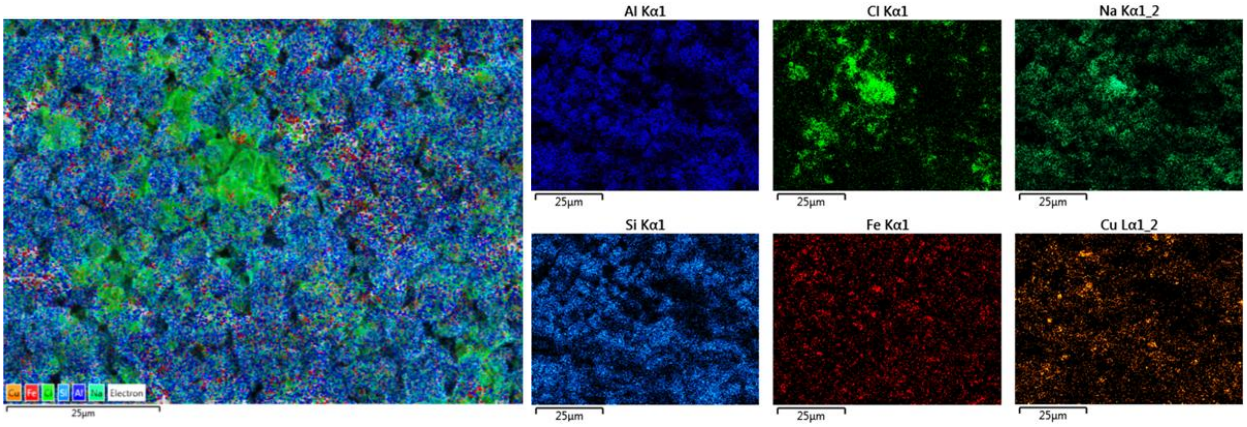

Figure 7.31 – SEM-EDS scans of M-CFA zeolite after desorption in NaCl solution showing the presence of Cu, Fe, Cl, Na, Si, and Al in the magnetic zeolite sample.

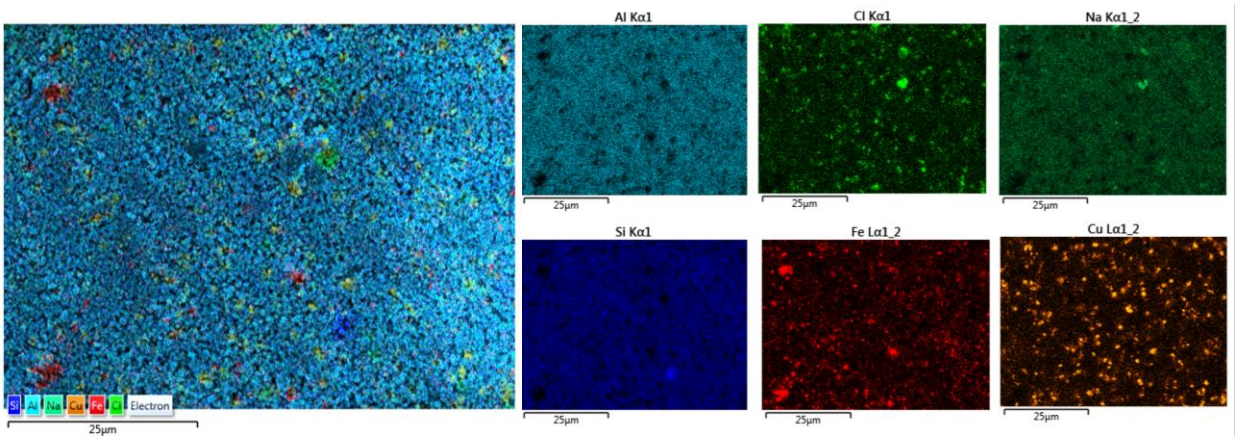

Figure 7.32 - SEM-EDS scans of M-LTA zeolite after desorption in NaCl solution showing the presence of Cu, Fe, Cl, Na, Si, and Al in magnetic zeolite sample.

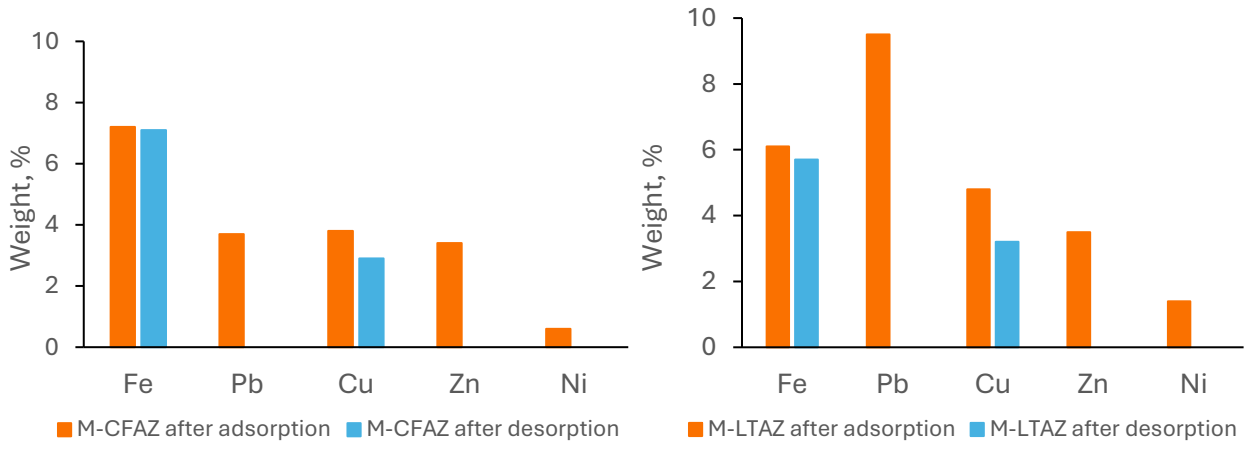

(a) (b)

Figure 7.33 – EDS results of (a) magnetic CFA zeolite and (b) magnetic LTA zeolite after adsorption and after desorption experiments excluding zeolites constituents.

Both zeolites show the presence of all adsorbed metal ions after adsorption experiments as well as Fe, indicating that zeolite remains magnetic. However, after desorption experiments, only Cu of the adsorbed ions was detected in the sample, suggesting the complete desorption of Pb, Zn, and Ni. The results indicate that about 70% of adsorbed Cu remained in the zeolite sample after desorption. Moreover, the results indicate minimal alteration of Fe, which implies that the magnetic properties of the zeolite were retained.

It is possible that the reason for Cu remaining in the sample is that the sites of the carbonized graphenic coke binder initially absorbed most of the Cu ions from the solution until these sites became saturated, after which the Cu ions began to adsorb onto the zeolite. When attempting to remove the Cu ions with a NaCl solution, only the Cu adsorbed on the zeolite is effectively desorbed, while the Cu retained in the graphenic sites of the binder remains unaffected by the NaCl solution which might be due the strong surface complexation of Cu ions with the oxygen-containing groups on the surface of graphene oxide [569]. Further investigation into this phenomenon would be of significant value, potentially uncovering new insights and deepening the knowledge of the underlying mechanisms.

To confirm these results, samples were taken from solution during adsorption and desorption experiments and the metal ion concentrations were measured using ICP-OES. Figure 7.34 shows adsorption (a) and desorption (b) kinetics of Pb, Cu, Zn and Ni ions per g M-CFAZ calculated using Equation 7.5:

$$Q = \frac{C_0 - C_e}{m} \times V \qquad 7.5$$

where Q is adsorption capacity (mg/g), V is solution volume (L), m is the adsorbent dosage (g), C_0 and C_e are the initial concentrations of metal ions in solution and after the adsorption process, respectively (mg/L).

Figure 7.35 shows the results of the same experiments using M-LTAZ. For ease of comparison, the amount of adsorbed and desorbed metal ions is shown for both zeolites in Figure 7.36.

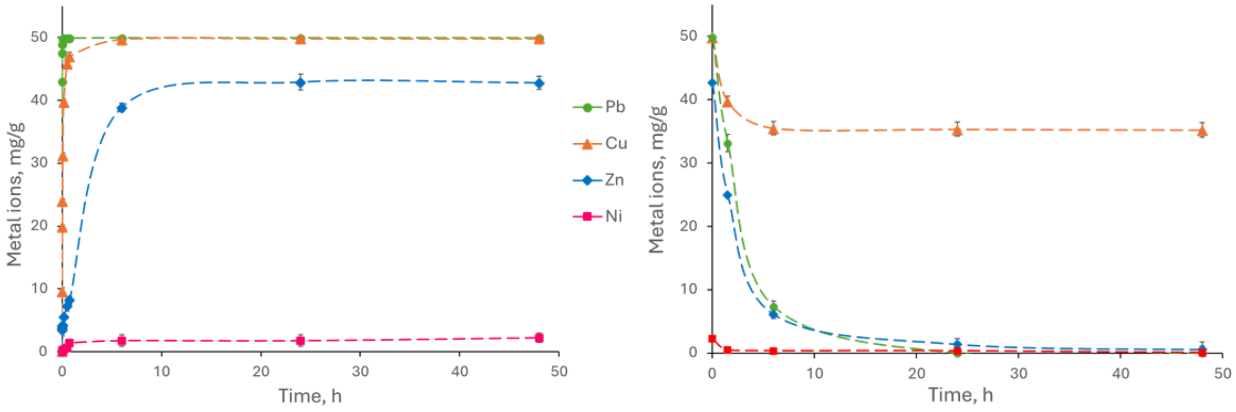

(a) (b)

Figure 7.34 – Metal ion concentrations in M-CFAZ in mg/g zeolite measured over time during (a) adsorption experiment and (b) desorption experiment. Curves are added as a visual aid.

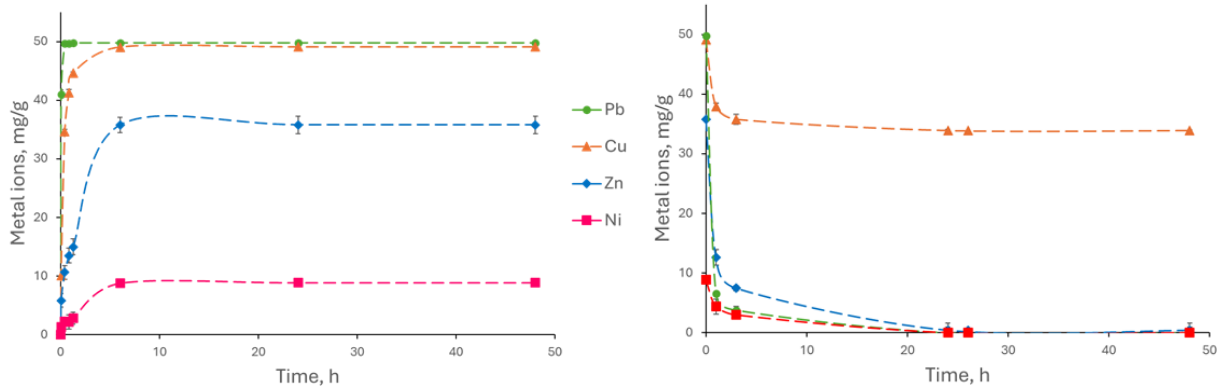

(a) (b)

Figure 7.35 – Metal ion concentrations in M-LTAZ in mg/g zeolite measured over time during (a) adsorption experiment and (b) desorption experiment. Curves are added as a visual aid.

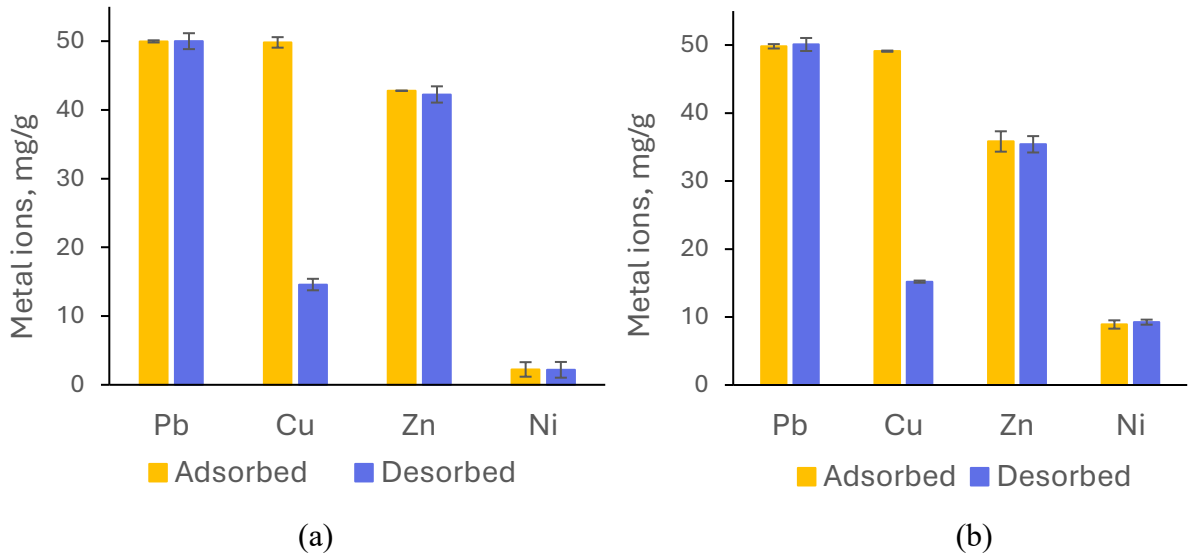

Figure 7.36 – Adsorbed and desorbed metal ions per g of (a) M-CFAZ and (b) M-LTAZ.

The results of Figures 7.34-7.36 show that both zeolites show high affinity for Pb and Cu adsorption and follow the selectivity order of adsorption Pb>Cu>Zn>Ni discussed in Section 7.2. However, in the desorption experiments, both the kinetics and the amount of desorbed metal ions are in the order of Pb, Zn, Ni > Cu. Figure 7.36 demonstrates that the same amounts of Pb, Zn, and Ni that were adsorbed by the zeolite were subsequently desorbed. Whereas only 15 mg/g of Cu was desorbed from both zeolites, indicating that about 70% of Cu remained in the zeolite. These results further confirm SEM-EDS results shown in Figures 7.31-7.33.

For calculating the desorption ratio of metal ions and comparing the desorption efficiency from M-CFAZ and M-LTAZ Equation 7.6 was used:

$$D = \frac{q_d}{q_t} \times 100\% \qquad 7.6$$

where D is the desorption ratio (%), q_d is the amount of metal desorbed per unit mass of desorbing (mg/g), and q_t is the amount of metal adsorbed onto the mineral per unit mass of adsorbent at equilibrium (mg/g).

Using Equation 7.5, the desorption ratio for the M-CFA zeolite was calculated to be 100% for Pb, 99% for Zn, 97% for Ni and 29% for Cu; for the M-LTA zeolite, desorption ratio was found as 100% for Pb and Ni, 99% for Zn and 31% for Cu. These results are summarized in Figure 7.37.

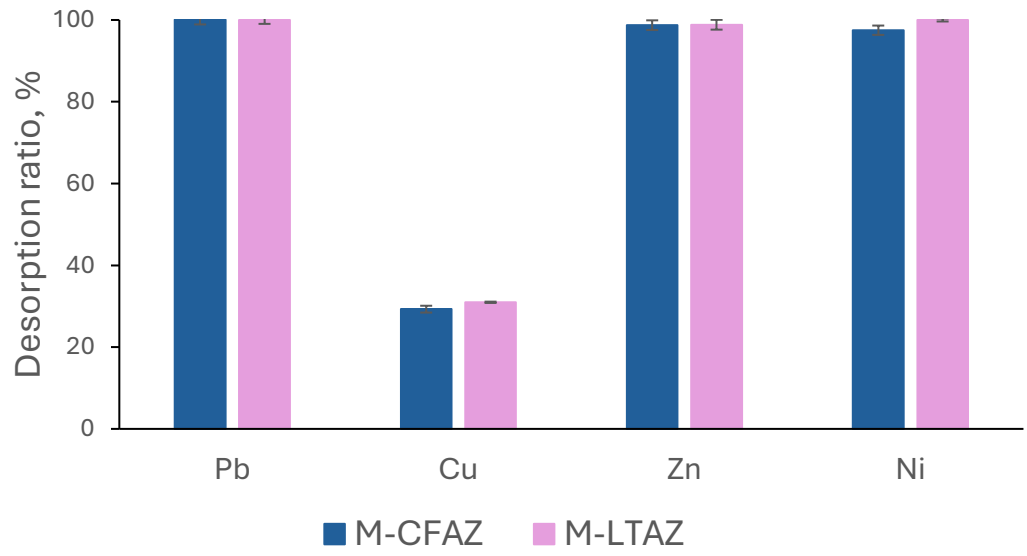

Figure 7.37 – Comparison of desorption ratio of M-CFAZ and M-LTAZ.

The results confirm the findings shown in Figures 8-10, and indicate that during desorption experiments Pb, Zn and Ni ions were completely removed from zeolite, while only removing approximately 30% of Cu.

7.7 Summary

This chapter covered the adsorption performance of magnetic LTAZ and CFAZ for heavy metal ion removal and compared it to the performance of non-magnetic zeolites under the same conditions. It was shown that CFAZ is an effective adsorbent material for water treatment for the investigated metal ions. Furthermore, when modified magnetically, M-CFAZ led to an enhanced adsorption capacity for Zn and Ni ions.

The XPS analyses demonstrated the absence of Na peaks on the CFAZ after adsorption whereas peaks for the adsorbed ions are clearly visible. Additionally, the investigated solutions maintained a constant pH over time, which suggests that the decrease in metal ions concentration was

attributed to the adsorption process. Based on these factors, an ion exchange mechanism may be implied in the removal of investigated metals from the liquid phase to CFAZ. These results provide further insight into the adsorption behavior of zeolite and the potential mechanisms underlying its ability to selectively remove heavy metals from water. Further research is necessary to understand the nature of CFAZ ion exchange properties and its influence on the adsorption efficiency.

Adsorption experiments using magnetic zeolite composites synthesized by the novel method designed in this work started with investigation of LTAZ modification with different loadings of iron oxide nano particles. The effect of different loading on adsorption capacity of synthesized magnetic zeolite was investigated for the case of M-LTAZ adsorption of Cu^{2+} ions. Thus, 10:1, 10:0.5, and 10:0.1 zeolite–iron oxide nanoparticles ratios were investigated in batch adsorption experiments. Although pure zeolite was more effective for Cu removal from aqueous solutions (maximum adsorption capacity was found to be 262 mg/g), all synthesized magnetic zeolites were found to be effective at removing Cu ions (151 mg/g, 154 mg/g, and 170 mg/g for 10:1, 10:0.5, and 10:0.1 loading, respectively). Furthermore, the findings indicate minimal fluctuation in the adsorption capacity of the synthesized magnetic zeolites. Therefore, adding a smaller number of iron oxide nanoparticles in the synthesis process would be more practical for further industrial applications and will not significantly affect the adsorption performance of magnetic zeolite.

The results obtained for M-CFAZ show that the zeolite synthesized from CFA has excellent adsorption properties for the investigated metal ions. Specifically, in a single ion system, the maximum adsorption capacity of CFA-zeolite was calculated as 495 mg/g for Pb^{2+}, 248 mg/g for Cu^{2+}, 177 mg/g for Zn^{2+}, and 130 mg/g for Ni^{2+}. When tested with the same dosage of zeolite in the mixed ions system, the adsorption capacity was found to be 276 mg/g for Pb^{2+} and 95 mg/g for Cu^{2+}, while Zn^{2+} and Ni^{2+} ions were not adsorbed. Furthermore, the results suggest that the magnetic zeolite composite has excellent adsorption properties. Thus, in the mixed ion system its maximum adsorption capacity was found to be 261 mg/g, 109 mg/g, 45 mg/g and 42 mg/g for Pb^{2+}, Cu^{2+}, Zn^{2+} and Ni^{2+} ions, respectively; the selectivity order of $Pb^{2+} > Cu^{2+} > Zn^{2+} > Ni^{2+}$ was therefore established for both systems. Additionally, magnetic zeolite was shown to be easily separated from the treated solution using high intensity magnetic separation. Various surface

characterization techniques were utilized to examine the zeolite's surface before and after the adsorption of metal ions, and the results suggest an ion exchange mechanism for the studied metals.

Moreover, the effectiveness of magnetic zeolites was tested in a continuous flow system under various operational conditions, maintaining a consistent selectivity order of Pb > Cu > Zn > Ni, repeating the selectivity order found in previous study of magnetic CFA zeolite in batch systems discussed in Chapter 7.

Furthermore, regeneration of metal-laden magnetic zeolites through desorption experiments was investigated by enhancing the ion-exchange process using a saturated NaCl solution. These results showed that Pb, Zn and Ni ions were completely removed from zeolite, whereas approximately 70% of the Cu remained adsorbed to the sample. Thus, the findings highlight the difference between adsorption and desorption selectivity order. Building on this, a sequential approach could be proposed, where a dedicated loop is designed for Cu removal, allowing the regeneration process to be specifically optimized to enhance Cu desorption efficiency from the metal-laden zeolite.

This research underscores the operational advantages of using magnetic LTA and CFA zeolites in industrial water treatment applications, illustrating their high adsorption capacity and straightforward desorption processes. These characteristics will assist in attaining economic and environmental sustainability through insights into their potential for further industrial application. When exhausted, metal-loaded zeolite can be incorporated into construction materials including concrete production [546-548]. It has been shown by several studies that zeolites not only add structural properties but also immobilize heavy metals, preventing environmental leaching [548,549]. Therefore, the proposed utilization of magnetic CFA-synthesized zeolite not only reduces CFA waste and treats industrial wastewater contaminated with heavy metal ions, but also potentially streamlines the recycling and repurposing of the used zeolite, consequently mitigating environmental impacts.

Chapter 8
Conclusions, Contributions and Future Work

This chapter summarizes the main conclusions drawn from the research presented in this thesis, highlights the contributions to original knowledge, and discusses recommendations for future work on the topics covered in this thesis.

8.1 Conclusions

8.1.1 Zeolites for Water Treatment

The literature reviews in Chapters 2, 3 and 4 of this thesis comprehensively examined water pollution and wastewater management, emphasizing heavy metal remediation. Different water treatment technologies were discussed, particularly focusing on the mining industry's wastewater contaminated with heavy metals. The reviews underscore the potential of natural and synthetic zeolites for effective heavy metal removal due to their superior adsorption capacities, ion exchange properties, and sustainability. The introduction of magnetic adsorbents offers a promising solution, as they can be effectively separated and reused, highlighting the significance of sustainable practices in water treatment. Thus, the reviews identified a knowledge gap in the synthesis of magnetic zeolites from CFA and their application in removing heavy metal ions from water in industrially relevant application. This gap underscores the need for further research and innovation in developing magnetic zeolites, and technology for their extraction from treated water, which served the motivation for this thesis.

8.1.2 Zeolite Synthesis

LTA and CFA zeolites were successfully synthesized and characterized using a variety of techniques including XRD, XPS, SEM, BET, and PSA. The results described in Chapter 6 confirmed that both zeolites exhibit the crystalline structure and morphology typical of type A (LTA) zeolites.

Additionally, a novel method was applied to synthesize magnetic zeolite composites. This involved binding iron oxide nanoparticles to the zeolite using a PVA solution, resulting in magnetic zeolite

composites with varying iron oxide nanoparticle loadings. Characterization of these magnetic zeolites confirmed that the type A structure of the zeolite was retained.

The presence of iron in the magnetic zeolites was confirmed, and it was shown that their magnetic properties improved with increased iron oxide content. Surface area and particle size analysis were also conducted, providing detailed insights into the specific surface area and particles size of the synthesized zeolites.

Furthermore, the VSM technique was used to measure the magnetic properties of synthesized magnetic zeolites. The results showed the superparamagnetic properties of iron oxide nanoparticles and revealed that when combined with the slightly diamagnetic zeolite, the saturation magnetization was shown to increase with the increase of the corresponding amount of added iron oxide nanoparticle content.

Following this comprehensive characterization, the synthesized zeolites were utilized in water treatment experiments. These experiments aimed to investigate their efficiency in the remediation of heavy metals from aqueous solutions, further demonstrating their potential in practical applications.

8.1.3 Adsorption Experiments

Chapter 7 investigated the application of synthesized zeolites in the removal of Pb, Cu, Zn and Ni ions from aqueous solutions in both single and mixed ions systems. Furthermore, magnetic zeolites were investigated in continuous flow system to explore its efficiency under conditions that more closely resemble real-life scenarios.

The results of metal ions removal by LTAZ and CFAZ revealed similar adsorption capacities of the zeolite for selected metal ions and favorable comparison of CFAZ to CFA-synthesized zeolites from literature. For mixed ions system, the results revealed selectivity between the investigated metal ions in the order of $Pb^{2+} > Cu^{2+} > Zn^{2+} > Ni^{2+}$.

Moreover, XPS analysis of zeolites before and after adsorption revealed the disappearance of Na peaks on the zeolite after adsorption, with the simultaneous increase of peaks corresponding to the adsorbed metal ions. Additionally, the pH of the investigated solutions remained constant over time, indicating that the metal ions stayed in solution and their decreased concentration was due

to the adsorption process. The combination of these factors offered deeper insight into the adsorption behavior of zeolite and the potential mechanisms responsible for its selective removal of heavy metals from water.

The adsorption experiments with M-CFAZ revealed a consistent pattern of sorption selectivity between the investigated metal ions. Specifically, the same selectivity order that was found for non-magnetic zeolite $Pb^{2+} > Cu^{2+} > Zn^{2+} > Ni^{2+}$. This trend of preferential adsorption for certain metal ions can be attributed by the difference in their nature, including parameters such as molar weight, electric charge, and ionic radius among ions. These factors can affect the strength of the interaction between metal ions and the adsorbent surface, influencing the adsorption behavior of the system. Overall, the findings suggest that the studied CFAZ exhibits potential as an effective adsorbent material for removing heavy metals from contaminated water.

Further investigations into the adsorption kinetics revealed a competitive nature between the metal ions for the free sites available on CFAZ. These results suggest that in an industrial scale application, it may be beneficial to employ a sequential adsorption process, whereby heavy metal ions are removed in multiple cycles. This approach could involve the removal of Pb in an initial cycle, followed by the removal of other metal ions in subsequent cycles, to avoid competition for available sites on the zeolite surface. This strategy could potentially enhance the efficiency and speed of the adsorption process, providing an effective means of heavy metal removal from water contaminated with a mixture of ions.

8.1.4 Magnetic Separation

The magnetic properties of synthesized magnetic zeolites enabled their removal from treated solution using magnetic separation technology. The results in Chapter 7 demonstrated that fine particles of magnetic zeolite can be efficiently extracted from a treated solution using a single cycle of wet high intensity magnetic separation (WHIMS). This holds great promise for the development of a more sustainable and cost-effective water treatment strategy, whereby the magnetic zeolite can be cleaned and reused in subsequent adsorption cycles.

The environmental importance of sustainable water treatment cannot be overstated. Effective removal of heavy metals from water is crucial for protecting ecosystems and human health. The

use of magnetic zeolites and their easy retrieval through magnetic separation offer a cleaner and more efficient alternative to traditional methods. This technology not only improves the efficiency of water treatment processes but also contributes to environmental conservation by promoting the reuse of materials and reducing waste.

For a deeper understanding of the practical application, sustainability, and further use of magnetic zeolites in heavy metal removal, particularly in industrially relevant applications, experiments were conducted in a continuous flow system.

8.1.5 Continuous flow

A continuous flow experimental setup was designed and built using peristaltic pumps that would pump treated water directly into WHIMS simulating industrially relevant water stream passing through a magnetic separator. M-CFAZ and M-LTAZ were compared in a continuous flow system to assess their ability to adsorb Pb, Cu, Zn, and Ni from mixed ions solutions. Both magnetic zeolites demonstrated the effective removal of Pb and Cu at the different flow rates and zeolite loadings, maintaining the selectivity order of Pb>Cu>Zn>Ni, consistent with findings from our previous batch adsorption experiments. The results show that the type of zeolite affects the adsorption efficiency of the metals, with M-CFA zeolite generally outperforming M-LTA zeolite in terms of metal uptake. This feature enhances the practical and operational benefits of using magnetic synthetic zeolite in real-world applications.

8.1.6 Regeneration of Zeolite

Desorption experiments were performed to regenerate used magnetic zeolite from metal ions and described in Chapter 7, Section 7.6. For that, metal-laden zeolite was stirred in saturated NaCl solutions to facilitate ion exchange. Both solution and zeolite surfaces were analyzed using ICP-OES and SEM-EDS techniques, respectively. The results indicated the effective removal of 100% Pb, Zn, and Ni and 30% of Cu from zeolite. However, it is possible that with the increase of NaCl solution volume where metal-laden zeolite is stirred in, would create more available Na^{2+} ions available to exchange with metal (Me^{2+}) ions and enhance Cu recovery.

The study highlighted the relationship between metal ions in adsorption and desorption processes, showing the importance of ion competition in designing adsorption systems for treating solutions

with multiple metal contaminants. Thus, the adsorption selectivity order was found as $Pb^{2+} > Cu^{2+} > Zn^{2+} > Ni^{2+}$, while in desorption experiments different selectivity order was observed, with Cu^{2+} ions remaining in the sample, while Pb^{2+}, Zn^{2+} and Ni^{2+} were completely removed. These could be due to the difference in bonds type and strength formed by metal ions with zeolite structure, as well as the difference in metal ions, including parameters such as molar weight, electric charge, and ionic radius among the different ions. Additionally, the regenerated magnetic zeolite shows promise for multiple reuses in subsequent water treatment cycles, thereby enhancing the sustainability of the process.

8.1.7 General Conclusions

Water contamination by heavy metals poses significant dangers and requires expensive and complex treatment methods. Finding a sustainable and effective adsorbent material is crucial for improving current water treatment technology. This study involved the successful synthesis of zeolite from coal fly ash (CFA) and its modification to a magnetic composite. Both were evaluated for their ability to adsorb heavy metals from aqueous solutions.

CFA derived zeolite demonstrated similar adsorption performance to non-magnetic zeolites of the same type. Magnetic zeolites were also successfully synthesized by the method developed in this work, binding iron oxide nanoparticles using a novel colloidal PVA solution. Characterization confirmed the presence of iron and retention of the original crystalline structure of Type A zeolite. Both magnetic and non-magnetic CFA zeolites were tested for their ability to remove Pb, Cu, Zn, and Ni from water. The magnetic CFA zeolite maintained its adsorption efficiency in mixed ion systems, with both systems showing selectivity order of Pb>Cu>Zn>Ni.

Surface analysis of the zeolites before and after adsorption suggests an ion exchange mechanism, where metal ions in solution are adsorbed by exchanging Na atoms from the zeolite structure. For zeolite regeneration, a desorption method was employed. Metal-laden zeolites were placed in saturated NaCl solutions, inducing a reverse ion exchange process where adsorbed metal ions were replaced by Na atoms from the solution. This desorption method successfully removed Pb, Zn, and Ni ions from zeolite, indicating that the zeolite can be regenerated and reused in multiple adsorption cycles. Furthermore, the characterization of zeolite after desorption showed that the

iron content in the sample remained the same as before desorption, meaning that magnetic properties of the zeolite were retained.

For industrial relevance, magnetic zeolites were tested in a continuous flow system built using WHIMS. The results showed effective removal of magnetic zeolites from treated water and maintained the selectivity order of adsorption in each cycle. This demonstrates the potential for tailoring zeolites for specific applications, allowing for sequential removal of different metals to optimize the treatment process.

This technology shows great promise for implementation in industrial water processing, particularly in industries like mining, where magnetic separators are already in use. It can also be integrated into the workflows of other industries and adapted to treat various water compositions. However, further research is needed to achieve these goals. The future work section will discuss in detail areas in need of further investigation.

8.2 Contributions to Original Knowledge

The contributions to original knowledge are summarized as follows:

1. Investigation of CFA-derived zeolite for the removal of Pb, Cu, Zn and Ni ions from mixed ions solutions.

2. Development of a novel method for magnetic zeolite synthesis by binding iron oxide nanoparticles to zeolite using PVA crosslinking method.

3. Determination of the optimal iron oxide loading for magnetic zeolite synthesis that maintains adsorption performance while allowing the zeolite to inherit superparamagnetic properties of iron oxide for its further extraction by the application of external magnetic field.

4. Application of magnetic separation technology for magnetic zeolite extraction from treated water. Although magnetic adsorbents have been previously studied, this work represents the first successful application of an industrially viable magnetic separation technique for the recovery of magnetic particles from treated solution.

5. Evaluation of the adsorption efficiency of magnetic CFA zeolite in a continuous flow system, using magnetic separation to extract magnetic zeolite while continuing the process.

6. Examination of magnetic zeolite regeneration using desorption method to removel metal ions from magnetic zeolite, demonstrating successful metal ions removal while retaining iron and, therefore, magnetic properties.

8.3 Future Work

The practical application of magnetic CFA-derived zeolite in real industrial wastewater scenarios should be thoroughly investigated. This includes testing the zeolite with different metal ion compositions, pH levels, and temperatures to determine its effectiveness in real-life conditions. Large-scale continuous flow experiments should be conducted to evaluate the efficiency of magnetic zeolites in industrial settings. Different flow speeds and zeolite loadings can be tested to find optimal conditions for specific need of the industry. The use of industrial-scale magnetic separators should be explored to integrate the suggested use of magnetic CFA zeolite into water treatment processing.

Further research would be complimentary to optimize the synthesis of magnetic zeolites for varying industrial conditions and water compositions. The modeling and synthesis of different magnetic zeolites tailored for specific applications can provide valuable insights. Future research should aim to tailor the zeolites more precisely for different remediation strategies, ensuring their effectiveness. This should involve refinement of the physical and chemical properties of the zeolites and the development of novel methods to customize them for specific contaminants and conditions. For example, the pore size of synthetic zeolite, their surface area, and magnetic properties could be adjusted for the removal of specific pollutants, which does not have to be limited by heavy metals but also include organic pollutants, microplastics and other emerging contaminants. By deepening the understanding of the mechanisms of zeolite pollutant removal, more efficient and precisely targeted zeolites can be synthesized and investigated for diverse environmental applications.

The regeneration and reuse of magnetic zeolites should be further studied to develop robust desorption techniques and improve the longevity of the adsorbents. Investigation of regenerated magnetic zeolite into more cycles of water treatment should be done to find the maximum number of adsorption-desorption cycles that the zeolite can undergo before it is exhausted.

The utilization of exhausted metal-laden zeolite should be investigated. As suggested in previous chapters, the application of zeolite in concrete production is a promising option.

Furthermore, sequential adsorption process could generate distinct effluent streams containing other elements, depending on the composition of solution. These separate streams could provide an opportunity for selective recovery and valorization of additional valuable elements, turning what might otherwise be considered waste into economically or industrially useful products. This approach could not only enhance the efficiency of resource recovery but also support the circular economy by minimizing waste generation and optimizing the utilization of secondary resources. Such a strategy could be particularly beneficial in industries dealing with complex wastewater compositions, such as mining or industrial manufacturing, where multiple valuable elements are often present in trace amounts. By leveraging the unique selectivity of the zeolite in each loop, this method could offer a scalable and sustainable pathway for advanced wastewater treatment and resource recovery.

References

1. Deblonde, T.; Cossu-Leguille, C.; Hartemann, P. Emerging pollutants in wastewater: A review of the literature. *International Journal of Hygiene and Environmental Health* **2011**, *214*, 442-448.
2. Khalid, S.; Shahid, M.; Bibi, I.; Sarwar, T.; Shah, A.H.; Niazi, N.K. A Review of Environmental Contamination and Health Risk Assessment of Wastewater Use for Crop Irrigation with a Focus on Low and High-Income Countries. *International Journal of Environmental Research and Public Health* **2018**, *15*.
3. He, X.; Yao, B.; Xia, Y.; Huang, H.; Gan, Y.; Zhang, W. Coal fly ash derived zeolite for highly efficient removal of Ni2+ inwaste water. *Powder Technology* **2020**, *367*, 40-46.
4. Govender, T.; Barnes, J.M.; Pieper, C.H. The Impact of Densification by Means of Informal Shacks in the Backyards of Low-Cost Houses on the Environment and Service Delivery in Cape Town , South Africa. *Environmental Health Insights* **2011**, *5*, 23-52.
5. Tarazona, J.V. Pollution, Water. *Encyclopedia of Toxicology* **2014**.
6. Jassby, D.; Cath, T.Y.; Buisson, H. The role of nanotechnology in industrial water treatment. *Nature Nanotechnology* **2018**, *13*, 670-672.
7. Duffus, J.H. " Heavy metals" a meaningless term?(IUPAC Technical Report). *Pure and applied chemistry* **2002**, *74*, 793-807.
8. Pourret, O.; Bollinger, J.-C.; Hursthouse, A. Heavy metal: a misused term? *Acta Geochimica* **2021**, *40*, 466-471.
9. Briffa, J.; Sinagra, E.; Blundell, R. Heavy metal pollution in the environment and their toxicological effects on humans. *Heliyon* **2020**, *6*, e04691.
10. Jaishankar, M.; Tseten, T.; Anbalagan, N.; Mathew, B.B.; Beeregowda, K.N. Toxicity, mechanism and health effects of some heavy metals. *Interdisciplinary Toxicology* **2014**, *7*, 60-72.
11. Qasem, N.A.A.; Mohammed, R.H.; Lawal, D.U. Removal of heavy metal ions from wastewater: a comprehensive and critical review. *Clean Water* **2021**, *4*, 36.
12. Huang, Y.; Zeng, X.; Guo, L.; Lan, J.; Zhang, L.; Cao, D. Heavy metal ion removal of wastewater by zeolite-imidazolate frameworks. *Separation and Purification Technology* **2018**, *194*, 462-469.
13. Fu, F.; Wang, Q. Removal of heavy metal ions from wastewaters: A review. *Journal of Environmental Management* **2011**, *92*, 407-418.
14. Wang, B.; Lan, J.; Bo, C.; Gong, B.; Ou, J. Adsorption of heavy metal onto biomass-derived activated carbon: review. *RSC Advances* **2023**, *13*, 4275-4302.
15. Gupta, A.; Sharma, V.; Sharma, K.; Kumar, V.; Choudhary, S.; Mankotia, P.; Kumar, B.; Mishra, H.; Moulick, A.; Ekielski, A.; et al. A Review of Adsorbents for Heavy Metal Decontamination: Growing Approach to Wastewater Treatment. *Materials* **2021**, *14*.
16. da Silva, A.d.S.; da Rocha, Z.N.; Mignoni, M.L.; dos Santos, J.H.Z. Solvent-free synthesis of modified zeolites using hybrid silicas as raw material. *Microporous and Mesoporous Materials* **2019**, *290*, 109684-109684.
17. Dusselier, M.; Davis, M.E. Small-pore zeolites: synthesis and catalysis. *Chemical Reviews* **2018**, *118*, 5265-5329.

18. Barrer, R.M. Zeolites and their synthesis. *Zeolites* **1981**, *1*, 130-140.
19. Davis, M.E.; Lobo, R.F. Zeolite and molecular sieve synthesis. *Chemistry of Materials* **1992**, *4*, 756-768.
20. Li, Y.; Zhu, G.; Wang, Y.; Chai, Y.; Liu, C. Preparation, mechanism and applications of oriented MFI zeolite membranes: A review. *Microporous and Mesoporous Materials* **2021**, *312*, 110790.
21. Kesraoui-Ouki, S.; Cheeseman, C.R.; Perry, R. Natural zeolite utilisation in pollution control: A review of applications to metals' effluents. *Journal of Chemical Technology & Biotechnology: International Research in Process, Environmental and Clean Technology* **1994**, *59*, 121-126.
22. Wang, S.; Peng, Y. Natural zeolites as effective adsorbents in water and wastewater treatment. *Chemical Engineering Journal* **2010**, *156*, 11-24.
23. Weitkamp, J. Zeolites and catalysis. *Solid State Ionics* **2000**, *131*, 175-188.
24. Król, M. Natural vs. Synthetic Zeolites. *Crystals* **2020**, *10(7): 622*.
25. Gottardi, G.; Galli, E. *Natural Zeolites*; Springer Science & Business Media: 2012; Volume 18.
26. Meiramkulova, K.; Kydyrbekova, A.; Devrishov, D.; Nurbala, U.; Tuyakbayeva, A.; Zhangazin, S.; Ualiyeva, R.; Kolpakova, V.; Yeremeyeva, Y.; Mkilima, T. Comparative analysis of natural and synthetic zeolite filter performance in the purification of groundwater. *Water* **2023**, *15*, 588.
27. Khaleque, A.; Alam, M.M.; Hoque, M.; Mondal, S.; Haider, J.B.; Xu, B.; Johir, M.A.H.; Karmakar, A.K.; Zhou, J.L.; Ahmed, M.B.; et al. Zeolite synthesis from low-cost materials and environmental applications: A review. *Environmental Advances* **2020**, *2*, 100019.
28. Breck, D.W. Crystalline molecular sieves. *Journal of Chemical Education* **1964**, *41*, 678-678.
29. Moshoeshoe, M.; Nadiye-Tabbiruka, M.S.; Obuseng, V. A review of the chemistry, structure, properties and applications of zeolites. *American Journal of Materials Science* **2017**, *7*, 196-221.
30. Yu, J. Chapter 3 - Synthesis of Zeolites. In *Studies in Surface Science and Catalysis*, Čejka, J., van Bekkum, H., Corma, A., Schüth, F., Eds.; Elsevier: 2007; Volume 168, pp. 39-103.
31. Jha, V.K.; Matsuda, M.; Miyake, M. Resource recovery from coal fly ash waste: an overview study. *Journal of the Ceramic Society of Japan* **2008**, *116*, 167-175.
32. Bukhari, S.; Behin, J.; Kazemian, H.; Rohani, S. Conversion of coal fly ash to zeolite utilizing microwave and ultrasound energies: A review. *Fuel* **2015**, *140*, 250-266.
33. Belviso, C.; Cavalcante, F.; Lettino, A.; Fiore, S. Zeolite Synthesised from Fused Coal Fly Ash at Low Temperature Using Seawater for Crystallization. *Coal Combustion and Gasification Products* **2009**, *1*, 7-13.
34. Blissett, R.S.; Rowson, N.A. A review of the multi-component utilisation of coal fly ash. *Fuel* **2012**, *97*, 1-23.
35. Borm, P.J. Toxicity and occupational health hazards of coal fly ash (CFA). A review of data and comparison to coal mine dust. *The Annals of Occupational Hygiene* **1997**, *41*, 659-676.
36. Harris, D. Ash as an internationally traded commodity. In *Coal Combustion Products (CCP's)*; Elsevier: 2017; pp. 509-529.

37. Vilakazi, A.Q.; Ndlovu, S.; Chipise, L.; Shemi, A. The recycling of coal fly ash: A review on sustainable developments and economic considerations. *Sustainability* **2022**, *14*, 1958.
38. Chen, Y.; Fan, Y.; Huang, Y.; Liao, X.; Xu, W.; Zhang, T. A comprehensive review of toxicity of coal fly ash and its leachate in the ecosystem. *Ecotoxicology and Environmental Safety* **2024**, *269*, 115905.
39. Belviso, C. State-of-the-art applications of fly ash from coal and biomass: A focus on zeolite synthesis processes and issues. *Progress in Energy and Combustion Science* **2018**, *65*, 109-135.
40. Franus, W.; Wdowin, M.; Franus, M. Synthesis and characterization of zeolites prepared from industrial fly ash. *Environmental Monitoring and Assessment* **2014**, *186*, 5721-5729.
41. Younas, F.; Mustafa, A.; Farooqi, Z.U.R.; Wang, X.; Younas, S.; Mohy-Ud-Din, W.; Ashir Hameed, M.; Mohsin Abrar, M.; Maitlo, A.A.; Noreen, S.; et al. Current and Emerging Adsorbent Technologies for Wastewater Treatment: Trends, Limitations, and Environmental Implications. *Water* **2021**, *13*, 215.
42. Castro, C.; Shyu, H.; Xaba, L.; Bair, R.; Yeh, D. Performance and onsite regeneration of natural zeolite for ammonium removal in a field-scale non-sewered sanitation system. *Science of The Total Environment* **2021**, *776*, 145938.
43. Maharana, M.; Sen, S. Magnetic zeolite: A green reusable adsorbent in wastewater treatment. *Materials Today: Proceedings* **2021**, *47*, 1490-1495.
44. Loiola, A.R.; Bessa, R.A.; Oliveira, C.P.; Freitas, A.D.; Soares, S.A.; Bohn, F.; Pergher, S.B. Magnetic zeolite composites: Classification, synthesis routes, and technological applications. *Journal of Magnetism and Magnetic Materials* **2022**, *560*, 169651.
45. Mehta, D.; Mazumdar, S.; Singh, S.K. Magnetic adsorbents for the treatment of water/wastewater—A review. *Journal of Water Process Engineering* **2015**, *7*, 244-265.
46. Ali, I.; Peng, C.; Naz, I.; Amjed, M.A. Water purification using magnetic nanomaterials: an overview. *Magnetic Nanostructures: Environmental and Agricultural Applications* **2019**, 161-179.
47. Allon, F.; Sofoulis, Z. Everyday Water: cultures in transition. *Australian Geographer* **2006**, *37*, 45-55.
48. Ahmed, J.; Thakur, A.; Goyal, A. Industrial Wastewater and Its Toxic Effects. In *Biological Treatment of Industrial Wastewater*, Shah, M.P., Ed.; The Royal Society of Chemistry: 2021; p. 420.
49. Xu, X.; Yang, H.; Li, C. Theoretical model and actual characteristics of air pollution affecting health cost: a review. *International Journal of Environmental Research and Public Health* **2022**, *19*, 3532.
50. Pltonykova, H.; Koeppel, S.; Bernardini, F.; Tiefenauer-Linardon, S.; de Strasser, L. The United Nations World Water Development Report 2020: Water and Climate Change. **2020**.
51. Vanham, D.; Alfieri, L.; Flörke, M.; Grimaldi, S.; Lorini, V.; de Roo, A.; Feyen, L. The number of people exposed to water stress in relation to how much water is reserved for the environment: a global modelling study. *The Lancet Planetary Health* **2021**, *5*, e766-e774.
52. Vanham, D.; Hoekstra, A.Y.; Wada, Y.; Bouraoui, F.; de Roo, A.; Mekonnen, M.M.; Van De Bund, W.; Batelaan, O.; Pavelic, P.; Bastiaanssen, W.G. Physical water scarcity metrics for monitoring progress towards SDG target 6.4: An evaluation of indicator 6.4. 2 “Level of water stress”. *Science of the Total Environment* **2018**, *613*, 218-232.

53. Biancalani, R.; Marinelli, M. Assessing SDG indicator 6.4.2 'level of water stress' at major basins level. *UCL Open Environment* **2021**, *3*, e026.
54. Babuji, P.; Thirumalaisamy, S.; Duraisamy, K.; Periyasamy, G. Human Health Risks due to Exposure to Water Pollution: A Review. *Water* **2023**, *15*, 2532.
55. Inyinbor Adejumoke, A.; Adebesin Babatunde, O.; Oluyori Abimbola, P.; Adelani-Akande Tabitha, A.; Dada Adewumi, O.; Oreofe Toyin, A. Water Pollution: Effects, Prevention, and Climatic Impact. In *Water Challenges of an Urbanizing World*, Matjaž, G., Ed.; IntechOpen: Rijeka, 2018; p. Ch. 3.
56. Lin, L.; Yang, H.; Xu, X. Effects of Water Pollution on Human Health and Disease Heterogeneity: A Review. *Frontiers in Environmental Science* **2022**, *10*.
57. Lawan, M.S.; Kumar, R.; Rashid, J.; Barakat, M.A.E.-F. Recent Advancements in the Treatment of Petroleum Refinery Wastewater. *Water* **2023**, *15*, 3676.
58. Azimi, A.; Azari, A.; Rezakazemi, M.; Ansarpour, M. Removal of Heavy Metals from Industrial Wastewaters: A Review. *ChemBioEng Reviews* **2017**, *4*, 37-59.
59. Barakat, M.A. New trends in removing heavy metals from industrial wastewater. *Arabian Journal of Chemistry* **2011**, *4*, 361-377.
60. Warren-Vega, W.M.; Campos-Rodríguez, A.; Zárate-Guzmán, A.I.; Romero-Cano, L.A. A Current Review of Water Pollutants in American Continent: Trends and Perspectives in Detection, Health Risks, and Treatment Technologies. *International Journal of Environmental Research and Public Health* **2023**, *20*.
61. Schoen, M.E.; Ashbolt, N.J. Assessing Pathogen Risk to Swimmers at Non-Sewage Impacted Recreational Beaches. *Environmental Science & Technology* **2010**, *44*, 2286-2291.
62. Munter, R. Industrial wastewater characteristics. *The Baltic University Programme (BUP), Sweden* **2003**, *185*.
63. Manasa, R.L.; Mehta, A. Wastewater: Sources of Pollutants and Its Remediation. In *Environmental Biotechnology Vol. 2*, Gothandam, K.M., Ranjan, S., Dasgupta, N., Lichtfouse, E., Eds.; Springer International Publishing: Cham, 2020; pp. 197-219.
64. Zamora-Ledezma, C.; Negrete-Bolagay, D.; Figueroa, F.; Zamora-Ledezma, E.; Ni, M.; Alexis, F.; Guerrero, V.H. Heavy metal water pollution: A fresh look about hazards, novel and conventional remediation methods. *Environmental Technology & Innovation* **2021**, *22*, 101504.
65. Viswanathan, S.P.; Kuriakose, G.M.; Neelamury, S.P.; Njazhakunnathu, G.V.; Paili, T.A. Biochar-based composites as environmentally sustainable functional materials for wastewater treatment. In *Reference Module in Materials Science and Materials Engineering*; Elsevier: 2023.
66. Matebese, F.; Mosai, A.K.; Tutu, H.; Tshentu, Z.R. Mining wastewater treatment technologies and resource recovery techniques: A review. *Heliyon* **2024**, *10*, e24730.
67. Wang, J.; Chen, C. Biosorbents for heavy metals removal and their future. *Biotechnology Advances* **2009**, *27*, 195-226.
68. Aslam, M.M.-A.; Kuo, H.-W.; Den, W.; Usman, M.; Sultan, M.; Ashraf, H. Functionalized carbon nanotubes (CNTs) for water and wastewater treatment: preparation to application. *Sustainability* **2021**, *13*, 5717.
69. Dutta, D.; Arya, S.; Kumar, S. Industrial wastewater treatment: Current trends, bottlenecks, and best practices. *Chemosphere* **2021**, *285*, 131245.

70. Demiral, İ.; Samdan, C.; Demiral, H. Enrichment of the surface functional groups of activated carbon by modification method. *Surfaces and Interfaces* **2021**, *22*, 100873.
71. Kumar, A.S.K.; Jiang, S.-J.; Tseng, W.-L. Effective adsorption of chromium (VI)/Cr (III) from aqueous solution using ionic liquid functionalized multiwalled carbon nanotubes as a super sorbent. *Journal of Materials Chemistry A* **2015**, *3*, 7044-7057.
72. Duan, C.; Ma, T.; Wang, J.; Zhou, Y. Removal of heavy metals from aqueous solution using carbon-based adsorbents: A review. *Journal of Water Process Engineering* **2020**, *37*, 101339.
73. Marciniak, M.; Goscianska, J.; Frankowski, M.; Pietrzak, R. Optimal synthesis of oxidized mesoporous carbons for the adsorption of heavy metal ions. *Journal of Molecular Liquids* **2019**, *276*, 630-637.
74. Owalude, S.O.; Tella, A.C. Removal of hexavalent chromium from aqueous solutions by adsorption on modified groundnut hull. *Beni-Suef University Journal of Basic and Applied Sciences* **2016**, *5*, 377-388.
75. Ngah, W.W.; Fatinathan, S. Adsorption of Cu (II) ions in aqueous solution using chitosan beads, chitosan–GLA beads and chitosan–alginate beads. *Chemical Engineering Journal* **2008**, *143*, 62-72.
76. Upadhyay, U.; Sreedhar, I.; Singh, S.A.; Patel, C.M.; Anitha, K. Recent advances in heavy metal removal by chitosan based adsorbents. *Carbohydrate Polymers* **2021**, *251*, 117000.
77. Abdur Razzak, S.; Faruque, M.O.; Alsheikh, Z.; Alsheikhmohamad, L.; Alkuroud, D.; Alfayez, A.; Hossain, S.M.; Hossain, M. A Comprehensive Review on Conventional and Biological-Driven Heavy Metals Removal from Industrial Wastewater. *Environmental Advances* **2022**, *7*, 100168.
78. Saleh, T.A.; Mustaqeem, M.; Khaled, M. Water treatment technologies in removing heavy metal ions from wastewater: A review. *Environmental Nanotechnology, Monitoring & Management* **2022**, *17*, 100617.
79. Mishra, V. Biosorption of zinc ion: a deep comprehension. *Applied Water Science* **2014**, *4*, 311-332.
80. Gao, X.; Meng, X. Photocatalysis for Heavy Metal Treatment: A Review. *Processes* **2021**, *9*, 1729.
81. Barakat, M. New trends in removing heavy metals from industrial wastewater. *Arabian Journal of Chemistry* **2011**, *4*, 361-377.
82. Marinho, B.A.; Djellabi, R.; Cristóvão, R.O.; Loureiro, J.M.; Boaventura, R.A.R.; Dias, M.M.; Lopes, J.C.B.; Vilar, V.J.P. Intensification of heterogeneous TiO2 photocatalysis using an innovative micro–meso-structured-reactor for Cr(VI) reduction under simulated solar light. *Chemical Engineering Journal* **2017**, *318*, 76-88.
83. Zhu, S.; Wang, D. Photocatalysis: Basic Principles, Diverse Forms of Implementations and Emerging Scientific Opportunities. *Advanced Energy Materials* **2017**, *7*, 1700841.
84. Macedo, O.; Menezes de Oliveira, A.; Santos, I. Zinc tungstate: a review on its application as heterogeneous photocatalyst. *Cerâmica* **2022**, *68*, 294-315.
85. Kyzas, G.Z.; Matis, K.A. Flotation in water and wastewater treatment. *Processes* **2018**, *6*, 116.
86. Deliyanni, E.A.; Kyzas, G.Z.; Matis, K.A. Various flotation techniques for metal ions removal. *Journal of Molecular Liquids* **2017**, *225*, 260-264.

87. Peleka, E.N.; Gallios, G.P.; Matis, K.A. A perspective on flotation: A review. *Journal of Chemical Technology & Biotechnology* **2018**, *93*, 615-623.
88. Clarke, A.N.; Wilson, D.J. *Foam Flotation–Theory and Applications*; Marcel Dekker Inc. : New York, 1983.
89. Chang, L.; Cao, Y.; Fan, G.; Li, C.; Peng, W. A review of the applications of ion floatation: wastewater treatment, mineral beneficiation and hydrometallurgy. *RSC Advances* **2019**, *9*, 20226-20239.
90. Wang, L.K.; Vaccari, D.A.; Li, Y.; Shammas, N.K. Chemical Precipitation. In *Physicochemical Treatment Processes*, Wang, L.K., Hung, Y.-T., Shammas, N.K., Eds.; Humana Press: Totowa, NJ, 2005; pp. 141-197.
91. Dąbrowski, A.; Hubicki, Z.; Podkościelny, P.; Robens, E. Selective removal of the heavy metal ions from waters and industrial wastewaters by ion-exchange method. *Chemosphere* **2004**, *56*, 91-106.
92. Barrera-Díaz, C.E.; Balderas-Hernández, P.; Bilyeu, B. Chapter 3 - Electrocoagulation: Fundamentals and Prospectives. In *Electrochemical Water and Wastewater Treatment*, Martínez-Huitle, C.A., Rodrigo, M.A., Scialdone, O., Eds.; Butterworth-Heinemann: 2018; pp. 61-76.
93. Almukdad, A.; Hawari, A.H.; Hafiz, M. An Enhanced Electrocoagulation Process for the Removal of Fe and Mn from Municipal Wastewater Using Dielectrophoresis (DEP). *Water* **2021**, *13*, 485.
94. Badawi, A.K.; Salama, R.S.; Mostafa, M.M.M. Natural-based coagulants/flocculants as sustainable market-valued products for industrial wastewater treatment: a review of recent developments. *RSC Advances* **2023**, *13*, 19335-19355.
95. Al-Muhtaseb, A.; Jamil, F.; Sarwer, A.; Al-Maawali, S. Chapter 6 - Valorization of microalgal biomass for food. In *Valorization of Microalgal Biomass and Wastewater Treatment*, Bandh, S.A., Malla, F.A., Eds.; Elsevier: 2023; pp. 81-112.
96. Johnson, C. 2.4 - Advances in Pretreatment and Clarification Technologies. In *Comprehensive Water Quality and Purification*, Ahuja, S., Ed.; Elsevier: Waltham, 2014; pp. 60-74.
97. Birniwa, A.H.; Habibu, S.; Abdullahi, S.S.a.; Mohammad, R.E.A.; Hussaini, A.; Magaji, H.; Al-dhawi, B.N.S.; Noor, A.; Jagaba, A.H. Membrane technologies for heavy metals removal from water and wastewater: A mini review. *Case Studies in Chemical and Environmental Engineering* **2024**, *9*, 100538.
98. Abdullah, N.; Yusof, N.; Lau, W.J.; Jaafar, J.; Ismail, A.F. Recent trends of heavy metal removal from water/wastewater by membrane technologies. *Journal of Industrial and Engineering Chemistry* **2019**, *76*, 17-38.
99. El Batouti, M.; Al-Harby, N.F.; Elewa, M.M. A Review on Promising Membrane Technology Approaches for Heavy Metal Removal from Water and Wastewater to Solve Water Crisis. *Water* **2021**, *13*, 3241.
100. Liao, Y.; Loh, C.-H.; Tian, M.; Wang, R.; Fane, A.G. Progress in electrospun polymeric nanofibrous membranes for water treatment: Fabrication, modification and applications. *Progress in Polymer Science* **2018**, *77*, 69-94.
101. Kyzas, G.Z.; Fu, J.; Matis, K.A. The Change from Past to Future for Adsorbent Materials in Treatment of Dyeing Wastewaters. *Materials* **2013**, *6*, 5131-5158.

102. Rajendran, S.; Priya, A.K.; Senthil Kumar, P.; Hoang, T.K.A.; Sekar, K.; Chong, K.Y.; Khoo, K.S.; Ng, H.S.; Show, P.L. A critical and recent developments on adsorption technique for removal of heavy metals from wastewater-A review. *Chemosphere* **2022**, *303*, 135146.
103. Barik, B.; Kumar, A.; Nayak, P.S.; Achary, L.S.K.; Rout, L.; Dash, P. Ionic liquid assisted mesoporous silica-graphene oxide nanocomposite synthesis and its application for removal of heavy metal ions from water. *Materials Chemistry and Physics* **2020**, *239*, 122028.
104. Hui, K.; Chao, C.Y.H.; Kot, S. Removal of mixed heavy metal ions in wastewater by zeolite 4A and residual products from recycled coal fly ash. *Journal of Hazardous Materials* **2005**, *127*, 89-101.
105. Mohan, S.; Gandhimathi, R. Solid waste characterisation and the assessment of the effect of dumping site leachate on groundwater quality: a case study. *International Journal of Environment and Waste Management* **2009**, *3*, 65-77.
106. Xu, X.; Cao, X.; Zhao, L. Comparison of rice husk-and dairy manure-derived biochars for simultaneously removing heavy metals from aqueous solutions: role of mineral components in biochars. *Chemosphere* **2013**, *92*, 955-961.
107. Lucassen-Reynders, E.H. Adsorption of Surfactant Monolayers at Gas/Liquid and Liquid/Liquid Interfaces. In *Progress in Surface and Membrane Science*, Cadenhead, D.A., Danielli, J.F., Eds.; Elsevier: 1976; Volume 10, pp. 253-360.
108. Patterson, H.B.W. Chapter 2 - Adsorption. In *Bleaching and Purifying Fats and Oils (Second Edition)*, List, G.R., Ed.; AOCS Press: 2009; pp. 53-67.
109. Satyam, S.; Patra, S. Innovations and challenges in adsorption-based wastewater remediation: A comprehensive review. *Heliyon* **2024**, *10*, e29573.
110. Dąbrowski, A. Adsorption — from theory to practice. *Advances in Colloid and Interface Science* **2001**, *93*, 135-224.
111. Xu, D.; Tan, X.; Chen, C.; Wang, X. Adsorption of Pb (II) from aqueous solution to MX-80 bentonite: effect of pH, ionic strength, foreign ions and temperature. *Applied Clay Science* **2008**, *41*, 37-46.
112. Rahman, M.S.; Islam, M.R. Effects of pH on isotherms modeling for Cu(II) ions adsorption using maple wood sawdust. *Chemical Engineering Journal* **2009**, *149*, 273-280.
113. Božić, D.; Stanković, V.; Gorgievski, M.; Bogdanović, G.; Kovačević, R. Adsorption of heavy metal ions by sawdust of deciduous trees. *Journal of Hazardous Materials* **2009**, *171*, 684-692.
114. Saleh, T.A. Simultaneous adsorptive desulfurization of diesel fuel over bimetallic nanoparticles loaded on activated carbon. *Journal of Cleaner Production* **2018**, *172*, 2123-2132.
115. Heidarinejad, Z.; Dehghani, M.H.; Heidari, M.; Javedan, G.; Ali, I.; Sillanpää, M. Methods for preparation and activation of activated carbon: a review. *Environmental Chemistry Letters* **2020**, *18*, 393-415.
116. Saravanan, A.; Kumar, P.S.; Hemavathy, R.V.; Jeevanantham, S.; Jawahar, M.J.; Neshaanthini, J.P.; Saravanan, R. A review on synthesis methods and recent applications of nanomaterial in wastewater treatment: Challenges and future perspectives. *Chemosphere* **2022**, *307*, 135713.
117. Sadegh, H.; Ali, G.A.; Gupta, V.K.; Makhlouf, A.S.H.; Shahryari-Ghoshekandi, R.; Nadagouda, M.N.; Sillanpää, M.; Megiel, E. The role of nanomaterials as effective

adsorbents and their applications in wastewater treatment. *Journal of Nanostructure in Chemistry* **2017**, *7*, 1-14.

118. Burakov, A.E.; Galunin, E.V.; Burakova, I.V.; Kucherova, A.E.; Agarwal, S.; Tkachev, A.G.; Gupta, V.K. Adsorption of heavy metals on conventional and nanostructured materials for wastewater treatment purposes: A review. *Ecotoxicology and Environmental Safety* **2018**, *148*, 702-712.
119. Chen, X.; Hossain, M.F.; Duan, C.; Lu, J.; Tsang, Y.F.; Islam, M.S.; Zhou, Y. Isotherm models for adsorption of heavy metals from water - A review. *Chemosphere* **2022**, *307*, 135545.
120. Chen, Z.; Ma, W.; Han, M. Biosorption of nickel and copper onto treated alga (Undaria pinnatifida): Application of isotherm and kinetic models. *Journal of Hazardous Materials* **2008**, *155*, 327-333.
121. Günay, A.; Arslankaya, E.; Tosun, I. Lead removal from aqueous solution by natural and pretreated clinoptilolite: adsorption equilibrium and kinetics. *Journal of Hazardous Materials* **2007**, *146*, 362-371.
122. Langmuir, I. The adsorption of gases on plane surfaces of glass, mica and platinum. *Journal of the American Chemical Society* **1918**, *40*, 1361-1403.
123. Liu, L.; Luo, X.-B.; Ding, L.; Luo, S.-L. 4 - Application of Nanotechnology in the Removal of Heavy Metal From Water. In *Nanomaterials for the Removal of Pollutants and Resource Reutilization*, Luo, X., Deng, F., Eds.; Elsevier: 2019; pp. 83-147.
124. Hodge, R.A.; Ericsson, M.; Löf, O.; Löf, A.; Semkowich, P. The global mining industry: corporate profile, complexity, and change. *Mineral Economics* **2022**, *35*, 587-606.
125. Ericsson, M.; Löf, O. Mining's contribution to national economies between 1996 and 2016. *Mineral Economics* **2019**, *32*, 223-250.
126. Northey, S.A.; Mudd, G.M.; Saarivuori, E.; Wessman-Jääskeläinen, H.; Haque, N. Water footprinting and mining: Where are the limitations and opportunities? *Journal of Cleaner Production* **2016**, *135*, 1098-1116.
127. Hosseinpour, M.; Osanloo, M.; Azimi, Y. Evaluation of positive and negative impacts of mining on sustainable development by a semi-quantitative method. *Journal of Cleaner Production* **2022**, *366*, 132955.
128. Zahoor, A.; Mao, G.; Jia, X.; Xiao, X.; Chen, J.L. Global research progress on mining wastewater treatment: a bibliometric analysis. *Environmental Science Advances* **2022**, *1*, 92-109.
129. Meißner, S. The impact of metal mining on global water stress and regional carrying capacities—a GIS-based water impact assessment. *Resources* **2021**, *10*, 120.
130. Ugya, A.; Ajibade, F.; Ajibade, T. Water pollution resulting from mining activity: An overview. In Proceedings of the 2018 annual conference of the school of engineering & engineering technology (SEET), The Federal University of Technology, Akure, Nigeria, 2018.
131. Kurniawan, S.B.; Ramli, N.N.; Said, N.S.M.; Alias, J.; Imron, M.F.; Abdullah, S.R.S.; Othman, A.R.; Purwanti, I.F.; Hasan, H.A. Practical limitations of bioaugmentation in treating heavy metal contaminated soil and role of plant growth promoting bacteria in phytoremediation as a promising alternative approach. *Heliyon* **2022**, *8(4): e08995*.
132. Asif, Z.; Chen, Z. Environmental management in North American mining sector. *Environmental Science and Pollution Research* **2016**, *23*, 167-179.

133. Khobragade, K. Impact of mining activity on environment: an overview. *International Journal of Scientific and Research Publications* **2020**, *10*, 784-791.
134. RoyChowdhury, A.; Sarkar, D.; Datta, R. Remediation of acid mine drainage-impacted water. *Current Pollution Reports* **2015**, *1*, 131-141.
135. Thomas, G.; Sheridan, C.; Holm, P.E. A critical review of phytoremediation for acid mine drainage-impacted environments. *Science of the Total Environment* **2022**, *811*, 152230.
136. Yaraghi, N.; Ronkanen, A.-K.; Haghighi, A.T.; Aminikhah, M.; Kujala, K.; Kløve, B. Impacts of gold mine effluent on water quality in a pristine sub-Arctic river. *Journal of Hydrology* **2020**, *589*, 125170.
137. Reid, C.; Bécaert, V.; Aubertin, M.; Rosenbaum, R.K.; Deschênes, L. Life cycle assessment of mine tailings management in Canada. *Journal of Cleaner Production* **2009**, *17*, 471-479.
138. Thomashausen, S.; Maennling, N.; Mebratu-Tsegaye, T. A comparative overview of legal frameworks governing water use and waste water discharge in the mining sector. *Resources Policy* **2018**, *55*, 143-151.
139. Zhang, L.; Huang, M.; Li, M.; Lu, S.; Yuan, X.; Li, J. Experimental study on evolution of fracture network and permeability characteristics of bituminous coal under repeated mining effect. *Natural Resources Research* **2021**, 1-24.
140. Zhang, L.; Huang, M.; Xue, J.; Li, M.; Li, J. Repetitive mining stress and pore pressure effects on permeability and pore pressure sensitivity of bituminous coal. *Natural Resources Research* **2021**, *30*, 4457-4476.
141. Sui, Y.; Abdulkreem Al-Huqail, A.; Suhatril, M.; Abed, A.M.; Zhao, Y.; Assilzadeh, H.; Amine Khadimallah, M.; Elhosiny Ali, H. Hydrogen energy of mining waste waters: Extraction and analysis of solving issues. *Fuel* **2023**, *331*, 125685.
142. Sánchez, F.; Hartlieb, P. Innovation in the Mining Industry: Technological Trends and a Case Study of the Challenges of Disruptive Innovation. *Mining, Metallurgy & Exploration* **2020**, *37*, 1385-1399.
143. Caron, J.; Durand, S.; Asselin, H. Principles and criteria of sustainable development for the mineral exploration industry. *Journal of Cleaner Production* **2016**, *119*, 215-222.
144. Napier-Munn, T.; Morrison, R. The potential for the dry processing of ores. **2003**.
145. Gunson, A.; Klein, B.; Veiga, M.; Dunbar, S. Reducing mine water requirements. *Journal of Cleaner Production* **2012**, *21*, 71-82.
146. Vick, S.G. *Planning, design, and analysis of tailings dams*; BiTech Publishers Ltd.: UBC Community and Partner Publications., 1990.
147. Davies, M. Filtered dry stacked tailings: the fundamentals. In Proceedings of the Tailings and Mine Waste 2011, Vancouver, BC, November 2011.
148. Ramirez-Llodra, E.; Trannum, H.C.; Evenset, A.; Levin, L.A.; Andersson, M.; Finne, T.E.; Hilario, A.; Flem, B.; Christensen, G.; Schaanning, M. Submarine and deep-sea mine tailing placements: a review of current practices, environmental issues, natural analogs and knowledge gaps in Norway and internationally. *Marine Pollution Bulletin* **2015**, *97*, 13-35.
149. Azam, S.; Li, Q. Tailings dam failures: a review of the last one hundred years. *Geotechnical News* **2010**, *28*, 50-54.
150. Hayward, J. The contents of a tailings pond are pictured flowing down the Hazeltine Creek into Quesnel Lake near the town of Likely, B.C. on August, 5, 2014. Available online: https://www.cbc.ca/news/canada/british-columbia/mount-polley-mine-disaster-5-years-later-emotions-accountability-unresolved-1.5236160 (accessed on 25 August, 2024).

151. Correia, B. An aerial view after a tailings dam collapsed near Brumadinho, Brazil. Brazilian mining company Vale SA said about 300 of its workers were in the area at the time, and hundreds of them remained unaccounted for. Available online: https://www.cbc.ca/news/world/brazil-vale-tailings-dam-collapse-1.4993711 (accessed on August 25, 2024).
152. Meseldzija, S.; Petrovic, J.; Onjia, A.; Volkov-Husovic, T.; Nesic, A.; Vukelic, N. Utilization of agro-industrial waste for removal of copper ions from aqueous solutions and mining-wastewater. *Journal of Industrial and Engineering Chemistry* **2019**, *75*, 246-252.
153. Samaei, S.M.; Gato-Trinidad, S.; Altaee, A. Performance evaluation of reverse osmosis process in the post-treatment of mining wastewaters: Case study of Costerfield mining operations, Victoria, Australia. *Journal of Water Process Engineering* **2020**, *34*, 101116.
154. Falconi, I.B.A.; Botelho, A.B.; Baltazar, M.d.P.G.; Espinosa, D.C.R.; Tenório, J.A.S. An overview of treatment techniques to remove ore flotation reagents from mining wastewater. *Journal of Environmental Chemical Engineering* **2023**, *11*, 111270.
155. Gupta, V.K.; Ali, I.; Saleh, T.A.; Nayak, A.; Agarwal, S. Chemical treatment technologies for waste-water recycling—an overview. *RSC Advances* **2012**, *2*, 6380-6388.
156. Mohan, D.; Pittman Jr, C.U. Arsenic removal from water/wastewater using adsorbents—a critical review. *Journal of Hazardous Materials* **2007**, *142*, 1-53.
157. Miller, K.D.; Bentley, M.J.; Ryan, J.N.; Linden, K.G.; Larison, C.; Kienzle, B.A.; Katz, L.E.; Wilson, A.M.; Cox, J.T.; Kurup, P.; et al. Mine Water Use, Treatment, and Reuse in the United States: A Look at Current Industry Practices and Select Case Studies. *American Chemical Society Environmental Science & Technology Engineering* **2022**, *2*, 391-408.
158. Minerals and the economy. Available online: https://natural-resources.canada.ca/our-natural-resources/minerals-mining/mining-data-statistics-and-analysis/minerals-and-the-economy/20529#GDP (accessed on May 2024).
159. Nadeau, S.; Badri, A.; Wells, R.; Neumann, P.; Kenny, G.; Morrison, D. Sustainable canadian mining:Occupational health and safety challenges. *Proceedings of the Human Factors and Ergonomics Society Annual Meeting* **2013**, *57*, 1071-1074.
160. Holeton, C.; Chambers, P.A.; Grace, L. Wastewater release and its impacts on Canadian waters. *Canadian Journal of Fisheries and Aquatic Sciences* **2011**, *68*, 1836-1859.
161. Russell, B.I.; Shapiro, D.; Vining, A.R. The evolution of the Canadian mining industry: The role of regulatory punctuation. *Resources Policy* **2010**, *35*, 90-97.
162. Fisheries Act Registry: pollution prevention. Available online: https://www.canada.ca/en/environment-climate-change/services/managing-pollution/fisheries-act-registry.html (accessed on May 2024).
163. Metal Mining Effluent Regulations. (SOR/2002-222). (2016). Minister of Justice of Canada. Available online: https://laws-lois.justice.gc.ca/eng/regulations/sor-2002-222/FullText.html (accessed on July 2024).
164. Trakal, L.; Šigut, R.; Šillerová, H.; Faturíková, D.; Komárek, M. Copper removal from aqueous solution using biochar: Effect of chemical activation. *Arabian Journal of Chemistry* **2014**, *7*, 43-52.
165. Ruyters, S.; Salaets, P.; Oorts, K.; Smolders, E. Copper toxicity in soils under established vineyards in Europe: A survey. *Science of The Total Environment* **2013**, *443*, 470-477.

166. Shrestha, R.; Ban, S.; Devkota, S.; Sharma, S.; Joshi, R.; Tiwari, A.P.; Kim, H.Y.; Joshi, M.K. Technological trends in heavy metals removal from industrial wastewater: A review. *Journal of Environmental Chemical Engineering* **2021**, *9*, 105688.
167. Ab Hamid, N.H.; bin Mohd Tahir, M.I.H.; Chowdhury, A.; Nordin, A.H.; Alshaikh, A.A.; Suid, M.A.; Nazaruddin, N.I.; Nozaizeli, N.D.; Sharma, S.; Rushdan, A.I. The Current State-Of-Art of Copper Removal from Wastewater: A Review. *Water* **2022**, *14*, 3086.
168. Yin, Z.; Zhu, L.; Mo, F.; Li, S.; Hu, D.; Chu, R.; Liu, C.; Hu, C. Preparation of biochar grafted with amino-riched dendrimer by carbonization, magnetization and functional modification for enhanced copper removal. *Journal of the Taiwan Institute of Chemical Engineers* **2021**, *121*, 349-359.
169. Paulino, A.T.; Minasse, F.A.; Guilherme, M.R.; Reis, A.V.; Muniz, E.C.; Nozaki, J. Novel adsorbent based on silkworm chrysalides for removal of heavy metals from wastewaters. *Journal of Colloid and Interface Science* **2006**, *301*, 479-487.
170. Liu, Y.; Wang, H.; Cui, Y.; Chen, N. Removal of Copper Ions from Wastewater: A Review. *International Journal of Environmental Research and Public Health* **2023**, *20*.
171. Al-Saydeh, S.A.; El-Naas, M.H.; Zaidi, S.J. Copper removal from industrial wastewater: A comprehensive review. *Journal of Industrial and Engineering Chemistry* **2017**, *56*, 35-44.
172. Gong, J.-L.; Wang, X.-Y.; Zeng, G.-M.; Chen, L.; Deng, J.-H.; Zhang, X.-R.; Niu, Q.-Y. Copper (II) removal by pectin–iron oxide magnetic nanocomposite adsorbent. *Chemical Engineering Journal* **2012**, *185-186*, 100-107.
173. Mallik, A.K.; Kabir, S.F.; Rahman, F.B.A.; Sakib, M.N.; Efty, S.S.; Rahman, M.M. Cu (II) removal from wastewater using chitosan-based adsorbents: a review. *Journal of Environmental Chemical Engineering* **2022**, *10*, 108048.
174. Varma V, G.; Misra, A.K. Copper contaminated wastewater–an evaluation of bioremedial options. *Indoor and Built Environment* **2018**, *27*, 84-95.
175. Margalioth, E.J.; Schenker, J.G.; Chevion, M. Copper and Zinc levels in normal and malignant tissues. *Cancer* **1983**, *52*, 868-872.
176. Ortega, P.; Sánchez, E.; Gil, E.; Matamoros, V. Use of cover crops in vineyards to prevent groundwater pollution by copper and organic fungicides. Soil column studies. *Chemosphere* **2022**, *303*, 134975.
177. Donnachie, R.L.; Johnson, A.C.; Moeckel, C.; Pereira, M.G.; Sumpter, J.P. Using risk-ranking of metals to identify which poses the greatest threat to freshwater organisms in the UK. *Environmental Pollution* **2014**, *194*, 17-23.
178. Boulaiche, W.; Hamdi, B.; Trari, M. Removal of heavy metals by chitin: equilibrium, kinetic and thermodynamic studies. *Applied Water Science* **2019**, *9*, 39.
179. Lee, C.-G.; Lee, S.; Park, J.-A.; Park, C.; Lee, S.J.; Kim, S.-B.; An, B.; Yun, S.-T.; Lee, S.-H.; Choi, J.-W. Removal of copper, nickel and chromium mixtures from metal plating wastewater by adsorption with modified carbon foam. *Chemosphere* **2017**, *166*, 203-211.
180. Gündoğan, R.; Acemioğlu, B.; Alma, M.H. Copper (II) adsorption from aqueous solution by herbaceous peat. *Journal of Colloid and Interface Science* **2004**, *269*, 303-309.
181. Doula, M.K.; Dimirkou, A. Use of an iron-overexchanged clinoptilolite for the removal of Cu2+ ions from heavily contaminated drinking water samples. *Journal of Hazardous Materials* **2008**, *151*, 738-745.

182. Aydın, H.; Bulut, Y.; Yerlikaya, Ç. Removal of copper (II) from aqueous solution by adsorption onto low-cost adsorbents. *Journal of Environmental Management* **2008**, *87*, 37-45.
183. Gaballah, I.; Goy, D.; Allain, E.; Kilbertus, G.; Thauront, J. Recovery of copper through decontamination of synthetic solutions using modified barks. *Metallurgical and Materials Transactions B* **1997**, *28*, 13-23.
184. Yuwei, C.; Jianlong, W. Preparation and characterization of magnetic chitosan nanoparticles and its application for Cu(II) removal. *Chemical Engineering Journal* **2011**, *168*, 286-292.
185. Albadarin, A.B.; Mo, J.; Glocheux, Y.; Allen, S.; Walker, G.; Mangwandi, C. Preliminary investigation of mixed adsorbents for the removal of copper and methylene blue from aqueous solutions. *Chemical Engineering Journal* **2014**, *255*, 525-534.
186. Alvarez-Ayuso, E.; Garcia-Sanchez, A.; Querol, X. Purification of metal electroplating waste waters using zeolites. *Water Research* **2003**, *37*, 4855-4862.
187. He, K.; Chen, Y.; Tang, Z.; Hu, Y. Removal of heavy metal ions from aqueous solution by zeolite synthesized from fly ash. *Environmental Science and Pollution Research* **2016**, *23*, 2778-2788.
188. Sireesha, S.; Agarwal, A.; Sopanrao, K.S.; Sreedhar, I.; Anitha, K.L. Modified coal fly ash as a low-cost, efficient, green, and stable adsorbent for heavy metal removal from aqueous solution. *Biomass Conversion and Biorefinery* **2022**, *12(5)*, 1-24.
189. Hidayat, E.; Yoshino, T.; Yonemura, S.; Mitoma, Y.; Harada, H. A Carbonized Zeolite/Chitosan Composite as an Adsorbent for Copper (II) and Chromium (VI) Removal from Water. *Materials* **2023**, *16*, 2532.
190. Gupta, V.K.; Agarwal, S.; Bharti, A.K.; Sadegh, H. Adsorption mechanism of functionalized multi-walled carbon nanotubes for advanced Cu (II) removal. *Journal of Molecular Liquids* **2017**, *230*, 667-673.
191. Awual, M.R. A novel facial composite adsorbent for enhanced copper(II) detection and removal from wastewater. *Chemical Engineering Journal* **2015**, *266*, 368-375.
192. Zhang, H.; Li, G.-W.; Feng, W.; Yao, Z.-Y. Cu(II) Adsorption from Aqueous Solution onto Poly(Acrylic Acid/Chestnut Shell Pigment) Hydrogel. *Water* **2022**, *14(21), 3500*.
193. Schaumlöffel, D. Nickel species: analysis and toxic effects. *Journal of Trace Elements in Medicine and Biology* **2012**, *26*, 1-6.
194. Genchi, G.; Carocci, A.; Lauria, G.; Sinicropi, M.S.; Catalano, A. Nickel: Human Health and Environmental Toxicology. *International Journal of Environmental Research and Public Health* **2020**, *17*.
195. Li, H.; Dong, X.; da Silva, E.B.; de Oliveira, L.M.; Chen, Y.; Ma, L.Q. Mechanisms of metal sorption by biochars: Biochar characteristics and modifications. *Chemosphere* **2017**, *178*, 466-478.
196. Borba, C.E.; Guirardello, R.; Silva, E.A.; Veit, M.T.; Tavares, C.R.G. Removal of nickel(II) ions from aqueous solution by biosorption in a fixed bed column: Experimental and theoretical breakthrough curves. *Biochemical Engineering Journal* **2006**, *30*, 184-191.
197. Raval, N.P.; Shah, P.U.; Shah, N.K. Adsorptive removal of nickel(II) ions from aqueous environment: A review. *Journal of Environmental Management* **2016**, *179*, 1-20.

198. Acheampong, M.A.; Pereira, J.P.C.; Meulepas, R.J.W.; Lens, P.N.L. Kinetics modelling of Cu(II) biosorption on to coconut shell and Moringa oleifera seeds from tropical regions. *Environmental Technology* **2012**, *33*, 409-417.
199. Coman, V.; Robotin, B.; Ilea, P. Nickel recovery/removal from industrial wastes: A review. *Resources, Conservation and Recycling* **2013**, *73*, 229-238.
200. Argun, M.E. Use of clinoptilolite for the removal of nickel ions from water: Kinetics and thermodynamics. *Journal of Hazardous Materials* **2008**, *150*, 587-595.
201. Srivastava, V.C.; Mall, I.D.; Mishra, I.M. Equilibrium modelling of single and binary adsorption of cadmium and nickel onto bagasse fly ash. *Chemical Engineering Journal* **2006**, *117*, 79-91.
202. Çoruh, S.; Ergun, O.N. Ni^{2+} removal from aqueous solutions using conditioned clinoptilolites: Kinetic and isotherm studies. *Environmental Progress & Sustainable Energy* **2009**, *28*, 162-172.
203. Panda, G.C.; Das, S.K.; Bandopadhyay, T.S.; Guha, A.K. Adsorption of nickel on husk of Lathyrus sativus: Behavior and binding mechanism. *Colloids and Surfaces B: Biointerfaces* **2007**, *57*, 135-142.
204. Katsou, E.; Malamis, S.; Haralambous, K.J.; Loizidou, M. Use of ultrafiltration membranes and aluminosilicate minerals for nickel removal from industrial wastewater. *Journal of Membrane Science* **2010**, *360*, 234-249.
205. Najafi, F.; Moradi, O.; Rajabi, M.; Asif, M.; Tyagi, I.; Agarwal, S.; Gupta, V.K. Thermodynamics of the adsorption of nickel ions from aqueous phase using graphene oxide and glycine functionalized graphene oxide. *Journal of Molecular Liquids* **2015**, *208*, 106-113.
206. Choksi, P.M.; Joshi, V.Y. Adsorption kinetic study for the removal of nickel (II) and aluminum (III) from an aqueous solution by natural adsorbents. *Desalination* **2007**, *208*, 216-231.
207. Zafar, M.N.; Nadeem, R.; Hanif, M.A. Biosorption of nickel from protonated rice bran. *Journal of Hazardous Materials* **2007**, *143*, 478-485.
208. Popuri, S.R.; Vijaya, Y.; Boddu, V.M.; Abburi, K. Adsorptive removal of copper and nickel ions from water using chitosan coated PVC beads. *Bioresource Technology* **2009**, *100*, 194-199.
209. Alabbad, E.; Al Dwairi, R. Removal of nickel (II) ions from water by Jordan natural zeolite as sorbent material. *Journal of Saudi Chemical Society* **2021**, 101233.
210. Vijaya, Y.; Popuri, S.R.; Boddu, V.M.; Krishnaiah, A. Modified chitosan and calcium alginate biopolymer sorbents for removal of nickel (II) through adsorption. *Carbohydrate Polymers* **2008**, *72*, 261-271.
211. Hoeber, L.; Steinlechner, S. A comprehensive review of processing strategies for iron precipitation residues from zinc hydrometallurgy. *Cleaner Engineering and Technology* **2021**, *4*, 100214.
212. Stefanidou, M.; Maravelias, C.; Dona, A.; Spiliopoulou, C. Zinc: a multipurpose trace element. *Archives of Toxicology* **2006**, *80*, 1-9.
213. Awofolu, O.R. A Survey of Trace Metals in Vegetation, Soil and Lower Animal Along Some Selected Major Roads in Metropolitan City of Lagos. *Environmental Monitoring and Assessment* **2005**, *105*, 431-447.

214. Cotruvo, J.A. 2017 WHO Guidelines for Drinking Water Quality: First Addendum to the Fourth Edition. *Journal AWWA* **2017**, *109*, 44-51.
215. Lebourg, A.; Sterckeman, T.; Ciesielski, H.; Proix, N. Trace Metal Speciation in Three Unbuffered Salt Solutions Used to Assess their Bioavailability in Soil. *Journal of Environmental Quality* **1998**, *27*, 584-590.
216. Noulas, C.; Tziouvalekas, M.; Karyotis, T. Zinc in soils, water and food crops. *Journal of Trace Elements in Medicine and Biology* **2018**, *49*, 252-260.
217. Zwain, H.M.; Vakili, M.; Dahlan, I. Waste Material Adsorbents for Zinc Removal from Wastewater: A Comprehensive Review. *International Journal of Chemical Engineering* **2014**, *2014*, 347912.
218. Zhang, H.; Tong, Z.; Wei, T.; Tang, Y. Removal characteristics of Zn(II) from aqueous solution by alkaline Ca-bentonite. *Desalination* **2011**, *276*, 103-108.
219. Dupont, L.; Bouanda, J.; Dumonceau, J.; Aplincourt, M. Biosorption of Cu(II) and Zn(II) onto a lignocellulosic substrate extracted from wheat bran. *Environmental Chemistry Letters* **2005**, *2*, 165-168.
220. Saeed, A.; Iqbal, M.; Akhtar, M.W. Removal and recovery of lead(II) from single and multimetal (Cd, Cu, Ni, Zn) solutions by crop milling waste (black gram husk). *Journal of Hazardous Materials* **2005**, *117*, 65-73.
221. Zhang, Y.; Chen, Y.; Kang, W.; Han, H.; Song, H.; Zhang, C.; Wang, H.; Yang, X.; Gong, X.; Zhai, C.; et al. Excellent adsorption of Zn(II) using NaP zeolite adsorbent synthesized from coal fly ash via stage treatment. *Journal of Cleaner Production* **2020**, *258*, 120736.
222. Izidoro, J.d.C.; Fungaro, D.A.; Abbott, J.E.; Wang, S. Synthesis of zeolites X and A from fly ashes for cadmium and zinc removal from aqueous solutions in single and binary ion systems. *Fuel* **2013**, *103*, 827-834.
223. Kumar, V.; Dwivedi, S.K.; Oh, S. A critical review on lead removal from industrial wastewater: Recent advances and future outlook. *Journal of Water Process Engineering* **2022**, *45*, 102518.
224. Naseem, R.; Tahir, S.S. Removal of Pb(II) from aqueous/acidic solutions by using bentonite as an adsorbent. *Water Research* **2001**, *35*, 3982-3986.
225. Davidson, A.J.; Binks, S.P.; Gediga, J. Lead industry life cycle studies: environmental impact and life cycle assessment of lead battery and architectural sheet production. *The International Journal of Life Cycle Assessment* **2016**, *21*, 1624-1636.
226. Awual, M.R. An efficient composite material for selective lead(II) monitoring and removal from wastewater. *Journal of Environmental Chemical Engineering* **2019**, *7*, 103087.
227. Zhang, J.; Hu, X.; Yan, J.; Long, L.; Xue, Y. Crayfish shell biochar modified with magnesium chloride and its effect on lead removal in aqueous solution. *Environmental Science and Pollution Research* **2020**, *27*, 9582-9588.
228. Jangkorn, S.; Youngme, S.; Praipipat, P. Comparative lead adsorptions in synthetic wastewater by synthesized zeolite A of recycled industrial wastes from sugar factory and power plant. *Heliyon* **2022**, *8, 4*, e09323.
229. Fan, Y.; Wang, H.; Deng, L.; Wang, Y.; Kang, D.; Li, C.; Chen, H. Enhanced adsorption of Pb(II) by nitrogen and phosphorus co-doped biochar derived from Camellia oleifera shells. *Environmental Research* **2020**, *191*, 110030.

230. Ge, Q.; Moeen, M.; Tian, Q.; Xu, J.; Feng, K. Highly effective removal of Pb^{2+} in aqueous solution by Na-X zeolite derived from coal gangue. *Environmental Science and Pollution Research* **2020**, *27*, 7398-7408.
231. Kharrazi, S.M.; Mirghaffari, N.; Dastgerdi, M.M.; Soleimani, M. A novel post-modification of powdered activated carbon prepared from lignocellulosic waste through thermal tension treatment to enhance the porosity and heavy metals adsorption. *Powder Technology* **2020**, *366*, 358-368.
232. Senthil Kumar, P. Adsorption of lead(II) ions from simulated wastewater using natural waste: A kinetic, thermodynamic and equilibrium study. *Environmental Progress & Sustainable Energy* **2014**, *33*, 55-64.
233. Sarı, A.; Tuzen, M.; Cıtak, D.; Soylak, M. Adsorption characteristics of Cu(II) and Pb(II) onto expanded perlite from aqueous solution. *Journal of Hazardous Materials* **2007**, *148*, 387-394.
234. Kobayashi, Y.; Ogata, F.; Saenjum, C.; Nakamura, T.; Kawasaki, N. Removal of Pb^{2+} from Aqueous Solutions Using K-Type Zeolite Synthesized from Coal Fly Ash. *Water* **2020**, *12*, 2375.
235. Pandey, P.K.; Sharma, S.K.; Sambi, S.S. Removal of lead(II) from waste water on zeolite-NaX. *Journal of Environmental Chemical Engineering* **2015**, *3*, 2604-2610.
236. Malamis, S.; Katsou, E.; Haralambous, K.J. Study of Ni(II), Cu(II), Pb(II), and Zn(II) Removal Using Sludge and Minerals Followed by MF/UF. *Water, Air, & Soil Pollution* **2011**, *218*, 81-92.
237. Hargreaves, A.J.; Vale, P.; Whelan, J.; Alibardi, L.; Constantino, C.; Dotro, G.; Cartmell, E.; Campo, P. Impacts of coagulation-flocculation treatment on the size distribution and bioavailability of trace metals (Cu, Pb, Ni, Zn) in municipal wastewater. *Water Research* **2018**, *128*, 120-128.
238. Kabra, K.; Chaudhary, R.; Sawhney, R.L. Solar photocatalytic removal of Cu(II), Ni(II), Zn(II) and Pb(II): Speciation modeling of metal–citric acid complexes. *Journal of Hazardous Materials* **2008**, *155*, 424-432.
239. MacArthur, E. Towards the circular economy. *Journal of Industrial Ecology* **2013**, *2*, 23-44.
240. Stahel, W.R. The circular economy. *Nature* **2016**, *531*, 435-438.
241. Arruda, E.H.; Melatto, R.A.P.B.; Levy, W.; Conti, D.d.M. Circular economy: A brief literature review (2015–2020). *Sustainable Operations and Computers* **2021**, *2*, 79-86.
242. Lieder, M.; Rashid, A. Towards circular economy implementation: a comprehensive review in context of manufacturing industry. *Journal of Cleaner Production* **2016**, *115*, 36-51.
243. Halog, A.; Anieke, S. A Review of Circular Economy Studies in Developed Countries and Its Potential Adoption in Developing Countries. *Circular Economy and Sustainability* **2021**, *1*, 209-230.
244. Mazur-Wierzbicka, E. Circular economy: advancement of European Union countries. *Environmental Sciences Europe* **2021**, *33*, 111.
245. Pesce, M.; Tamai, I.; Guo, D.; Critto, A.; Brombal, D.; Wang, X.; Cheng, H.; Marcomini, A. Circular Economy in China: Translating Principles into Practice. *Sustainability* **2020**, *12*, 832.
246. Koop, S.H.; van Leeuwen, C.J. The challenges of water, waste and climate change in cities. *Environment, Development and Sustainability* **2017**, *19*, 385-418.

247. Morseletto, P.; Mooren, C.E.; Munaretto, S. Circular Economy of Water: Definition, Strategies and Challenges. *Circular Economy and Sustainability* **2022**, *2*, 1463-1477.
248. Voulvoulis, N. Water reuse from a circular economy perspective and potential risks from an unregulated approach. *Current Opinion in Environmental Science & Health* **2018**, *2*, 32-45.
249. Rao, S.R.; Finch, J.A. A review of water re-use in flotation. *Minerals Engineering* **1989**, *2*, 65-85.
250. Broman, P.G. Water Reuse at Sulfide Ore Concentrators in Sweden: Practice, Experience and Current Developments. *Complex Sulphide Ores, The Institution of Mining and Metallurgy, London* **1980**, 28-39.
251. Abd, A.A.; Othman, M.R.; Naji, S.Z.; Hashim, A.S. Methane enrichment in biogas mixture using pressure swing adsorption: process fundamental and design parameters. *Materials Today Sustainability* **2021**, *11-12*, 100063.
252. Brião, G.d.V.; da Silva, M.G.; Vieira, M.G.A. Adsorption potential for the concentration and recovery of rare earth metals from NdFeB magnet scrap in the hydrometallurgical route: A review in a circular economy approach. *Journal of Cleaner Production* **2022**, *380*, 135112.
253. Singh, R.; Pandey, A.; Sagar, N.A.; Kumar, N. Chapter 10 - Advances in dye removal technologies from wastewater by microbes. In *Synergistic Approaches for Bioremediation of Environmental Pollutants : Recent Advances and Challenges*, Kapoor, R.T., Shah, M.P., Eds.; Academic Press: 2022; pp. 185-197.
254. Yu, C.; Han, X. Adsorbent material used in water treatment-a review. In Proceedings of the 2015 2nd International Workshop on Materials Engineering and Computer Sciences, 2015; pp. 286-289.
255. Letsoalo, M.R.; Sithole, T.; Mufamadi, S.; Mazhandu, Z.; Sillanpaa, M.; Kaushik, A.; Mashifana, T. Efficient detection and treatment of pharmaceutical contaminants to produce clean water for better health and environmental. *Journal of Cleaner Production* **2023**, *387*, 135798.
256. Rodriguez-Narvaez, O.M.; Peralta-Hernandez, J.M.; Goonetilleke, A.; Bandala, E.R. Treatment technologies for emerging contaminants in water: A review. *Chemical Engineering Journal* **2017**, *323*, 361-380.
257. Akinola, T.E.; Bonilla Prado, P.L.; Wang, M. Experimental studies, molecular simulation and process modelling\simulation of adsorption-based post-combustion carbon capture for power plants: A state-of-the-art review. *Applied Energy* **2022**, *317*, 119156.
258. Karnib, M.; Kabbani, A.; Holail, H.; Olama, Z. Heavy metals removal using activated carbon, silica and silica activated carbon composite. *Energy Procedia* **2014**, *50*, 113-120.
259. Yuna, Z. Review of the natural, modified, and synthetic zeolites for heavy metals removal from wastewater. *Environmental Engineering Science* **2016**, *33*, 443-454.
260. Catalfamo, P.; Di Pasquale, S.; Corigliano, F.; Mavilia, L. Influence of the calcium content on the coal fly ash features in some innovative applications. *Resources, Conservation and Recycling* **1997**, *20*, 119-125.
261. Moreno, N.; Querol, X.; Ayora, C.; Pereira, C.F.; Janssen-Jurkovicová, M. Utilization of zeolites synthesized from coal fly ash for the purification of acid mine waters. *Environmental Science & Technology* **2001**, *35*, 3526-3534.

262. Silva, M.; Lecus, A.; Gajdardziska-Josifovska, M.; Schofield, D.; Virnoche, M.; Chang, J.; Chen, J.; Garman, D. Graphene-oxide loading on natural zeolite particles for enhancement of adsorption properties. *RSC Advances* **2020**, *10*, 4589-4597.
263. Čejka, J.; Millini, R.; Opanasenko, M.; Serrano, D.P.; Roth, W.J. Advances and challenges in zeolite synthesis and catalysis. *Catalysis Today* **2020**, *345*, 2-13.
264. Roque-Malherbe, R. Chapter 12 - Applications of Natural Zeolites in Pollution Abatement and Industry In *Handbook of Surfaces and Interfaces of Materials*, Nalwa, H.S., Ed.; Academic Press: Burlington, 2001; pp. 495-522.
265. Pérez-Botella, E.; Valencia, S.; Rey, F. Zeolites in Adsorption Processes: State of the Art and Future Prospects. *Chemical Reviews* **2022**, *122*, 17647-17695.
266. Ernst, S. Zeolites and Catalysis. Synthesis, Reactions and Applications. Edited by Jiri Cejka, Avelino Corma and Stacey Zones. *Angewandte Chemie International Edition* **2011**, *50*, 5425-5426.
267. Speight, J.G. *Heavy oil recovery and upgrading*; Gulf Professional Publishing: 2019.
268. Kühl, G.H. Modification of Zeolites. In *Catalysis and Zeolites: Fundamentals and Applications*, Weitkamp, J., Puppe, L., Eds.; Springer Berlin Heidelberg: Berlin, Heidelberg, 1999; pp. 81-197.
269. Shi, J.; Yang, Z.; Dai, H.; Lu, X.; Peng, L.; Tan, X.; Shi, L.; Fahim, R. Preparation and application of modified zeolites as adsorbents in wastewater treatment. *Water Science and Technology* **2018**, *2017*, 621-635.
270. Mallette, A.J.; Seo, S.; Rimer, J.D. Synthesis strategies and design principles for nanosized and hierarchical zeolites. *Nature Synthesis* **2022**, *1*, 521-534.
271. Xu, H.; Wu, P. New progress in zeolite synthesis and catalysis. *National Science Review* **2022**, *9*.
272. Misaelides, P. Application of natural zeolites in environmental remediation: A short review. *Microporous and Mesoporous Materials* **2011**, *144*, 15-18.
273. Moliner, M. Design of Zeolites with Specific Architectures Using Self-Assembled Aromatic Organic Structure Directing Agents. *Topics in Catalysis* **2015**, *58*, 502-512.
274. Mitra, S.; Chakraborty, A.J.; Tareq, A.M.; Emran, T.B.; Nainu, F.; Khusro, A.; Idris, A.M.; Khandaker, M.U.; Osman, H.; Alhumaydhi, F.A.; et al. Impact of heavy metals on the environment and human health: Novel therapeutic insights to counter the toxicity. *Journal of King Saud University - Science* **2022**, *34*, 101865.
275. Masters, A.F.; Maschmeyer, T. Zeolites – From curiosity to cornerstone. *Microporous and Mesoporous Materials* **2011**, *142*, 423-438.
276. Flanigen, E.M. Chapter 2 Zeolites and molecular sieves: An historical perspective. In *Studies in Surface Science and Catalysis*, van Bekkum, H., Flanigen, E.M., Jacobs, P.A., Jansen, J.C., Eds.; Elsevier: 2001; Volume 137, pp. 11-35.
277. Barrer, R. Separation of mixtures using zeolites as molecular sieves. I. Three classes of molecular-sieve zeolite. *Journal of the Society of Chemical Industry* **1945**, *64*, 130.
278. Barrer, R.M. 435. Syntheses and reactions of mordenite. *Journal of the Chemical Society (Resumed)* **1948**, 2158-2163.
279. Vaughan, O. Porous by design. *Nature Publishing Group* **2014**, *11*, 1-1.
280. The International Zeolite Association. Database of zeolite structures. Available online: https://america.iza-structure.org/IZA-SC/ftc_table.php (accessed on May 2024).

281. Misaelides, P. Application of natural zeolites in environmental remediation: A short review. *Microporous and Mesoporous Materials* **2011**.
282. Silva, M.R.; Lecus, A.; Gajdardziska-josifovska, M.; Scho, M.; Virnoche, M. Graphene-oxide loading on natural zeolite particles for enhancement of adsorption properties. *RSC Advances* **2020**, 4589-4597.
283. Cao, J.-l.; Liu, X.-W.; Fu, R.; Tan, Z.-y. Magnetic P zeolites: Synthesis, characterization and the behavior in potassium extraction from seawater. *Separation and Purification Technology* **2008**, *63*, 92-100.
284. Huang, Y.; Dong, D.; Yao, J.; He, L.; Ho, J.; Kong, C.; Hill, A.J.; Wang, H. In Situ Crystallization of Macroporous Monoliths with Hollow NaP Zeolite Structure. *Chemistry of Materials* **2010**, *22*, 5271-5278.
285. Deng, L.; Xu, Q.; Wu, H. Synthesis of zeolite-like material by hydrothermal and fusion methods using municipal solid waste fly ash. *Procedia Environmental Sciences* **2016**, *31*, 662-667.
286. Mastinu, A.; Kumar, A.; Maccarinelli, G.; Bonini, S.A.; Premoli, M.; Aria, F.; Gianoncelli, A.; Memo, M. Zeolite Clinoptilolite: Therapeutic Virtues of an Ancient Mineral. *Molecules* **2019**, *24*, 1517.
287. Zeng, X.; Hu, X.; Song, H.; Xia, G.; Shen, Z.-Y.; Yu, R.; Moskovits, M. Microwave synthesis of zeolites and their related applications. *Microporous and Mesoporous Materials* **2021**, *323*, 111262.
288. Jha, V.K.; Nagae, M.; Matsuda, M.; Miyake, M. Zeolite formation from coal fly ash and heavy metal ion removal characteristics of thus-obtained Zeolite X in multi-metal systems. *Journal of Environmental Management* **2009**, *90*, 2507-2514.
289. Weitkamp, J.; Puppe, L. *Catalysis and zeolites: fundamentals and applications*; Springer Science & Business Media: 2013.
290. Weckhuysen, B.M. Zeolites shine bright. *Nature Materials* **2016**, *15*, 933-934.
291. Li, Y.; Li, L.; Yu, J. Applications of Zeolites in Sustainable Chemistry. *Chem* **2017**, *3*, 928-949.
292. Limlamthong, M.; Tesana, S.; Yip, A.C.K. Metal encapsulation in zeolite particles: A rational design of zeolite-supported catalyst with maximum site activity. *Advanced Powder Technology* **2020**, 1-6.
293. Kühl, G.H. Modification of Zeolites BT - Catalysis and Zeolites: Fundamentals and Applications. Weitkamp, J., Puppe, L., Eds.; Springer Berlin Heidelberg: Berlin, Heidelberg, 1999; pp. 81-197.
294. Auerbach, S.M.; Carrado, K.A.; Dutta, P.K. *Handbook of Zeolite Science and Technology*; CRC press: 2003.
295. De Smedt, C.; Someus, E.; Spanoghe, P. Potential and actual uses of zeolites in crop protection. *Pest Management Science* **2015**, *71*, 1355-1367.
296. Wang, S.; Peng, Y. Natural zeolites as effective adsorbents in water and wastewater treatment. **2010**, *156*, 11-24.
297. Roque-Malherbe, R. *Applications of Natural Zeolites in Pollution Abatement and Industry*; Academic Press: 2001; Volume 5, pp. 495-522.
298. Jia, X.; Khan, W.; Wu, Z.; Choi, J.; Yip, A.C.K. Modern synthesis strategies for hierarchical zeolites: Bottom-up versus top-down strategies. *Advanced Powder Technology* **2019**, *30*, 467-484.

299. García-Martínez, J.; Li, K.; Krishnaiah, G. A mesostructured Y zeolite as a superior FCC catalyst – from lab to refinery. *Chemical Communications* **2012**, *48*, 11841-11843.
300. Kanezashi, M.; O'Brien, J.; Lin, Y.S. Thermal stability improvement of MFI-type zeolite membranes with doped zirconia intermediate layer. *Microporous and Mesoporous Materials* **2007**, *103*, 302-308.
301. Inglezakis, V.J.; Zorpas, A.A. *Handbook of natural zeolites*; Bentham Science Publishers: 2012.
302. Barrer, R.M. 33. Synthesis of a zeolitic mineral with chabazite-like sorptive properties. *Journal of the Chemical Society (Resumed)* **1948**, 127-132.
303. Querol, X.; Moreno, N.; Umaña, J.C.; Alastuey, A.; Hernández, E.; López-Soler, A.; Plana, F. Synthesis of zeolites from coal fly ash: an overview. *International Journal of Coal Geology* **2002**, *50*, 413-423.
304. Maruyama, A.; Adachi, N.; Takatsuki, T.; Torii, M.; Sanui, K.; Ogata, N. Enantioselective Permeation of a-Amino Acid Isomers through Poly (amino acid) - Derived Membranes. *Macromolecules* **1990**, *23(10)*, 2748-2752.
305. Inoue, K.; Miyahara, A.; Itaya, T. Enantioselective Permeation of Amino Acids across Membranes Prepared from 3α-Helix Bundle Polyglutamates with Oxyethylene Chains. *Journal of the American Chemical Society* **1997**, *119*, 6191-6192.
306. Higashi, B.N.; Koga, T.; Niwa, M. Dendrimers with Attached Helical Peptides. *Advanced Materials* **2000**, *12*, 1373-1375.
307. Aoi, K.; Itoh, K.; Okada, M. Globular Carbohydrate Macromolecules "Sugar Balls". 1. Synthesis of Novel Sugar-Persubstituted Poly(amido amine) Dendrimers. *Macromolecules* **1995**, *28(15)*, 5391-5393.
308. Helfrich, J.; Hentschke, R. Molecular Dynamics Simulation of Macromolecular Interactions in Solution: Poly(.gamma.-benzyl glutamate) in Dimethylformamide and Tetrahydrofuran. *Macromolecules* **1995**, *28*, 3831-3841.
309. Chang, Y.-C.; Frank, C.W. Grafting of Poly(γ-benzyl-l-glutamate) on Chemically Modified Silicon Oxide Surfaces. *Langmuir* **1996**, *12*, 5824-5829.
310. Higashi, N.; Nishikawa, R.; Koga, T.; Niwa, M. Effects of Helical Sense and Macrodipole on Helix Interaction in Poly(glutamic acid) Monolayers at the Air–Water Interface. *Journal of Colloid and Interface Science* **1999**, *220*, 362-366.
311. Higashi, N.; Yamamoto, T.; Yokoyama, K.; Niwa, M. Facilitated Formation of Helical Polypeptide Assemblies in a Lipid Monolayer by an Interfacial Polyion Complexation. *Macromolecules* **1995**, 2585-2587.
312. Cooper, A.I.; Londono, J.D.; Wignall, G.; McClain, J.B.; Samulski, E.T.; Lin, J.S.; Dobrynin, A.; Rubinstein, M.; Burke, A.L.C.; Fréchet, J.M.J.; et al. Extraction of a hydrophilic compound from water into liquid CO_2 using dendritic surfactants. *Nature* **1997**, *389*, 368-371.
313. Chechik, V.; Zhao, M.; Crooks, R.M. Self-Assembled Inverted Micelles Prepared from a Dendrimer Template : Phase Transfer of Encapsulated Guests. *Journal of the American Chemical Society* **1999**, 4910-4911.
314. United States Geological Survey. Zeolites Statistics and Information. Reston, VA: National Minerals Information Center;. Available online: https://www.usgs.gov/centers/nmic/zeolites-statistics-and-information (accessed on May 2024).

315. Dong, Y.; Caruge, J.-m.; Zhou, Z.; Hamilton, C.; Popovic, Z.; Ho, J.; Stevenson, M.; Liu, G.; Bulovic, V.; Ls, O.N. Ultra-Bright , Highly Efficient , Low Roll-off Inverted Quantum-Dot Light Emitting Devices (QLEDs). In Proceedings of the SID Symposium Digest of Technical Papers, 46, 2015; pp. 270-273.
316. Karge, H.G. Modification of Zeolites and New Routes to Ion Exchange BT - Zeolite Microporous Solids: Synthesis, Structure, and Reactivity. Derouane, E.G., Lemos, F., Naccache, C., Ribeiro, F.R., Eds.; Springer Netherlands: Dordrecht, 1992; pp. 273-290.
317. Čejka, J.; Corma, A.; Zones, S. *Zeolites and Catalysis: Synthesis, Reactions and Applications. Zeolites and Catalysis: Synthesis*; Weinheim: Wiley-VCH: 2010.
318. Baccouche, A.; Srasra, E.; El Maaoui, M. Preparation of Na-P1 and sodalite octahydrate zeolites from interstratified illite–smectite. *Applied Clay Science* **1998**, *13*, 255-273.
319. Du, Y.; Shi, S.; Dai, H. Water-bathing synthesis of high-surface-area zeolite P from diatomite. *Particuology* **2011**, *9*, 174-178.
320. Barrer, R.M.; White, E.A.D. 286. The hydrothermal chemistry of silicates. Part II. Synthetic crystalline sodium aluminosilicates. *Journal of the Chemical Society (Resumed)* **1952**, 1561-1571.
321. Petrov, I.; Michalev, T. Synthesis of Zeolite A: A Review. In Proceedings of the Chemical Technologies, 51, 2012.
322. Zheng, Y.; Li, X.; Dutta, P.K. Exploitation of Unique Properties of Zeolites in the Development of Gas Sensors. *Sensors* **2012**, *12*, 5170-5194.
323. Tanaka, H.; Eguchi, H.; Fujimoto, S.; Hino, R. Two-step process for synthesis of a single phase Na–A zeolite from coal fly ash by dialysis. *Fuel* **2006**, *85*, 1329-1334.
324. Musyoka, N.M.; Petrik, L.F.; Hums, E.; Baser, H.; Schwieger, W. In situ ultrasonic monitoring of zeolite A crystallization from coal fly ash. *Catalysis Today* **2012**, *190*, 38-46.
325. McCusker, L.B.; Liebau, F.; Engelhardt, G. Nomenclature of structural and compositional characteristics of ordered microporous and mesoporous materials with inorganic hosts(IUPAC Recommendations 2001). *Pure and Applied Chemistry* **2001**, *73*, 381-394.
326. Hammond, C. Chapter 15 - Sn-Substituted Zeolites as Heterogeneous Catalysts for Liquid-Phase Catalytic Technologies. In *Morphological, Compositional, and Shape Control of Materials for Catalysis*, Paolo Fornasiero, M.C., Ed.; Studies in Surface Science and Catalysis; Elsevier: 2017; Volume 177, pp. 567-611.
327. Malekpour, A.; Millani, M.R.; Kheirkhah, M. Synthesis and characterization of a NaA zeolite membrane and its applications for desalination of radioactive solutions. *Desalination* **2008**, *225*, 199-208.
328. Cheng, S.; Zhang, G.; Javed, M.; Gao, W.; Mazonde, B. Solvent-Free Synthesis of 1D Cancrinite Zeolite for Unexpectedly Improved Gasoline Selectivity. **2018**, 2115-2119.
329. Sommerville, R.; Blissett, R.; Rowson, N.; Blackburn, S. Producing a synthetic zeolite from improved fly ash residue. *International Journal of Mineral Processing* **2013**, *124*, 20-25.
330. Cundy, C.S.; Cox, P.A. The Hydrothermal Synthesis of Zeolites: History and Development from the Earliest Days to the Present Time. *Chemical Reviews* **2003**, *103*, 663-702.
331. Feng, S.H.; Li, G.H. Chapter 4 - Hydrothermal and Solvothermal Syntheses. In *Modern Inorganic Synthetic Chemistry*, 2 ed.; Xu, R., Xu, Y., Eds.; Elsevier: Amsterdam, 2017; pp. 73-104.

332. Bux, H.; Liang, F.; Li, Y.; Cravillon, J.; Wiebcke, M.; Caro, J. Zeolitic Imidazolate Framework Membrane with Molecular Sieving Properties by Microwave-Assisted Solvothermal Synthesis. *Journal of the American Chemical Society* **2009**, *131*, 16000-16001.
333. Morris, R.E. Ionothermal synthesis — ionic liquids as functional solvents in the preparation of crystalline materials. *Chemical Communications* **2009**.
334. Parnham, E.R.; Morris, R.E. Ionothermal Synthesis of Zeolites, Metal–Organic Frameworks, and Inorganic–Organic Hybrids. *Accounts of Chemical Research* **2007**, *40*, 1005-1013.
335. Feijen, E.J.P.; Martens, J.A.; Jacobs, P.A. Zeolites and their Mechanism of Synthesis. *Studies in Surface Science and Catalysis* **1994**, *84*, 3-21.
336. Barrer, R.M. *Hydrothermal Chemistry of Zeolites*; London : Academic Press: 1982.
337. Kaissaratos, M.; Filobelo, L.; Vekilov, P.G. Two-Step Crystal Nucleation Is Selected Because of a Lower Surface Free Energy Barrier. *Crystal Growth & Design* **2021**, *21*, 5394-5402.
338. Jeon, S.; Heo, T.; Hwang, S.Y.; Ciston, J.; Bustillo, K.C.; Reed, B.W.; Ham, J.; Kang, S.; Kim, S.; Lim, J.; et al. Reversible disorder-order transitions in atomic crystal nucleation. *Science* **2021**, *371*, 498-503.
339. Gibbs, J.W. On the equilibrium of heterogeneous substances. *Transactions of the Connecticut Academy of Arts and Sciences* **1876**, *III*, pp. 108–248, Oct. 1875–May, 1876, and pp. 1343–1524, May, 1877–July, 1878.
340. Asgar Pour, Z.; Alassmy, Y.A.; Sebakhy, K.O. A Survey on Zeolite Synthesis and the Crystallization Process: Mechanism of Nucleation and Growth Steps. *Crystals* **2023**, *13*, 959.
341. Volmer, M.; Weber, A. Keimbildung in übersättigten Gebilden. *Zeitschrift für Physikalische Chemie* **1926**, *119U*, 277-301.
342. Mullin, J.W. *Crystallization*; Elsevier: 2001.
343. Duchstein, P.; Ectors, P.; Zahn, D. Chapter Thirteen - Molecular simulations of crystal growth: From understanding to tailoring. In *Advances in Inorganic Chemistry*, van Eldik, R., Puchta, R., Eds.; Academic Press: 2019; Volume 73, pp. 507-529.
344. Randolph, A. *Theory of particulate processes: analysis and techniques of continuous crystallization*; Elsevier: 2012.
345. Wedlock, D.J. *Controlled particle, droplet and bubble formation*; Butterworth-Heinemann: 2012.
346. Kashchiev, D. *Nucleation*; Elsevier: 2000.
347. Thompson, R.W. Nucleation, growth, and seeding in zeolite synthesis. In *Verified Syntheses of Zeolitic Materials*; Elsevier: 2001; pp. 21-23.
348. Kellogg, R.M.; Leeman, M. 9.16 Crystallization as a Tool in Industrial Applications of Asymmetric Synthesis. In *Comprehensive Chirality*, Carreira, E.M., Yamamoto, H., Eds.; Elsevier: Amsterdam, 2012; pp. 367-399.
349. Myerson, A. *Handbook of industrial crystallization*; Butterworth-Heinemann: 2002.
350. Simon, L.L.; Simone, E.; Abbou Oucherif, K. Chapter 9 - Crystallization process monitoring and control using process analytical technology. In *Computer Aided Chemical Engineering*, Singh, R., Yuan, Z., Eds.; Elsevier: 2018; Volume 41, pp. 215-242.

351. Wise, W.S. MINERALS | Zeolites. In *Encyclopedia of Geology*, Selley, R.C., Cocks, L.R.M., Plimer, I.R., Eds.; Elsevier: Oxford, 2005; pp. 591-600.
352. Cundy, C.S.; Cox, P.A. The hydrothermal synthesis of zeolites: Precursors, intermediates and reaction mechanism. *Microporous and Mesoporous Materials* **2005**, *82*, 1-78.
353. Sommerville, R.P.Z. Utilisation of fly ash in the manufacture of zeolites. School of Chemical Engineering, University of Birmingham. PhD Thesis., **2017**.
354. Burriesci, N.; Crisafulli, M.L.; Giordano, N.; Bart, J.C.J. Factors affecting formation of zeolite a from alumino-silicate gels. *Materials Letters* **1984**, *2*, 401-406.
355. Zones, S. Translating new materials discoveries in zeolite research to commercial manufacture. *Microporous and Mesoporous Materials* **2011**, *144*, 1-8.
356. Hui, K.S.; Chao, C.Y.H. Effects of step-change of synthesis temperature on synthesis of zeolite 4A from coal fly ash. *Microporous and Mesoporous Materials* **2006**, *88*, 145-151.
357. Georgiev, D.; Bogdanov, B.; Angelova, K.; Markovska, I.; Hristov, Y. Synthetic zeolites–Structure, classification, current trends in zeolite synthesis. In Proceedings of the Economics and society development on the base of knowledge: International Scientific Conference 2009.
358. Wałek, T.T.; Saito, F.; Zhang, Q. The effect of low solid/liquid ratio on hydrothermal synthesis of zeolites from fly ash. *Fuel* **2008**, *87*, 3194-3199.
359. Murayama, N.; Yamamoto, H.; Shibata, J. Mechanism of zeolite synthesis from coal fly ash by alkali hydrothermal reaction. *International Journal of Mineral Processing* **2002**, *64*, 1-17.
360. Rabenau, B.A. The Role of Hydrothermal Synthesis in Preparative Chemistry. *Angewandte Chemie International Edition* **1985**, *24*, 1026-1040.
361. Król, M. Hydrothermal synthesis of zeolite aggregate with potential use as a sorbent of heavy metal cations. *Journal of Molecular Structure* **2019**, *1183*, 353-359.
362. Sherman, J.D. Synthetic zeolites and other microporous oxide molecular sieves. *Proceedings of the National Academy of Sciences* **1999**, *96*, 3471 LP-3478.
363. Motsi, T.; Rowson, N.A.; Simmons, M.J.H. Adsorption of heavy metals from acid mine drainage by natural zeolite. *International Journal of Mineral Processing* **2009**, *92*, 42-48.
364. Subotić, B.; Škrtić, D.; Šmit, I.; Sekovanić, L. Transformation of zeolite A into hydroxysodalite: I. An approach to the mechanism of transformation and its experimental evaluation. *Journal of Crystal Growth* **1980**, *50*, 498-508.
365. Byrappa, K.; Yoshimura, M. *Handbook of Hydrothermal Technology*; William Andrew: 2012.
366. Schuiling, R. Carbon dioxide sequestration, Weathering approaches to. In *Geoengineering Responses to Climate Change: Selected Entries from the Encyclopedia of Sustainability Science and Technology*; Springer: 2012; pp. 141-167.
367. Fukasawa, T.; Karisma, A.D.; Shibata, D.; Huang, A.-N.; Fukui, K. Synthesis of zeolite from coal fly ash by microwave hydrothermal treatment with pulverization process. *Advanced Powder Technology* **2017**, *28*, 798-804.
368. UN Climate Change Conference UKCOP26. Available online: https://ukcop26.org/global-coal-to-clean-power-transition-statement/ (accessed on May 2024).
369. Scheetz, B.E.; Earle, R. Utilization of fly ash. *Current Opinion in Solid State and Materials Science* **1998**, *3*, 510-520.

370. Kukier, U.; Ishak, C.F.; Sumner, M.E.; Miller, W.P. Composition and element solubility of magnetic and non-magnetic fly ash fractions. *Environmental Pollution* **2003**, *123*, 255-266.
371. Vassilev, S.V.; Vassileva, C.G. Methods for Characterization of Composition of Fly Ashes from Coal-Fired Power Stations: A Critical Overview. *Energy & Fuels* **2005**, *19*, 1084-1098.
372. Blissett, R.S.; Smalley, N.; Rowson, N.A. An investigation into six coal fly ashes from the United Kingdom and Poland to evaluate rare earth element content. *Fuel* **2014**, *119*, 236-239.
373. Hower, J.C.; Dai, S.; Seredin, V.V.; Zhao, L.; Kostova, I.J.; Silva, L.F.; Mardon, S.M.; Gurdal, G. A note on the occurrence of yttrium and rare earth elements in coal combustion products. *Coal Combustion and Gasification Products* **2013**, *5*, 39-47.
374. Cao, S.; Zhou, C.; Pan, J.; Liu, C.; Tang, M.; Ji, W.; Hu, T.; Zhang, N. Study on Influence Factors of Leaching of Rare Earth Elements from Coal Fly Ash. *Energy & Fuels* **2018**, *32*, 8000-8005.
375. Dere Ozdemir, O.; Piskin, S. A Novel Synthesis Method of Zeolite X From Coal Fly Ash: Alkaline Fusion Followed by Ultrasonic-Assisted Synthesis Method. *Waste and Biomass Valorization* **2019**, *10*, 143-154.
376. Inada, M.; Eguchi, Y.; Enomoto, N.; Hojo, J. Synthesis of zeolite from coal fly ashes with different silica–alumina composition. *Fuel* **2005**, *84*, 299-304.
377. Kelechi, S.; Adamu, M.; Uche, O.; Okokpujie, I.; Ibrahim, Y.E.; Obianyo, I. A comprehensive review on coal fly ash and its application in the construction industry. *Cogent Engineering* **2022**, *9*, 2114201.
378. Inada, M.; Tsujimoto, H.; Eguchi, Y.; Enomoto, N.; Hojo, J. Microwave-assisted zeolite synthesis from coal fly ash in hydrothermal process. *Fuel* **2005**, *84*, 1482-1486.
379. Singh, N.; Agarwal, A.; De, A.; Singh, P. Coal fly ash: An emerging material for water remediation. *International Journal of Coal Science & Technology* **2022**, *9*, 44.
380. Mushtaq, F.; Zahid, M.; Bhatti, I.A.; Nasir, S.; Hussain, T. Possible applications of coal fly ash in wastewater treatment. *Journal of Environmental Management* **2019**, *240*, 27-46.
381. Yao, Z.T.; Ji, X.S.; Sarker, P.K.; Tang, J.H.; Ge, L.Q.; Xia, M.S.; Xi, Y.Q. A comprehensive review on the applications of coal fly ash. *Earth-Science Reviews* **2015**, *141*, 105-121.
382. Kravchenko, J.; Lyerly, H.K. The impact of coal-powered electrical plants and coal ash impoundments on the health of residential communities. *North Carolina Medical Journal* **2018**, *79*, 289-300.
383. Wang, S.; Zhang, C.; Chen, J. Utilization of Coal Fly Ash for The Production of Glass-ceramics with Unique Performances: A Brief Review. *Journal of Materials Science & Technology* **2014**, *30*.
384. Projected electricity generation capacity worldwide from 2018 to 2050;. Available online: https://www.statista.com/statistics/859178/projected-world-electricity-generation-capacity-by-energy-source/ (accessed on April 2024).
385. Verma, C.; Hussain, A.; Madan, S.; Kumar, V. Assessment of heavy metal pollution in groundwater with respect to distance from ash pond by using heavy metal evaluation index. *Applied Water Science* **2021**, *11*, 1-6.
386. Verrecchia, G.; Cafiero, L.; de Caprariis, B.; Dell'Era, A.; Pettiti, I.; Tuffi, R.; Scarsella, M. Study of the parameters of zeolites synthesis from coal fly ash in order to optimize their CO_2 adsorption. *Fuel* **2020**, *276*, 118041.

387. Lee, Y.-R.; Soe, J.T.; Zhang, S.; Ahn, J.-W.; Park, M.B.; Ahn, W.-S. Synthesis of nanoporous materials via recycling coal fly ash and other solid wastes: A mini review. *Chemical Engineering Journal* **2017**, *317*, 821-843.
388. Ahmaruzzaman, M. A review on the utilization of fly ash. *Progress in Energy and Combustion Science* **2010**, *36*, 327-363.
389. Gollakota, A.R.K.; Shu, C.-M.; Gautam, S. Turning Coal Fly Ash into Zeolite for Effective Waste Management BT - Pollutants from Energy Sources: Characterization and Control. Agarwal, R.A., Agarwal, A.K., Gupta, T., Sharma, N., Eds.; Springer Singapore: Singapore, 2019; pp. 269-290.
390. Holler, H.; Wirsching, U. Zeolite formation from fly-ash. *Fortschritte der Mineralogie* **1985**, *63*, 21-43.
391. Wang, C.-F.; Li, J.-S.; Wang, L.-J.; Sun, X.-Y. Influence of NaOH concentrations on synthesis of pure-form zeolite A from fly ash using two-stage method. *Journal of Hazardous Materials* **2008**, *155*, 58-64.
392. Berkgaut, V.; Singer, A. High capacity cation exchanger by hydrothermal zeolitization of coal fly ash. *Applied Clay Science* **1996**, *10*, 369-378.
393. Tanaka, H.; Miyagawa, A.; Eguchi, H.; Hino, R. Synthesis of a Single-Phase Na-A Zeolite from Coal Fly Ash by Dialysis. *Industrial & Engineering Chemistry Research* **2004**, *43*, 6090-6094.
394. Chang, H.-L.; Shih, W.-H. Synthesis of Zeolites A and X from Fly Ashes and Their Ion-Exchange Behavior with Cobalt Ions. *Industrial & Engineering Chemistry Research* **2000**, *39*, 4185-4191.
395. Tanaka, H.; Sakai, Y.; Hino, R. Formation of Na-A and -X zeolites from waste solutions in conversion of coal fly ash to zeolites. *Materials Research Bulletin* **2002**, *37*, 1873-1884.
396. Chareonpanich, M.; Namto, T.; Kongkachuichay, P.; Limtrakul, J. Synthesis of ZSM-5 zeolite from lignite fly ash and rice husk ash. *Fuel Processing Technology* **2004**, *85*, 1623-1634.
397. Rubio, S.J.; Casino, B. A note on cooperative versus non-cooperative strategies in international pollution control. *Resource and Energy Economics* **2002**, *24*, 251-261.
398. Borowiak-Resterna, A.; Cierpiszewski, R.; Prochaska, K. Kinetic and equilibrium studies of the removal of cadmium ions from acidic chloride solutions by hydrophobic pyridinecarboxamide extractants. *Journal of Hazardous Materials* **2010**, *179*, 828-833.
399. Senapati, M.R. Fly ash from thermal power plants–waste management and overview. *Current Science* **2011**, 1791-1794.
400. Sahoo, P.K.; Kim, K.; Powell, M.; Equeenuddin, S.M. Recovery of metals and other beneficial products from coal fly ash: A sustainable approach for fly ash management. *International Journal of Coal Science & Technology* **2016**, *3*, 267-283.
401. Weibel, G.; Eggenberger, U.; Kulik, D.A.; Hummel, W.; Schlumberger, S.; Klink, W.; Fisch, M.; Mäder, U.K. Extraction of heavy metals from MSWI fly ash using hydrochloric acid and sodium chloride solution. *Waste Management* **2018**, *76*, 457-471.
402. Leelarungroj, K.; Likitlersuang, S.; Chompoorat, T.; Janjaroen, D. Leaching mechanisms of heavy metals from fly ash stabilised soils. *Waste Management & Research* **2018**, *36*, 616-623.
403. Meer, I.; Nazir, R. Removal techniques for heavy metals from fly ash. *Journal of Material Cycles and Waste Management* **2018**, *20*, 703-722.

404. Dwivedi, A.; Jain, M.K. Fly ash–waste management and overview: A Review. *Recent Research in Science and Technology* **2014**, *6(1)*, 30-35.
405. Yadav, V.K.; Fulekar, M.H. Advances in methods for recovery of ferrous, alumina, and silica nanoparticles from fly ash waste. *Ceramics* **2020**, *3*, 384-420.
406. Amrhein, C.; Haghnia, G.H.; Kim, T.S.; Mosher, P.A.; Gagajena, R.C.; Amanios, T.; De La Torre, L. Synthesis and properties of zeolites from coal fly ash. *Environmental Science and Technology* **1996**, *30*, 735-742.
407. Bandura, L.; Franus, M.; Józefaciuk, G.; Franus, W. Synthetic zeolites from fly ash as effective mineral sorbents for land-based petroleum spills cleanup. *Fuel* **2015**, *147*, 100-107.
408. Belviso, C.; Cavalcante, F.; Fiore, S. Synthesis of zeolite from Italian coal fly ash: Differences in crystallization temperature using seawater instead of distilled water. *Waste Management* **2010**, *30*, 839-847.
409. Belviso, C.; Cavalcante, F.; Huertas, F.J.; Lettino, A.; Ragone, P.; Fiore, S. The crystallisation of zeolite (X-and A-type) from fly ash at 25 C in artificial sea water. *Microporous and Mesoporous Materials* **2012**, *162*, 115-121.
410. Wang, C.; Li, J.; Sun, X.; Wang, L.; Sun, X. Evaluation of zeolites synthesized from fly ash as potential adsorbents for wastewater containing heavy metals. *Journal of Environmental Sciences* **2009**, *21*, 127-136.
411. Slangen, P.M.; Jansen, J.C.; van Bekkum, H. The effect of ageing on the microwave synthesis of zeolite NaA. *Microporous Materials* **1997**, *9*, 259-265.
412. Mishra, T.; Tiwari, S. Studies on sorption properties of zeolite derived from Indian fly ash. *Journal of Hazardous Materials* **2006**, *137*, 299-303.
413. Querol, X.; Umaña, J.C.; Plana, F.; Alastuey, A.; Lopez-Soler, A.; Medinaceli, A.; Valero, A.; Domingo, M.J.; Garcia-Rojo, E. Synthesis of zeolites from fly ash at pilot plant scale. Examples of potential applications. *Fuel* **2001**, *80*, 857-865.
414. Srinivasan, A.; Grutzeck, M.W. The adsorption of SO2 by zeolites synthesized from fly ash. *Environmental Science & Technology* **1999**, *33*, 1464-1469.
415. Park, M.; Choi, C.L.; Lim, W.T.; Kim, M.C.; Choi, J.; Heo, N.H. Molten-salt method for the synthesis of zeolitic materials: I. Zeolite formation in alkaline molten-salt system. *Microporous and Mesoporous Materials* **2000**, *37*, 81-89.
416. Ansari, M.; Aroujalian, A.; Raisi, A.; Dabir, B.; Fathizadeh, M. Preparation and characterization of nano-NaX zeolite by microwave assisted hydrothermal method. *Advanced Powder Technology* **2014**, *25*, 722-727.
417. Moriyama, R.; Takeda, S.; Onozaki, M.; Katayama, Y.; Shiota, K.; Fukuda, T.; Sugihara, H.; Tani, Y. Large-scale synthesis of artificial zeolite from coal fly ash with a small charge of alkaline solution. *Fuel* **2005**, *84*, 1455-1461.
418. Kim, J.K.; Lee, H.D. Effects of step change of heating source on synthesis of zeolite 4A from coal fly ash. *Journal of Industrial and Engineering Chemistry* **2009**, *15*, 736-742.
419. Querol, X.; Alastuey, A.; López-Soler, A.; Plana, F.; Andrés, J.M.; Juan, R.; Ferrer, P.; Ruiz, C.R. A Fast Method for Recycling Fly Ash: Microwave-Assisted Zeolite Synthesis. *Environmental Science & Technology* **1997**, *31*, 2527-2533.
420. Tanaka, H.; Fujii, A.; Fujimoto, S.; Tanaka, Y. Microwave-Assisted Two-Step Process for the Synthesis of a Single-Phase Na-A Zeolite from Coal Fly Ash. *Advanced Powder Technology* **2008**, *19*, 83-94.

421. Molina, A.; Poole, C. A comparative study using two methods to produce zeolites from fly ash. *Minerals Engineering* **2004**, *17*, 167-173.
422. Hollman, G.G.; Steenbruggen, G.; Janssen-Jurkovičová, M. A two-step process for the synthesis of zeolites from coal fly ash. *Fuel* **1999**, *78*, 1225-1230.
423. Querol, X.; Andres, M.; Janssen, M.; Nugteren, H. Pure zeolite synthesis from silica extracted from coal fly ashes. **2002**, *279*, 6-8.
424. Font, O.; Moreno, N.; Díez, S.; Querol, X.; López-Soler, A.; Coca, P.; García Peña, F. Differential behaviour of combustion and gasification fly ash from Puertollano Power Plants (Spain) for the synthesis of zeolites and silica extraction. *Journal of Hazardous Materials* **2009**, *166*, 94-102.
425. Tanaka, H.; Fujii, A. Effect of stirring on the dissolution of coal fly ash and synthesis of pure-form Na-A and -X zeolites by two-step process. *Advanced Powder Technology* **2009**, *20*, 473-479.
426. Rayalu, S.S.; Udhoji, J.S.; Munshi, K.N.; Hasan, M.Z. Highly crystalline zeolite — a from flyash of bituminous and lignite coal combustion. *Journal of Hazardous Materials* **2001**, *88*, 107-121.
427. Hui, K.S.; Chao, C.Y.H. Pure, single phase, high crystalline, chamfered-edge zeolite 4A synthesized from coal fly ash for use as a builder in detergents. *Journal of Hazardous Materials* **2006**, *137*, 401-409.
428. Fukui, K.; Kanayama, K.; Yamamoto, T.; Yoshida, H. Effects of microwave irradiation on the crystalline phase of zeolite synthesized from fly ash by hydrothermal treatment. *Advanced Powder Technology* **2007**, *18*, 381-393.
429. Shigemoto, N.; Hayashi, H.; Miyaura, K. Selective formation of Na-X zeolite from coal fly ash by fusion with sodium hydroxide prior to hydrothermal reaction. *Journal of Materials Science* **1993**, *28*, 4781-4786.
430. Chang, H.-L.; Shih, W.-H. A general method for the conversion of fly ash into zeolites as ion exchangers for cesium. *Industrial and Engineering Chemistry Research* **1998**, *37*, 71-78.
431. Wu, D.; Zhang, B.; Yan, L.; Kong, H.; Wang, X. Effect of some additives on synthesis of zeolite from coal fly ash. *International Journal of Mineral Processing* **2006**, *80*, 266-272.
432. Ayele, L.; Pérez-Pariente, J.; Chebude, Y.; Díaz, I. Conventional versus alkali fusion synthesis of zeolite A from low grade kaolin. *Applied Clay Science* **2016**, *132-133*, 485-490.
433. Kumar, P.; Mal, N.; Oumi, Y.; Yamana, K.; Sano, T. Mesoporous materials prepared using coal fly ash as the silicon and aluminium source. *Journal of Materials Chemistry* **2001**, *11*, 3285-3290.
434. Lau, Y.J.; Khan, F.S.A.; Mubarak, N.M.; Lau, S.Y.; Chua, H.B.; Khalid, M.; Abdullah, E.C. Chapter 10 - Functionalized carbon nanomaterials for wastewater treatment. Thomas, S., Grohens, Y., Pottathara, Y., Eds.; Elsevier: 2019; pp. 283-311.
435. Zou, Y.; Wang, X.; Khan, A.; Wang, P.; Liu, Y.; Alsaedi, A.; Hayat, T.; Wang, X. Environmental Remediation and Application of Nanoscale Zero-Valent Iron and Its Composites for the Removal of Heavy Metal Ions: A Review. *Environmental Science & Technology* **2016**, *50*, 7290-7304.
436. Khosravi, J.; Alamdari, A. Copper removal from oil-field brine by coprecipitation. *Journal of Hazardous Materials* **2009**, *166*, 695-700.

437. Uluozlu, O.D.; Tuzen, M.; Mendil, D.; Soylak, M. Coprecipitation of trace elements with Ni^{2+}/2-Nitroso-1-naphthol-4-sulfonic acid and their determination by flame atomic absorption spectrometry. *Journal of Hazardous Materials* **2010**, *176*, 1032-1037.
438. Wang, Z.; Feng, Y.; Hao, X.; Huang, W.; Feng, X. A novel potential-responsive ion exchange film system for heavy metal removal. *Journal of Materials Chemistry A* **2014**, *2*.
439. Koyuncu, I.; Akcin, N.; Akcin, G.; Mutlu, K. Comparative Study of Ion-exchange and Flotation Processes for the Removal of Cu^{2+} and Pb^{2+} Ions from Natural Waters. *Reviews in Analytical Chemistry* **2010**, *29*.
440. Al-Shannag, M.; Al-Qodah, Z.; Bani-Melhem, K.; Qtaishat, M.R.; Alkasrawi, M. Heavy metal ions removal from metal plating wastewater using electrocoagulation: Kinetic study and process performance. *Chemical Engineering Journal* **2015**, *260*, 749-756.
441. Lu, J.; Li, Y.; Yin, M.; Ma, X.; Lin, S. Removing heavy metal ions with continuous aluminum electrocoagulation: A study on back mixing and utilization rate of electro-generated Al ions. *Chemical Engineering Journal* **2015**, *267*, 86-92.
442. Trần, T.K.; Chiu, K.-F.; Lin, C.-Y.; Leu, H.-J. Electrochemical treatment of wastewater: Selectivity of the heavy metals removal process. *International Journal of Hydrogen Energy* **2017**, *42*.
443. Yadanaparthi, S.K.R.; Graybill, D.; von Wandruszka, R. Adsorbents for the removal of arsenic, cadmium, and lead from contaminated waters. *Journal of Hazardous Materials* **2009**, *171*, 1-15.
444. Zhu, C.; Guan, F.; Wang, C.; Jin, L.H. The Protective Effects of Rhodiola crenulata Extracts on Drosophila melanogaster Gut Immunity Induced by Bacteria and SDS Toxicity. *Phytotherapy Research* **2014**, *28*, 1861-1866.
445. Stewart, D.I.; Burke, I.T.; Hughes-Berry, D.V.; Whittleston, R.A. Microbially mediated chromate reduction in soil contaminated by highly alkaline leachate from chromium containing waste. *Ecological Engineering* **2010**, *36*, 211-221.
446. Mohsen-Nia, M.; Montazeri, P.; Modarress, H. Removal of Cu^{2+} and Ni^{2+} from wastewater with a chelating agent and reverse osmosis processes. *Desalination* **2007**, *217,1-3*, 276-281.
447. Abia, A.A. A bioseparation process for removing heavy metals from waste water using biosorbents. *African Journal of Biotechnology* **2006**, *5*, 1167-1179.
448. Renault, F.; Sancey, B.; Badot, P.-M.; grégorio, C. Chitosan for Coagulation/Flocculation Processes—An Eco-Friendly Approach. *European Polymer Journal* **2009**, *45*, 1337-1348.
449. Margeta, K.; Zabukovec Logar, N.a.; Siljeg, M.; Farkas, A. Natural Zeolites in Water Treatment – How Effective is Their Use. *Water Treatment* **2013**.
450. Jiménez-Castañeda, M.E.; Medina, D.I. Use of Surfactant-Modified Zeolites and Clays for the Removal of Heavy Metals from Water. *Water* **2017**, *9*, 235.
451. Erdem, E.; Karapinar, N.; Donat, R. The removal of heavy metal cations by natural zeolites. *Journal of colloid and interface science* **2004**, *280*, 309-314.
452. Blanchard, G.; Maunaye, M.; Martin, G. Removal of heavy metals from waters by means of natural zeolites. *Water Research* **1984**, *18*, 1501-1507.
453. Zhang, Y.; Dong, J.; Guo, F.; Shao, Z.; Wu, J. Zeolite synthesized from coal fly ash produced by a gasification process for Ni^{2+} removal from water. *Minerals* **2018**, *8*, 116.

454. Visa, M. Synthesis and characterization of new zeolite materials obtained from fly ash for heavy metals removal in advanced wastewater treatment. *Powder Technology* **2016**, *294*, 338-347.
455. Álvarez-Ayuso, E.; García-Sánchez, A.; Querol, X. Purification of metal electroplating waste waters using zeolites. *Water Research* **2003**, *37*, 4855-4862.
456. Wang, Y.; Guo, Y.; Yang, Z.; Cai, H.; Xavier, Q. Synthesis of zeolites using fly ash and their application in removing heavy metals from waters. *Science in China Series D: Earth Sciences* **2003**, *46*, 967-976.
457. Wu, C.N.; Tang, Y.C.; Tang, L.H. Removal of heavy metal from wastewater using zeolite from fly ash. *Advanced Materials Research* **2012**, *518*, 2736-2739.
458. Yang, Y.; Zhang, P.; Jiang, J.; Dai, Y.; Wu, M.; Pan, Y.; Ni, L. Synthesis and properties of magnetic zeolite with good magnetic stability from fly ash. *Journal of Sol-Gel Science and Technology* **2018**, *87*, 408-418.
459. Wang, P.; Sun, Q.; Zhang, Y.; Cao, J. Hydrothermal synthesis of magnetic zeolite P from fly ash and its properties. *Materials Research Express* **2020**, *7*.
460. Huiping, S.; Huaigang, C.; Zepeng, Z.; Fangqin, C. Adsorption properties of zeolites synthesized from coal fly ash for Cu (II). *Journal of Environmental Biology* **2014**, *35*, 983.
461. Merrikhpour, H.; Jalali, M. Comparative and competitive adsorption of cadmium, copper, nickel, and lead ions by Iranian natural zeolite. *Clean Technologies and Environmental Policy* **2013**, *15*, 303-316.
462. Hernández-Montoya, V.; Pérez-Cruz, M.A.; Mendoza-Castillo, D.I.; Moreno-Virgen, M.; Bonilla-Petriciolet, A. Competitive adsorption of dyes and heavy metals on zeolitic structures. *Journal of Environmental Management* **2013**, *116*, 213-221.
463. Ji, X.; Ma, Y.; Peng, S.; Gong, Y.; Zhang, F. Simultaneous removal of aqueous Zn^{2+}, Cu^{2+}, Cd^{2+}, and Pb^{2+} by zeolites synthesized from low-calcium and high-calcium fly ash. *Water Science and Technology* **2017**, *76*, 2106-2119.
464. Qiu, Q.; Jiang, X.; Lv, G.; Chen, Z.; Lu, S.; Ni, M.; Yan, J.; Deng, X. Adsorption of heavy metal ions using zeolite materials of municipal solid waste incineration fly ash modified by microwave-assisted hydrothermal treatment. *Powder Technology* **2018**, *335*, 156-163.
465. Nascimento, M.; Soares, P.S.M.; de Souza, V.P. Adsorption of heavy metal cations using coal fly ash modified by hydrothermal method. *Fuel* **2009**, *88*, 1714-1719.
466. Mihaly-Cozmuta, L.; Mihaly-Cozmuta, A.; Peter, A.; Nicula, C.; Tutu, H.; Silipas, D.; Indrea, E. Adsorption of heavy metal cations by Na-clinoptilolite: Equilibrium and selectivity studies. *Journal of Environmental Management* **2014**, *137*, 69-80.
467. Joseph, L.; Jun, B.-M.; Flora, J.R.V.; Park, C.M.; Yoon, Y. Removal of heavy metals from water sources in the developing world using low-cost materials: A review. *Chemosphere* **2019**, *229*, 142-159.
468. Bai, S.; Chu, M.; Zhou, L.; Chang, Z.; Zhang, C.; Liu, B. Removal of heavy metals from aqueous solutions by X-type zeolite prepared from combination of oil shale ash and coal fly ash. *Energy Sources, Part A: Recovery, Utilization, and Environmental Effects* **2022**, *44*, 5113-5123.
469. Koshlak, H. Synthesis of Zeolites from Coal Fly Ash Using Alkaline Fusion and Its Applications in Removing Heavy Metals. *Materials* **2023**, *16*, 4837.
470. Li, G.; Li, M.; Zhang, X.; Cao, P.; Jiang, H.; Luo, J.; Jiang, T. Hydrothermal synthesis of zeolites-calcium silicate hydrate composite from coal fly ash with co-activation of Ca (OH)

2-NaOH for aqueous heavy metals removal. *International Journal of Mining Science and Technology* **2022**, *32*, 563-573.

471. Li, X.-b.; Ye, J.-j.; Liu, Z.-h.; Qiu, Y.-q.; Li, L.-j.; Mao, S.; Wang, X.-c.; Zhang, Q. Microwave digestion and alkali fusion assisted hydrothermal synthesis of zeolite from coal fly ash for enhanced adsorption of Cd(II) in aqueous solution. *Journal of Central South University* **2018**, *25*, 9-20.
472. Yao, Q.; Peng, Y.; Chen, M.; Wang, Y.; Ding, J.; Ma, B.; Wang, Q.; Lu, S. One-step high efficiency synthesis of zeolite from fly ash by mechanochemical method as a low-cost adsorbent for cadmium removal. *Journal of Environmental Chemical Engineering* **2024**, *12*, 111877.
473. Remenárová, L.; Pipíška, M.; Florková, E.; Horník, M.; Rozložník, M.; Augustín, J. Zeolites from coal fly ash as efficient sorbents for cadmium ions. *Clean Technologies and Environmental Policy* **2014**, *16*, 1551-1564.
474. Wu, D.; Sui, Y.; He, S.; Wang, X.; Li, C.; Kong, H. Removal of trivalent chromium from aqueous solution by zeolite synthesized from coal fly ash. *Journal of Hazardous Materials* **2008**, *155*, 415-423.
475. Ghasemi, Z.; Sourinejad, I.; Kazemian, H.; Hadavifar, M.; Rohani, S.; Younesi, H. Kinetics and thermodynamic studies of Cr (VI) adsorption using environmental friendly multifunctional zeolites synthesized from coal fly ash under mild conditions. *Chemical Engineering Communications* **2020**, *207*, 808-825.
476. Liu, Z.; Cheng, X. Preparation and characterization of P-type zeolite for adsorption of Cr^{3+}, Ni^{2+}, and Co^{2+}. *Environmental Science and Pollution Research* **2024**, *31*, 23664-23679.
477. Attari, M.; Bukhari, S.S.; Kazemian, H.; Rohani, S. A low-cost adsorbent from coal fly ash for mercury removal from industrial wastewater. *Journal of Environmental Chemical Engineering* **2017**, *5*, 391-399.
478. Tauanov, Z.; Tsakiridis, P.E.; Mikhalovsky, S.V.; Inglezakis, V.J. Synthetic coal fly ash-derived zeolites doped with silver nanoparticles for mercury (II) removal from water. *Journal of Environmental Management* **2018**, *224*, 164-171.
479. Lee, C.-H.; Suh, J.-H. Adsorption characteristics of cobalt ion with zeolite synthesized by coal fly ash. *Journal of Korean Society of Environmental Engineers* **2009**, *31*, 941-946.
480. Hui, K.S.; Chao, C.Y.H.; Kot, S.C. Removal of mixed heavy metal ions in wastewater by zeolite 4A and residual products from recycled coal fly ash. *Journal of Hazardous Materials* **2005**, *127*, 89-101.
481. Joseph, I.V.; Tosheva, L.; Doyle, A.M. Simultaneous removal of Cd(II), Co(II), Cu(II), Pb(II), and Zn(II) ions from aqueous solutions via adsorption on FAU-type zeolites prepared from coal fly ash. *Journal of Environmental Chemical Engineering* **2020**, *8*, 103895.
482. Philippova, O.; Barabanova, A.; Molchanov, V.; Khokhlov, A. Magnetic polymer beads: Recent trends and developments in synthetic design and applications. *European Polymer Journal* **2011**, *47*, 542-559.
483. Kharissova, O.V.; Dias, H.V.R.; Kharisov, B.I. Magnetic adsorbents based on micro- and nano-structured materials. *RSC Advances* **2015**, *5*, 6695-6719.
484. Ali, A.; Shah, T.; Ullah, R.; Zhou, P.; Guo, M.; Ovais, M.; Tan, Z.; Rui, Y. Review on Recent Progress in Magnetic Nanoparticles: Synthesis, Characterization, and Diverse Applications. *Frontiers in Chemistry* **2021**, *9*, 629054.

485. Tahoon, M.A.; Siddeeg, S.M.; Salem Alsaiari, N.; Mnif, W.; Ben Rebah, F. Effective Heavy Metals Removal from Water Using Nanomaterials: A Review. *Processes* **2020**, *8(6), 645*.
486. Li, N.; Li, Z.; Zhang, L.; Shi, H.; Li, J.; Zhang, J.; Zhang, Z.; Dang, F. One-step fabrication of bifunctional self-assembled oligopeptides anchored magnetic carbon nanoparticles and their application in copper (II) ions removal from aqueous solutions. *Journal of Hazardous Materials* **2020**, *382*, 121113.
487. Maksoud, M.I.A.; Elgarahy, A.; Farrell, C.; Ala; Al-Muhtaseb, A.a.; Rooney, D.; Osman, A. Insight on water remediation application using magnetic nanomaterials and biosorbents. *Coordination Chemistry Reviews* **2019**, *403, 213096*.
488. Iranmanesh, M.; Hulliger, J. Magnetic separation: Its application in mining, waste purification, medicine, biochemistry and chemistry. *Chemical Society Reviews* **2017**, *46*.
489. Sharma, A.; Mangla, D.; Shehnaz; Chaudhry, S.A. Recent advances in magnetic composites as adsorbents for wastewater remediation. *Journal of Environmental Management* **2022**, *306*, 114483.
490. Martinez-Boubeta, C.; Simeonidis, K. Chapter 20 - Magnetic Nanoparticles for Water Purification. In *Nanoscale Materials in Water Purification*, Thomas, S., Pasquini, D., Leu, S.-Y., Gopakumar, D.A., Eds.; Elsevier: 2019; pp. 521-552.
491. Brião, G.d.V.; de Andrade, J.R.; da Silva, M.G.C.; Vieira, M.G.A. Removal of toxic metals from water using chitosan-based magnetic adsorbents. A review. *Environmental Chemistry Letters* **2020**, *18*, 1145-1168.
492. Nisticò, R. Magnetic materials and water treatments for a sustainable future. *Research on Chemical Intermediates* **2017**, *43*, 6911-6949.
493. Ghosh, N.; Sen, S.; Biswas, G.; Saxena, A.; Haldar, P.K. Adsorption and Desorption Study of Reusable Magnetic Iron Oxide Nanoparticles Modified with Justicia adhatoda Leaf Extract for the Removal of Textile Dye and Antibiotic. *Water, Air, & Soil Pollution* **2023**, *234*, 202.
494. Wahajuddin, M.; Arora, S. Superparamagnetic iron oxide nanoparticles: Magnetic nanoplatforms as drug carriers. *International Journal of Nanomedicine* **2012**, *7*, 3445-3471.
495. Reichel, V.; Kovács, A.; Kumari, M.; Bereczk-Tompa, É.; Schneck, E.; Diehle, P.; Pósfai, M.; Hirt, A.M.; Duchamp, M.; Dunin-Borkowski, R.E. Single crystalline superstructured stable single domain magnetite nanoparticles. *Scientific Reports* **2017**, *7*, 45484.
496. Liosis, C.; Papadopoulou, A.; Karvelas, E.; Karakasidis, T.E.; Sarris, I.E. Heavy Metal Adsorption Using Magnetic Nanoparticles for Water Purification: A Critical Review. *Materials (Basel)* **2021**, *14*.
497. Teja, A.S.; Koh, P.-Y. Synthesis, properties, and applications of magnetic iron oxide nanoparticles. *Progress in Crystal Growth and Characterization of Materials* **2009**, *55*, 22-45.
498. Tadic, M.; Trpkov, D.; Kopanja, L.; Vojnovic, S.; Panjan, M. Hydrothermal synthesis of hematite (α-Fe2O3) nanoparticle forms: Synthesis conditions, structure, particle shape analysis, cytotoxicity and magnetic properties. *Journal of Alloys and Compounds* **2019**, *792*, 599-609.
499. Gallegos-Garcia, M.; Ramírez-Muñiz, K.; Song, S. Arsenic Removal from Water by Adsorption Using Iron Oxide Minerals as Adsorbents: A Review. *Mineral Processing and Extractive Metallurgy Review* **2012**, *33*, 301-315.

500. Siddiqui, S.I.; Chaudhry, S.A. Iron oxide and its modified forms as an adsorbent for arsenic removal: A comprehensive recent advancement. *Process Safety and Environmental Protection* **2017**, *111*, 592-626.
501. Nassar, N.N. Iron oxide nanoadsorbents for removal of various pollutants from wastewater: an overview. *Application of Adsorbents for Water Pollution Control* **2012**, 81-118.
502. Liu, J.; Yu, Y.; Zhu, S.; Yang, J.; Song, J.; Fan, W.; Yu, H.; Bian, D.; Huo, M. Synthesis and characterization of a magnetic adsorbent from negatively-valued iron mud for methylene blue adsorption. *PLoS One* **2018**, *13*, e0191229.
503. Zhu, J.; Wei, S.; Chen, M.; Gu, H.; Rapole, S.B.; Pallavkar, S.; Ho, T.C.; Hopper, J.; Guo, Z. Magnetic nanocomposites for environmental remediation. *Advanced Powder Technology* **2013**, *24*, 459-467.
504. Turan, N.B.; Erkan, H.S.; Engin, G.O.; Bilgili, M.S. Nanoparticles in the aquatic environment: Usage, properties, transformation and toxicity—A review. *Process Safety and Environmental Protection* **2019**, *130*, 238-249.
505. Bhateria, R.; Singh, R. A review on nanotechnological application of magnetic iron oxides for heavy metal removal. *Journal of Water Process Engineering* **2019**, *31*, 100845.
506. Liosis, C.; Karvelas, E.G.; Karakasidis, T.; Sarris, I.E. Numerical study of magnetic particles mixing in waste water under an external magnetic field. *Journal of Water Supply: Research and Technology—AQUA* **2020**, *69*, 266-275.
507. Karvelas, E.; Liosis, C.; Karakasidis, T.; Sarris, I. Micromixing nanoparticles and contaminated water under different velocities for optimum heavy metal ions adsorption. *Environmental Sciences Proceedings* **2020**, *2*, 65.
508. Matis, K.A.; Zouboulis, A.I.; Gallios, G.P.; Erwe, T.; Blöcher, C. Application of flotation for the separation of metal-loaded zeolites. *Chemosphere* **2004**, *55*, 65-72.
509. Castro, C.J.; Shyu, H.Y.; Xaba, L.; Bair, R.; Yeh, D.H. Performance and onsite regeneration of natural zeolite for ammonium removal in a field-scale non-sewered sanitation system. *Science of The Total Environment* **2021**, *776*, 145938.
510. Younas, F.; Mustafa, A.; Farooqi, Z.U.; Wang, X.; Younas, S.; Mohy-Ud-Din, W.; Ashir Hameed, M.; Mohsin Abrar, M.; Maitlo, A.A.; Noreen, S.; et al. Current and Emerging Adsorbent Technologies for Wastewater Treatment: Trends, Limitations, and Environmental Implications. *Water* **2021**, *13, 215*.
511. Loiola, A.R.; Bessa, R.A.; Oliveira, C.P.; Freitas, A.D.L.; Soares, S.A.; Bohn, F.; Pergher, S.B.C. Magnetic zeolite composites: Classification, synthesis routes, and technological applications. *Journal of Magnetism and Magnetic Materials* **2022**, *560*, 169651.
512. Fungaro, D.; Yamaura, M.; Carvalho, T.; Graciano, J. Zeolite from fly ash-iron oxide magnetic nanocomposite: Synthesis and application as an adsorbent for removal of contaminants from aqueous solution. *Zeolites: Synthesis, Chemistry and Applications* **2012**.
513. Ambashta, R.D.; Sillanpää, M. Water purification using magnetic assistance: A review. *Journal of Hazardous Materials* **2010**, *180*, 38-49.
514. Younas, F.; Mustafa, A.; Ur, Z.; Farooqi, Z.U.; Xiukang, W.; Younas, S.; Mohy-Ud-Din, W.; Hameed, M.; Abrar, M.M.; Maitlo, A.L.I.; et al. Current and Emerging Adsorbent Technologies for Wastewater Treatment: Trends, Limitations, and Environmental Implications. *Water* **2021**, *13*, 215.

515. Liu, H.; Peng, S.; Shu, L.; Chen, T.; Bao, T.; Frost, R.L. Magnetic zeolite NaA: synthesis, characterization based on metakaolin and its application for the removal of Cu^{2+}, Pb^{2+}. *Chemosphere* **2013**, *91*, 1539-1546.
516. Oliveira, L.C.A.; Petkowicz, D.I.; Smaniotto, A.; Pergher, S.B.C. Magnetic zeolites: A new adsorbent for removal of metallic contaminants from water. *Water Research* **2004**, *38*, 3699-3704.
517. Mthombeni, N.H.; Onyango, M.S.; Aoyi, O. Adsorption of hexavalent chromium onto magnetic natural zeolite-polymer composite. *Journal of the Taiwan Institute of Chemical Engineers* **2015**, *50*, 242-251.
518. Praipipat, P.; Ngamsurach, P.; Roopkhan, N. Zeolite A powder and beads from sugarcane bagasse fly ash modified with iron(III) oxide-hydroxide for lead adsorption. *Scientific Reports* **2023**, *13*, 1873.
519. Yuan, M.; Song, C.; Yan, G. Some Research on the Magnetic X Zeolite Composites. *Advanced Materials Research* **2011**, *311-313*, 2040-2047.
520. Yang, Y.; Zhang, P.; Jiang, J.; Dai, Y.; Wu, M.; Pan, Y.; Ni, L. Synthesis and properties of magnetic zeolite with good magnetic stability from fly ash. *Journal of Sol-Gel Science and Technology* **2018**, *87*.
521. Salem Attia, T.M.; Hu, X.L.; Yin, D.Q. Synthesised magnetic nanoparticles coated zeolite (MNCZ) for the removal of arsenic (As) from aqueous solution. *Journal of Experimental Nanoscience* **2014**, *9*, 551-560.
522. Boycheva, S.; Zgureva, D.; Miteva, S.; Marinov, I.; Behunová, D.; Trendafilova, I.; Popova, M.; Václaviková, M. Studies on the Potential of Nonmodified and Metal Oxide-Modified Coal Fly Ash Zeolites For Adsorption of Heavy Metals and Catalytic Degradation of Organics for Waste Water Recovery. *Processes* **2020**, *8, (7)*.
523. Faghihian, H.; Moayed, M.; Firooz, A.; Iravani, M. Synthesis of a novel magnetic zeolite nanocomposite for removal of Cs^{+} and Sr^{2+} from aqueous solution: kinetic, equilibrium, and thermodynamic studies. *J Colloid Interface Sci* **2013**, *393*, 445-451.
524. Gill, C.B. Magnetic Separation. In *Materials Beneficiation*, Gill, C.B., Ed.; Springer New York: New York, NY, 1991; pp. 128-140.
525. Chen, L.; Xiong, D. Chapter Seven - Magnetic Techniques for Mineral Processing. In *Progress in Filtration and Separation*, Tarleton, S., Ed.; Academic Press: Oxford, 2015; pp. 287-324.
526. Wills, B.A.; Finch, J.A. Magnetic and Electrical Separation (8^{th} Edition). In *Wills' Mineral Processing Technology*; Butterworth-heinemann: 2016; pp. 381-407.
527. Adeleke, A.A. Magnetic Separation. In *Mineral Processing Technology (1^{st} Edition)*; CRC Press: 2023; pp. 181-196.
528. Liu, J.; Xie, S.; Li, X.; Lu, D.; Wang, H.; Yao, Q.; Yang, X.; Fu, Y. Separating efficiency of ferromagnetic particles and principle of low-intensity dry magnetic separator under different air supply modes: Based on multi-physical modeling. *Powder Technology* **2023**, *415*, 118155.
529. Foner, S. The vibrating sample magnetometer: Experiences of a volunteer. *Journal of Applied Physics* **1996**, *79*, 4740-4745.
530. Svoboda, J. *Magnetic techniques for the treatment of materials*; Springer Science & Business Media: 2004.

531. Stradling, A. Development of a mathematical model of a crossbelt magnetic separator. *Minerals Engineering* **1991**, *4*, 733-745.
532. Nesset, J.; Todd, I.; Hollingworth, M.; Finch, J. A loading equation for high gradient magnetic separation. *IEEE Transactions on Magnetics* **1980**, *16*, 833-835.
533. Cavanough, G.L.; Holtham, P.N.; Powell, T.M. Magnetic susceptibility measurement applied to the minerals industry. *Minerals Engineering* **2006**, *19*, 1588-1595.
534. Marion, C. A Mineralogical Investigation into the Beneficiation of a Rare-Earth Mineral Deposit Using Physical Separations. PhD Thesis, Department of Mining and Materials Engineering, McGill University, Montreal, Canada, 2020.
535. Bennett, L.H.; Page, C.H.; Swartzendruber, L.J. Comments on Units in Magnetism. *Journal of Research of the National Bureau of Standards* **1978**, *83*, 9-12.
536. Svoboda, J.; Fujita, T. Recent developments in magnetic methods of material separation. *Minerals Engineering* **2003**, *16*, 785-792.
537. Oberteuffer, J. Magnetic separation: A review of principles, devices, and applications. *IEEE Transactions on Magnetics* **1974**, *10*, 223-238.
538. Lawver, J.E.; Hopstock, D.M. Wet Magnetic Separation of Weakly Magnetic Minerals. *Minerals Engineering* **1974**, *6(3)*, 154-172.
539. Svoboda, J. Magnetic Separation. In *Encyclopedia of Materials: Science and Technology*, Buschow, K.H.J., Cahn, R.W., Flemings, M.C., Ilschner, B., Kramer, E.J., Mahajan, S., Veyssière, P., Eds.; Elsevier: Oxford, 2005; pp. 1-7.
540. Kamimoto, Y.; Hagio, T.; Jung, Y.-J.; Ichino, R.; Gil, K. Development of Synthetic Magnetic Zeolite Adsorbents and Application to Ammonium Ion Removal. *KSCE Journal of Civil Engineering* **2020**, *24*, 1395-1399.
541. Huang, X.; Wang, N.; Kang, Z.; Yang, X.; Pan, M. An Investigation into the Adsorption of Ammonium by Zeolite-Magnetite Composites. *Minerals* **2022**, *12*, 256.
542. Nah, I.W.; Hwang, K.Y.; Shul, Y.G.; Jeon, C. Removal of ammonium ion from aqueous solution using magnetically modified zeolite. *Environmental Technology* **2008**, *29*, 633-639.
543. Babalar, M.; Siddiqua, S.; Sakr, M.A. A novel polymer coated magnetic activated biochar-zeolite composite for adsorption of polystyrene microplastics: Synthesis, characterization, adsorption and regeneration performance. *Separation and Purification Technology* **2024**, *331*, 125582.
544. Sossou, K.; Prasad, S.B.; Agbotsou, E.K.; Saidou Souley, H. Evaluation of the performance of magnetic zeolite nanocomposites in removing various water contaminants as heavy metals, organic pollutants, and emerging contaminants: A review. *Next Nanotechnology* **2024**, *6*, 100075.
545. Shahadat, M.; Isamil, S. Regeneration performance of clay-based adsorbents for the removal of industrial dyes: a review. *RSC Advances* **2018**, *8*, 24571-24587.
546. V, A.; Cioffi, R.; Michele, P.; C, C. Disposal of Lead-Containing Zeolite Sludges in Cement Matrix. *Environmental Technology* **1995**, *16*, 147-156.
547. Girskas, G.; Pundienė, I.; Pranckevičienė, J. The Effect of Natural and Synthesised Zeolites on Cement-Based Materials Hydration and Hardened State Properties. *Materials (Basel)* **2023**, *16*.

548. Lu, X.; Wang, F.; Li, X.-y.; Shih, K.; Zeng, E.Y. Adsorption and Thermal Stabilization of Pb^{2+} and Cu^{2+} by Zeolite. *Industrial & Engineering Chemistry Research* **2016**, *55*, 8767-8773.
549. Kordala, N.; Wyszkowski, M. Zeolite Properties, Methods of Synthesis, and Selected Applications. *Molecules* **2024**, *29*, 1069.
550. Thompson, R.; Franklin, K. Chapter 55—LTA Linde Type A Si (50), Al (50). *Verified Syntheses of Zeolitic Materials; Robson, H., Lillerud, KP, Eds* **2001**, 179-181.
551. Ramachandran, V.S.; Beaudoin, J.J. *Handbook of analytical techniques in concrete science and technology: principles, techniques and applications*; Elsevier: 2000.
552. Stevie, F.A.; Donley, C.L. Introduction to x-ray photoelectron spectroscopy. *Journal of Vacuum Science & Technology A* **2020**, *38*.
553. Cortez-Trejo, M.C.; Manríquez, J.; Mendoza, S. 5 - Characterization of natural gums: emphasizing distinctive spectroscopic techniques. In *Natural Gums*, Ahmed, S., Ali, A., Eds.; Elsevier: 2023; pp. 123-161.
554. Helaluddin, A.; Khalid, R.S.; Alaama, M.; Abbas, S.A. Main analytical techniques used for elemental analysis in various matrices. *Tropical Journal of Pharmaceutical Research* **2016**, *15*, 427-434.
555. Reed, T.B.; Breck, D.W. Crystalline Zeolites. II. Crystal Structure of Synthetic Zeolite, Type A. *Journal of the American Chemical Society* **1956**, *78*, 5972-5977.
556. Loiola, A.R.; Andrade, J.C.R.A.; Sasaki, J.M.; da Silva, L.R.D. Structural analysis of zeolite NaA synthesized by a cost-effective hydrothermal method using kaolin and its use as water softener. *Journal of Colloid and Interface Science* **2012**, *367*, 34-39.
557. Mohamed, R.M.; Ismail, A.A.; Kini, G.; Ibrahim, I.A.; Koopman, B. Synthesis of highly ordered cubic zeolite A and its ion-exchange behavior. *Colloids and Surfaces A: Physicochemical and Engineering Aspects* **2009**, *348*, 87-92.
558. Leiggener, C.; Currao, A.; Calzaferri, G. Zeolite A and ZK-4. In *Materials Syntheses: A Practical Guide*, Schubert, U., Hüsing, N., Laine, R.M., Eds.; Springer Vienna: Vienna, 2008; pp. 21-28.
559. Painer, F.; Baldermann, A.; Gallien, F.; Eichinger, S.; Steindl, F.; Dohrmann, R.; Dietzel, M. Synthesis of Zeolites from Fine-Grained Perlite and Their Application as Sorbents. *Materials* **2022**, *15*, 4474.
560. de Lima, R.C.F.; Oliveira, D.d.S.; Pergher, S.B.C. Interzeolitic Transformation of Clinoptilolite into GIS and LTA Zeolite. *Minerals* **2021**, *11*, 1313.
561. Song, H.; Cheng, H.; Zhang, Z.; Cheng, F. Adsorption properties of zeolites synthesized from coal fly ash for Cu (II). *Journal of environmental biology / Academy of Environmental Biology, India* **2014**, *35*, 983-988.
562. Wu, C.N.; Tang, Y.C.; Tang, L.H. Removal of heavy metal from wastewater using zeolite from fly ash. In Proceedings of the Advanced Materials Research, 2012; pp. 2736-2739.
563. Li, G.; Li, M.; Zhang, X.; Cao, P.; Jiang, H.; Luo, J.; Jiang, T. Hydrothermal synthesis of zeolites-calcium silicate hydrate composite from coal fly ash with co-activation of Ca(OH)2-NaOH for aqueous heavy metals removal. *International Journal of Mining Science and Technology* **2022**, *32*, 563-573.
564. Jangkorn, S.; Youngme, S.; Praipipat, P. Comparative lead adsorptions in synthetic wastewater by synthesized zeolite A of recycled industrial wastes from sugar factory and power plant. *Heliyon* **2022**, *8 (4)*, e09323.

565. Chang, H.L.; Shih, W.H. A general method for the conversion of fly ash into zeolites as ion exchangers for cesium. *Industrial and Engineering Chemistry Research* **1998**, *37*, 71-78.
566. Nightingale, E.R., Jr. Phenomenological Theory of Ion Solvation. Effective Radii of Hydrated Ions. *The Journal of Physical Chemistry* **1959**, *63*, 1381-1387.
567. Ayawei, N.; Ebelegi, A.N.; Wankasi, D. Modelling and Interpretation of Adsorption Isotherms. *Journal of Chemistry* **2017**, *2017*, 3039817.
568. Boycheva, S.; Zgureva, D.; Miteva, S.; Marinov, I.; Behunová, D.M.; Trendafilova, I.; Popova, M.; Václaviková, M. Studies on the Potential of Nonmodified and Metal Oxide-Modified Coal Fly Ash Zeolites For Adsorption of Heavy Metals and Catalytic Degradation of Organics for Waste Water Recovery. *Processes* **2020**, *8*, 778.
569. Sitko, R.; Turek, E.; Zawisza, B.; Malicka, E.; Talik, E.; Heimann, J.; Gagor, A.; Feist, B.; Wrzalik, R. Adsorption of divalent metal ions from aqueous solutions using graphene oxide. *Dalton Transactions* **2013**, *42*, 5682-5689.
570. Wang, J.; Guo, X. Adsorption isotherm models: Classification, physical meaning, application and solving method. *Chemosphere* **2020**, *258*, 127279.
571. Freundlich, H. Über die adsorption in lösungen. *Zeitschrift für Physikalische Chemie* **1907**, *57*, 385-470.
572. Redlich, O.; Peterson, D.L. A useful adsorption isotherm. *Journal of Physical Chemistry* **1959**, *63*, 1024-1024.
573. Temkin, M. Kinetics of ammonia synthesis on promoted iron catalysts. *Acta Physiochim. URSS* **1940**, *12*, 327-356.
574. Langmuir, I. The constitution and fundamental properties of solids and liquids. Part I. Solids. *Journal of the American Chemical Society* **1916**, *38*, 2221-2295.
575. Volmer, M. Thermodynamische Folgerungen ans der Zustandsgleichung für adsorbierte Stoffe. *Zeitschrift für Physikalische Chemie* **1925**, *115*, 253-260.
576. Brunauer, S.; Emmett, P.H.; Teller, E. Adsorption of gases in multimolecular layers. *Journal of the American Chemical Society* **1938**, *60*, 309-319.
577. Aranovich, G. The theory of polymolecular adsorption. *Langmuir* **1992**, *8*, 736-739.

Appendix

Appendix A Different adsorption isotherm models.

Some of the commonly used adsorption models are presented in Appendix A. For a detailed review of these and other adsorption models, please refer to Wang and Guo [570].

Table A1 - Commonly used adsorption models.

Classification	**Model's name**	**Model equation**	**References**
Adsorption empirical isotherm models	Linear isotherm model (Henry's law)	$q_e=KC_e$	-
	Freundlich isotherm model	$q_e = K_F C_e^{1/n}$	[571]
	Redlich–Peterson (R–P) isotherm model	$q_e = \frac{\mathrm{K_{RP}} C_e}{1 + \alpha_{\mathrm{RP}} C_e^{g}}$	[572]
	Temkin isotherm model	$q_e = \frac{RT}{\mathrm{b}} \ln (AC_e)$	[573]
Chemical adsorption models	Langmuir isotherm model	$q_e = \frac{q_m \mathrm{K_L} C_e}{1 + K_{\mathrm{L}} C_e}$	[574]
	Volmer isotherm model	$b_V C_e = \frac{q_e}{q_{mV} - q_{\mathrm{e}}} e^{\frac{q_e}{q_{mV} - q_{\mathrm{e}}}}$	[575]
Physical adsorption models	BET isotherm model (n = ∞)	$q_e = \frac{q_{mBET} \mathrm{K}_{BET1} C_e}{(1 - K_{\mathrm{BET2}} C_e)[1 - K_{\mathrm{BET2}} C_e + \mathrm{K}_{BI}$	[576]
	Aranovich isotherm model	$q_e = \frac{q_{mA} C_A \frac{C_e}{C_{sA}}}{\sqrt{\left(1 - \frac{C_e}{C_{sA}}\right)} \left(1 + C_A \frac{C_e}{C_{sA}}\right)}$	[577]

Appendix B Absolute adsorption capacities of different zeolites synthesized from CFA for heavy metal ions remediation

Table B1 - Absolute adsorption capacities of different zeolites synthesized from CFA in single-ion solutions – Ni.

Ion	**Zeolite type**	**Surface area of zeolite, m^2/g**	**CEC, meq/g**	**Zeolite Adsorption Capacity, mg/g**	**Adsorbent Dosage, g/L**	**pH**	**Metal Ion Concentration, mg/L**	**Solution Volume, mL**	**Reference**
Ni	Zeolite A	90.04	NA	47	2	7	100	100	He et al. [3]
Ni	Zeolite X	NA	2.70	16	2.5	5	100	100	Zhang et al. [453]
Ni	CFA Zeolite	346.6	NA	61	5	5	10-500	100	Sireesha et al. [188]
Ni	CFA Zeolite	12.7	1.64	34	1	5	100	100	He et al. [187]
Ni	NaP1 Zeolite	27.7	1.95	20	2.5	6	100	20	Alvarez-Ayuso et al. [455]

Table B2 - Absolute adsorption capacities of different zeolites synthesized from CFA in single-ion solutions – Cu.

Ion	**Zeolite type**	**Surface area of zeolite, m^2/g**	**CEC, meq/g**	**Zeolite Adsorption Capacity, mg/g**	**Adsorbent Dosage, g/L**	**pH**	**Metal Ion Concentration, mg/L**	**Solution Volume, mL**	**Reference**
Cu	CFA Zeolite	12.7	1.64	56	1	5	100	100	He et al. [187]
Cu	NaP1 Zeolite	27.7	1.95	51	2.5	5	100	20	Alvarez-Ayuso et al. [455]
Cu	CFA Zeolite	NA	NA	71	1	6	500	50	Wu et al. [457]
Cu	Zeolite A	NA	NA	50	NA	3	250	50	Yang et al. [458]
	Magnetic CFA-zeolites	NA	NA	49		3			
Cu	CFA zeolite	NA	NA	69-141	4	5	40-500	NA	Huiping et al. [460]
Cu	CFA Zeolite	346.6	NA	96	5	5	10-500	100	Sireesha et al. [188]

Table B3 - Absolute adsorption capacities of different zeolites synthesized from CFA in single-ion solutions – Zn.

Ion	**Zeolite type**	**Surface area of zeolite, m^2/g**	**CEC, meq/g**	**Zeolite Adsorption Capacity, mg/g**	**Adsorbent Dosage, g/L**	**pH**	**Metal Ion Concentration, mg/L**	**Solution Volume, mL**	**Reference**
Zn	NaP1 Zeolite	27.7	1.95	33	2.5	6	100	20	Alvarez-Ayuso et al. [455]
Zn	NaP Zeolite	26.8	NA	37	2.5	5	100	20	Zhang et al. [221]
	NaP-CyOH	80.4		40					
	NaP-AMP	28.6		39					
	NaP-PEG	24.3		35					
Zn	Zeolite X	249.7	3.10	205	10	6.8	NA	50	Izidoro et al. [222]
	Zeolite A	15.7	3.90	220					

Table B4 - Absolute adsorption capacities of different zeolites synthesized from CFA in single-ion solutions – Pb.

Ion	Zeolite type	Surface area of zeolite, m^2/g	CEC, meq/g	Zeolite Adsorption Capacity, mg/g	Adsorbent Dosage, g/L	pH	Metal Ion Concentration, mg/L	Solution Volume, mL	Reference
Pb	CFA Zeolite	12.7	1.64	66	1	5	100	100	He et al. [187]
Pb	Zeolite A	10.4	NA	556	0.1	5	200	200	Jangkorn et al. [228]
Pb	K-type Zeolite (FA48)	47.3	0.986–0.999	56	0.2	2-5	50	50	Kobayashi et al. [234]
Pb	CFA Composite Zeolite	96.5	NA	409	0.5	4.5	100±10	100	Li et al. [470]

Table B5 - Absolute adsorption capacities of different zeolites synthesized from CFA in single-ion solutions – Cd.

Ion	Zeolite type	Surface area of zeolite, m^2/g	CEC, meq/g	Zeolite Adsorption Capacity, mg/g	Adsorbent Dosage, g/L	pH	Metal Ion Concentration, mg/L	Solution Volume, mL	Reference
Cd	Zeolite X	249.7	3.10	156	10	6.6	NA	50	Izidoro et al. [222]
	Zeolite A	15.7	3.90	185					
Cd	P1 Zeolite	88.4	2.21	131	0.05	5	25-250	50	Yao et al. [472]
Cd	CFA Zeolite	12.7	1.64	52	1	5	100	100	He et al. [187]
Cd	CFA synthesized Faujasite	75.7	NA	87	0.5	6	20	50	Li et al. [470]
Cd	NaP1 Zeolite	27.7	1.95	51	2.5	6	100	20	Alvarez-Ayuso et al. [455]
Cd	CFA Zeolite	NA	NA	83	1	6	500	50	Wu et al. [457]
Cd	Zeolitic material ZM1	NA	NA	71	2.5	6	450	300	Remenarova et al. [473]
	Zeolitic material ZM3	NA	NA	130					

Table B6 - Absolute adsorption capacities of different zeolites synthesized from CFA in single-ion solutions – Cr.

Ion	**Zeolite type**	**Surface area of zeolite, m^2/g**	**CEC, meq/g**	**Zeolite Adsorption Capacity, mg/g**	**Adsorbent Dosage, g/L**	**pH**	**Metal Ion Concentration, mg/L**	**Solution Volume, mL**	**Reference**
Cr	NaP1 Zeolite	27.7	1.95	44	2.5	4	100	20	Alvarez-Ayuso et al. [455]
Cr	High calcium Wujin F Zeolite	NA	< 3	51	10	4	400	40	Wu et al. [474]
Cr	KP-Na-P1	41.5	NA	49	0.5	2	50	100	Ghasemi et al. [475]
Cr	HDTMA-Na-P1		NA	338					

Table B7 - Absolute adsorption capacities of different zeolites synthesized from CFA in single-ion solutions – Hg.

Ion	**Zeolite type**	**Surface area of zeolite, m^2/g**	**CEC, meq/g**	**Zeolite Adsorption Capacity, mg/g**	**Adsorbent Dosage, g/L**	**pH**	**Metal Ion Concentration, mg/L**	**Solution Volume, mL**	**Reference**
Hg	CFA-Linde Type A	127.11	NA	0.4	50	2.5	10	10	Attari et al. [477]
Hg	CFA zeolite with AgNP	105	NA	6	7.5	2	10	100	Tauanov et al. [478]
Hg	K-type zeolite (FA48)	47.3	8.98	12	0.2	3	50	50	Kobayashi et al. [234]

Table B8 - Absolute adsorption capacities of different zeolites synthesized from CFA in single-ion solutions – Co.

Ion	Zeolite type	Surface area of zeolite, m^2/g	CEC, meq/g	Zeolite Adsorption Capacity, mg/g	Adsorbent Dosage, g/L	pH	Metal Ion Concentration, mg/L	Solution Volume, mL	Reference
Co	CFA zeolite (Z-C1)	NA	NA	94	NA	NA	NA	NA	Lee et al. [479]

Table B9 - Absolute adsorption capacities of different zeolites synthesized from CFA in single-ion solutions – Mn.

Ion	Zeolite type	Surface area of zeolite, m^2/g	CEC, meq/g	Zeolite Adsorption Capacity, mg/g	Adsorbent Dosage, g/L	pH	Metal Ion Concentration, mg/L	Solution Volume, mL	Reference
Mn	CFA Zeolite	12.7	1.64	31	1	5	100	100	He et al. [187]

Table B10 - Absolute adsorption capacities of different zeolites synthesized from CFA in mixed-ion systems.

Zeolite type	Surface area of zeolite, (m^2/g)	CEC, (meq/g)	Metal ions in mixed-ion system	Adsorption Capacity (mg/g)	Adsorbent Dosage, (g/L)	pH	Metal Ion Concentration (mg/L)	Solution Volume (mL)	Reference
Magnetic zeolite P	29.5	NA	Cu	25	NA	NA	NA	50	Wang et al. [459]
			Pb	20					
Zeolite P	22.4	NA	Cu	30					
			Pb	28					
ZCET40	52.44	NA	Pb	88	4	6.6	0-1000	50	Visa et al. [454]
			Cd	27			0-600		
			Cu	21			0-250		
			Zn	8			0-260		
			Ni	6			0-250		
ZDs40	37.30	NA	Pb	98			0-1000		
			Cu	89			0-600		
			Cd	18			0-250		
			Zn	8			0-260		
			Ni	5			0-250		
4A	54.82	NA	Cu	50	5	3	50-300	100	Hui et al. [104]
			Cr	42					
			Zn	31					
			Co	14					
			Ni	9					
CFA Zeolite	12.7	1.64	Pb	45	1	5	100	100	He et al. [187]
			Cu	33					
			Cd	27					
			Ni	16					

Zeolite type	**Surface area of zeolite, (m^2/g)**	**CEC, (meq/g)**	**Metal ions in mixed-ion system**	**Adsorption Capacity (mg/g)**	**Adsorbent Dosage, (g/L)**	**pH**	**Metal Ion Concentration (mg/L)**	**Solution Volume (mL)**	**Reference**
			Mn	15					
NaP1	NA	NA	Cu	10	20	7	200	50	Wang et al. [456]
			Pb	1					
			Cd	0.3					
FAU-type zeolite (CFZ10−68)	432	NA	Pb	110	5	NA	100-500	20	Joseph et al. [481]
			Cu	58					
			Cd	53					
			Zn	37					
			Co	12					
Low calcium FA zeolite	3.26	3.06	Cu	198	10	6	100	100	Ji et al. [463]
			Pb	186					
			Zn	156					
			Cd	124					
High calcium FA zeolite	8.36	3.56	Cu	183					
			Pb	182					
			Zn	154					
			Cd	119					
Municipal solid waste incineration FA zeolite	40.12	0.498	Pb	50	12.5	3-4	500	20	Qiu et al. [464]
			Cu	28					
			Zn	20					
			Mn	15					
			Ni	14					
			Cd	11					
Zeolite A	NA	NA	Cu	38	5	3	300	100	

Zeolite type	**Surface area of zeolite, (m^2/g)**	**CEC, (meq/g)**	**Metal ions in mixed-ion system**	**Adsorption Capacity (mg/g)**	**Adsorbent Dosage, (g/L)**	**pH**	**Metal Ion Concentration (mg/L)**	**Solution Volume (mL)**	**Reference**
			Zn	30					
Zeolite X	NA	NA	Cu	29					Wang et al. [410]
			Zn	22					
CFA Zeolite	NA	NA	Pb	195	10	4-5	100-3000	50	Nascimento et al. [465]
			Cu	77					
			Mn	60					
			Zn	59					
Zeolite X	288.5	NA	Pb	112	1	7	100	50	Bai et al. [468]
			Cr	62					
			Cu	54					
			Zn	45					
			Cd	38					
CFA Composite Zeolite	96.5	NA	Pb	122	0.5	4.5	100±10	100	Li et al. [470]
			Cr	71					
			Cu	34					
			Zn	28					
			Cd	10					
			Ni	5					

Appendix C SEM-EDS results of synthesized M-CFAZ showing map scans and point IDs.

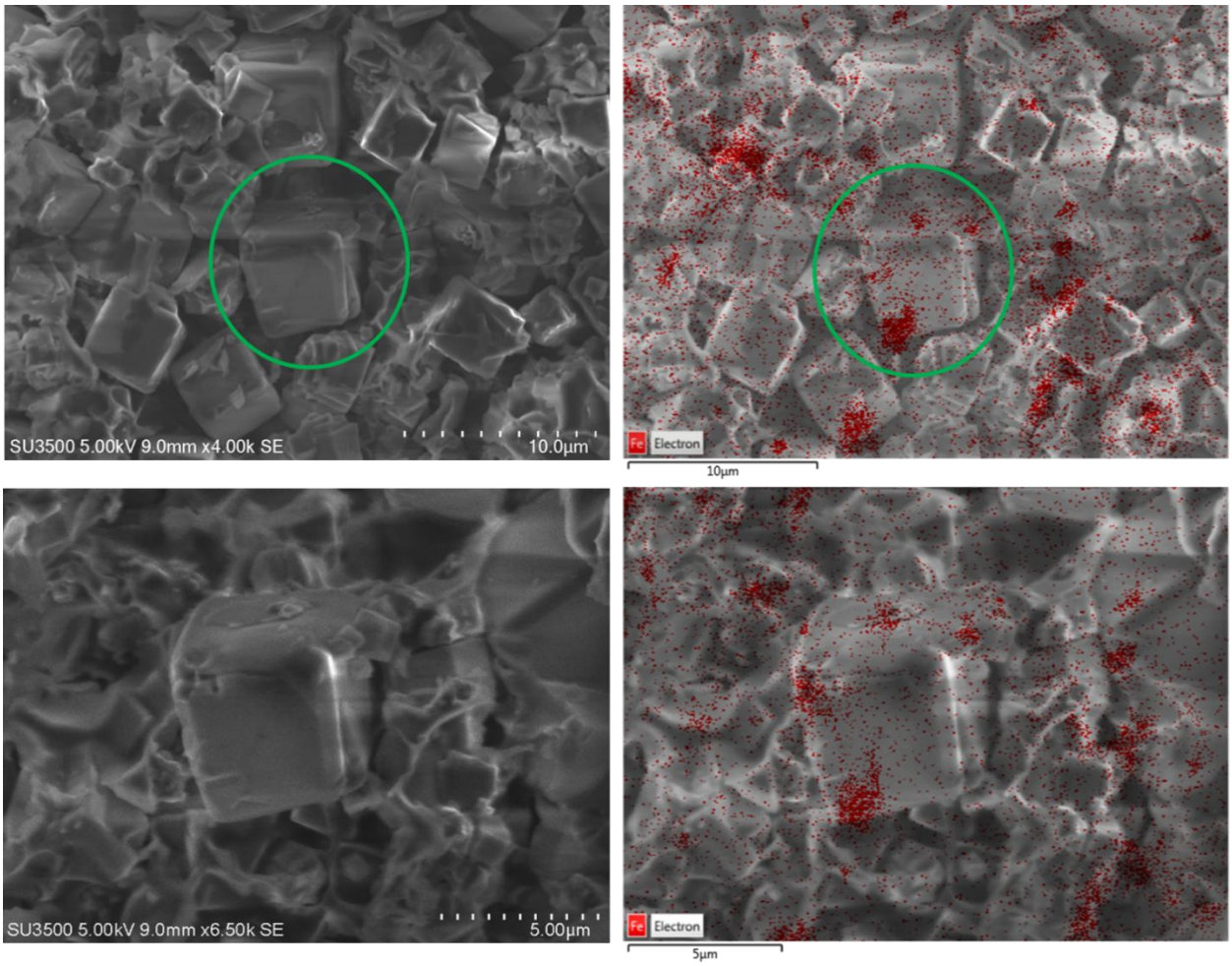

Figure C1 – SEM-EDS map scans of individual M-CFAZ particle showing iron presence in the sample.

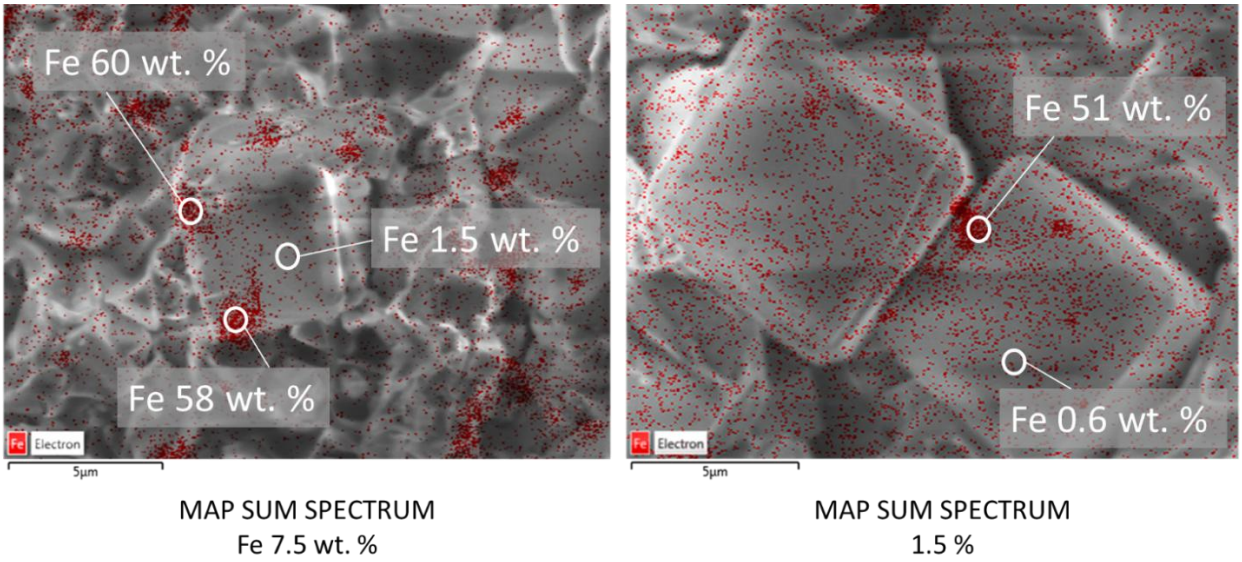

Figure C2 – SEM-EDS point analysis of M-CFAZ particles at high magnification showing iron presence in weight % in the sample.